6-2006

Experimental investigation of the Aerodynamic Ground Effect of a Tailless LAMBDA-Shaped UCAV with Wing Flaps

Jason T. Mostaccio

EXPERIMENTAL INVESTIGATION OF THE AERODYNAMIC GROUND EFFECT OF A TAILLESS LAMBDA-SHAPED UCAV WITH WING FLAPS

THESIS

Jason T. Mostaccio, Ensign, USN

AFIT/GAE/ENY/06-J11

DEPARTMENT OF THE AIR FORCE
AIR UNIVERSITY

AIR FORCE INSTITUTE OF TECHNOLOGY

Wright-Patterson Air Force Base, Ohio

AFIT/GAE/ENY/06-J11

EXPERIMENTAL INVESTIGATION OF THE AERODYNAMIC GROUND EFFECT OF A TAILLESS LAMBDA-SHAPED UCAV WITH WING FLAPS

THESIS

Presented to the Faculty

Department of Aeronautics and Astronautics

Graduate School of Engineering and Management

Air Force Institute of Technology

Air University

Air Education and Training Command

In Partial Fulfillment of the Requirements for the

Degree of Master of Science in Aeronautical Engineering

Jason T. Mostaccio, BS

Ensign, USN

June 2006

AFIT/GAE/ENY/06-J11

EXPERIMENTAL INVESTIGATION OF THE AERODYNAMIC GROUND EFFECT OF A TAILLESS LAMBDA-SHAPED UCAV WITH WING FLAPS

Jason T. Mostaccio, BS
Ensign, USN

Approved:

_____	_____
Dr. Milton E. Franke (Chairman)	Date
_____	_____
Dr. Mark F. Reeder (Member)	Date
_____	_____
Lt Col Eric J. Stephen (Member)	Date

Abstract

This experimental study adequately identified the ground effect region of a lambda-shaped unmanned combat air vehicle (UCAV). The lambda planform used in this study was originally tested in a previous experiment to determine the stability and control characteristics generated out-of-ground-effect. The following study extends the existing database by analyzing the inherent aerodynamic behavior that is produced by employing trailing edge flap deflections while flying in-ground-effect (IGE). To accomplish this objective, static ground effect tests were performed in the AFIT 3' x 3' subsonic wind tunnel where a ground plane was used to simulate the forces and moments on the UCAV IGE. Removable aluminum flap pieces were attached to the model, in a split flap configuration, along the midboard and outboard trailing edges of the UCAV, and the corresponding IGE data was collected for symmetric and asymmetric deflections of $+10^{o}$ and $+20^{o}$.

Based on the results of this study, the ground effect region for the lambda UCAV, with flaps deployed was characterized by an increase in the lift, a reduction in the induced drag but an increase in the overall drag, and an increase in the lift-to-drag ratio. These trends were noted in previous ground effect studies for aircraft with trailing edge flaps, and similar aspect ratios and wing sweep. Additionally, a flow visualization analysis revealed that a vortical flow pattern, that is characteristic of delta wing configurations, developed over the upper surface of the wing at high angles of attack.

To my parents and sister who have always supported me in all of my endeavors and to my grandfather; may he have the courage and strength to face every day with a newfound hope.

Acknowledgments

I would first and foremost like to thank and express my sincerest gratitude to my Lord God from whom I have received all the blessings in my life and who has given me the strength and motivation to complete this thesis, and to my loving family who continually support me in every endeavor of my life. Also, I would like to thank my thesis advisor, Dr. Franke for his insightfulness and experience and for allowing me to spearhead this entire project, from start to finish. I would also like to thank Mr. Ryan Plumley of the Air Vehicles Directorate of the Air Force Research Lab for his numerous suggestions and support for this project. Lastly, I would like to express my sincere gratitude to Dwight Gehring and John Hixenbaugh, AFIT/ENY, for their patience and hard work that without would have made this project impossible to finish. They helped immensely with the set-up and operation of the wind tunnel, from installing the ground planes to calibrating the equipment.

Jason T. Mostaccio

Table of Contents

Page

Abstract iv

Acknowledgments vi

List of Figures ix

List of Tables xv

List of Symbols xix

I. Introduction 1

Section 1 – Wing-in-Ground Effect 1
Section 2 - Wing-In-Ground Vehicles 2
Section 3 – Unmanned Aerial Vehicles (UAVs) 4
Section 4 – Motivation 6

II. Literature Review 7

Section 1 – Ground Effect Theory 7
Section 1.1 – Induced Drag 7
Section 1.2 – Lift 9
Section 2 – Boundary Layer Interaction with the Ground Plane 11
Section 2.1 – Static and Dynamic Ground Effect Tests 11
Section 2.1 – Boundary Layer Theory 11
Section 2.3 – Boundary Layer Removal 14
Section 3 – Adverse Ground Effect 16
Section 4 – Experimental Objectives 18

III. Experimental Equipment 20

Section 1 – UCAV Model 20
Section 2 – Ground Representation 23
Section 3 – Wind Tunnel 25
Section 4 – Strain Gage Balance 28
Section 5 – Dantec Hot-wire Anemometer 29

IV. Experimental Procedures 31

Section 1 – Hot-wire Anemometer 31
Section 1.1 – Hot-wire Calibration 31
Section 1.2 – Blockage Corrections 32

Page

Section 2 – Data Acquisition 36
Section 3 – Data Reduction 38

V. Results & Analysis 39

Section 1 – Hot-wire Anemometer & Wind Tunnel Blockage Corrections 39
Section 2 - Wind Tunnel Ground Effect Tests 42
Section 2.1 – Longitudinal Stability Characteristics, OGE 43
Section 2-1.1 Midboard and Outboard Trailing Edge Flaps 48
Section 2.2 – Longitudinal Characteristics, IGE 53
Section 2.2.1 – Lift Coefficient IGE 53
Section 2.2.2 – Drag Coefficient IGE 63
Section 2.2.3 – Lift-to-Drag IGE 72
Section 3 – Lambda UCAV Flow Visualization 75
Section 3.1 – OGE Flow Visualization 76
Section 3.2 – IGE Flow Visualization 78
Section 4 – Height-to-Span Ratio and Angle of Attack 80

VI. Conclusions and Recommendations 83

Section 1 – Conclusions 83
Section 2 – Recommendations 85

Appendix A: Additional UCAV Pictures 87

Appendix B: Ground Plane Schematics 89

Appendix C: MATLAB Data Reduction Sample Calculation 92

Appendix D: Ground Plane Boundary Layer Analysis 101

Appendix E: Additional Plots 107

Appendix F: Data Tables 130

Appendix G: MATLAB Data Reduction Code 169

Appendix H: Lambda UCAV Flap Specifications 182

References 184

Vita 187

List of Figures

Figure Page

Figure 1: Percent Lift Increase in Ground Effect for Various Aircraft 10

Figure 2: Theoretical Boundary Layer Analysis of the Ground Plane 13

Figure 3: Requirements for the Application of an Endless-Belt Moving Ground Plane . 16

Figure 4: Adverse Ground Effect for the F-106, AOA = 14^{o} 17

Figure 5: Adverse Ground Effect for the Lambda UCAV 18

Figure 6: Original Scale Lambda UCAV..... 20

Figure 7: Four Views of the ½ - Scaled Lambda Model OGE and IGE (h/b = 0.05) with Mid/Outboard Trailing Edge Split Flap Deflections 22

Figure 8: Top and Separated View of the Removable Ground Plane 25

Figure 9: Dimensions of the Wind Tunnel Intake and Convergent Section 26

Figure 10: Hot-wire Probe Access Panels 27

Figure 11: AFIT 3'x3' Wind Tunnel Schematic 28

Figure 12: Wind Tunnel Coordinates 30

Figure 13: Hot-wire Location for Blockage Measurements 33

Figure 14: Hot-wire Test Grid for Blockage Measurements 34

Figure 15: Hot-wire Test Grid for Boundary Layer Measurements 35

Figure 16: Wind Tunnel Velocity Differences Between the Hot-wire and Pressure Transducer..... 40

Figure 17: Hot-wire Velocity Comparison 41

Figure 18: Aerodynamic Comparison of the Lift Coefficient, No Flaps..... 43

Page

Figure 19: Lift Comparison Based on In's Blockage Corrections..... 45

Figure 20: C_m vs. AOA, OGE, No Flaps 47

Figure 21: C_m vs. C_L, OGE, No Flaps..... 47

Figure 22: Effect of Flap Deflections on the Lift Coefficient, Vel. = 100 mph 50

Figure 23: Effect of Flap Deflections on the Drag Polar, Vel. = 100 mph..... 50

Figure 24: Flap Effectiveness Stability Analysis, Vel. = 100 mph..... 52

Figure 25: Lift Curve Comparison IGE, No Flaps, Vel. = 100 mph 54

Figure 26: Lift Curve Comparison, Flaps +10^o, Vel. = 100 mph 55

Figure 27: Lift Curve Comparison, Flaps +20^o, Vel. = 100 mph 55

Figure 28: Effect of Height and Flap Deflection on the Lift Axis Intercept..... 56

Figure 29: Effect of Height and Flap Deflection on the Lift Curve Slope 57

Figure 30: Ground Effect, C_L vs. (h/b), No Flaps, Vel. = 100 mph..... 58

Figure 31: Ground Effect, C_L vs. (h/b), Flaps +10^o, Vel. = 100 mph..... 59

Figure 32: Ground Effect, C_L vs. (h/b), Flaps +20^o, Vel. = 100 mph..... 59

Figure 33: Effect of Flap Deflections on the Maximum Lift Increase at h/b = 0.05, Vel. =100 mph 62

Figure 34: Ground Effect, VORLAX Panel Prediction, C_L vs. (h/b), Re = 1.4E6 63

Figure 35: Ground Effect, C_D vs. (h/b), Flaps Retracted, Vel. = 100 mph..... 64

Figure 36: Ground Effect, C_D vs. (h/b), Flaps +10^o, Vel. = 100 mph..... 65

Figure 37: Ground Effect, C_D vs. (h/b), Flaps +20^o, Vel. = 100 mph..... 65

Figure 38: Effect of Height on the Drag Polar, Flaps +20^o, Re = 7.25E5 66

Page

Figure 39: Induced Drag Factor Comparison, Flaps +20°, Vel. = 100 mph 68

Figure 40: Effect of Height and Flap Deflection on the Induced Drag Factor, k 69

Figure 41: Effect of Height and Flap Deflection on McCormick's Induced Drag Factor 70

Figure 42: Effect of Height and Flap Deflection on the Parasite Drag..... 71

Figure 43: Ground Effect, L/D vs. (h/b), No Flaps, Vel. = 100 mph 73

Figure 44: Ground Effect, L/D vs. (h/b), Flaps +10°, Vel. = 100 mph..... 73

Figure 45: Ground Effect, L/D vs. (h/b), Flaps +20°, Vel. = 100 mph..... 74

Figure 46: OGE, Vel. = 100 mph, alpha = -10° 77

Figure 47: OGE, Vel. = 100 mph, alpha = 0° 77

Figure 48: OGE, Vel. = 100 mph, alpha = +20° 78

Figure 49: IGE (h/b = 0.05), Vel. = 100 mph, alpha = -4°..... 79

Figure 50: IGE (h/b = 0.05), Vel. = 100 mph, alpha = 0° 79

Figure 51: IGE (h/b = 0.05), Vel. = 100 mph, alpha = +13°..... 80

Figure 52: Variance of Height-Span-Ratio with AOA 81

Figure 53: Lambda Model OGE with +20° Symmetric Flap Deflections, AOA = +4° 87

Figure 54: Lambda Model with +20° Symmetric Flap Deflections, AOA = 0° 87

Figure 55: Original Lambda UCAV Model..... 88

Figure 56: ½-Scaled Lambda UCAV with Mid/Outboard Trailing Edge Split Flaps 88

Figure 57: Dimensions of the ground plane circular plate 89

Figure 58: Dimensions of the ground plane front plate 90

Figure 59: Dimensions of the ground plane mounting legs 91

Page

Figure 60: Boundary Layer Velocity Profiles, h/b = 0.05, $U_{\infty,corr}$ = 36.52 mph 102

Figure 61: Boundary Layer Velocity Profiles, h/b = 0.05, $U_{\infty,corr}$ = 90.88 mph 102

Figure 62: Ground Plane Boundary Layer Comparison, h/b = 0.05 104

Figure 63: C_D vs. AOA, OGE, No Flaps 107

Figure 64: C_L vs. C_D, OGE, No Flaps 108

Figure 65: L/D vs. AOA, OGE, No Flaps 108

Figure 66: L/D vs. AOA, OGE, Flap Deflection Comparison, Vel. = 100 mph 109

Figure 67: C_m vs. AOA, OGE, Flap Deflection Comparison, Vel. = 100 mph 109

Figure 68: Ground Effect, C_L vs. (h/b), No Flaps, 40 mph 110

Figure 69: Ground Effect, C_L vs. (h/b), Flaps $+10^o$, 40 mph 110

Figure 70: Ground Effect, C_L vs. (h/b), Flaps $+20^o$, 40 mph 111

Figure 71: Ground Effect, C_L vs. (h/b), No Flaps, 60 mph 111

Figure 72: Ground Effect, C_L vs. (h/b), Flaps $+10^o$, 60 mph 112

Figure 73: Ground Effect, C_L vs. (h/b), Flaps $+20^o$, 60 mph 112

Figure 74: Ground Effect, C_L vs. (h/b), No Flaps, 80 mph 113

Figure 75: Ground Effect, C_L vs. (h/b), Flaps $+10^o$, 80 mph 113

Figure 76: Ground Effect, C_L vs. (h/b), Flaps $+20^o$, 80 mph 114

Figure 77: Ground Effect, C_D vs. (h/b), No Flaps, 40 mph 114

Figure 78: Ground Effect, C_D vs. (h/b), Flaps $+10^o$, 40 mph 115

Figure 79: Ground Effect, C_D vs. (h/b), Flaps $+20^o$, 40 mph 115

Figure 80: Ground Effect, C_D vs. (h/b), No Flaps, 60 mph 116

Page

Figure 81: Ground Effect, C_D vs. (h/b), Flaps +10^o, 60 mph 116

Figure 82: Ground Effect, C_D vs. (h/b), Flaps +20^o, 60 mph 117

Figure 83: Ground Effect, C_D vs. (h/b), No Flaps, 80 mph 117

Figure 84: Ground Effect, C_D vs. (h/b), Flaps +10^o, 80 mph 118

Figure 85: Ground Effect, C_D vs. (h/b), Flaps +20^o, 80 mph 118

Figure 86: Ground Effect, L/D vs. (h/b), No Flaps, 40 mph 119

Figure 87: Ground Effect, L/D vs. (h/b), Flaps +10^o, 40 mph 119

Figure 88: Ground Effect, L/D vs. (h/b), Flaps +20^o, 40 mph 120

Figure 89: Ground Effect, L/D vs. (h/b), No Flaps, 60 mph 120

Figure 90: Ground Effect, L/D vs. (h/b), Flaps +10^o, 60 mph 121

Figure 91: Ground Effect, L/D vs. (h/b), Flaps +20^o, 60 mph 121

Figure 92: Ground Effect, L/D vs. (h/b), No Flaps, 80 mph 122

Figure 93: Ground Effect, L/D vs. (h/b), Flaps +10^o, 80 mph 122

Figure 94: Ground Effect, L/D vs. (h/b), Flaps +20^o, 80 mph 123

Figure 95: Ground Effect, C_m vs. (h/b), No Flaps, 40 mph 123

Figure 96: Ground Effect, C_m vs. (h/b), Flaps +10^o, 40 mph 124

Figure 97: Ground Effect, C_m vs. (h/b), Flaps +20^o, 40 mph 124

Figure 98: Ground Effect, C_m vs. (h/b), No Flaps, 60 mph 125

Figure 99: Ground Effect, C_m vs. (h/b), Flaps +10^o, 60 mph 125

Figure 100: Ground Effect, C_m vs. (h/b), Flaps +20^o, 60 mph 126

Figure 101: Ground Effect, C_m vs. (h/b), No Flaps, 80 mph 126

Page

Figure 102: Ground Effect, C_m vs. (h/b), Flaps +10^o, 80 mph..... 127

Figure 103: Ground Effect, C_m vs. (h/b), Flaps +20^o, 80 mph..... 127

Figure 104: Ground Effect, C_m vs. (h/b), No Flaps, 100 mph 128

Figure 105: Ground Effect, C_m vs. (h/b), Flaps +10^o, 100 mph..... 128

Figure 106: Ground Effect, C_m vs. (h/b), Flaps +20^o, 100 mph..... 129

List of Tables

Table Page

Table 1: Preliminary Boundary Layer Analysis for h/b = 0.05 14

Table 2: Conventional Ground Plane Justification 16

Table 3: Model Specifications of the Original and Scaled Lambda-Shaped UCAV..... 21

Table 4: Trailing Edge Flap Specifications for the Original and Scaled Lambda UCAV 23

Table 5: Dimensions and Specifications of the Ground Plane Assembly 24

Table 6: Operating Specifications of the Toshiba Premium Efficiency Fan Motor and the Siemens Adjustable Frequency Tunnel Controller 25

Table 7: Maximum Loads of the AFIT 100 lb Balance..... 29

Table 8: Hot-wire Position Along Ground Plane..... 35

Table 9: Experimental Test Matrix 37

Table 10: Correction Factors Used to Adjust Velocity for Wind Tunnel Blockage..... 42

Table 11: Summary of Corrected Wind Tunnel Velocities 42

Table 12: Lift Curve Comparison 44

Table 13: Longitudinal Characteristics, OGE, No Flap Deflections 48

Table 14: Lift Comparison for Maximum Flap Deflection 49

Table 15: Longitudinal Effects of Mid/Outboard Flap Deflections, Vel. = 100 mph 52

Table 16: IGE Lift Comparison for Various Flap Deflections 60

Table 17: Effect of Flap Deflections on the L/D IGE..... 74

Table 18: Variance of (h/b) Datum for Various AOA 82

Table 19: Model specifications and test room conditions 93

Page

Table 20: Corrected Tunnel Flight Parameters for Solid Blockage Effects 95

Table 21: Corrected Balance Measured Forces and Moments 96

Table 22: Model Center of Mass and Corresponding Moments..... 98

Table 23: Drag Coefficient Correction Factors 100

Table 24: MATLAB Reduction Code Flight Parameter Comparison 100

Table 25: Boundary Layer Comparison, h/b = 0.05 105

Table 26: Vertical Extensions of Trailing Edge Flaps into the Boundary Layer, h/b=0.05 106

Table 27: U_∞ = 40 mph, h/b = 1.05(OGE), $\delta_{mid/out}$ = +10^o, Symmetric Deflections 130

Table 28: U_∞ = 40 mph, h/b = 0.3, $\delta_{mid/out}$ = +10^o, Symmetric Deflections..... 131

Table 29: U_∞ = 40 mph, h/b = 0.15, $\delta_{mid/out}$ = +10^o, Symmetric Deflections..... 132

Table 30: U_∞ = 40 mph, h/b = 0.1, $\delta_{mid/out}$ = +10^o, Symmetric Deflections..... 133

Table 31: U_∞ = 40 mph, h/b = 0.05, $\delta_{mid/out}$ = +10^o, Symmetric Deflections..... 134

Table 32: U_∞ = 60 mph, h/b = 1.05 (OGE), $\delta_{mid/out}$ = +10^o, Symmetric Deflections..... 135

Table 33: U_∞ = 60 mph, h/b = 0.3, $\delta_{mid/out}$ = +10^o, Symmetric Deflections 136

Table 34: U_∞ = 60 mph, h/b = 0.15, $\delta_{mid/out}$ = +10^o, Symmetric Deflections..... 137

Table 35: U_∞ = 60 mph, h/b = 0.1, $\delta_{mid/out}$ = +10^o, Symmetric Deflections..... 138

Table 36: U_∞ = 60 mph, h/b = 0.05, $\delta_{mid/out}$ = +10^o, Symmetric Deflections 139

Table 37: U_∞ = 80 mph, h/b = 1.05 (OGE), $\delta_{mid/out}$ = +10^o, Symmetric Deflections..... 140

Table 38: U_∞ = 80 mph, h/b = 0.3, $\delta_{mid/out}$ = +10^o, Symmetric Deflections..... 141

Table 39: U_∞ = 80 mph, h/b = 0.15, $\delta_{mid/out}$ = +10^o, Symmetric Deflections..... 142

Page

Table 40: U_∞ = 80 mph, h/b = 0.1, $\delta_{mid/out}$ = +10°, Symmetric Deflections 143

Table 41: U_∞ = 80 mph, h/b = 0.05, $\delta_{mid/out}$ = +10°, Symmetric Deflections 144

Table 42: U_∞ = 100 mph, h/b = 1.05, $\delta_{mid/out}$ = +10°, Symmetric Deflections 145

Table 43: U_∞ = 100 mph, h/b = 0.3, $\delta_{mid/out}$ = +10°, Symmetric Deflections 146

Table 44: U_∞ = 100 mph, h/b = 0.15, $\delta_{mid/out}$ = +10°, Symmetric Deflections 147

Table 45: U_∞ = 100 mph, h/b = 0.1, $\delta_{mid/out}$ = +10°, Symmetric Deflections 148

Table 46: U_∞ = 100 mph, h/b = 0.05, $\delta_{mid/out}$ = +10°, Symmetric Deflections 149

Table 47: U_∞ = 40 mph, h/b = 1.05 (OGE), $\delta_{mid/out}$ = +20°, Symmetric Deflections 149

Table 48: U_∞ = 40 mph, h/b = 0.3, $\delta_{mid/out}$ = +20°, Symmetric Deflections 150

Table 49: U_∞ = 40 mph, h/b = 0.15, $\delta_{mid/out}$ = +20°, Symmetric Deflections 151

Table 50: U_∞ = 40 mph, h/b = 0.1, $\delta_{mid/out}$ = +20°, Symmetric Deflections 152

Table 51: U_∞ = 40 mph, h/b = 0.05, $\delta_{mid/out}$ = +20°, Symmetric Deflections 153

Table 52: U_∞ = 60 mph, h/b = 1.05 (OGE), $\delta_{mid/out}$ = +20°, Symmetric Deflections 154

Table 53: U_∞ = 60 mph, h/b = 0.3, $\delta_{mid/out}$ = +20°, Symmetric Deflections 155

Table 54: U_∞ = 60 mph, h/b = 0.15, $\delta_{mid/out}$ = +20°, Symmetric Deflections 156

Table 55: U_∞ = 60 mph, h/b = 0.1, $\delta_{mid/out}$ = +20°, Symmetric Deflections 157

Table 56: U_∞ = 60 mph, h/b = 0.05, $\delta_{mid/out}$ = +20°, Symmetric Deflections 158

Table 57: U_∞ = 80 mph, h/b = 1.05, $\delta_{mid/out}$ = +20°, Symmetric Deflections 159

Table 58: U_∞ = 80 mph, h/b = 0.3, $\delta_{mid/out}$ = +20°, Symmetric Deflections 160

Table 59: U_∞ = 80 mph, h/b = 0.15, $\delta_{mid/out}$ = +20°, Symmetric Deflections 161

Table 60: U_∞ = 80 mph, h/b = 0.1, $\delta_{mid/out}$ = +20°, Symmetric Deflections 162

Page

Table 61: U_∞ = 80 mph, h/b = 0.05, $\delta_{mid/out}$ = +20°, Symmetric Deflections..... 163

Table 62: U_∞ = 100 mph, h/b = 1.05, $\delta_{mid/out}$ = +20°, Symmetric Deflections..... 164

Table 63: U_∞ = 100 mph, h/b = 0.3, $\delta_{mid/out}$ = +20°, Symmetric Deflections..... 165

Table 64: U_∞ = 100 mph, h/b = 0.15, $\delta_{mid/out}$ = +20°, Symmetric Deflections..... 166

Table 65: U_∞ = 100 mph, h/b = 0.1, $\delta_{mid/out}$ = +20°, Symmetric Deflections..... 167

Table 66: U_∞ = 100 mph, h/b = 0.05, $\delta_{mid/out}$ = +20°, Symmetric Deflections..... 168

List of Symbols

A	Axial Force (Body Axis)
A_1	Balance Axial Sensor
AR	Aspect Ratio
a	Speed of Sound
body	Body Axis Frame
bc	Body Centered
b	Wing Span
C	Tunnel Cross Sectional Area
C_D	Coefficient of Drag
C_{Do}	Profile Drag
ΔC_{D_M}	Wave Drag
C_L	Coefficient of Lift
C_{L_α}	Lift Curve Slope
$C_{L_{MAX}}$	Maximum Lift Coefficient
C_m	Pitch Moment Coefficient
C_{m_α}	Pitch Curve Slope
C_P	Pressure Coefficient
CG	Center of Gravity
cm	Center of Mass
cmb	Balance Center of Mass
corr	Corrected
$\bar{c}$, MAC	Mean Aerodynamic Chord
c_r	Wing Root Chord
D	Drag Force in Wind Axes
ΔD_i	Change in Induced Drag
e	Oswald's Efficiency Factor
h	Height Above Ground
h/b	Height-to-Span Ratio
k	Induced Drag Constant
L	Lift Force in Wind Axis
L/D	Lift-to-Drag Ratio
l	Roll Moment
ℓ_1	Balance Roll Moment Sensor
M	Mach Number
m	Pitch Moment
N	Normal Force in Body Axis
N_1 & N_2	Balance Normal Sensors
P	Test Room Pressure
q_∞	Freestream Dynamic Pressure
R	Specific Gas Constant
Re	Reynolds Number
S*	Side Force (Wind Axis)

S	Wing Planform Area
S_1 & S_2	Balance Side Sensors
T	Test Room Temperature
U	Boundary Layer Velocity
U_e	Velocity at Boundary Layer Edge
U_∞	Freestream Velocity
$U_{\infty,corr}$	Corrected Freestream Velocity
UAV	Unmanned Aerial Vehicle
UCAV	Unmanned Combat Air Vehicle
u	Uncorrected, Instantaneous Velocity in Boundary Layer
u_e	Boundary Layer Edge Velocity
WIG	Wing-in-Ground
wind	Wind Axis Frame
w	Angle Between x_{cg} and x-Axis At $\alpha = 0^o$
Y	Side Force in Body Axis
x,y,z	Wind Tunnel Coordinates
α,θ	Angle of Attack
α_{corr}	Corrected Angle of Attack
$\Delta\alpha_w$	Angle of Attack Correction Factor
ε_{GP}	Solid Blockage Correction Factor of the Ground Plane
$\varepsilon_{sb,wing}$	Solid Blockage Correction Factor of the Model
ε_{tc}	Blockage Correction Factor of the Hot-Wire and Pressure Transducer
ε_{vel}	Total Velocity Correction Factor
γ	Ratio of Specific Heats
δ_{lam}	Laminar Boundary Layer Thickness
δ_{lam}^*	Laminar Boundary Layer Displacement Thickness
δ_{turb}	Turbulent Boundary Layer Thickness
δ_{turb}^*	Turbulent Boundary Layer Displacement Thickness
$\delta_{mid/out}$	Midboard/Outboard Flap Deflection Angle
ρ	Air Density
μ	Air Viscosity
ϕ	McCormack's Induced Drag Factor
ψ	Yaw Angle

EXPERIMENTAL INVESTIGATION OF THE AERODYNAMIC GROUND EFFECT OF A TAILLESS LAMBDA-SHAPED UCAV WITH WING FLAPS

I. Introduction

Section 1 – Wing-in-Ground Effect

During the first few moments of takeoff, an aircraft usually remains close to the ground, in an almost nearly horizontal flight position, as the pilot gains the appropriate airspeed necessary to initiate a safe and efficient climb. While in close proximity to the ground, additional lift is generated, which would only be possible by means of a greater power setting and fuel expense if the aircraft were in flight (1). This peculiar phenomenon can be traced back to the early days of manned flight when, during the landing phase, pilots would experience a noticeable change in the aerodynamic handling qualities of their aircraft. In particular, they would notice that the airplane would seem to float above the surface as if the air trapped between the wing and the runway had created a cushion of air. Throughout the twentieth century, it has come to be known that what these pilots experienced was an aerodynamic phenomenon known as wing-in-ground effect (WIG) (2). It is during this interaction with the ground that, either during takeoff or landing, the efficiency of the aircraft will be improved in the form of increased lift and decreased drag (3).

The drag of an aircraft can be divided into two categories: friction drag and induced drag. For the wing of an aircraft to generate positive lift, the static pressure on the lower surface must be higher than on the upper surface. Consequently, the conditions necessary to generate lift cause complications at the ends of a finite wing: trailing

cylindrical vortices develop and are shed when the high pressure area on the lower side curls around the wingtips to meet the low pressure area on the upper side. When the energy of the vortices is dissipated, the aircraft experiences an increase in drag (2). Therefore, it can be concluded that the aerodynamic advantages associated with ground effect are not only a result of ground proximity but also of the drag due to lift (3).

From previous research, it is generally accepted that an aircraft will experience ground effect when it is within one wingspan of the ground (3). Under these conditions, the presence of the ground significantly modifies the flow around the airplane. As the aircraft approaches the surface, the vortices trailing aft of the lifting wings do not have enough space to fully develop and therefore become weaker as the amount of leakage of pressure from the lower side diminishes (2). This effect reduces the downwash induced on the wings as the vortices are pushed outward by the ground (4).

Based on the phenomena described above, both theory and experiment indicate that ground proximity generally decreases the drag and increases the lift and pitching moments of the aircraft. With a decrease in drag and an increase in lift, the aircraft efficiency, in terms of the lift-to-drag ratio, is ultimately increased. It is the realization of these advantages associated with ground effect that led engineers to develop Wing-In-Ground (WIG) vehicles (3).

Section 2 - Wing-In-Ground Vehicles

During the flight intensive years of World War I, many technological advances were made in the engineering field of aeronautics. It was during this time that engineers truly began to study and apply the benefits of flying in-ground effect (IGE) to the design of new aircraft. In 1932, T. Kaario, a Finnish engineer, built the first true WIG concept

(5). The aircraft was basically a flying wing based on ram-wing configurations studied almost a decade earlier by Warner in the 1920s. The aircraft was reported to fly well near the ground but would develop severe instabilities at higher altitudes (1).

About the same time T. Kaario was developing his experimental concepts, N. Troong, an engineer from Switzerland, was taking the revolutionary WIG theory a step further by designing an aircraft that weighed up to thirty tons; an idea, that up to that time, was unheard of in the aviation community. Based on his research, it became apparent that less energy was required within one chord length of the ground, to sustain flight of heavier-than-air machines (5). Unfortunately, his studies were never completed, but paved the way for the future of WIG vehicles (1).

As the 20th century progressed beyond World War II, improved theories and technologies relating to ground effect not only popularized the idea of WIG vehicles but extended its advantages to marine transportation. In the early 1960s, the first WIG boats were designed independently by the Russian ship designer, Rostislav Alexeiev, and the German aeronautical engineer, Alexander Lippisch. With a background in ship design, Alexeiev thought of WIG boats as hydrofoils that would travel above the surface, rather than submerged, whereas Lippisch was intrigued by the potential of increasing the overall efficiency of the aircraft by flying in ground effect (2).

Based on the WIG research of Alexeiev, Russia, under the auspices of Alexeiev himself, began to develop “ekranoplans” that were designed to take full advantage of all the benefits that ground effect had to offer (3). Consequently, once the Soviet military realized the vast potential of these vehicles, Soviet President, Kruchev, generously awarded unlimited financial resources to Alexeiev that eventually led to the development

of the 550 ton KM Caspian Sea Monster (3). The Caspian Sea Monster was one of the most ambitious projects attempted by Akexeiev; the vehicle was not only to travel fast over the water, but was expected to weigh more than 100 times that of the heaviest ekranoplan built to date. Fortunately, the KM project was a success but was eventually terminated when funding was lost due to the fall of the Soviet Union in 1991 (2).

Just as Russia realized the potential of WIG vehicles, so did the United States. In order to meet the growing demands in mass transportation for both the military and the civilian workplace, Boeing Phantom Works is currently designing a low-flying, surface skimming aircraft similar to that of past Russian WIG concepts. It is officially known as the Pelican project and is projected to be twice the size of the world's largest aircraft, the Russian An225, with the capability of carrying payloads up to 1,400 tons (6). By flying low, the Pelican will capitalize on the aerodynamic benefits of ground effect; a significant fraction of the drag will be reduced resulting in an outstanding cruise efficiency that will not only reduce operating costs but, more importantly, revolutionize the future for marine transportation (6).

Section 3 – Unmanned Aerial Vehicles (UAVs)

With today's advances in technology, it is possible to achieve controlled flight of an aircraft without the presence of a pilot. Throughout history, these unmanned vehicles have been called many things such as drones, pilot-less and remote-piloted vehicles but became known in the early 1990s, by military forces around the world, as unmanned aerial vehicles (UAV) (7). The Department of Defense explicitly defines a UAV as

> a powered, aerial vehicle that does not carry a human operator, uses aerodynamic forces to provide vehicle lift, can fly autonomously or be piloted remotely, can be expendable or recoverable, and carry a lethal or nonlethal payload. Ballistic or

> semiballistic vehicles, cruise missiles, and artillery projectiles are not considered unmanned aerial vehicles (Joint Publication 1-02). (8)

Taken literally, this definition implies that a UAV can be anything from a wind-powered kite to a radio-controlled model airplane; however, when speaking about UAVs, the military restricts their classification only to reusable heavier-than-air craft (7).

Throughout the late 20th century, advances in communications, guidance, navigation, and computing capabilities have significantly increased the reliability of unmanned vehicles (3). Lately, the U.S. military has gained a greater interest in UAVs because they not only offer the possibility of cheaper, more capable fighting machines but, more importantly, offer efficient operation without risk to aircrews (7).

Initially, the military used UAVs for the tactical purposes of battlefield reconnaissance, damage assessment, and visual surveillance but lately, through technological advances, have extended their mission capabilities by fitting new designs with weapons for warefare/defense suppression; a UAV of this type, is commonly referred to as a UCAV or an unmanned combat aerial vehicle (7). Two of the most well known UCAVs in current use by the U.S. Armed Forces, are the General Atomics Predator, and the Teledyne-Ryan Global Hawk. Based on the success and military effectiveness of the Global Hawk and Predator programs, the military foresees the applications of UAVs extending well into the 21st century (9).

Currently, the primary organization involved with the development of UCAVs is the joint unmanned air systems (J-UCAS) program that is designed to

> demonstrate the technical feasibility, military utility and operational value for a networked system of high performance, weaponized unmanned air vehicles to effectively and affordably prosecute 21st century combat missions, including Suppression of Enemy Air Defenses (SEAD), surveillance, and precision strike within the emerging global command and control architecture. (3)

The program is currently studying two advanced, unconventional designs, the Boeing X-45 and the Northrop Grumman X-47; both employ a blended, swept wing, no tail configuration. This alone presents stability and control challenges, but further complicates the issue when coupled with the ground effect that is encountered during the takeoff and landing phases of flight. Therefore, in order to properly design an autonomous vehicle that will operate effectively in this region, it becomes imperative for the control engineer to study and apply the aerodynamic effects associated with flying IGE (3).

Section 4 – Motivation

In an effort to quantify the aerodynamic characteristics of moderately swept, low aspect ratio, tailless, blended wing planforms, Lt. Shad Reed of the Air Vehicles Directorate (VAAA/AFRL) conducted two subsonic wind tunnel investigations of three advanced configurations: a lambda-shaped, a chevron-shaped, and a diamond-shaped wing planform. In particular, the test program defined the stability and control characteristics associated with these configurations through the applications of trailing edge flaps; the results are found in reference 10.

To extend the database established by Reed, Capt. Won In studied the aerodynamic ground effects associated with the lambda-shaped planform without the application of wing flaps; the results of In's study are found in reference 11. Therefore, in order to assist with the ongoing control challenges imposed with flying near the surface, it is important to analyze and study the inherent aerodynamic behavior that is produced by employing trailing edge flap deflections while flying IGE.

II. Literature Review

Section 1 – Ground Effect Theory

Ever since the early days of flight, aircraft designers have noticed a change in the aerodynamic characteristics of a wing when operating near the surface of the earth. One of the most significant effects first observed was a decrease in the landing speed that was almost immediately attributed to the lift increase generated while flying in-ground-effect (3). It was soon realized that not only was the lift affected but so was the drag. Whereas the lift was increased, the induced drag was decreased, therefore improving the overall efficiency of the wing in terms of the lift-to-drag ratio (2). It was aerodynamic changes such as these that led engineers around the world to investigate the benefits of ground effect (1).

Section 1.1 – Induced Drag

In 1921, Wieselsberger studied the effects of a wing flying near the ground and found that, "the wing resistance diminishes on approaching the ground, while the lift increases somewhat, thereby making the lift-drag ratio more favorable" (12). In order to investigate the incremental change in induced drag (ΔD_i) near the ground, Wieselsberger utilized the principle of reflection whereby the ground surface was replaced by a mirror image of the wing above (1). Based on this theoretical set-up, equation [1] (1) is used to determine the change in induced drag under the assumptions that the wing, of height h, above the surface, generates a lift of L_1, while the reflected image, positioned below the surface at the same height, produces a lift of L_2 (12).

$$\Delta D_i = \frac{\sigma L_1(-L_2)}{\pi q h_1 h_2} \quad [1]$$

where σ is the influence coefficient based on the height-to-span ratio, h/b (12):

$$\sigma = \frac{1 - 0.66(h/b)}{1.05 + 5.7(h/b)} \quad [2]$$

Because the reflected images are symmetric about the ground plane, the distances h_1 and h_2, and the lift values L_1 and L_2, are equal, therefore simplifying equation [1] to the following form (1):

$$\Delta D_i = \frac{-\sigma L^2}{\pi q h^2} \quad [3]$$

Based on equation [3], the total induced drag generated by the wing in-ground-effect, is represented by equation [4] (1). It should be noted that the first term is the induced drag produced out-of-ground effect (13).

$$D_i = \frac{L^2}{\pi q h^2} - \frac{\sigma L^2}{\pi q h^2} = \frac{L^2}{\pi q h^2}(1 - \sigma) \quad [4]$$

In terms of a drag coefficient, equation [5] is derived by dividing equation [3] by the dynamic pressure (q) and the planform area (S) (1):

$$\Delta C_{D_i} = \frac{-\sigma L^2}{\pi q^2 S h^2} = \frac{-\sigma S}{\pi h^2} C_L{}^2 \quad [5]$$

It is apparent from equation [5] that while in ground effect, the reduction of induced drag is directly proportional to the lift squared. Based on equations [1]-[5], the results of Wieselsberger have not only been experimentally verified in the 1930s and 40s, as seen in references 14-16, but have become the standard for predicting the drag effects related to ground proximity (3).

In a similar manner to the approach followed by Wieselsberger, McCormick has also estimated the change in induced drag by utilizing the theory of reflection. McCormick was able to simulate the ground by replacing a rectangular wing with a simple horseshoe vortex that was reflected in such a way that the resulting vertical velocities produced by each image were zero along the plane of reflection (3,13). By applying the Biot-Savart law, McCormick then determined the effect of the ground on the downwash midway between a pair of vortices that led him to develop a relationship between the induced drag experienced in-ground-effect and out-of-ground effect (13):

$$\phi = \frac{C_{D_i}(IGE)}{C_{D_i}(OGE)} = \frac{16(h/b)^2}{1+16(h/b)^2} \qquad [6]$$

Based on McCormick's induced drag factor, one can predict the effect of ground proximity on the total drag of an airplane by multiplying the drag due-to-lift term (kC_L^2) of equation [7] (18) by the induced drag factor, ϕ, in order to correct the OGE k value (31); the final result is seen in equation [8] (31).

$$C_D = C_{D0} + kC_L^2 \qquad [7]$$

$$C_D = C_{D0} + \phi k_{OGE} C_L^2 \qquad [8]$$

Section 1.2 – Lift

It has been proven in many studies (1,3,10-11,16) that as an aircraft approaches the surface within one wingspan, the lift coefficient (C_L) is generally greater than the lift coefficient obtained out-of-ground effect (1). This effect is primarily due to the fact that while in-ground-effect, the magnitude of the overall lift vector is increased as the lift-due-to-drag vector component is decreased; the lift-due-to-drag component is decreased because the strength of the trailing vortices is reduced when they interact with the surface

(16). Equation [9] displays the new C_L that is a combination of the freestream lift ($C_{L\infty}$) and the incremental change experienced in-ground effect ($\Delta C_{L,IGE}$) (1).

$$C_L = C_{L\infty} + \Delta C_{L,IGE} \quad [9]$$

It should be noted that since the value for $\Delta C_{L,IGE}$ is positive, the total lift is greater than when out-of-ground effect (1).

The prediction of the incremental change in lift can be quantified based on the results of Corda, et al. (19) who performed a series of tests on an F-15 to determine the changes in aerodynamic characteristics caused by dynamic ground effects. Based on their results, presented in Figure 1, they fit the following equation to the dynamic data for a wing (3,19):

$$\%\Delta C_{L,IGE} = \left(\frac{0.2}{AR} + 0.4\right) * 100 \quad [10]$$

From this equation, it can be predicted that the lambda UCAV should experience an 11.9% increase in lift due to ground effect.

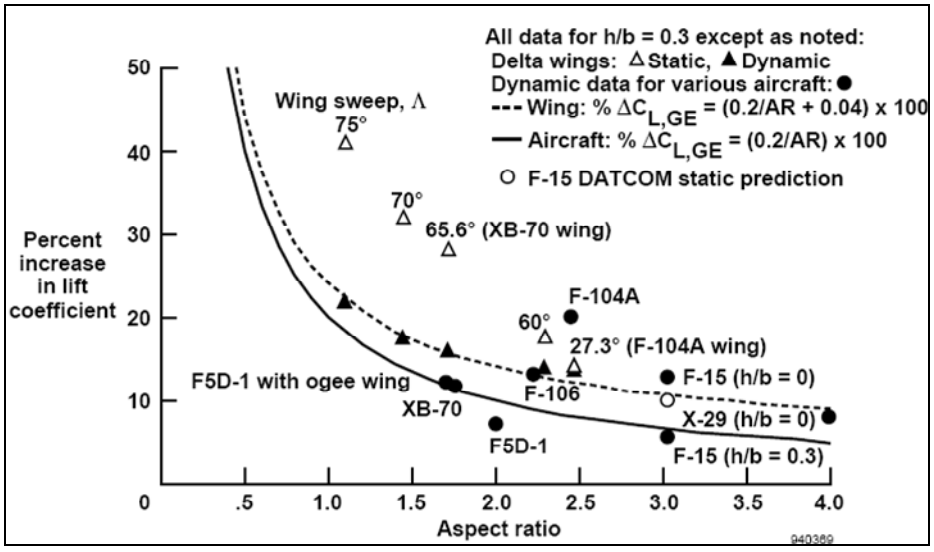

Figure 1: Percent Lift Increase in Ground Effect for Various Aircraft (19)

Section 2 – Boundary Layer Interaction with the Ground Plane

Section 2.1 – Static and Dynamic Ground Effect Tests

Based on the results presented by Jones (3), it was concluded that a static ground effect test for the lambda UCAV would be adequate. Because the lambda UCAV has an aspect ratio comparable to that of the F-15, it is apparent from Figure 2 that the static prediction for the F-15 and therefore the lambda UCAV will produce results similar to that of a dynamic test (3).

In order to simulate a static ground effect test, a conventional approach was followed in this study whereby the aerodynamic forces and moments of a stationary model were measured at various heights above a flat plate (19). Unfortunately, one of the limitations associated with the use of a ground plane in a wind tunnel is the boundary layer that forms across the top surface that if developed enough, can interact with the model. Therefore, it becomes imperative to predict and monitor the boundary layer growth over the ground plane.

Section 2.1 – Boundary Layer Theory

Consider the case of parallel flow over a flat plate. As air passes over the ground plane, the particles in direct contact with the surface are brought to rest due to the no-slip condition. As one travels vertically away from the wall, successive layers of the fluid are retarded as a momentum deficit is diffused from layer to layer through the production of shear stresses between adjacent fluid particles. The result is a relatively thin layer of fluid, known as the boundary layer, that has a velocity slower than the freestream (13). It is customary to define the edge of the boundary layer, and thus its thickness, as the distance where the velocity within the boundary layer is 99% of the freestream velocity

(20). If the Reynolds number is less than 91,000, the point at which instabilities are predicted to first appear (21), the boundary layer is considered to be laminar and the following equations, based on the Blasius solution for a flat plate, are used to estimate the boundary layer thickness (δ) and the displacement thickness (δ^*) (21):

$$\delta_{lam} = \frac{5x}{\sqrt{\mathrm{Re}_x}} \qquad [11]$$

$$\delta_{lam}{}^* = \frac{1.7208x}{\sqrt{\mathrm{Re}_x}} \qquad [12]$$

Beyond the critical Reynolds number of 91,000, disturbances in the boundary layer, due to surface roughness, are no longer damped out and the instabilities begin to amplify. The region that develops is significantly thicker than the laminar one and is characterized by an average velocity profile that is a combination of the instantaneous velocities and the small randomly fluctuating velocity components associated with the growing instabilities (13). This region is known as the transition region, and is rather complicated to quantify theoretically; however, there do exist correlations based on empirical results, such as the two-step method of Granville, that can estimate the final onset of fully turbulent flow (21). Based on the turbulent boundary layer integral-momentum equations derived by Kármán in 1921, it was suggested by Prandtl that a simple one-seventh power law would suffice in the derivation of the following boundary layer equations for turbulent flow over a flat plate (21):

$$\delta_{turb} \approx \frac{0.16x}{\mathrm{Re}_x{}^{\frac{1}{7}}} \qquad [13]$$

$$\delta_{turb}{}^* = \int_0^{\delta} (1 - \frac{u}{u_e}) dy \qquad [14]$$

One must note that equations [13] and [14] assume that $\delta = 0$ at $x = 0$.

In this study, the lambda model was tested at four different speeds, 40, 60, 80, and 100 mph. At the higher speeds, the Reynolds numbers are larger, therefore implying that the onset of turbulence will occur at a location closer to the front of the ground plane. Because of this, the model, at the closest ground plane setting (h/b =0.05), might interact with the boundary layer. Therefore, based on the above equations, and assuming a linear relation for the transition region, a first approximation of the boundary layer growth over the ground plane can be seen in Figure 2 for standard atmospheric conditions. The boundary layer is only presented for a freestream velocity of 100 mph because it is assumed that at this test condition, the turbulent region of the boundary layer will be the most developed.

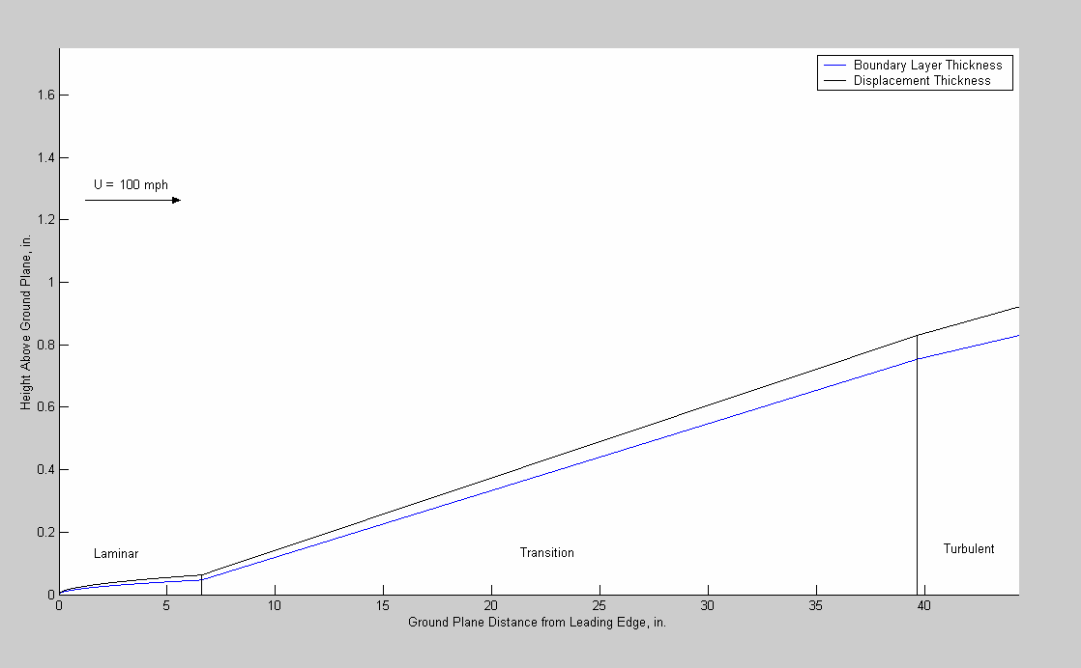

Figure 2: Theoretical Boundary Layer Analysis of the Ground Plane

For a preliminary analysis, measurements were made from the leading edge of the ground plane to the nose (x_{nose}) and trailing edge ($x_{t.e.}$) of the lambda model. Because the closest ground plane setting is assumed to be the limiting case for boundary layer interactions with the model, vertical heights corresponding to the nose (z_{nose}) and trailing edge ($z_{t.e.}$) locations were measured for the range of angle of attacks tested. Table 1 lists the model measurements and the predicted boundary layer thicknesses, as seen in Figure 2, for the specified locations along the ground plane. Based on these results, it can be assumed that the model should not interact with the boundary layer in the limiting test case (U = 100 mph, h/b = 0.05) and therefore the other combinations of test conditions.

Table 1: Preliminary Boundary Layer Analysis for h/b = 0.05

	$\alpha = -4^o$	**$\alpha = 0^o$**	**$\alpha = +13^o$**
x_{nose}	16.63”	16.63”	16.63”
z_{nose}	0.56”	1.31”	3.75”
δ_{nose}	0.26”	0.26”	0.26”
δ^*_{nose}	0.29”	0.29”	0.29”
$x_{t.e}$	27.38”	27.38”	27.38”
$z_{t.e}$	1.0”	1.0”	1.0”
$\delta_{t.e.}$	0.5”	0.5”	0.5”
$\delta^*_{t.e.}$	0.54”	0.54”	0.54”

Section 2.3 – Boundary Layer Removal

Even though a preliminary analysis shows that the boundary layer should not interact with the lambda model, varying test conditions and the presence of freestream turbulence within the wind tunnel might cause a boundary layer interference. If such a case existed, one method of boundary layer removal could be achieved through the application of a moving-belt ground plane. The basic premise of a moving-belt ground plane is that if the belt were to spin at the same speed of the freestream, but in the

opposite direction, the resultant velocity over the surface will be zero; this in turn would better simulate an aircraft flying over the surface (3).

While the removal of the boundary layer seems essential to achieve accurate flight dynamics, two independent studies conducted by Kemmerly and Paulson, Jr. (22) and Turner (23) showed when an endless-belt ground plane would be required as opposed to a conventional ground plane for ground effect wind tunnel testing (3). Kemmerly and Paulson, Jr. concluded that the application of a moving belt ground plane would only be necessary in the study of ground effect if the condition in equation [15] was satisfied whereas Turner concluded that the use of a moving belt ground plane was dependent on $C_{L_{MAX}}$ and the height above the ground.

$$\frac{(h/b)}{C_L} < 0.05 \qquad [15]$$

Based on the above criteria established by Kemmerly and Paulson, Jr. and Turner, and the maximum C_L achieved in Reed's study (10) for the lambda UCAV in a $+20^o$ flap configuration, Figure 3 and Table 2 were generated for the test conditions of this experiment. It is apparent from Figure 4 and Table 2 that for a $C_{L_{MAX}}$ of 0.867 and the range of height-to-span ratios that were tested in previous ground effect studies (see reference 3 and 11), that the use of an endless-belt moving ground plane should not be required for this experiment.

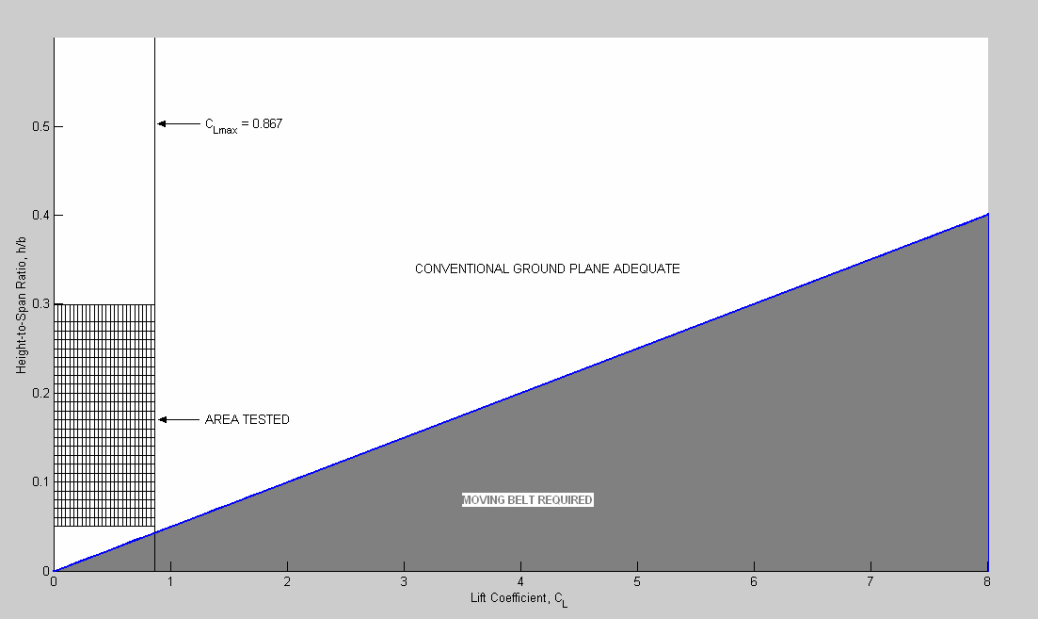

Figure 3: Requirements for the Application of an Endless-Belt Moving Ground Plane (22)

Table 2: Conventional Ground Plane Justification

h/b	C_{Lmax}*	(h/b)/C_{Lmax}
0.3	0.867	0.35
0.15	0.867	0.17
0.1	0.867	0.12
0.05	0.867	0.06
* denotes Reed's data		

Section 3 – Adverse Ground Effect

While many studies substantiate the fact that lift is increased and drag is decreased while flying in-ground effect, not all aircraft experience these benefits (3). One such study was conducted by Lee et al. (24) who performed static and dynamic ground effect tests on a 60^o delta wing and models of an F-106B and XB-70 aircraft in a 36 in. x 51 in. wind tunnel; tests were made with and without flap deflections and a Reynolds number range of $3x10^5$ to $7.5x10^5$. A sample of their drag coefficient (C_D) data for the F-106 is presented in Figure 4; the results indicate an average 12% increase in C_D at the

positive angles of attack while IGE with various flap deflections. Similar trends were also seen in the C_D results obtained for the XB-70 (24).

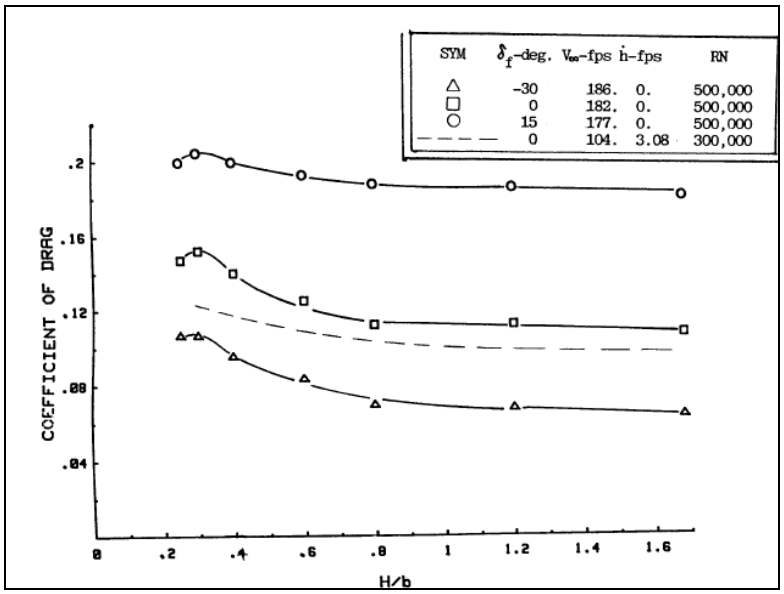

Figure 4: Adverse Ground Effect for the F-106, AOA = 14^o (24)

Even though Lee et al. did not focus on the adverse drag effects, it was concluded by Jones (3) that a possible explanation for this phenomenon was the aspect ratios and wing sweep angles of the models tested; the F-106, XB-70, and the 60^o delta wing had the following aspect ratios: 2.4, 1.78, and 2.3, respectively. The F-106 had a wing sweep of 60^o whereas the XB-70 had a wing sweep of 65^o. Just as these models had similar characteristics as the chevron UCAV tested by Jones, so to were they similar to the lambda UCAV studied in this experiment.

Similarly, the lambda model used in this experiment was previously tested by In (11). He tested the model, with zero flap deflections, in-ground effect and out-of-ground effect in the AFIT 3' x 3' wind tunnel at speeds of 40, 60, 80 and 100 mph. His results showed that the model experienced an increase in lift and drag while in-ground effect. A

plot of the C_D vs. (h/b) for the lambda UCAV, with zero flap deflections, is shown in Figure 5. Based on In's data, the lambda UCAV is expected to experience an average 11% increase in C_D while flying IGE.

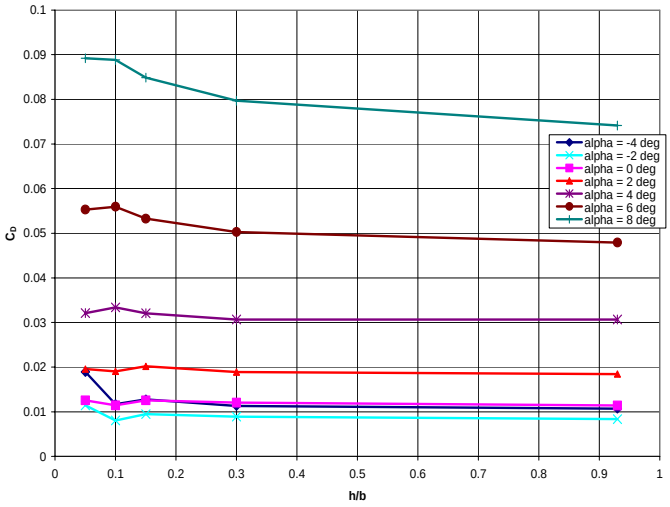

Figure 5: Adverse Ground Effect for the Lambda UCAV (11)

Additionally, Cury and Owens (25) noted that the Tu-144 also experienced an increase in the total drag when the aircraft flew close to the ground (3).

Section 4 – Experimental Objectives

To extend the database established by Reed (10) and In (11), a ground effect analysis will further the investigation of the aerodynamics of an advanced UCAV configuration. Since almost every present-day aircraft is equipped with high-lift devices, it is of particular importance to study the inherent aerodynamic behavior that is produced by employing trailing edge flap deflections while flying IGE.

The goals of this study are to:

1. Expand the current aerodynamic database for moderately swept, low aspect ratio, tailless, blended body UCAVs by testing the lambda configuration in ground effect with flaps added to the midboard and outboard trailing edges.

2. Compare and validate aerodynamic out-of-ground effect parameters with experimental results obtained from the research of Reed (10) and In (11).

3. Compare wind tunnel results to theoretical data obtained from a VORLAX panel code.

4. Analyze the boundary layer over the ground plane.

5. Verify McCormick's induced drag factor (13) for an aircraft with flap deflections.

6. Determine the flow characteristics of the lambda UCAV by means of a flow visualization technique (tufts).

The following chapters will include a detailed description of the experimental apparatus and procedures, analysis of the results, concluding remarks and recommendations.

III. Experimental Equipment

This chapter describes the equipment that was used to collect and analyze the wind tunnel data associated with the longitudinal and lateral stability of the lambda UCAV IGE and OGE.

Section 1 – UCAV Model

The model used in this study was based on a wing planform originally tested in the Boeing St. Louis Low Speed Wind Tunnel (LSWT) and the AFRL Subsonic Aerodynamic Research Laboratory (SARL) by Reed (10). The original lambda-shaped model (shown in Figure 6) was designed and built by Dynamic Engineering, Inc. Table 3 lists the dimensions and specifications of the original model and of the scaled model used in this experiment.

Figure 6: Original Scale Lambda UCAV

Table 3: Model Specifications of the Original and Scaled Lambda-Shaped UCAV

	Original Model	Scaled Model
Material	Ren 450 & Aluminum	Photopolymer Plastic
Wing Area, in^2	366.91	78.31
Span, in	32.00	14.62
MAC, in	14.46	6.36
Root Chord, in	22.79	10.55
Tip Cord, in	0.00	0.00
Aspect Ratio	2.791	2.729
Leading-Edge Sweep, deg	50.00	50.0
Trailing-Edge Sweep, deg	50/-30	50/-30
Dihedral, deg	0.00	0.00

The original lambda model has a wingspan of 32 in. and would just fit, with minimal clearance, in the AFIT 3' x 3' wind tunnel. Therefore, in order to avoid flow interference with the test section walls, a ½-scaled lambda model was manufactured with the AFIT/ENY 3-D rapid prototype machine; for a comprehensive explanation of the machining process refer to reference 3.

The ½-scaled lambda model was originally tested in the AFIT 3' x 3' subsonic wind tunnel by In (11), and because the ground effect results were only based on a clean aerodynamic configuration, with zero flap deflections, removable aluminum flap pieces were designed and manufactured for this study. It should be noted that the original model tested by Reed (10) utilized a plain flap configuration that was machined into the model and could be manually adjusted. Because the trailing edge of the ½-scaled lambda model, used in this experiment, was extremely thin, the model could not be machined for an adjustable plain flap installation; therefore, a removable split flap configuration was selected as an alternate design choice.

Based on the dimensions shown in Appendix H, two sets of midboard and outboard flap pieces were machined in order to simulate a $+10^o$ and $+20^o$ deflection

angle. The flap pieces were fixed to the model with Loctite 608 Hysol Epoxy Adhesive. Figure 7 illustrates the positive flap convention used in this experiment and the lambda UCAV positioned over the closest ground plane (h/b = 0.05). Table 4 lists the nominal dimensions and properties of the original plain flaps utilized by Reed (10) and of the split flaps used in this experiment. Additional pictures of the lambda model are given in Appendix A.

Figure 7: Four Views of the ½ - Scaled Lambda Model OGE and IGE (h/b = 0.05) with Mid/Outboard Trailing Edge Split Flap Deflections

Table 4: Trailing Edge Flap Specifications for the Original and Scaled Lambda UCAV

	Original Model	Scaled Model
Midbaord		
Material	Ren 450	Aluminum
Area (per side), in^2	7.22	4.313
Span (per side), in	4.52	2.875
Chord, in	2.38	1.50
Outboard		
Material	Ren 450	Aluminum
Area (per side), in^2	8.97	0.875
Span (per side), in	6.10	1.75
Chord, in	1.75	0.50

Section 2 – Ground Representation

As was established in chapter 2, section 2.1, a variable height ground plane will be sufficient for the study of ground effect. Therefore, to properly simulate an aircraft flying in close proximity to the ground, a flat plate was mounted to the base of the wind tunnel. The ground plane assembly consists of two flat plates and four sets of eight removable cylindrical legs; each set of legs was dimensioned in accordance with the height-to-span (h/b) ratios that were tested. Table 5 lists the dimensions and specifications of the ground plane assembly (3).

Table 5: Dimensions and Specifications of the Ground Plane Assembly (3)

Plate		
	material	hot-rolled steel
	max length, in	44.313
	width/diameter, in	35.313
	thickness, in	0.25
Mounting Legs		
	material	cold-rolled steel
	diameter, in	1.50
	length, in	
	h/b = 0.3	9.77
	h/b = 0.15	12.17
	h/b = 0.10	12.97
	h/b = 0.05	13.77

In order to accommodate rotation about the yaw axis, the ground plane was designed and built in two sections. Figure 8 and the ground plane blueprints, Appendix B, clearly illustrate the geometries of the flat plates. To properly simulate yaw, the ground plane must be placed in the test section such that the ground plane circular plate is located directly above and mounted to the circular plate located at the base of the test section; in doing so, the ground plane circular plate is free to rotate with the model through various angles of yaw.

Figure 8: Top and Separated View of the Removable Ground Plane (3)

Section 3 – Wind Tunnel

The AFIT 3'x3' subsonic wind tunnel, built by the New York Blower Company, was used for this experiment. The tunnel is equipped with an ACF/PLR Class IV fan and a Toshiba Premium Efficiency (EQP III) fan motor that are both controlled by a Siemens (13710) Adjustable Frequency Tunnel Controller. Table 6 lists the basic specifications of the fan motor and controller.

Table 6: Operating Specifications of the Toshiba Premium Efficiency Fan Motor and the Siemens Adjustable Frequency Tunnel Controller

Controller	Motor
	3 phase induction
	1785 RPM operating speed
	Maximum theoretical speed – 150 mph
	Maximum tested speed – 148 mph
250 max HP	200 brake horsepower
460 volts	230/460 volts
315 amps	444/222 amps
	60 Hz
	4 poles

The tunnel is an Eiffel-type, open circuit configuration with a closed test section. The fan is located at the end of the tunnel and sucks ambient air in from the room through

a 122”w x 111”h x 70”l intake plenum. In order to assure that well-defined laminar streamlines pass through the test section, the plenum is constructed with four steel, mesh anti-turbulence screens and a ¼ in. aluminum honeycomb flow-straightener that has a minimum aspect ratio of 15. After the flow passes through the screens, it travels to the test section through a 95.5 in. long convergent duct that has a contraction ratio of 9:5:1. The height of the tunnel at the beginning of the test section is 31.5 in. Figure 9 displays the dimensions of the wind tunnel intake and convergent channel.

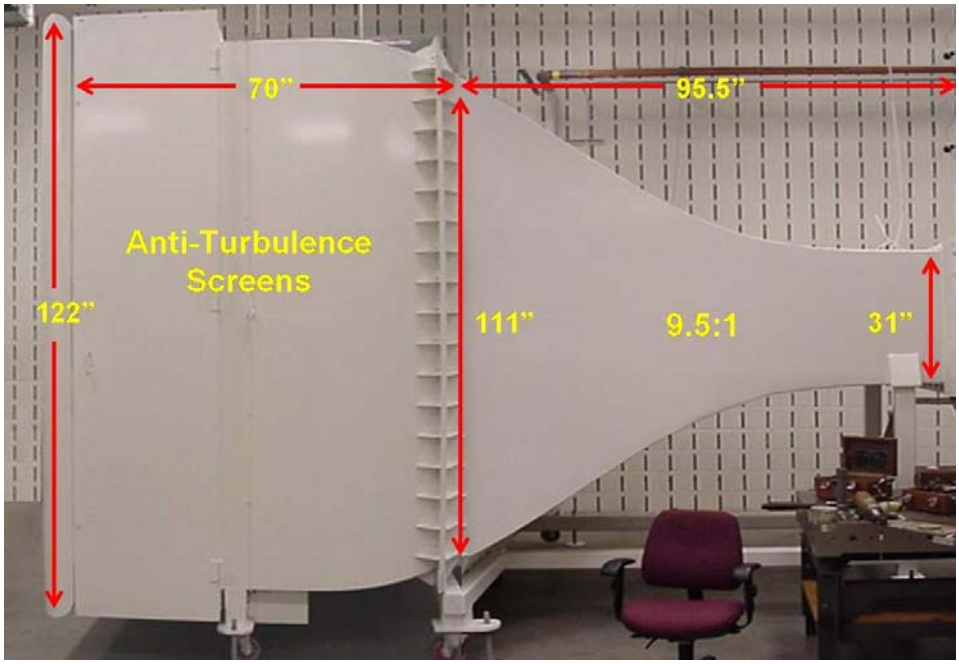

Figure 9: Dimensions of the Wind Tunnel Intake and Convergent Section (3)

The test section is 31”h x 44”w x 72”l and is geometrically shaped like an octagon to eliminate the effects of corner interference. The test section is accessible through gas-actuated Plexiglas doors that are located on both sides of the chamber. In addition, as seen in Figure 10, the test section can accommodate a traversing hot-wire anemometer by means of six, removable Plexiglas panels that are located directly above the test section.

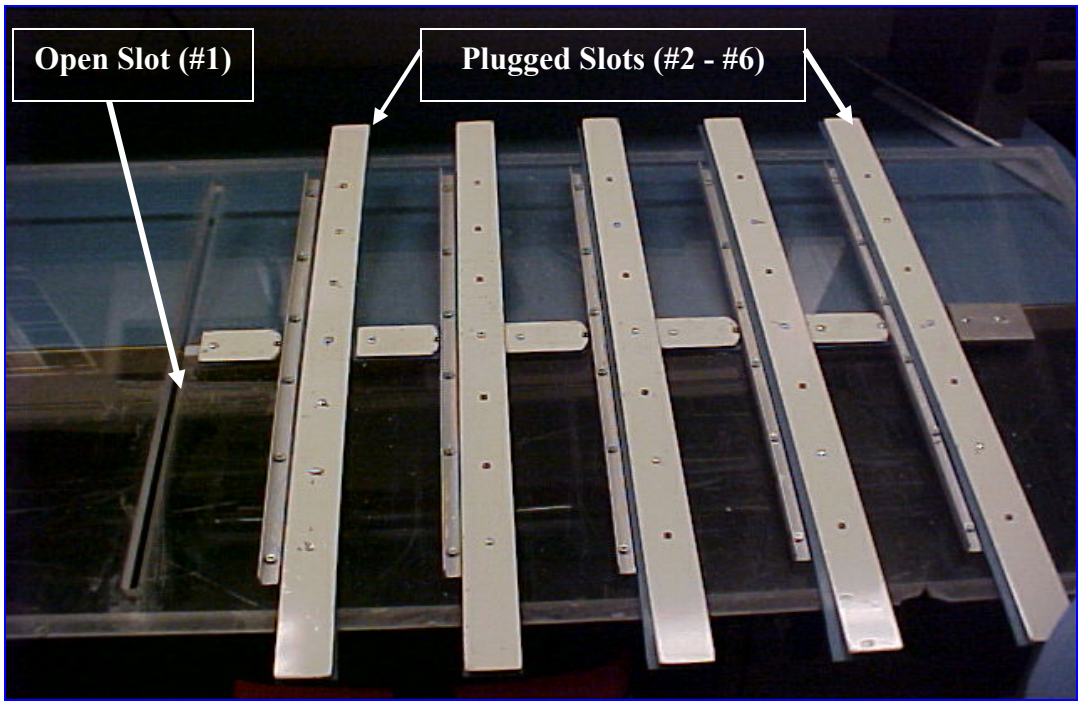

Figure 10: Hot-wire Probe Access Panels (3)

Within the test section, a model sting support is mounted to the test section floor, through a slot in the circular traverse plate. The sting mechanism is remotely controlled allowing the model angle of attack to vary from -25^{o} to +25^{o}. In order to test various angles of yaw, the sting support is automatically rotated with the circular traverse plate as it sweeps the model through a yaw range of -20^{o} to +20^{o}.

Beyond the test section, the air flows downstream through the 26 ft. divergent section, and leaves the tunnel through the vertical exhaust pipe. In case of model failure, a safety fence, located within the divergent section, prevents debris from damaging the fan and motor. Figure 11 displays the various components of the AFIT 3' x 3' wind tunnel.

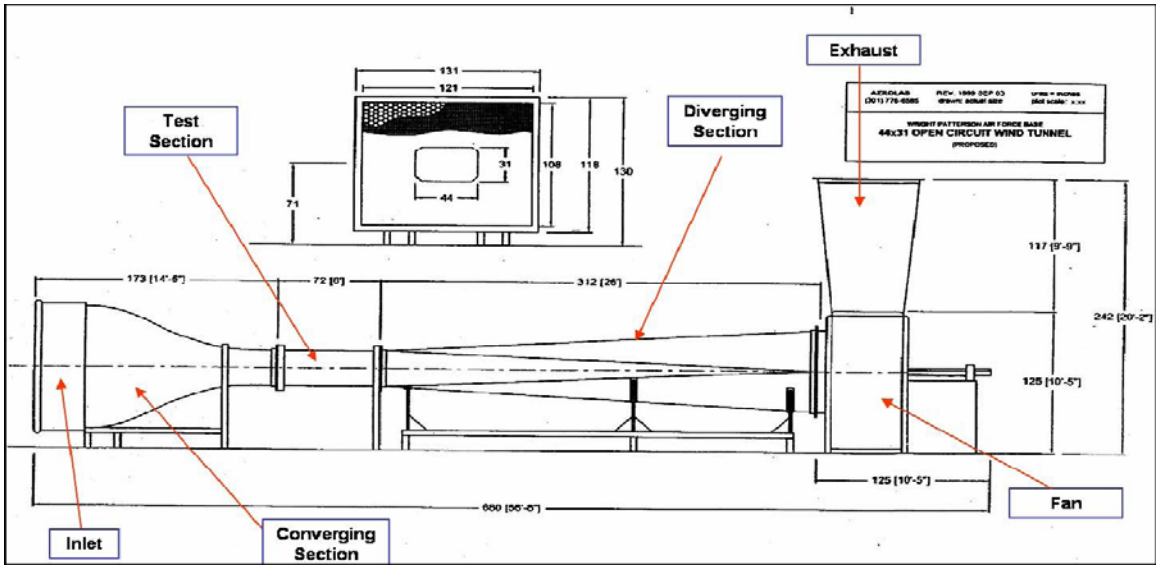

Figure 11: AFIT 3'x3' Wind Tunnel Schematic (3)

Section 4 – Strain Gage Balance

The aerodynamic forces and moments exerted on the lambda UCAV were measured in the AFIT wind tunnel via a 100 lb, six component, internal strain gage balance manufactured by the Able Corporation. The balance used for this test was a 0.50 Mk V series capable of the loads listed in Table 7**.** The six components of the balance consist of two normal force elements for the measurement of a normal force and pitching moment, two side force elements for a side force and yawing moment, and a dual axial force component for the determination of a dual roll element. The balance was accurate in all gauges to at least $\pm$ 0.25% of the maximum applied load.

Before acquiring data, the balance was manually calibrated by the wind tunnel technician. For this process, the calibration constants were manually adjusted in the data collection software as known weights were added to the balance and matched to the associated loads registered in the program. The key to proper calibration was to ensure

that the voltages measured in each balance component related linearly to the increase of added weights (3).

Table 7: Maximum Loads of the AFIT 100 lb Balance

Directional Component	Maximum Load
Normal Force (N1)	100 lbs
Pitch Moment (N2)	100 in-lbs
Side Force (S1)	50 lbs
Yaw Moment (S2)	50 in-lbs
Axial Force (A1)	50 lbs
Roll Moment (L1)	40 in-lbs

Section 5 – Dantec Hot-wire Anemometer

The AFIT 3' x 3' subsonic wind tunnel is equipped with a Streamline 90N10 Constant Temperature Anemometer by Dantec Dynamics. The anemometer used in this experiment was a tri-axial probe that measured velocities in each of the three coordinate axes and was mounted in the tunnel test section by means of a vertical attachment that was connected to a fully motorized, programmable, 3-axis traversing mechanism. Based on the test section geometry, the maximum range of the probe in both the y- and z-directions is 19.7 in. whereas the maximum range in the longitudinal x-direction is about 3 ft. Figure 12 illustrates the wind tunnel coordinate axes; for clarification, the +y axis extends to the right as one looks in the –x direction. A data acquisition program called Streamware, designed specifically for the hot-wire, collects, processes and formats the data.

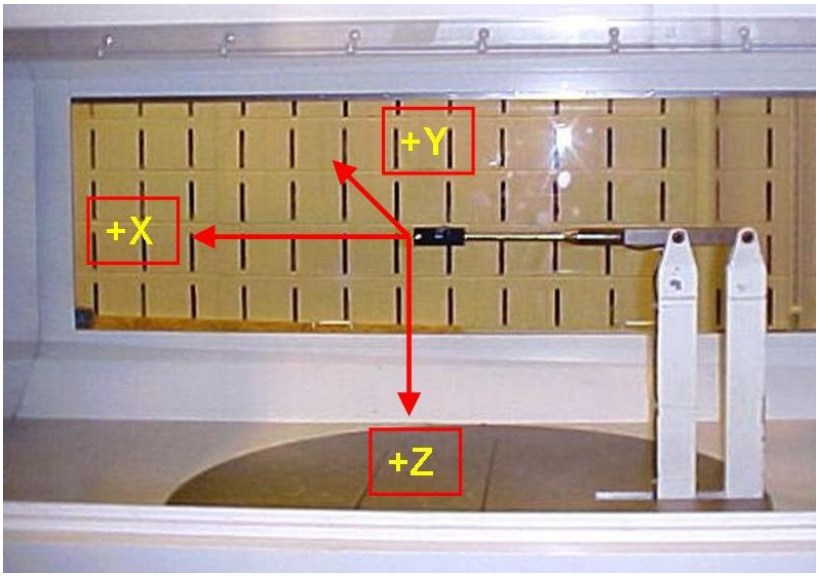

Figure 12: Wind Tunnel Coordinates (3)

IV. Experimental Procedures

The following section describes the procedures and methodologies that were associated with the wind tunnel data collection process followed in this experiment.

Section 1 – Hot-wire Anemometer

A Dantec hot-wire anemometer was used in this experiment to: determine the velocity differences between the pressure transducer and those measured at the model, calculate the solid blockage corrections associated with ground plane interference, and study the boundary layer growth over the ground plane.

Section 1.1 – Hot-wire Calibration

The tri-axial hot-wire was calibrated outside of the tunnel by using the Dantec automatic calibrator. To calibrate the wire that measures velocities in the x-direction, the automatic calibrator, with an attaching nozzle, blew air over the single wire within the calibration velocity range of 4.5 to 161 mph. To calibrate the remaining two wires, the probe axis (x-direction) was tilted 30^{o} with respect to the flow and rotated 360^{o}, in 15^{o} steps, while the remaining wires were exposed to the mid-calibration velocity of 80.5 mph. As the known velocities increased, or as the probe was rotated 360^{o}, the anemometer measured the voltages required to maintain a constant temperature throughout the three wires. Throughout the calibration process, the Streamware acquisition program automatically created the appropriate conversion factors required to convert the recorded voltages to metric-based velocities (3).

Section 1.2 – Blockage Corrections

As the air flow travels downstream through the test section, the freestream velocity does not remain constant. Because the cross-sectional area of the test section increases in the negative x-direction (see Figure 12), the freestream velocity decreases in order to satisfy continuity. As a result, the velocity measured by the upstream transducer is greater than the velocity at the model. Because the data files of a given test only contain the velocities measured by the transducer, the MATLAB data reduction code would output results based on the velocities measured upstream at the transducer and not the actual velocities at the model.

In a similar manner, the ground planes also affect the flow around the model. In this case, the ground planes decrease the cross-sectional area of the test section and consequently increase the freestream velocity at the model. To account for this difference, solid blockage correction factors are determined by comparing the velocities measured by the hot-wire in the open tunnel configuration to the velocities measured with the hot-wire above the ground planes. The following experiments were set up to account for these errors.

For the solid blockage and velocity correction measurements, the hot-wire probe was positioned in the tunnel test section through the #6, removable, top Plexiglas panel; the remaining slots were plugged according to the longitudinal station of interest. As shown in Figure 13**,** the centerline of the hot-wire probe was positioned 2 in. above the centerline and 4 ¾ in. in front of the balance support. The hot-wire recorded the velocities at this location in an open tunnel configuration (without the ground planes), and then with each ground plane in the test section at speeds of 40, 60, 80, and 100 mph.

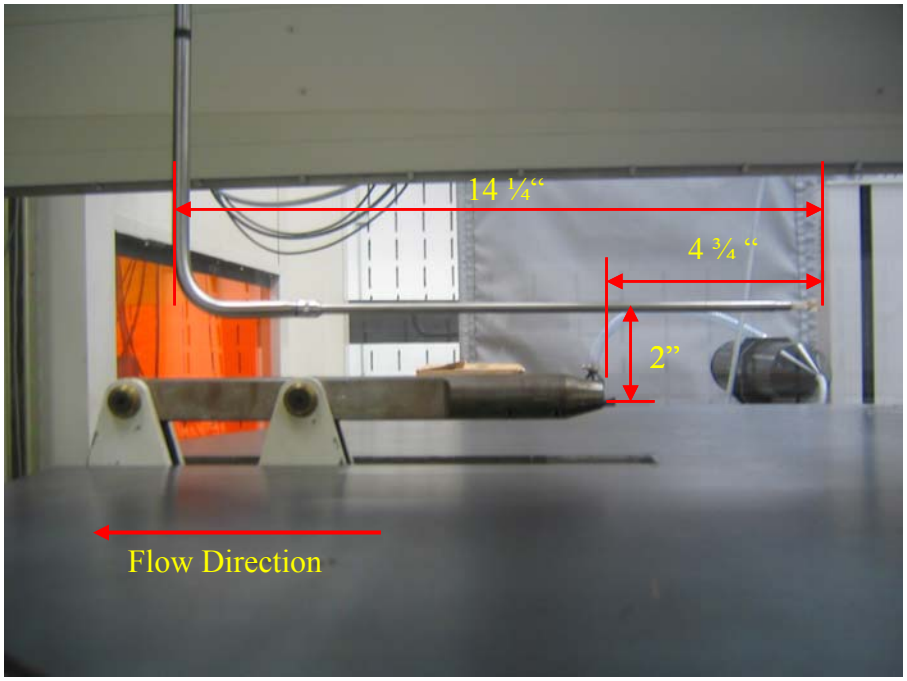

Figure 13: Hot-wire Location for Blockage Measurements

The hot-wire started measuring freestream velocities, at 1 kHz, directly above the sting support and continued to record data as the probe was automatically translated, in 0.1 mm increments, in the negative z- and y- directions. Based on this test pattern, the hot-wire measured velocities within a 1.0 mm^2 plane offset to the right of the sting support, as seen from the positive x-direction. Figure 14 illustrates the path followed by the hot-wire. It should be noted that the hot-wire control software is based on SI units.

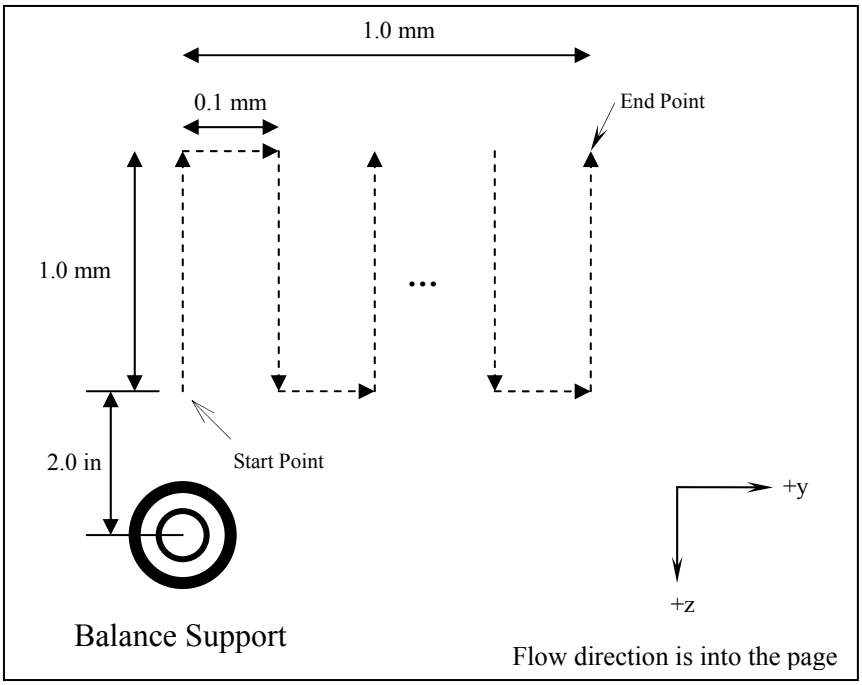

Figure 14: Hot-wire Test Grid for Blockage Measurements

For the boundary layer measurements a similar approach was followed, except in this case the hot-wire only measured data in the negative z-direction while remaining fixed in the other two coordinate axes. For a given ground plane height, the x-position, as measured from the leading edge of the plate, was fixed according to the top Plexiglas panel the hot-wire probe was installed through. Table 8 lists the Plexiglas panels and the corresponding x-locations along the ground plane that were tested in this boundary layer analysis. It should be noted that in order to position the hot-wire probe within the boundary layer, it was offset 1 ¼ in. in the negative y-direction to avoid interference with the balance support. Figure 15 displays the nominal test grid used to analyze the boundary layer at each x-location. Based on this grid pattern, the hot-wire measured velocities in the negative z-direction, from ½ in. to 3 ¼ in. above the ground plane, in 0.197 in.(5 mm) increments. The boundary layer was only measured over the closest ground plane (h/b = 0.05) for two reasons: at this height, the model is most susceptible to

the adverse effects of the boundary layer because it is the closest to the plate as compared to the other heights; and the physical limitations of the mechanical traverse placed the hot-wire in such a position over the plate that it was not able to measure the velocities within the boundary layer.

Table 8: Hot-wire Position Along Ground Plane

Plexiglas Panel #	Distance from Plate Leading Edge, in
1	2.75
2	12.75
3	27.625

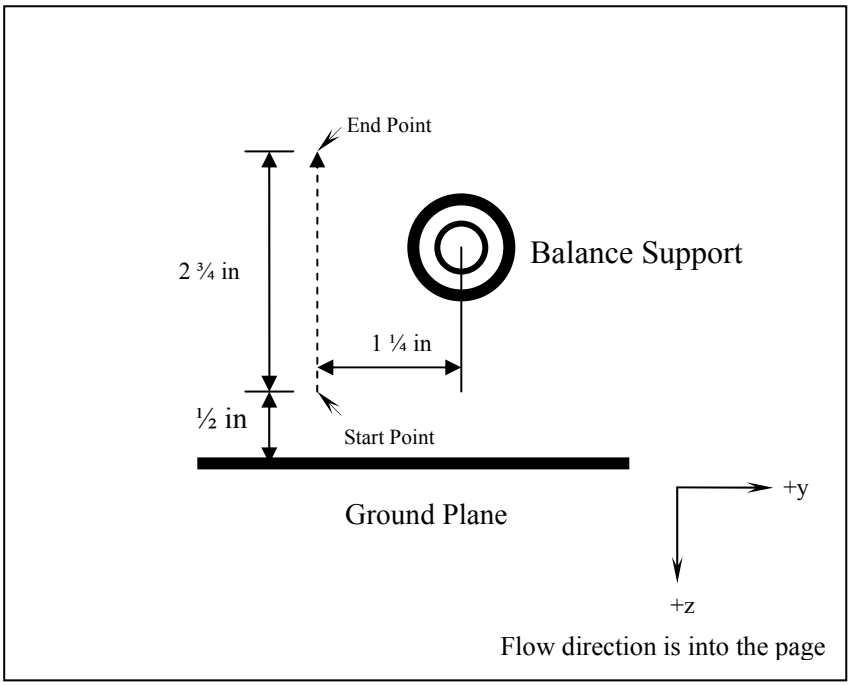

Figure 15: Hot-wire Test Grid for Boundary Layer Measurements

The Dantec Streamware software originally saved the recorded measurements in raw form, as voltage outputs. These values were later converted to physical velocity measurements at each point within the program. It should be noted that the hot-wire text files include the following data sets for each measurement location: the x,y,z coordinates

(see Figure 12) of the probe (as referenced to the start position), and the mean and root mean squared velocities, in metric units, for each direction of motion.

Section 2 – Data Acquisition

After the balance was calibrated and placed in the wind tunnel test section via the sting mechanism, the lambda UCAV was fixed to the balance along the longitudinal x-axis of the model. Because the static weight of the model inherently applied a load to the axial sensor of the balance, a wind-off or tare run was performed each time the model was removed from the balance. During the dynamic tests, a computer equipped with a LabView Virtual Instrument interface was used to control the angle of attack, yaw angle, and tunnel speed. In addition, the following analog backup instruments were used to monitor the performance of the LabView interface: sting mounted optical encoders for the angle of attack and sideslip; and a pressure transducer and pitot-static tube for the velocity.

For this experiment the lambda UCAV was tested OGE and IGE with symmetric and asymmetric split flap configurations; symmetric deflections refer to midboard and outboard flap extensions on both the left and right side of the model whereas asymmetric deflections refer only to midboard and outboard extensions on the right wing of the model. In this study, the following flap deflections were tested in a symmetric and asymmetric configuration: $\delta_{mid/out} = 0^o$ (no flaps), $+10^o$, and $+20^o$; it should be noted that the zero deflection configuration corresponds to the lambda model without flaps attached to the trailing edge. The OGE and IGE tests were performed to analyze flap effectiveness in terms of the longitudinal forces and moments exerted on the model in an open tunnel

and with the addition of the ground planes placed at four different heights. Table 9 lists the test matrix that was applied to the lambda UCAV for each flap configuration.

Table 9: Experimental Test Matrix

Tunnel Speed (mph)	OGE Model only	Plane 1 h/b = 0.3	Plane 2 h/b = 0.15	Plane 3 h/b = 0.10	Plane 4 h/b = 0.05
40	-10<α<+20	-10<α<+20	-10<α<+20	-10<α<+20	-4<α<+13
60	-10<α<+20	-10<α<+20	-10<α<+20	-9<α<+20	-4<α<+13
80	-10<α<+20	-10<α<+20	-10<α<+20	-8<α<+20	-4<α<+13
100	-10<α<+20	-10<α<+20	-10<α<+20	-8<α<+20	-4<α<+13

Table 9 shows that the ranges of tested angles of attack were limited with planes 3 and 4. This was necessary for two reasons: first, because the model would vibrate more intensely at the higher tunnel speeds, the UCAV would consequently collide with the ground plane; in a similar manner, at the highest ground plane setting (plane 4), the sting mechanism would also collide with the ground plane at angles greater than $+13^{o}$.

The forces and moments measured by the balance were recorded at a 2 Hz sampling rate by the data acquisition program within the control computer. The measured data from the balance was stored in the form of two normal force components, N_1 and N_2, two side force components, S_1 and S_2, an axial force component, A_1, and a roll moment, l_1 (3). As the flow velocity of the tunnel was slowly increased to the desired test speed, the balance was monitored for any data acquisition anomalies. After ensuring that the balance was accurately measuring the applied loads, the model was pitched through the various angles of attack while data was recorded for 10 sec for each angle. It should be noted that the angle of attack was increased in 2^{o} increments between -10^{o} and $+10^{o}$ and 1^{o} increments between $+10^{o}$ and $+20^{o}$; because the angle of attack range was limited for plane 4, 1^{o} increments were used that particular test. This process was repeated until the model or sting mechanism collided with the ground plane.

Section 3 – Data Reduction

The force and moment data acquired for a given test was reduced with a MATLAB code originally written by DeLuca (26) and Gebbie (27)**,** and later altered by In (11) for use with the 100 lb balance. The program simultaneously loaded a tare file and test file and then averaged the measured forces and moments to a single test point for each angle of attack. For convenience, the MATALB code generated an Excel output file that was used to produce the standard aerodynamic plots presented in this report. The following flight parameters were listed in the Excel output files for the range of angles tested: Mach number, Reynolds number, dynamic pressure (lb_f/ft^2), velocity (mph), corrected angle of attack, lift, drag, and side force coefficients, and roll, pitch, and yaw moment coefficients. Appendix C presents a sample calculation that corresponds to the algorithm applied in the MATLAB reduction code. For more detail regarding the MATLAB program refer to references (9) and (26).

V. Results & Analysis

This chapter presents the data acquired from the wind tunnel tests for the lambda UCAV. The results of the hot-wire anemometer experiments for the wind tunnel blockage effects will be presented first followed by the out-of-ground-effect and in-ground-effect results, the flow visualization, and the ground plane boundary layer analysis.

Section 1 – Hot-wire Anemometer & Wind Tunnel Blockage Corrections

As the air flows through the tunnel test section, the freestream velocity decreases as the cross-sectional area of the test section increases. As a result, the velocity measured by the upstream transducer is greater than the velocity at the model. Because the data files saved by the wind tunnel computer only contain the velocities measured by the transducer, the MATLAB data reduction code would output results based on the velocities measured upstream at the transducer and not the actual velocities at the model. To account for this difference, a hot-wire was used to compare the velocities at the model, in an open-tunnel (no ground plane) test configuration, to the velocities measured by the upstream pressure transducer. The results for each test speed are presented in Figure 16.

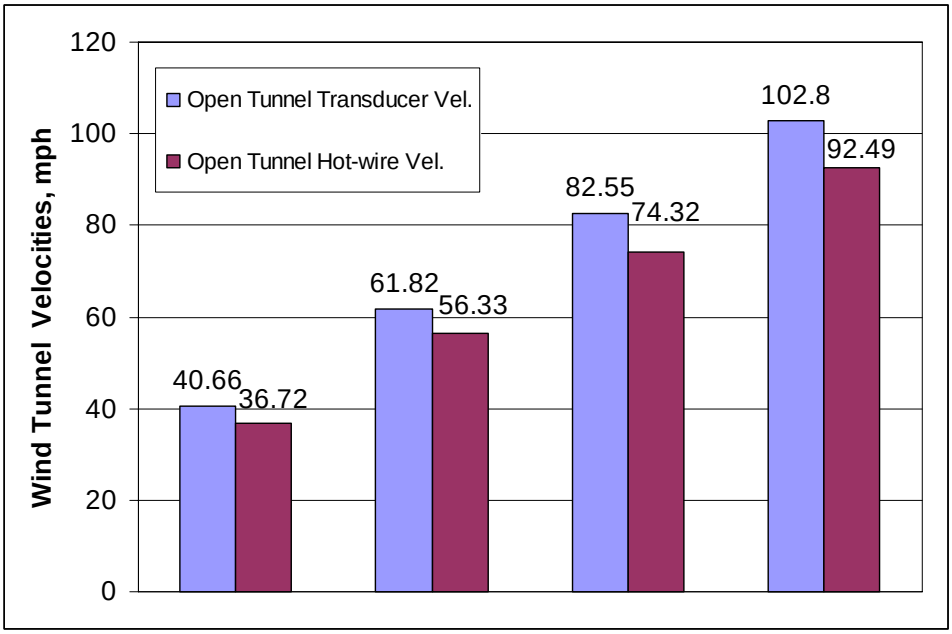

Figure 16: Wind Tunnel Velocity Differences Between the Hot-wire and Pressure Transducer

Based on Figure 16, it is apparent that the freestream velocity does not remain constant throughout the test section. For each test speed, the velocities measured by the hot-wire, at the location of the model, are approximately 10% less than those measured by the upstream pressure transducer; a similar percentage difference was reported by Jones (3) in his ground-effect study. The velocity differences were then accounted for in the MATLAB data reduction code in the form of blockage correction factors based on the following equation (28):

$$\varepsilon_{tc} = \frac{U_{OT}}{U_{Tr}} \qquad [15]$$

In a similar manner, the presence of the ground planes also affected the flow through the tunnel. With an enclosed test section, the tunnel cross-sectional area is decreased by the addition of the ground planes and model. As a result, the air velocity increases in the vicinity of the UCAV. To account for this difference, and to make the

results as accurate as possible, additional solid blockage correction factors were determined by comparing the velocities measured by the hot-wire in the open tunnel configuration to the velocities measured with the hot-wire above each ground plane. The results are presented in Figure 17. It should be noted that because the measured hot-wire velocities for a given test speed were within 1%-2% of each other, the values shown in Figure 17 are the averaged velocities for all four ground plane heights tested. It is apparent from the figure that the freestream velocities increased within the tunnel test section due to the presence of the ground planes.

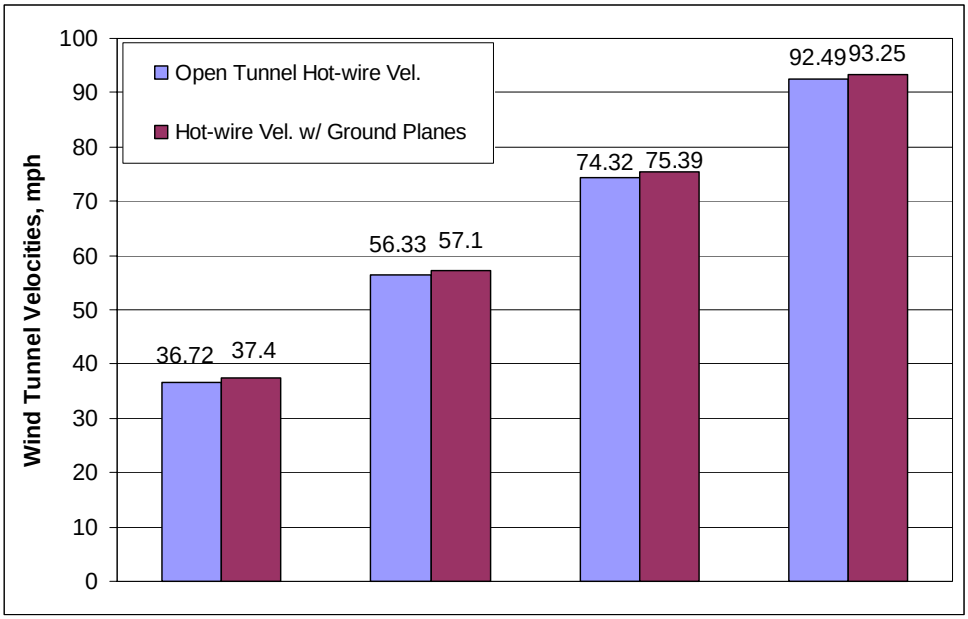

Figure 17: Hot-wire Velocity Comparison

Equation [16] was used to calculate the solid blockage correction factors that were associated with the ground plane interference.

$$\varepsilon_{GP} = \frac{U_{GP}}{U_{OT}} \qquad [16]$$

Table 10 summarizes both the velocity and solid blockage correction factors that were applied to the MATLAB data reduction code for this experiment.

Table 10: Correction Factors Used to Adjust Velocity for Wind Tunnel Blockage

Correction Factors	40 mph	60 mph	80 mph	100 mph
ε_{tc}	0.903	0.911	0.900	0.8997
ε_{GP}				
Plane 1, h/b = 0.3	1.026	1.015	1.016	1.011
Plane 2, h/b = 0.15	1.008	1.010	1.0104	1.005
Plane 3, h/b = 0.10	1.029	1.011	1.015	1.007
Plane 4, h/b = 0.05	1.010	1.016	1.016	1.009

Section 2 - Wind Tunnel Ground Effect Tests

The following section examines the OGE and IGE data collected for the lambda UCAV. The ground-effect region is identified by analyzing the following longitudinal characteristics of the model: lift, drag, and pitching moment coefficients. Data related to the lateral stability of the UCAV, in terms of the roll, pitch, and yawing moments, were collected for asymmetric flap deflections but will not be presented in this section; for further analysis, see the raw data files presented in Appendix F.

It should be noted that the wind tunnel velocities labeled on the figures and tables in this section and Appendices E and F are the nominal test speeds that do not account for the solid blockage effects and velocity measurement errors that are presented in Table 10. Table 11 lists the actual corrected tunnel velocities for the nominal test speeds of 40, 60, 80, and 100 mph.

Table 11: Summary of Corrected Wind Tunnel Velocities

$U_{\infty,corr}$ (mph)				
OGE	**IGE** h/b = 0.3	**IGE h/b = 0.15**	**IGE h/b = 0.10**	**IGE h/b = 0.05**
36.16	37.10	36.45	37.21	36.52
54.72	55.54	55.26	55.32	55.60
72.08	73.23	73.23	73.16	73.23
90.07	91.10	90.52	90.70	90.88

Section 2.1 – Longitudinal Stability Characteristics, OGE

The purpose of the tunnel tests conducted without the ground planes was to verify the results with the longitudinal characteristics identified by Reed (10) and In (11), and to identify the aerodynamic OGE performance of the lambda UCAV with various flap deflections. Figure 18 shows similar trends between the lift coefficients measured with the original lambda UCAV and the scaled down version used in this study and by In (11).

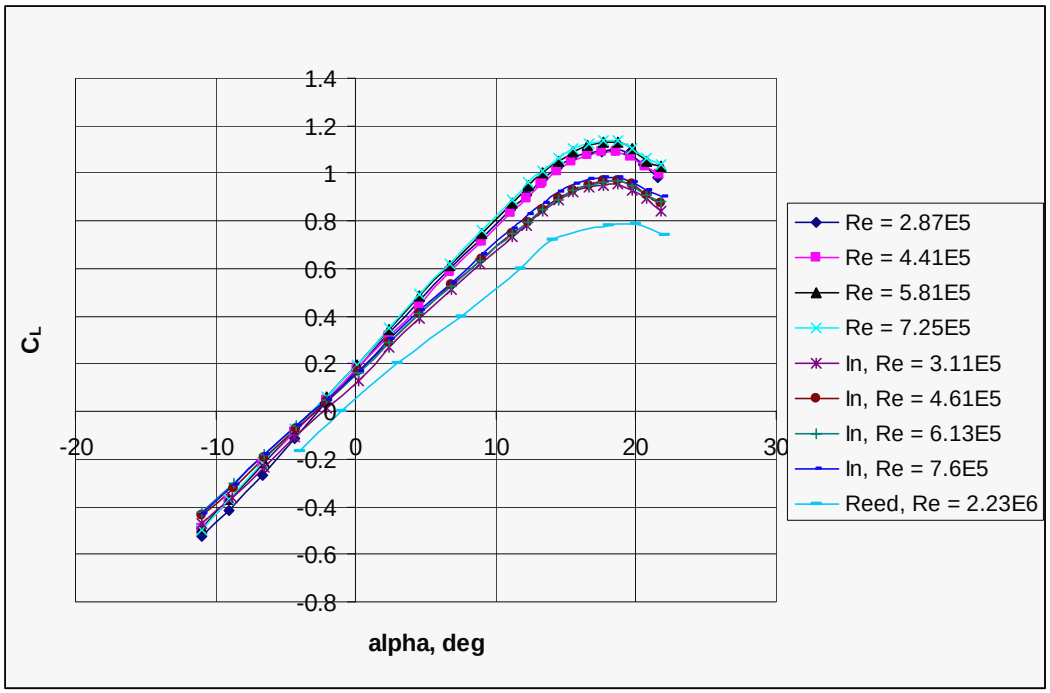

Figure 18: Aerodynamic Comparison of the Lift Coefficient, No Flaps

Based on the data presented in Figure 18, Table 12 lists a comparison of the lift curve slopes (C_{L_α}) and $C_{L_{MAX}}$ for the results obtained in this study to those of Reed and In. It is apparent from Figure 19 that the lift curve slopes remain relatively constant for a given series of tests, therefore an average C_{L_α} is shown in Table 12; just for comparison,

only the $C_{L_{MAX}}$ values corresponding to the largest Reynolds numbers tested are presented in the table.

Table 12: Lift Curve Comparison

	Current Study	In	Reed
C_{L_α} (per deg)	0.0621	0.0545	0.0470
$C_{L_{MAX}}$	1.14	0.950	0.785

Because the same lambda model was tested by In, one would expect the results to be very similar. On the contrary, it can be seen that the lift curve slope and the maximum lift coefficient vary by 12.2% and 16.67%, respectively. This discrepancy is a direct result of the blockage corrections used by In (11), which are on the same order as those determined for this study but differ by approximately +0.07 OGE and +0.005 IGE. These differences in blockage factors are most likely attributed to varying test room conditions, such as temperature, pressure, and density that occur between day-to-day operations of the wind tunnel.

When the OGE, no-flap configuration lift coefficient data of this experiment was re-analyzed with In's blockage correction factors, the results matched with minimal discrepancies, as seen in Figure 19. This indicates repeatability of results for the wind tunnel used in this experiment. It should be noted that the data presented in the remainder of this report is based on the blockage factors listed in Table 10, that were calculated for this study.

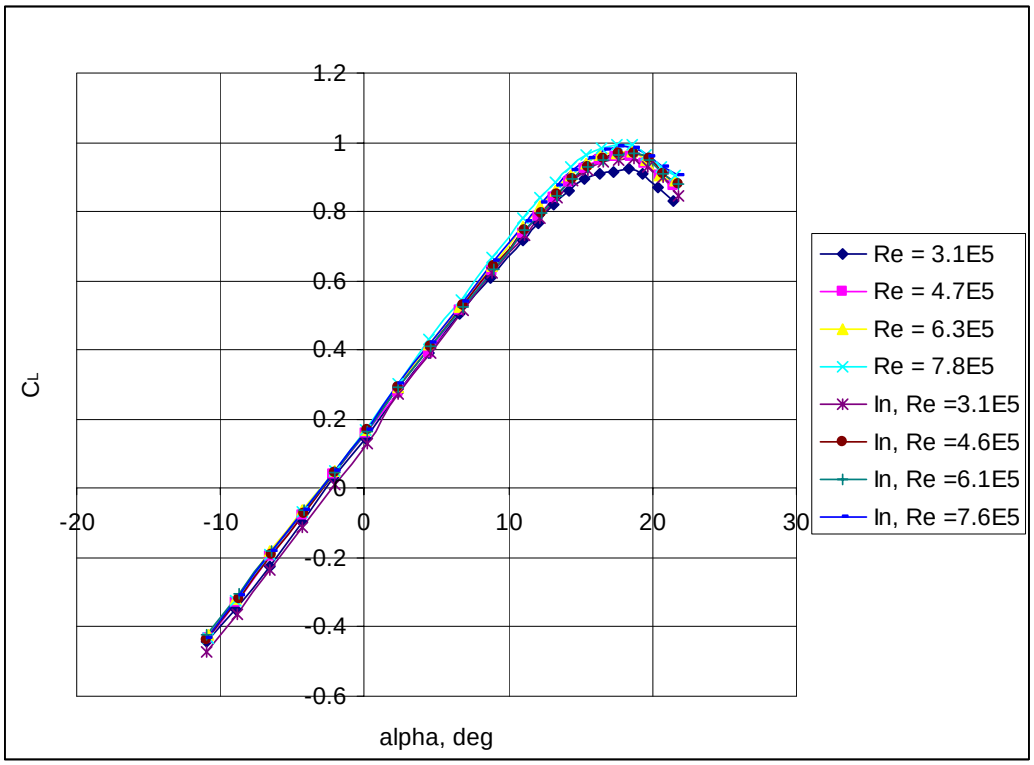

Figure 19: Lift Comparison Based on In's Blockage Corrections

The differences related to Reed's data, in particular, the 31% variance in $C_{L_{MAX}}$, is not as easy to explain. Based on convention, at higher Reynolds numbers, $C_{L_{MAX}}$ should be greater for similar planform shapes (28). According to the results displayed in Figure 18, the opposite is true. A possible explanation of this phenomena is that the ½-scaled model used in this study was not fabricated in exact proportions to the original model therefore reducing the repeatability of the results. However, even though the results are not in good agreement with the original study performed by Reed, it should be realized that the results are in good agreement with In's data when a consistent set of blockage corrections are utilized.

In the same manner, similar discrepancies are evident for the drag coefficient and the drag polar which can be attributed to the above explanations; see Appendix E for plots of the OGE, drag coefficient and drag polar comparisons.

Static longitudinal stability is defined as the tendency of an aircraft to return to a trimmed equilibrium condition when it is disturbed (10). Therefore, for an airplane to be statically stable in pitch and trim, the following requirements must be met (13):

$$C_{m_\alpha} < 0 \qquad [17]$$

$$\frac{\partial C_m}{\partial C_L} < 0 \qquad [18]$$

$$C_{m_{\alpha=0}} > 0 \qquad [19]$$

Based on Figures 20 and 21, it is apparent that only one of the above conditions is met. For each speed tested, $C_{m_{\alpha=0}} > 0$, but neither C_{m_α} or ($\partial C_m / \partial C_L$) is less than zero; as a result, the lambda UCAV is not longitudinally stable. In order to achieve stability and to counteract the nose-up tendency of the UCAV, the current model might need to be modified such that the trailing edge is reflexed with a negative camber (13) or that the lift distribution is varied along the span by adding wing twist (29).

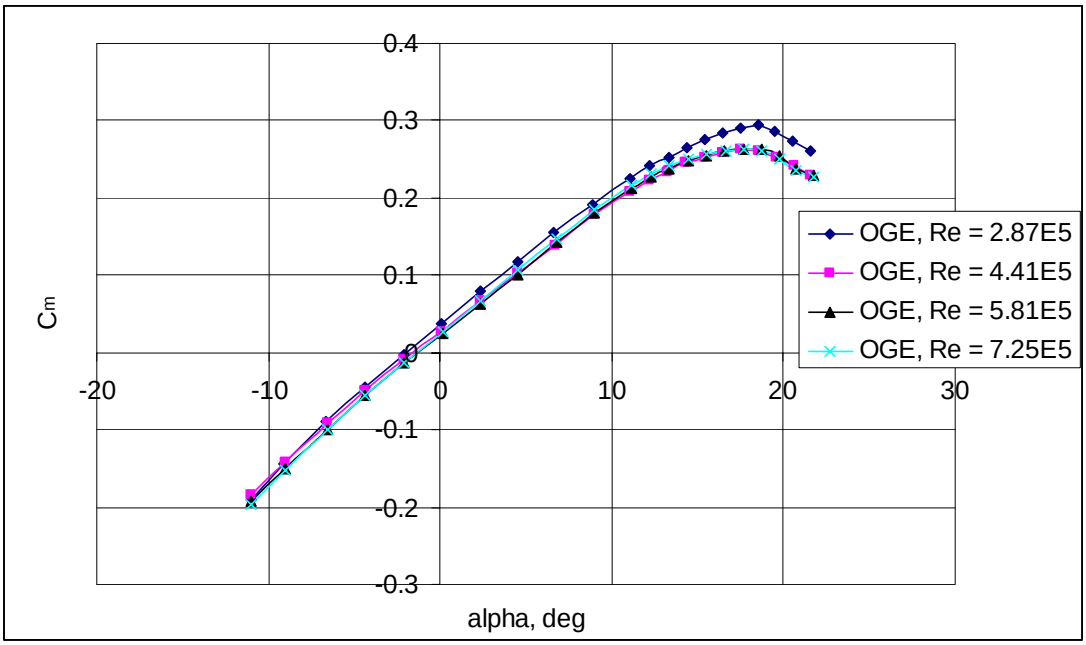

Figure 20: C_m vs. AOA, OGE, No Flaps

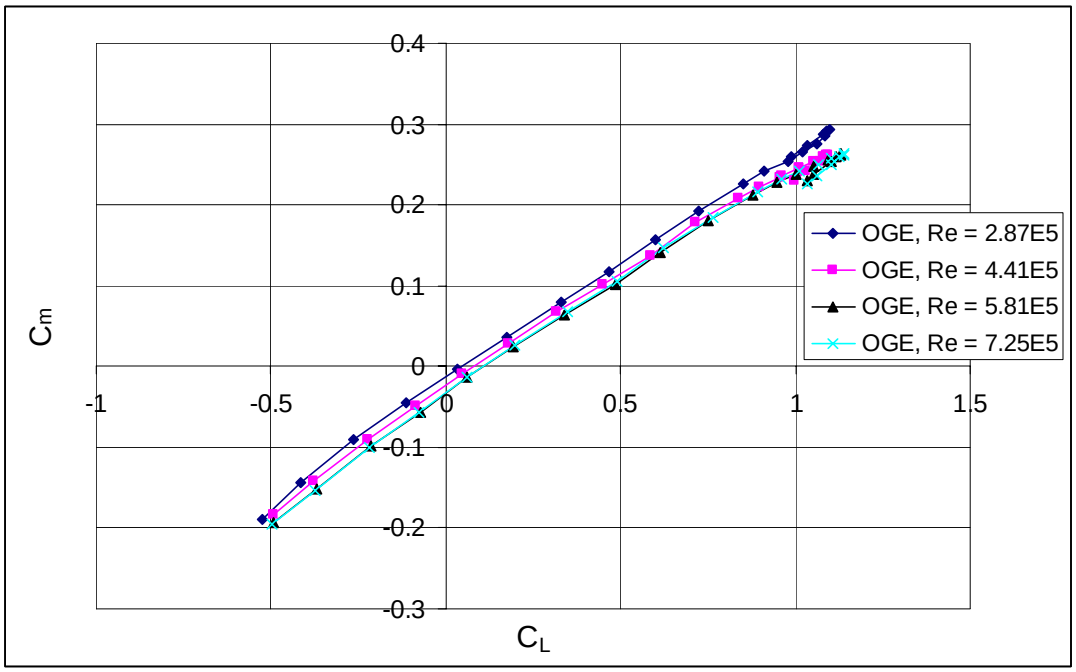

Figure 21: C_m vs. C_L, OGE, No Flaps

Based on the data analyzed in this section, Table 13 summarizes the key longitudinal characteristics of the lambda UCAV, flying OGE, without flap deflections for the four tunnel speeds studied in this experiment.

Table 13: Longitudinal Characteristics, OGE, No Flap Deflections

	Re=2.87E5	Re=4.41E5	Re=5.81E5	Re=7.25E5
C_{L_α}	0.0627	0.0606	0.0622	0.0630
C_{L_o}	0.166	0.174	0.187	0.189
$C_{L_{MAX}}$	1.10	1.09	1.13	1.14
L/D_{MAX}	25	17	16	18
C_{m_α}	0.0138	0.0127	0.0129	0.0129
C_{m_o}	0.035	0.026	0.023	0.024
$\partial C_m / \partial C_L$	0.298	0.277	0.278	0.276
$C_{D_{MIN}}$	0.0070	0.0080	0.0107	0.0120

Section 2-1.1 Midboard and Outboard Trailing Edge Flaps

The lambda UCAV had two flap positions along the trailing edge, midboard and outboard, that were deflected $+10^o$ and $+20^o$. In this study, data was collected for symmetric and asymmetric flap deflections where asymmetric deflections refer to the model configuration in which the flaps were only extended on the right wing. Because similar trends based on flap effectiveness were seen between each test speed, only the data for the 100 mph test case is presented in this section; additional plots are included in Appendix E.

The effect of the flaps on the longitudinal control characteristics of the UCAV, in terms of the lift and drag, can be seen in Figures 22 and 23. First, it should be noted that as with the zero deflection (no flaps) case presented in Figure 18, there exists a discrepancy between the data analyzed in this study and that of Reed. Based on the

comparisons shown in Table 14, it is apparent that the lift curve slopes are similar with only a 4.3% difference whereas the $C_{L_{MAX}}$ values differ by 33.1%. The large error related to $C_{L_{MAX}}$ can best be explained in terms of the different flap configurations studied. The lambda model tested by Reed was manufactured with plain flaps and the lambda model studied in this experiment utilized split flaps. Because leakage through the gap at the leading edge of the plain flap can decrease $C_{L_{MAX}}$ by approximately 0.4 (13), a similar effect should be seen in Reed's data. Based on the results shown in Table 14, a 0.43 difference exists between the $C_{L_{MAX}}$ values estimated from Figure 22. Additional sources of error might be attributed to imprecise scaling of the model and flaps from the original UCAV studied by Reed.

Table 14: Lift Comparison for Maximum Flap Deflection

	Current Study	Reed
C_{L_α} (per deg)	0.047	0.045
$C_{L_{MAX}}$	1.3	0.87

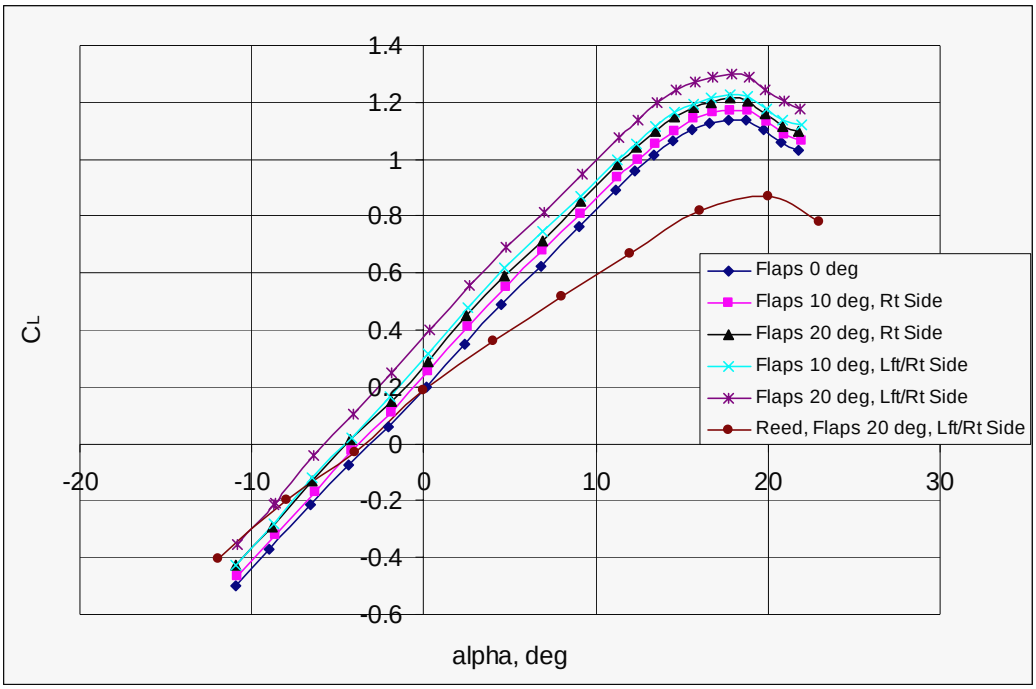

Figure 22: Effect of Flap Deflections on the Lift Coefficient, Vel. = 100 mph

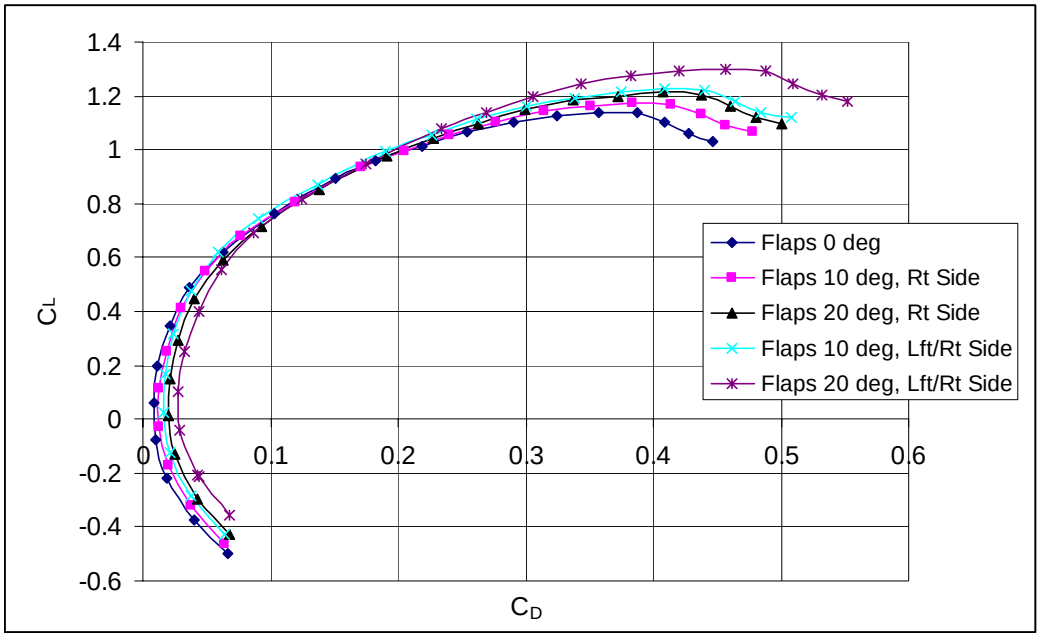

Figure 23: Effect of Flap Deflections on the Drag Polar, Vel. = 100 mph

Based on the results presented in Figures 22 and 23, it can be verified that the longitudinal characteristics of the model follow the trends that are to be expected for an aircraft with flaps deflected. As seen from Figure 22, the lift curves are shifted upward without changing the slope (13). In reference to the drag, with the extension of flaps, a greater wake region is created behind the UCAV therefore increasing the drag as compared to a clean aircraft configuration. As approximated from the drag polars (Figure 23), it is apparent that the deflection of the flaps does increase the drag. It is interesting to note that the lift and drag generated by a symmetric deflection of $+10^{o}$ is very similar to that of an asymmetric deflection of $+20^{o}$. This is because the projected areas normal to the freestream flow for these two flap configurations are nearly identical; 1.21 in^2 for the $+10^{o}$ symmetric deflection and 1.22 in^2 for the $+20^{o}$ asymmetric deflection.

As was determined from the data shown for the no-flap configuration in the previous section, it was determined that the lambda UCAV is longitudinally unstable. Figure 24 displays the pitching moment as a function of the lift coefficient for the various flap configurations studied. Although the UCAV remains longitudinally unstable with the flaps deflected, they do provide a beneficial effect. As subtle as it may be by inspection of Figure 24, the slopes of the curves do vary. In general, as the flaps are deflected from 0^{o} to $+20^{o}$, the value of $\partial C_m / \partial C_L$ decreases. For instance, at zero flap deflections, the slope is 0.276 while at $+20^{o}$ symmetric deflections, the slope is 0.2645. Even though this is a relatively small change, it does suggest that positive deflections aft of the c.g. can increase the stability of the UCAV.

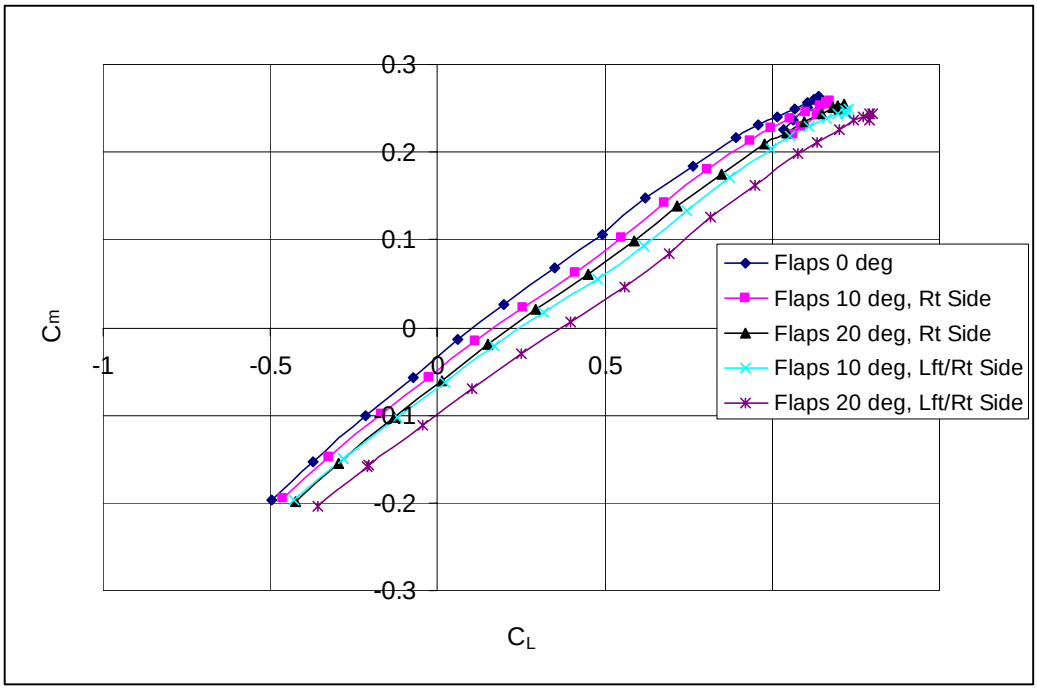

Figure 24: Flap Effectiveness Stability Analysis, Vel. = 100 mph

Based on the data analyzed in this section, Table 15 summarizes the key longitudinal control characteristics of the lambda UCAV, flying OGE, with various split flap deflections.

Table 15: Longitudinal Effects of Mid/Outboard Flap Deflections, Vel. = 100 mph

	$\delta_{mid/out}=0^o$ Symmetric	$\delta_{mid/out}=+10^o$ Asymmetric	$\delta_{mid/out}=+20^o$ Asymmetric	$\delta_{mid/out}=+10^o$ Symmetric	$\delta_{mid/out}=+20^o$ Symmetric
C_{L_α}	0.063	0.0466	0.0466	0.0472	0.0469
C_{L_o}	0.189	0.230	0.270	0.300	0.370
$C_{L_{MAX}}$	1.14	1.17	1.21	1.23	1.3
L/D_{MAX}	18	15.5	12.25	14.70	10.20
C_{m_α}	0.0129	0.0127	0.0126	0.0125	0.0124
C_{m_o}	0.024	0.018	0.016	0.013	0.002
$\partial C_m / \partial C_L$	0.276	0.2720	0.2710	0.2646	0.2648
$C_{D_{MIN}}$	0.012	0.014	0.021	0.019	0.034

Section 2.2 – Longitudinal Characteristics, IGE

The following section investigates the effect of decreasing height above the ground on the longitudinal stability of the lambda UCAV with deflections of the trailing edge split flaps. For this experiment, the datum chosen as the reference point for vertical measurements above the ground plane was the interface between the 100 lb balance and the wind tunnel balance support. As was mentioned in Chapter IV, data was collected at four tunnel speeds, but because similar trends exist between each test speed for a given stability parameter, only the aerodynamic properties plotted as a function of h/b for the 100 mph test condition is presented. Please refer to Appendix E for the lambda UCAV longitudinal IGE flight data obtained for the other test speeds of 40, 60, and 80 mph.

Section 2.2.1 – Lift Coefficient IGE

Figures 25-27 show the results of flying IGE with split flap deflections on the lift data for a nominal tunnel speed of 100 mph. The other tunnel speeds provided similar trends. Based on previous ground effect studies, several lift curve trends are to be expected when IGE: for a no-flap configuration, the lift curve slope increases as the wing moves closer to the surface, and the lift axis intercept decreases for the same conditions (31); for split flap deflections, the lift curve slope and the lift axis intercept increase as the wing approaches the ground plane (16). The lift axis intercept decrease associated with a no-flap, wing configuration has been well documented in previous work and is attributed to the Venturi effect that is generated when the area between the wing and ground decrease as the airfoil moves closer to the surface (31). On the other hand, it is not clear why the lift axis intercept increases IGE with flap deflections but has been noted

in Recant's (16) ground effect work with a NACA 23012 tapered wing with split flaps. A possible explanation for the lift axis increase is that the additional lift generated by deflecting the flaps dominates the lift decrease produced by the Venturi effect.

It should be noted that the point where the lift curves cross shift for the different flap deflections. For the no-flap case, and the $+10^{o}$ and $+20^{o}$ deflection configuration, the lift curves cross at the following approximate angles of attack for a tunnel speed of 100 mph: 0^{o}, -0.6^{o}, and -1.6^{o}, respectively. It is at these angles of attack that the lift remains unaffected by the height above the ground. The lift curves for the other test speeds revealed that the curves crossed at the same angles of attack, therefore suggesting that the point of intersection is a function of the wing geometry and not the velocity.

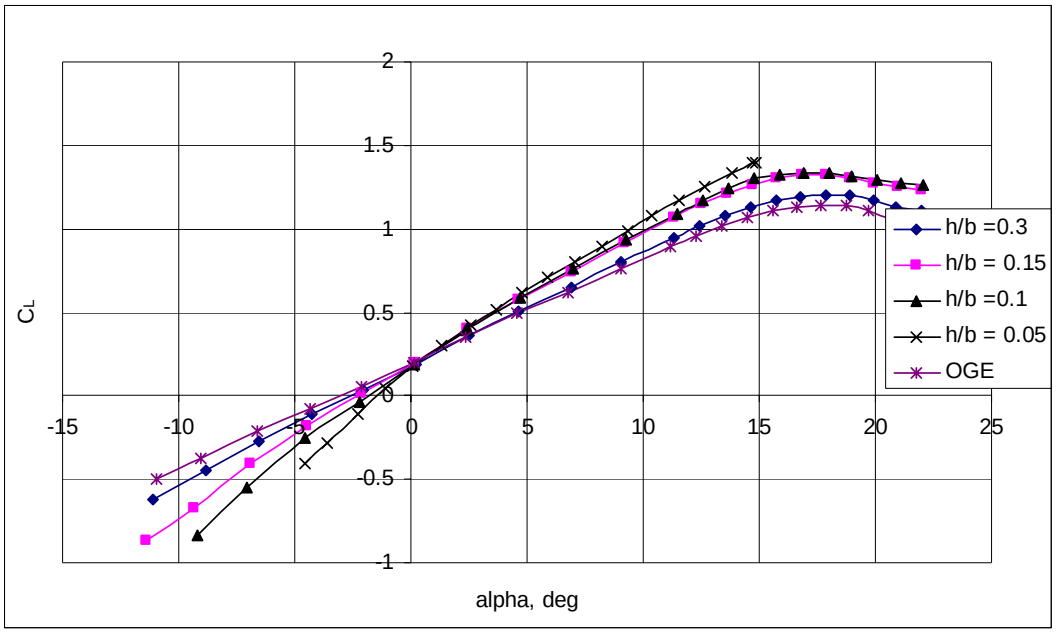

Figure 25: Lift Curve Comparison IGE, No Flaps, Vel. = 100 mph

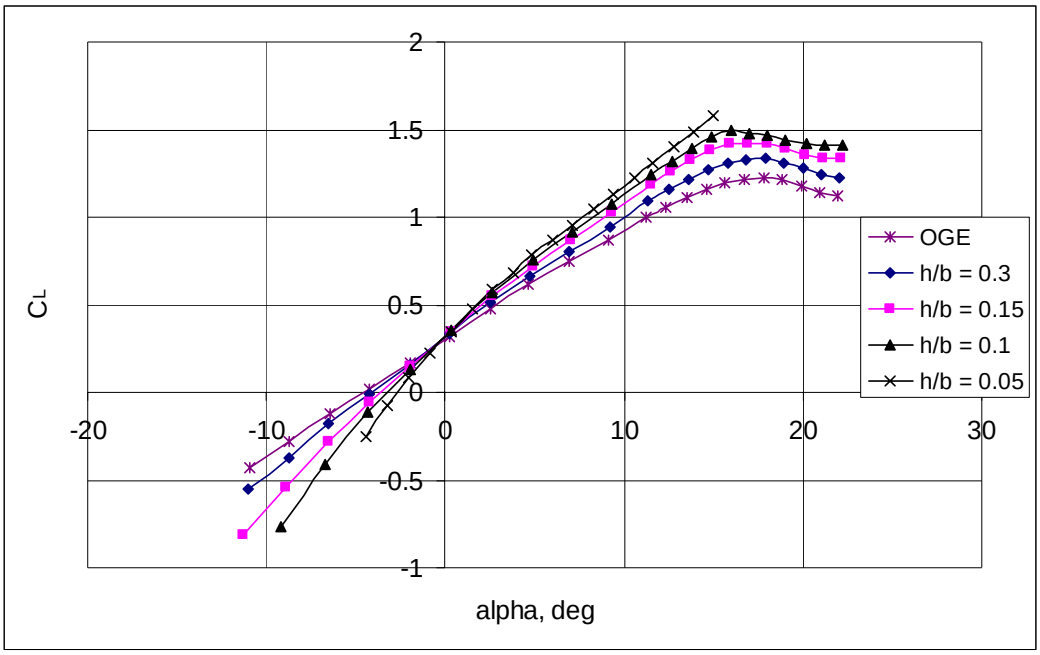

Figure 26: Lift Curve Comparison, Flaps +10°, Vel. = 100 mph

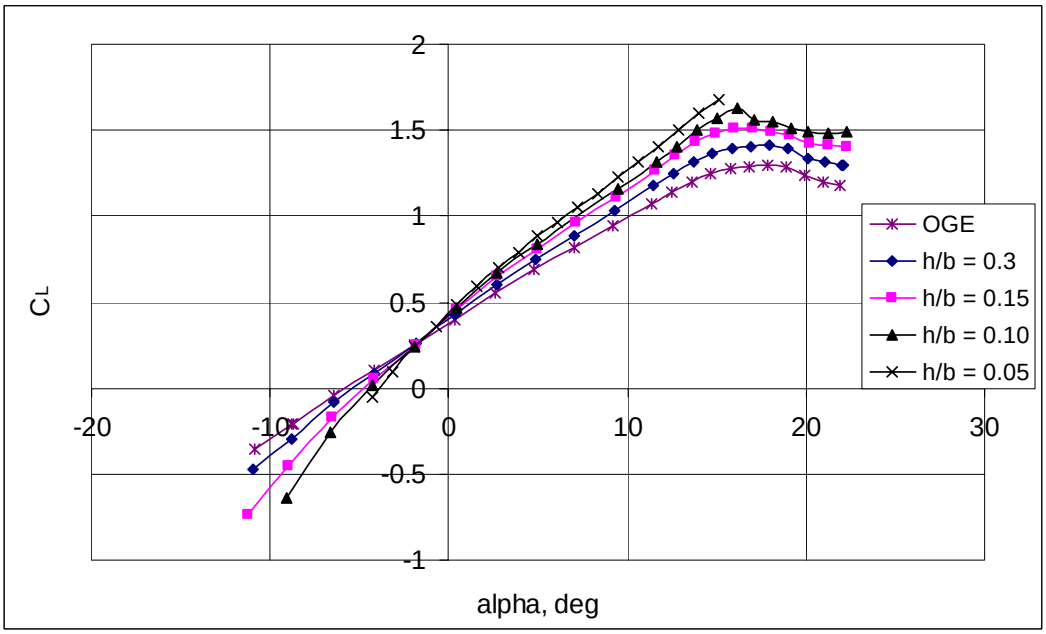

Figure 27: Lift Curve Comparison, Flaps +20°, Vel. = 100 mph

The lift results for all tunnel speeds and flap configurations studied in this experiment are presented in Figures 28 and 29. In particular, theses two graphs compare the variations in the lift curve slope and the lift axis intercept with respect to the flap

deflections. The data presented in these figures are consistent with the expected trends mentioned above.

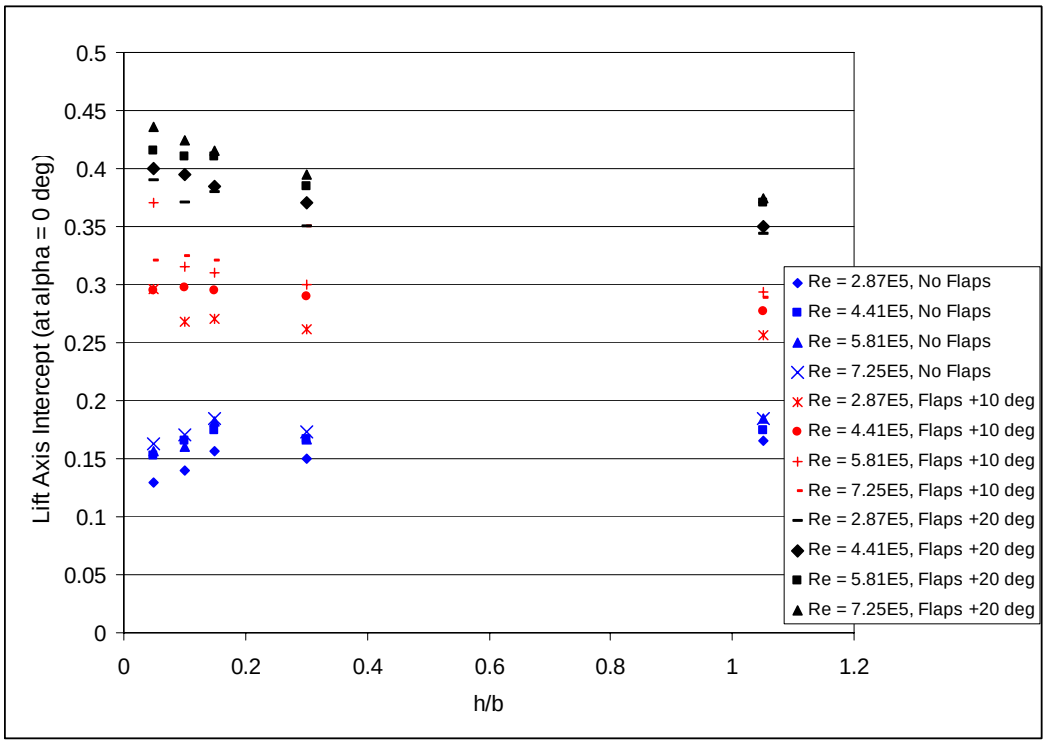

Figure 28: Effect of Height and Flap Deflection on the Lift Axis Intercept

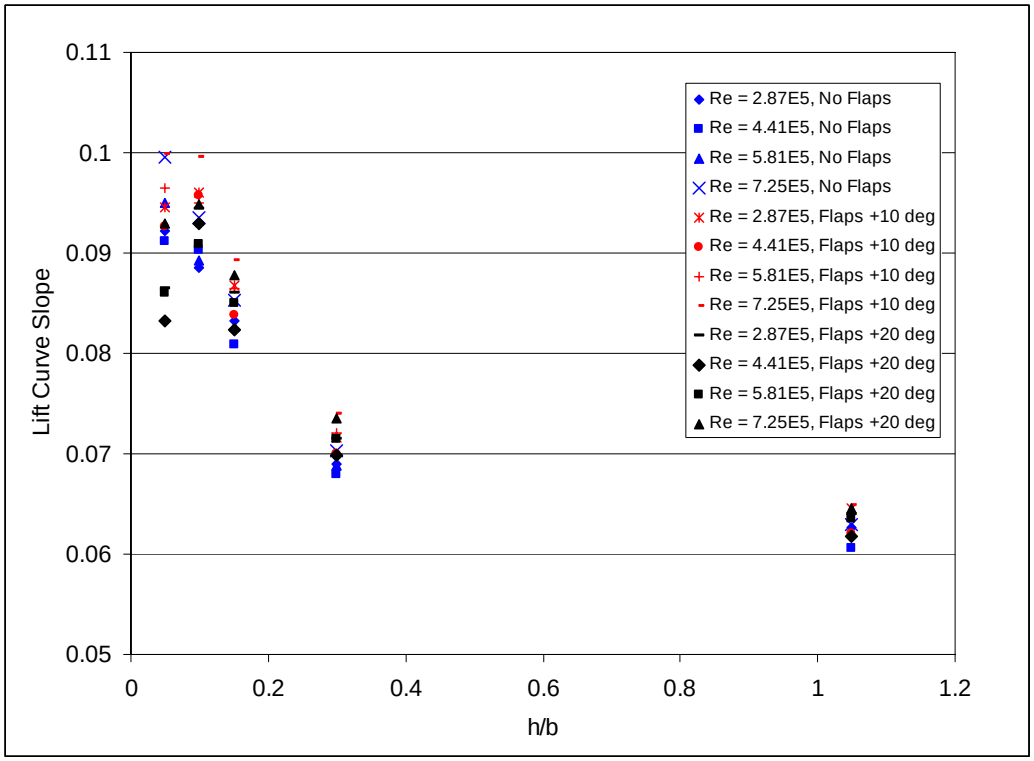

Figure 29: Effect of Height and Flap Deflection on the Lift Curve Slope

To better understand the variations of lift IGE, traditional ground effect plots were generated. Figures 30-32 display the lift coefficient at several angles of attack as a function of the height above the ground plane for a nominal tunnel speed of 100 mph; similar trends were noted for the other test speeds. In particular, these figures illustrate the effect of symmetric flap deflections on the lift while flying in close proximity to the ground. It is important to realize that the results obtained for the no-flap configuration are in good agreement with the results of In's study (11); in particular, the lift increases as the UCAV is positioned closer to the ground plane. The lift increase IGE was seen in Figures 25-27 for each flap configuration and is to be expected because as the UCAV approaches the surface, the ground partially blocks the trailing vortices and reduces the amount of downwash generated by the wing; this reduction in downwash increases the effective angle of attack and ultimately, the lift produced (4).

Again, there are small discrepancies between the results of this study and those of In. The lift coefficient data, at each angle of attack, presented in Figure 30 is approximately 18% greater than the results calculated by In. This discrepancy is due to the fact that In used different blockage correction factors in the analysis of his wind tunnel data. As was determined in Section 2.1, because different blockage factors were used, the lift coefficients should vary by approximately 17%.

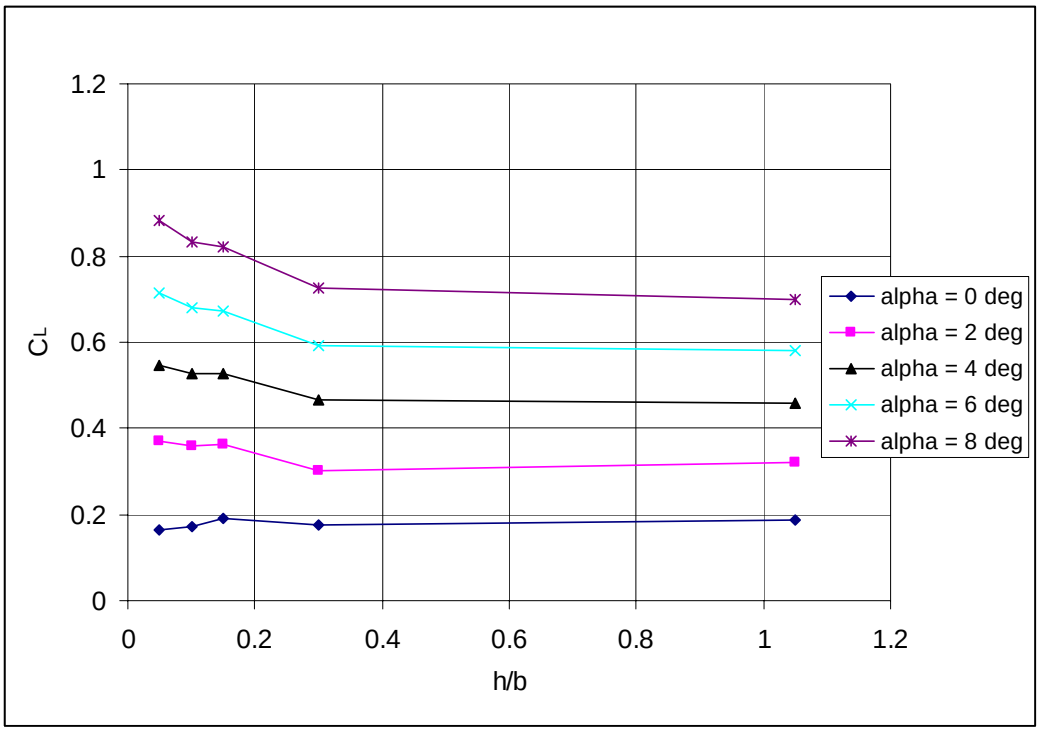

Figure 30: Ground Effect, C_L vs. (h/b), No Flaps, Vel. = 100 mph

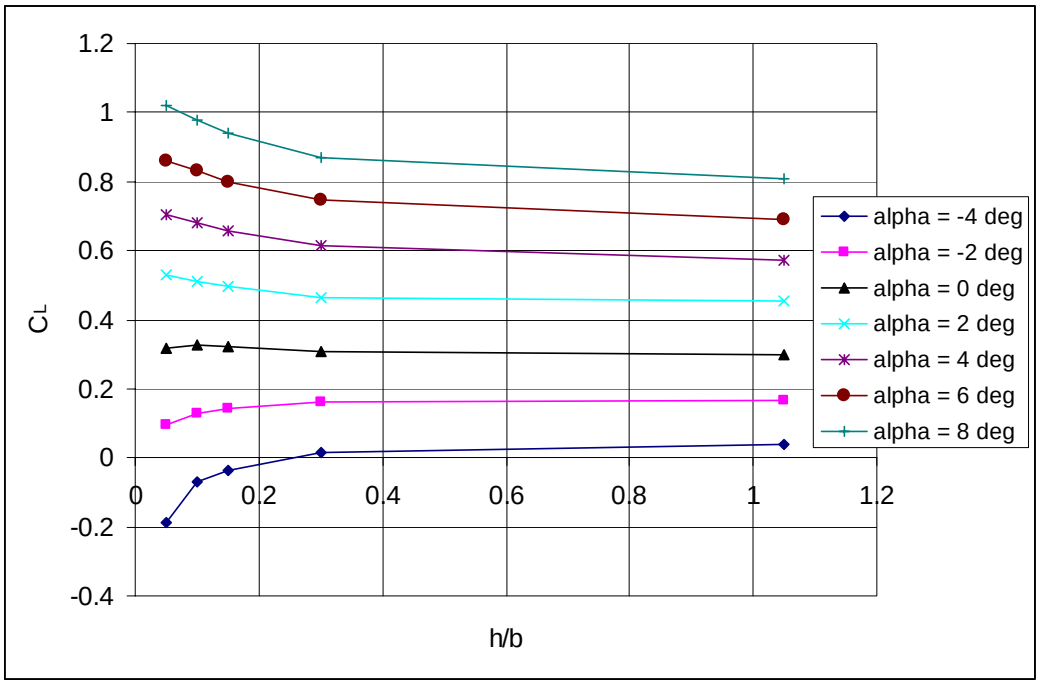

Figure 31: Ground Effect, C_L vs. (h/b), Flaps +10°, Vel. = 100 mph

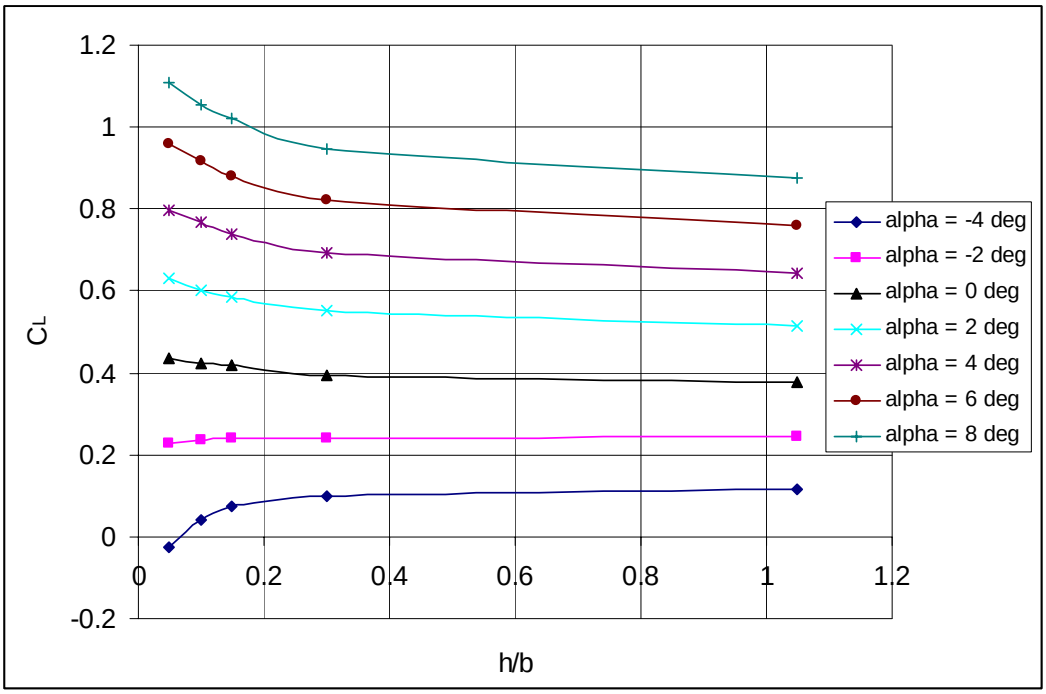

Figure 32: Ground Effect, C_L vs. (h/b), Flaps +20°, Vel. = 100 mph

Based on the results presented in Figures 30-32, Table 16 compares the main differences in lift for the various symmetric flap deflections. The $\%\Delta C_{L,IGE}$ compares the lift achieved OGE (h/b =1.05) to the height above the ground plane where the greatest change in lift is achieved IGE; the greatest lift change occurs at h/b = 0.05. The second major difference seen between these figures if the rate at which the lift varies ($dC_L/d(h/b)$) when the UCAV transitions from the OGE region to the first IGE point where h/b = 0.3. Beyond this point, it is apparent that the lift increases at a higher rate in a near parabolic fashion; it is within this region that the benefits of ground effect are most pronounced.

Table 16: IGE Lift Comparison for Various Flap Deflections

	$\delta_{mid/out} = 0^o$		$\delta_{mid/out} = +10^o$		$\delta_{mid/out} = +20^o$	
AOA (deg)	$\%\Delta C_{L,IGE}$	$\frac{dC_L}{d(h/b)}$	$\%\Delta C_{L,IGE}$	$\frac{dC_L}{d(h/b)}$	$\%\Delta C_{L,IGE}$	$\frac{dC_L}{d(h/b)}$
0	16.0*	0.019	6.0	-0.015	13.5	-0.025
2	13.5	0.025	14.0	-0.013	18.0	-0.048
4	16.0	-0.007	19.0	-0.059	19.0	-0.064
6	18.8	-0.019	19.8	-0.073	21.0	-0.080
8	21.0	-0.039	21.0	-0.084	21.0	-0.093
* denotes a percent decrease						

Based on the pitch angles analyzed, it can be seen that for a fixed angle of attack up to 8^o, the percent increase in lift generally increases with an increase in the flap deflection angle which suggests that positive deflections of the midboard/outboard flaps enhance the beneficial lift effects related to ground effect for the lambda UCAV.

As the UCAV transitions from OGE to the IGE region where h/b = 0.3, it is apparent from Figures 30-32 and Table 16 that the flap deflections alter the rate in which the lift varies for a given angle of attack. In general, the deflection of the flaps increases the slopes ($dC_L/d(h/b)$) as compared to the no-flap case. The greatest effect is seen when

the flaps are deflected +20^{o}. It should be noted that the slopes are positive for the no-flap configuration at angles of attack of 0 and 2^{o}. Even though at an AOA of 2^{o} the final lift achieved IGE is greater than that achieved OGE, the lift actually decreases as the UCAV transitions from OGE to IGE at h/b = 0.3 (see Figure 30). A similar trend is experienced at an AOA of 0^{o}.

In order to determine the effectiveness of the midboard/outboard flaps, the percent increase in the maximum C_L achieved at each angle of attack, as compared to the no-flap case, was computed and plotted in Figure 33 for the two deflection angles studied in this experiment; the maximum achievable lift occurs at h/b = 0.05. The results indicate that at the lower angles of attack, for either deflection angle, the maximum achievable lift IGE is substantially greater than when the flaps are not extended. For instance, at an AOA of 0^{o}, the maximum lift increases 95% for the +10^{o} deflection and 168% for the +20^{o} flap deflection. As the AOA is increased, the percent increase decreases exponentially towards an asymptotic value. This is due to the fact that as the AOA is increased, greater separation begins to occur, starting at the wingtip, over the upper surface of the UCAV, therefore reducing the effectiveness of the flaps. But even though the effectiveness of the flaps reaches a limiting value, the maximum lift generated, when the flaps are deflected, remains greater than the no-flap configuration.

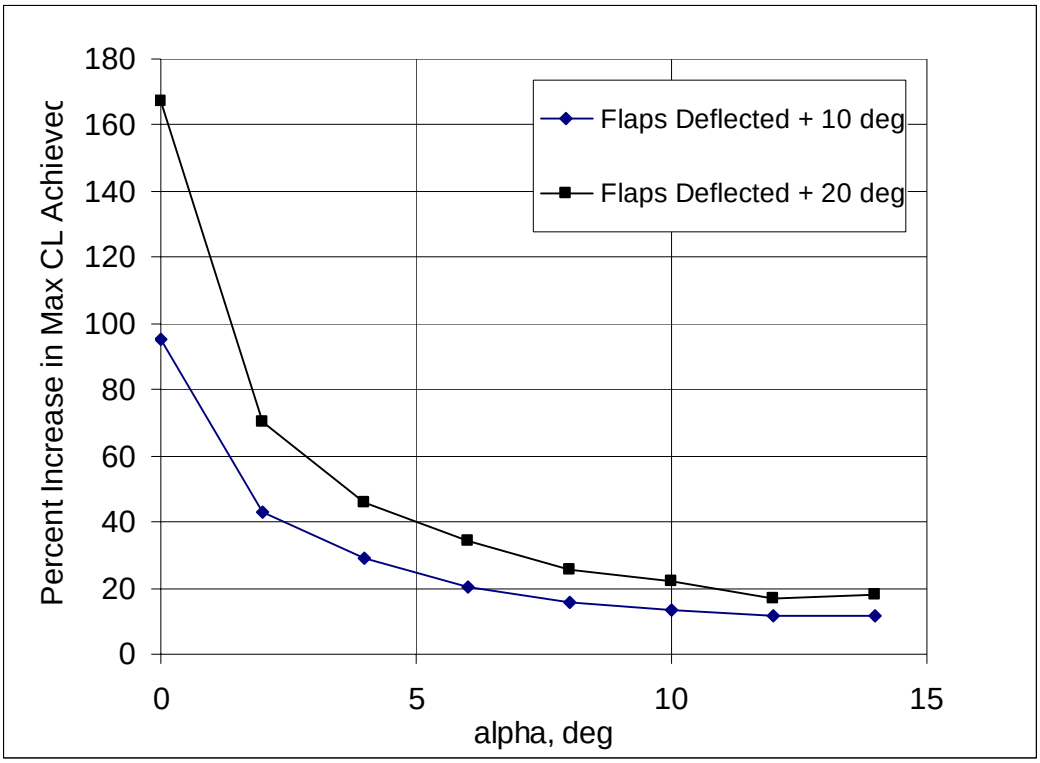

Figure 33: Effect of Flap Deflections on the Maximum Lift Increase at h/b = 0.05, Vel. =100 mph

Based on the results presented in this section, it can be concluded that the positive flap deflections, both $+10^{o}$ and $+20^{o}$, enhance the overall lift benefits that are attributed to ground effect. The maximum achievable lift is increased in addition to the rates in which they increase. In order to validate the trends associated with the flap deflections, a 2-D VORLAX panel code was used to theoretically predict the lift variation IGE for a lambda-shaped UCAV; the results are shown in Figure 34. The results were generated by Plumley (30) of the Air Vehicles Directorate at AFRL, prior to this study, for a 0^{o} and $+20^{o}$ deflection of the midboard/outboard trailing edge flaps; the results were acquired at a Reynolds number similar to that tested by Reed (10), Re = 1.4E6. In general, the panel code predicts lift increases that are higher than the measured values presented in Figures

30 and 32. This over-prediction is to be expected because the panel code only models the circulation about the wing and does not account for the Venturi effect that occurs when the wing approaches the ground (31). The program also does not account for changes in the shape of the wake or flow separation which becomes significant when the flaps are deflected (31) and it only models the lifting surface as a flat plate without camber. Even though the experimental lift values do not match well with the predicted values, it can be concluded that the trends of the curves are similar and that the results of the VORLAX code validate that flap deflections are to enhance the lift benefits associated with flying IGE.

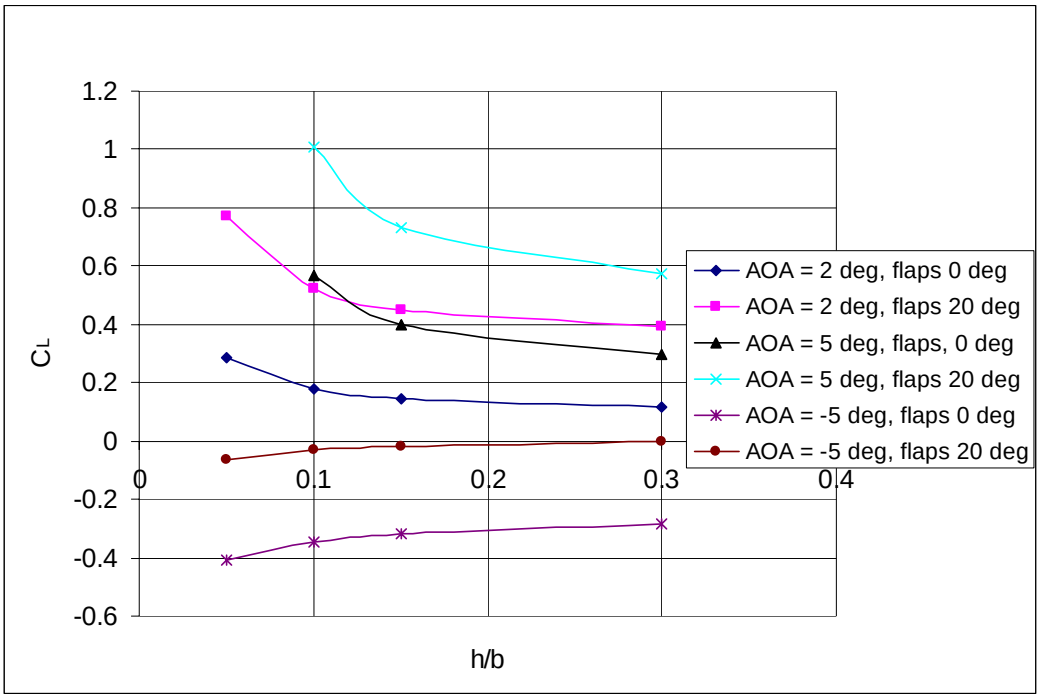

Figure 34: Ground Effect, VORLAX Panel Prediction, C_L vs. (h/b), Re = 1.4E6

Section 2.2.2 – Drag Coefficient IGE

The effect of the ground and the symmetric deflections of the midboard/outboard trailing edge flaps on the drag coefficient of the lambda UCAV are shown in Figures 35-

37 for a nominal tunnel speed of 100 mph. It is apparent from the figures that several common trends exist: unlike the variation in lift, the drag coefficient generally increased within the ground effect region for each flap configuration tested; the drag is seen to change rapidly as the UCAV transitioned further into the ground effect region beyond h/b = 0.3; in general, at an h/b of 0.15, the drag decreased; the drag increases when the flaps are deflected because of the greater momentum loss generated when the flaps are extended into the freestream flow.

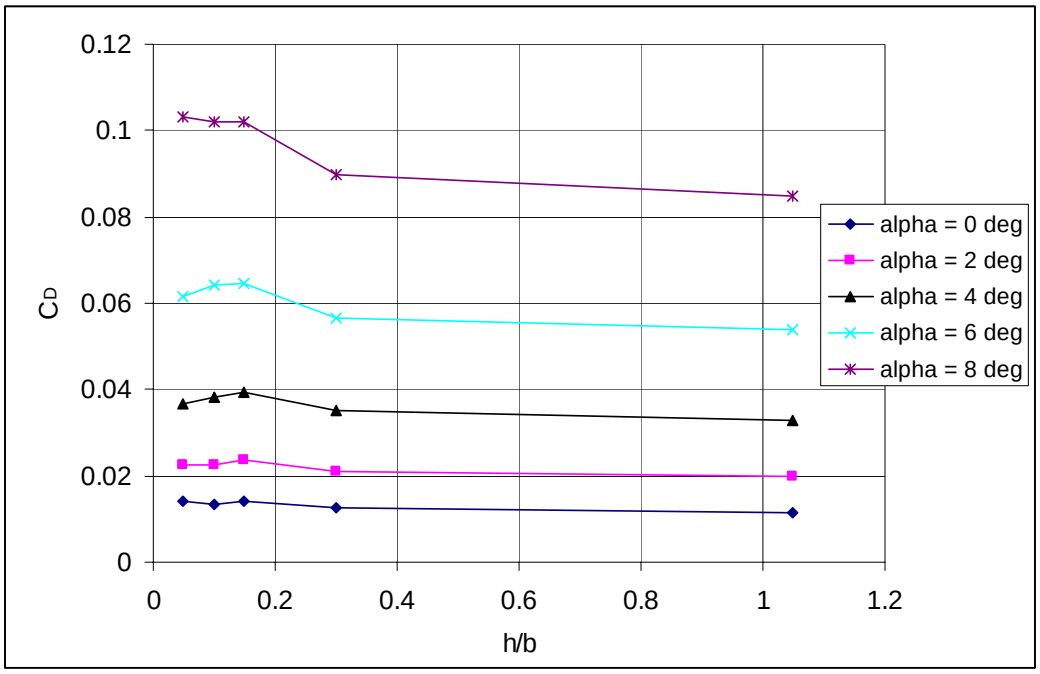

Figure 35: Ground Effect, C_D vs. (h/b), Flaps Retracted, Vel. = 100 mph

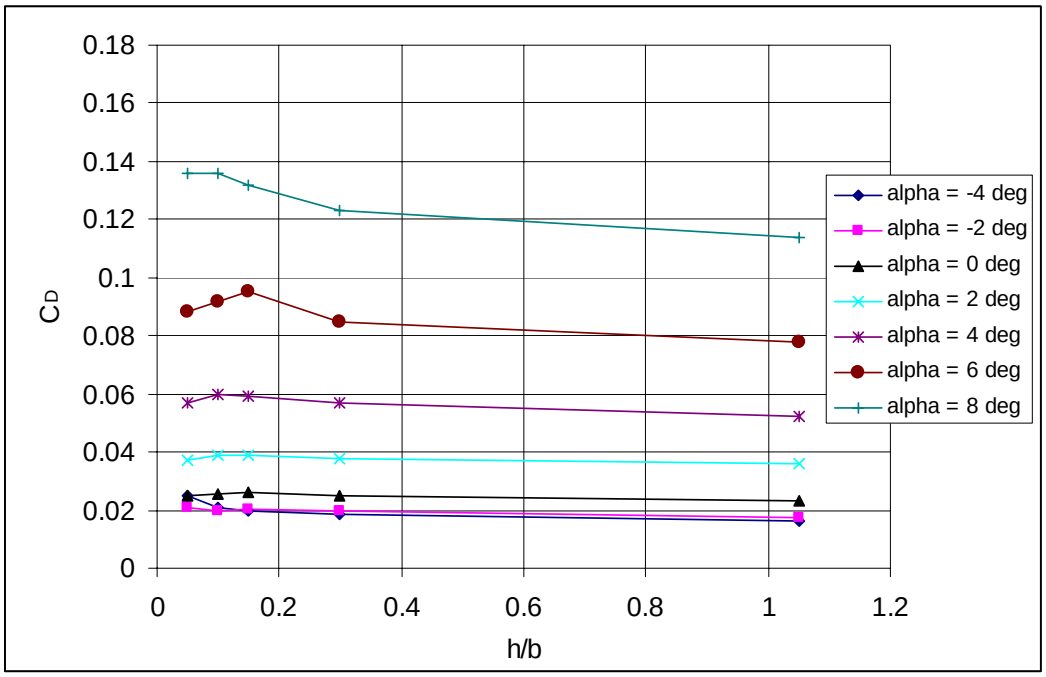

Figure 36: Ground Effect, C_D vs. (h/b), Flaps +10°, Vel. = 100 mph

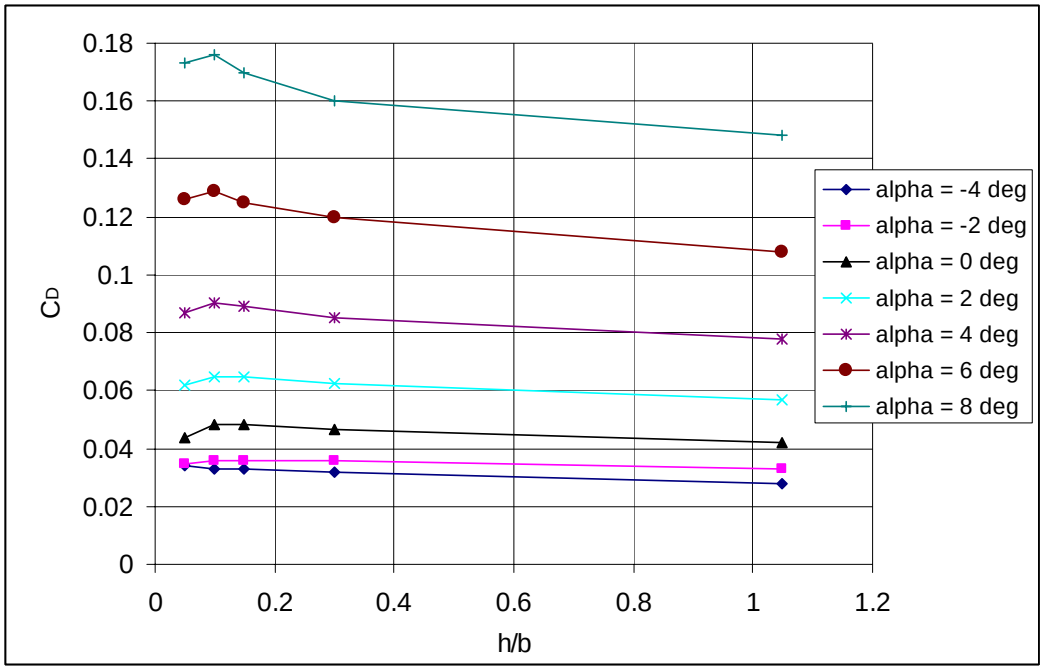

Figure 37: Ground Effect, C_D vs. (h/b), Flaps +20°, Vel. = 100 mph

In order to explain the drag increase that is seen in Figures 35-37 for each flap configuration, it is imperative to analyze the trends seen in the drag polar. Figure 38

displays the drag polar for all the heights tested at a tunnel speed of 100 mph, and a flap deflection angle of +20°; similar trends were seen in the drag polar for the no-flap and +10° deflection configuration. From the figure, it is apparent that as the lambda UCAV approaches the ground, the parabolic curves become wider, indicating a reduction in the induced drag which is consistent with previous ground effect studies (31). On the other hand, as the wing approaches the surface, the curves shift to the right, suggesting an increase in parasite drag (C_{D0}). This increase in C_{D0} is not consistent with many ground effect studies but was seen to be characteristic of the chevron UCAV, tested IGE by Jones (3). Because the parasite drag increase is more significant than the induced drag reduction, the total drag is increased IGE for any angle of attack.

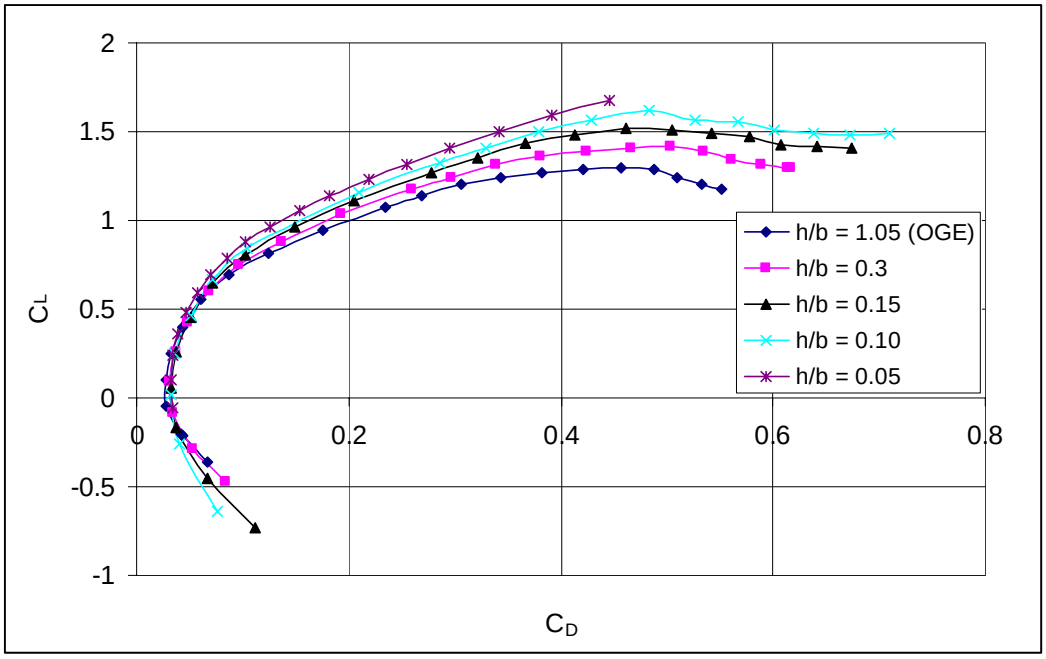

Figure 38: Effect of Height on the Drag Polar, Flaps +20°, Re = 7.25E5

In order to analyze the various components of drag and to investigate the validity of McCormick's induced drag factor (see Chapter II, Section 1.1), the drag coefficient

data shown in Figure 38, for a +20^{o} flap deflection, was assumed to take the form of Equation 20 from Bertin (18):

$$C_D = C_{D0} + kC_L{}^2 + \Delta C_{D_M} \qquad [20]$$

where C_{D0} is the parasite drag that exists when the configuration generates zero lift; $kC_L{}^2$ is the drag due to lift; and ΔC_{D_M} is the drag associated with compressibility effects. For this analysis, ΔC_{D_M} is zero.

The induced drag factor (k) in equation [20] is an indication of how much drag is associated with the production of lift and is traditionally represented as the slope of the C_D vs. $C_L{}^2$ curve (28):

$$k = \frac{C_D}{C_L{}^2} \qquad [21]$$

Figure 39 shows the C_D vs. $C_L{}^2$ curves associated with the data presented in Figure 38. The trends observed in Figure 39 are also representative of the data related to the other tunnel speeds and flap configurations analyzed in this experiment.

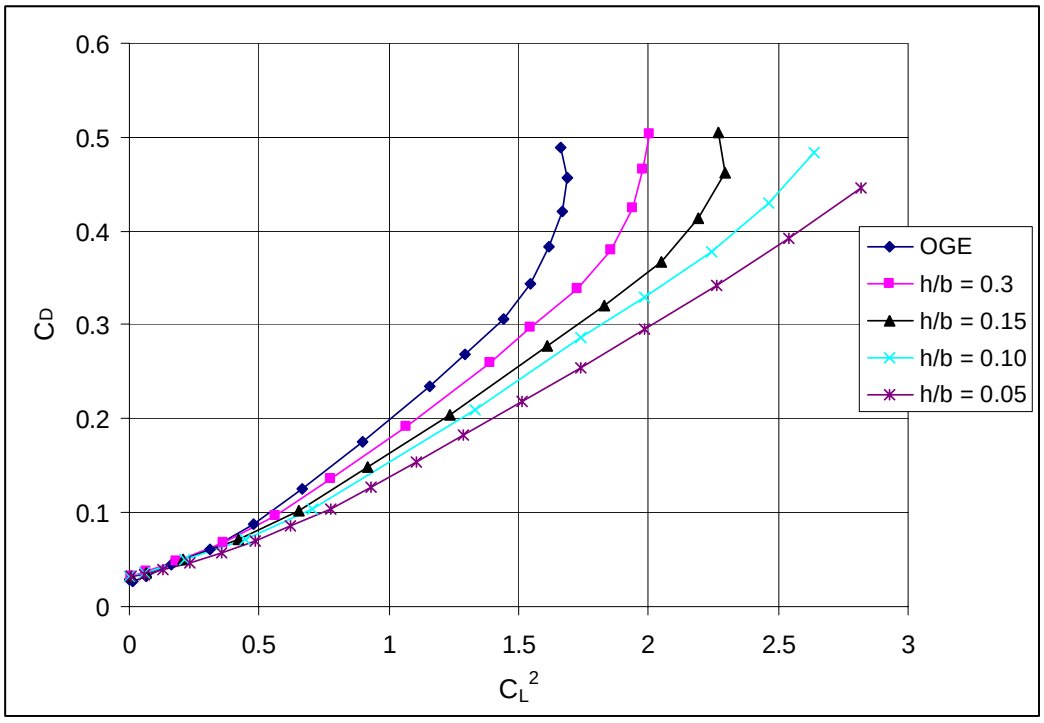

Figure 39: Induced Drag Factor Comparison, Flaps +20^o, Vel. = 100 mph

Because a non-linear relationship exists for the results presented in Figure 39, the k values for each test speed, height-to-span ratio, and flap configuration studied, were determined through a least squares curve fit to the data in the nearly linear region found between $0 \leq C_L^2 \leq 0.5$; the k values are shown in Figure 40. The results reveal several trends: for a given flap deflection angle, k decreases as the UCAV approaches the surface; as the flaps are deflected, the k values decrease as compared to the no-flap configuration, therefore suggesting that the flaps reduce the downwash on the wing; and, in general, as the tunnel speed is increased, the k values decrease. These trends were also characteristic of the chevron UCAV tested by Jones (31) and is due to the fact that the vorticity in the wake, as compared to the vorticity generated OGE, is unable to produce additional downwash on the wing, which would cause the lift vector to rotate aft and produce additional drag (31).

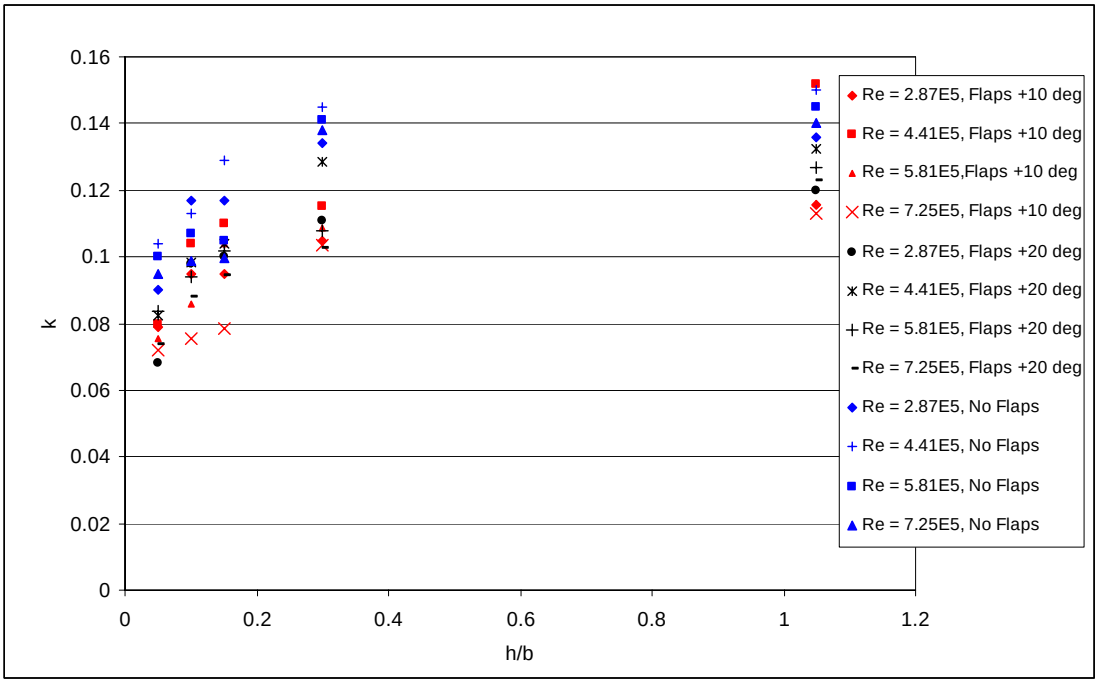

Figure 40: Effect of Height and Flap Deflection on the Induced Drag Factor, k

In order to investigate the theoretical prediction of McCormick's induced drag factor, the k values from Figure 40 were non-dimensionalized by dividing the data by the OGE k values at h/b = 1.05; this method adjusts for the velocity dependent shift seen at each h/b value. From this approach, the non-dimensional k values are comparable to McCormick's induced drag term, ϕ, seen in Equations [6] and [8]. Figure 41 compares the non-dimensional k values of this experiment to McCormick's induced drag factor. From the figure, it can be concluded that even when the flaps are extended, the induced drag experienced by the lambda UCAV IGE, follows the prediction of McCormick's inviscid flow model. A similar agreement was seen for the chevron UCAV tested IGE by Jones (31).

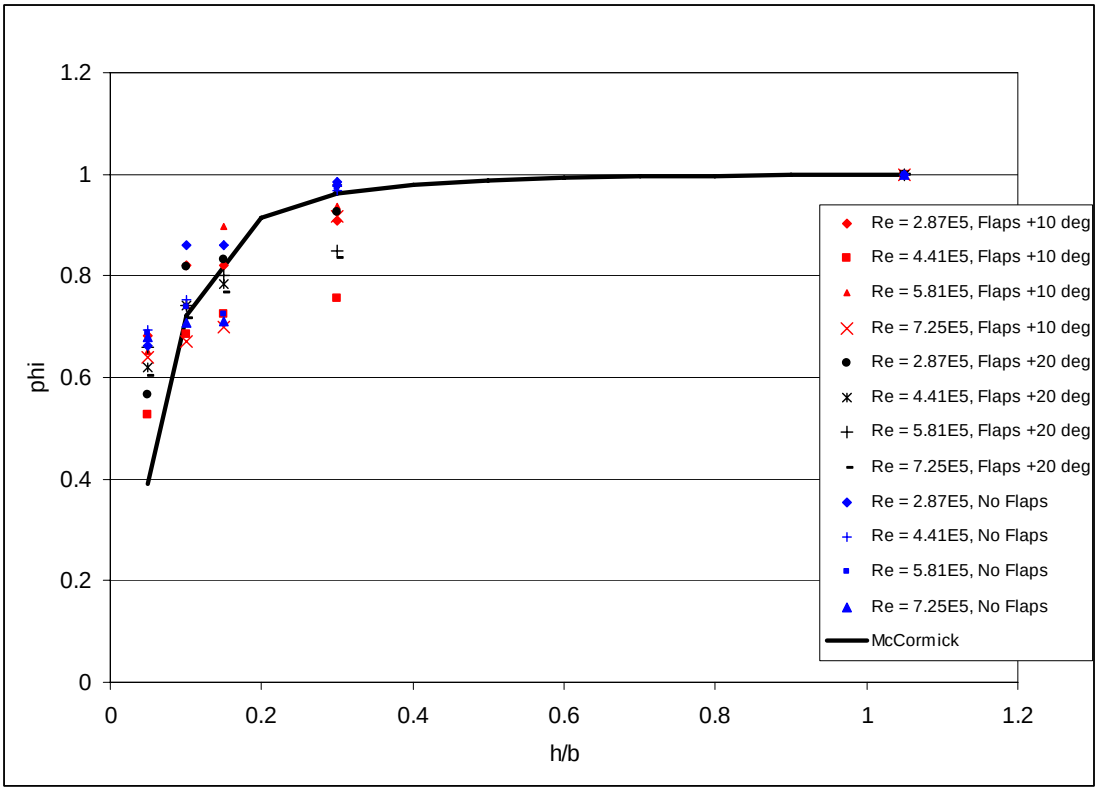

Figure 41: Effect of Height and Flap Deflection on McCormick's Induced Drag Factor

By further analyzing the curve fits for the drag polars, it was possible to estimate the parasite drag coefficients generated throughout the ground effect region for each flap configuration; the results are shown in Figure 42.

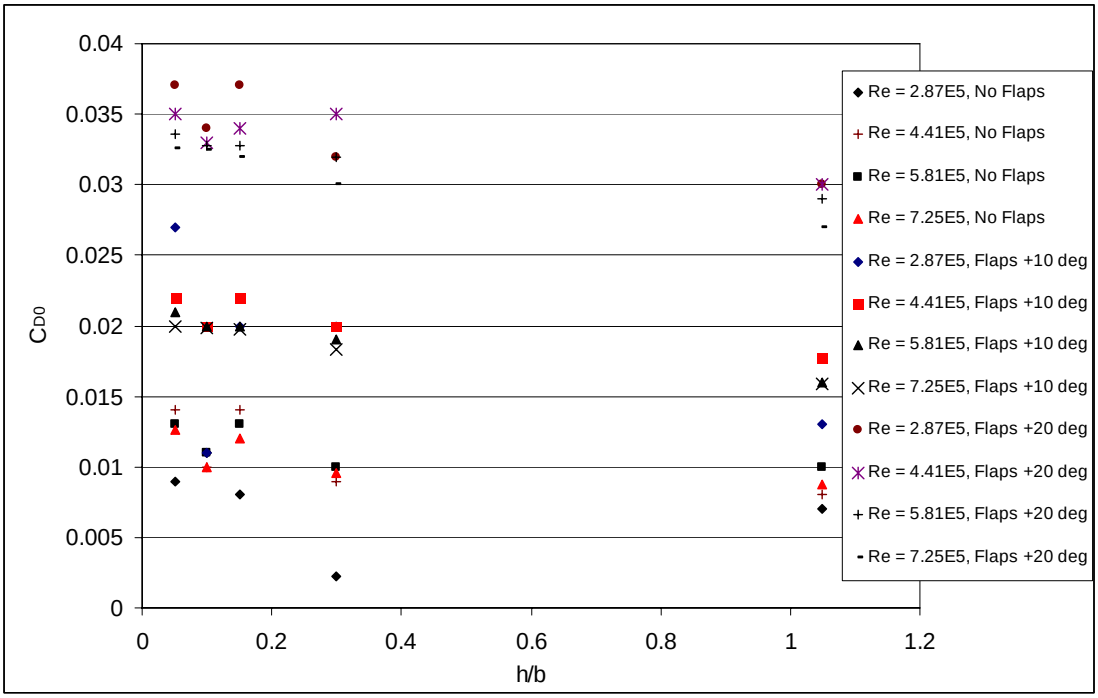

Figure 42: Effect of Height and Flap Deflection on the Parasite Drag

Based on the data presented in Figure 42, the following trends are seen: for a given flap deflection angle, the parasite drag generally increases as the UCAV approaches the ground, and the parasite drag is greater when the flaps are deflected, which is to be expected as the flaps create a greater momentum deficit when they are deployed. The results also indicate a Reynolds number dependence that seems to increase as the UCAV approaches the ground plane. A similar trend was observed for the chevron UCAV but differed in that the Reynolds dependence decreased as the wing approached the surface. It was concluded in reference 31 that the increase in parasite drag and the Reynolds number dependence was possibly a function of the flow separation behavior, in that the separation point remains fixed as the wing moves closer to the surface.

With respect to the drag, it was determined in this section that the drag coefficient increases as the lambda UCAV moves closer to the ground plane. This adverse effect is a result of the parasite drag increase that dominates the induced drag reduction at each angle of attack for a given flap configuration. The drag increase was further amplified as a greater momentum loss was experienced when the flaps were deflected.

Section 2.2.3 – Lift-to-Drag IGE

In an effort to draw some conclusions to the results presented above for the lift and drag and to better understand the complexities of the ground effect region for the lambda UCAV with flaps deployed, the lift-to-drag ratio (L/D) was analyzed. In a typical ground effect study, the L/D is presented in order to show the overall improved or unimproved efficiency that results from flying in close proximity to the ground. Based on the data collected for a nominal tunnel speed of 100 mph, Figures 43-45 illustrate that the L/D generally increases IGE, at positive angles of attack, for the three flap configurations studied in this experiment.

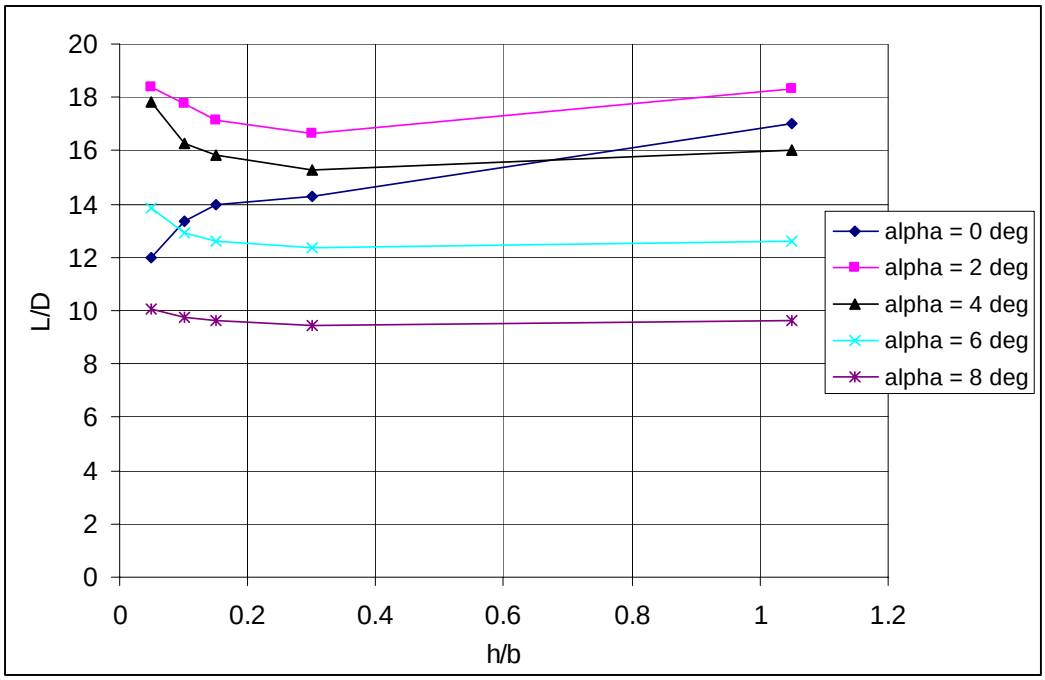

Figure 43: Ground Effect, L/D vs. (h/b), No Flaps, Vel. = 100 mph

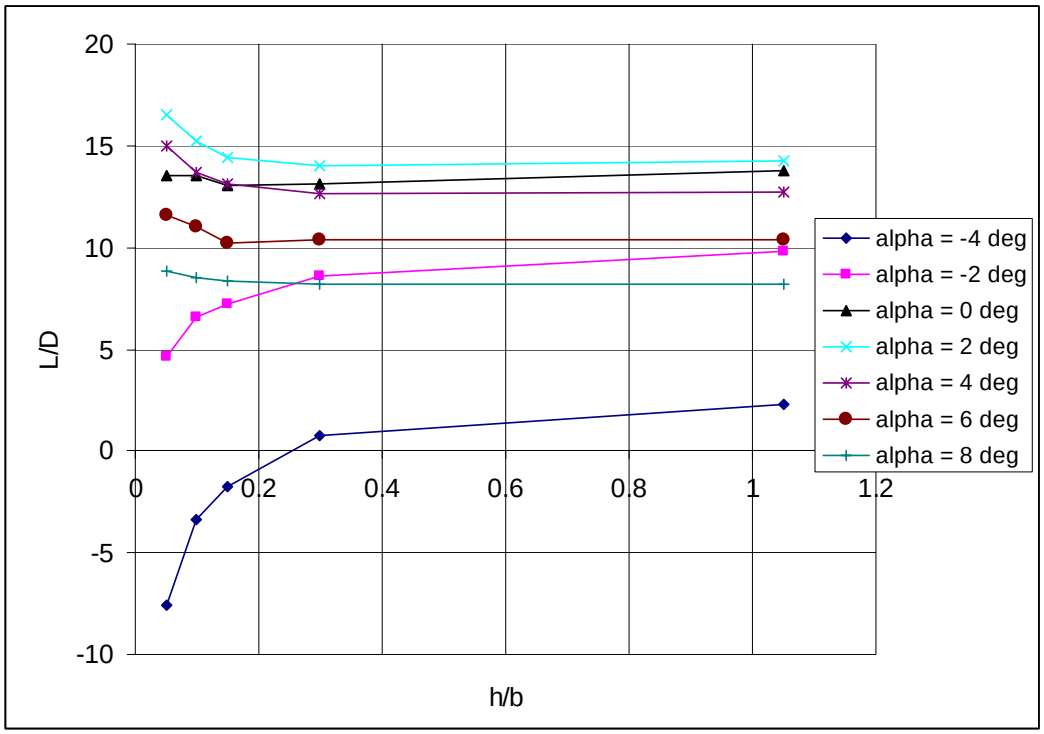

Figure 44: Ground Effect, L/D vs. (h/b), Flaps +10^{o}, Vel. = 100 mph

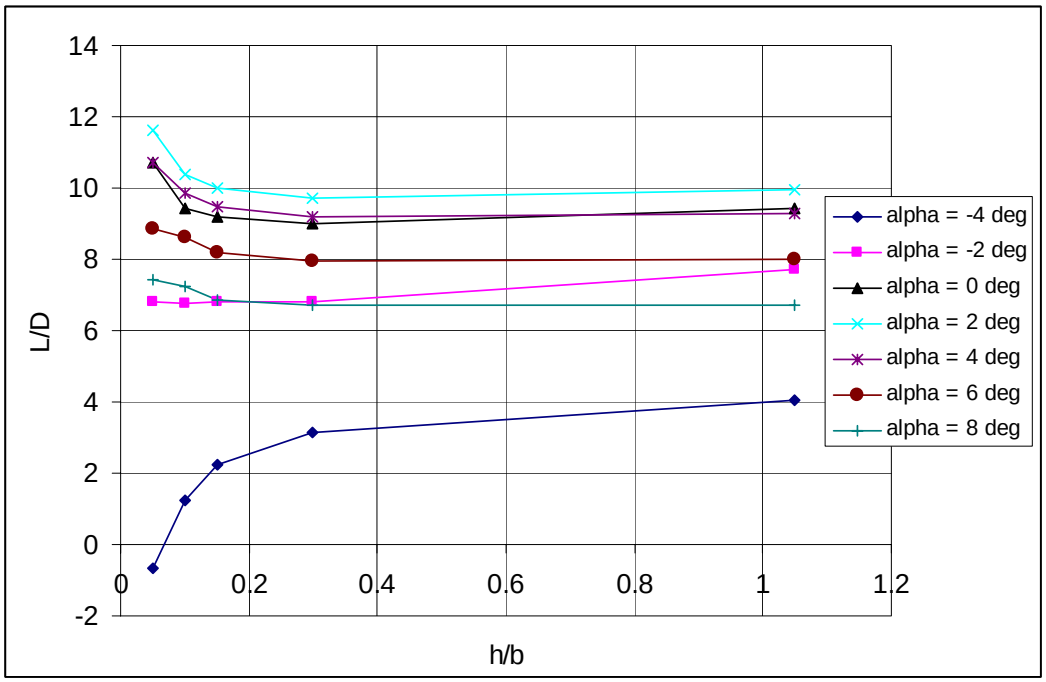

Figure 45: Ground Effect, L/D vs. (h/b), Flaps +20°, Vel. = 100 mph

Based on the data presented in Figures 43-45, the effect of the flap deflections can be quantified by comparing the L/D measured IGE at h/b = 0.05 to the L/D achieved for the no-flap configuration IGE at h/b = 0.05. The results are displayed in Table 17.

Table 17: Effect of Flap Deflections on the L/D IGE

	$\delta_{mid/out} = +10^{o}$	$\delta_{mid/out} = +20^{o}$
AOA	$\%\Delta(L/D)_{IGE(h/b)=0.05}$	$\%\Delta(L/D)_{IGE(h/b)=0.05}$
0	13.0^{+}	10.7
2	10.3	37.0
4	16.0	40.0
6	16.0	36.0
8	11.8	26.0
+ denotes a positive increase		

From the results, it can be concluded that positive deflections of the midboard/outboard trailing edge flaps decreases the overall efficiency of the lambda UCAV at each angle of attack, as compared to the no-flap configuration. This is because

for a given flap deflection angle, the associated increase in drag is greater than the additional lift produced by the flaps and the ground effect region combined. A similar trend was observed in a previous ground effect study by Recant (16) who analyzed a NACA 23012 tapered wing with a full span split flap deflection of $+60^{o}$. Even though Recant tested the wing with a greater flap deflection than that studied in this experiment, his results indicated that the overall efficiency of the wing decreased for a positive split flap deflection IGE. In particular, he noted that the L/D decreased by approximately 46% for the extended flap configuration which is on the same order of magnitude and close in value to the percent differences calculated for the lambda UCAV with a $+20^{o}$ flap deflection.

Based on the results presented in this section, it was determined that for each flap configuration tested, the lift benefits associated with flying in close proximity to the ground outweighed the adverse drag rise and therefore increased the L/D of the lambda UCAV IGE. On the other hand, in terms of the flap effectiveness, it was seen that the incremental drag increase associated with the flap deflections increased the total drag IGE and therefore decreased the L/D as compared to the no-flap UCAV configuration.

Section 3 – Lambda UCAV Flow Visualization

In order to study the flow characteristics of the lambda UCAV, a flow visualization was performed IGE (at the highest ground plane setting) and OGE with the midboard/outboard trailing edge flaps deflected $+20^{o}$. The visualization was achieved by attaching 1.5 in. long string tufts to the upper surface of the model, which were spaced approximately 1 in. apart across the span of the UCAV. The tufts were spaced closer together along the trailing edge in order to adequately reveal the flow around the back

end of the model. The flow visualization was conducted at 40, 60, 80 and 100 mph IGE and OGE. For the IGE runs, the angles of attack studied were: -4^o, 0^o and $+13^o$. For the OGE runs, visualizations were acquired for the following angles of attack: -10^o, 0^o and $+20^o$. Because the flow characteristics varied the most at 100 mph, only the visualizations associated with this test speed are presented.

Section 3.1 – OGE Flow Visualization

The flow characteristics of the lambda UCAV OGE are presented in Figures 46-48. It can be seen that at the angles of attack of -10^o and 0^o, the flow is relatively laminar and remains attached across the span of the upper surface of the model. The pictures also indicate that trailing vortices are shed as the flow curls around the trailing edges of the model from the high pressure region on the lower surface to the low pressure region on the suction side of the airfoil. Unfortunately, no intermediate pictures were taken for angles between 0^0 and $+20^o$, therefore providing limited insight into the separation patterns that lead to stall. On the other hand, it can be seen from Figure 48 that at an angle of attack of $+20^o$, most of the flow over the upper surface of the model has separated; as seen in Figure 22 of Section 2-1.1 , at this angle of attack and flap deflection angle, the lambda UCAV is within the stall region. In addition to the separated flow over the surface, the tuft pattern also indicates a spanwise outflow that is representative of delta wing configurations. Delta wings encounter this effect because at subsonic speeds and high angles of attack, a free shear layer is formed when the boundary layer on the lower surface separates as it flows outward over the leading edge. The shear layer then curves upward and inboard creating a core of high vorticity across the upper

surface of the wing. Beneath this vortex sheet, a spanwise outflow is induced in the direction of the leading edge (18).

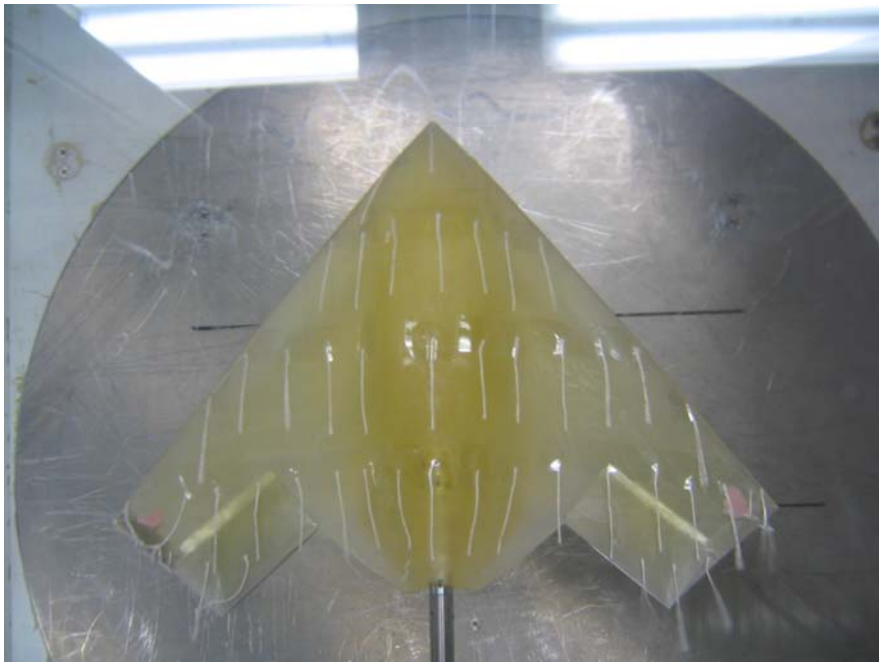

Figure 46: OGE, Vel. = 100 mph, alpha = -10^{o}

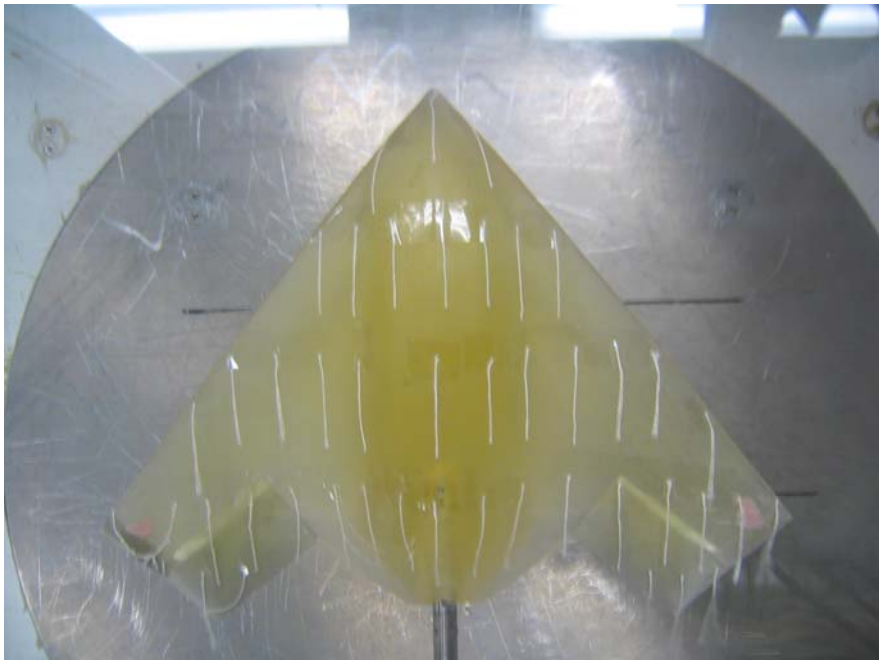

Figure 47: OGE, Vel. = 100 mph, alpha = 0^{o}

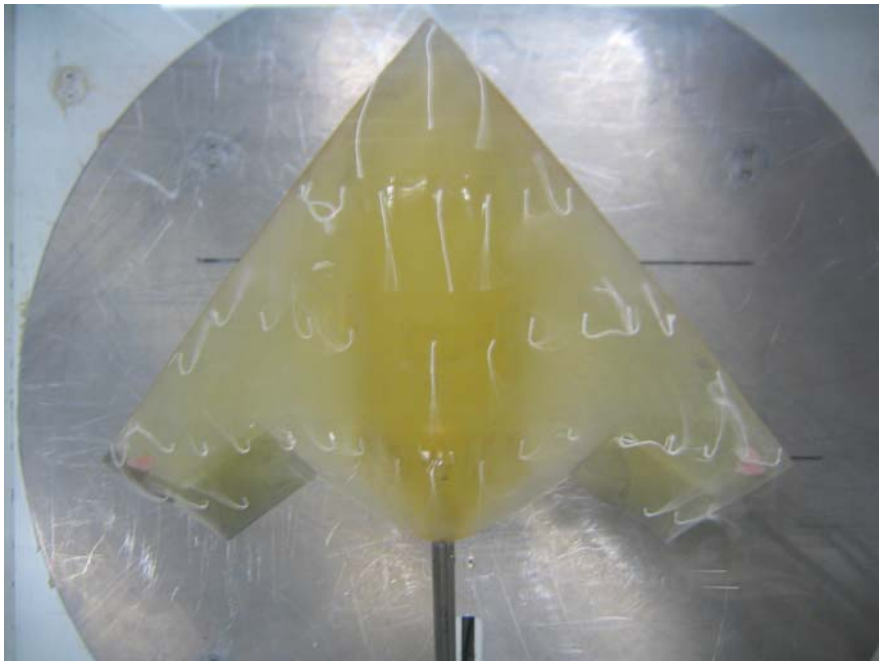

Figure 48: OGE, Vel. = 100 mph, alpha = +20^{o}

Section 3.2 – IGE Flow Visualization

Based on Figures 49-51, it is apparent that the flow remains laminar and well attached to the upper surface of the model for an AOA of -4^{o} and 0^{o}. Unlike the flow pictures obtained for the OGE runs, Figure 51 not only indicates increased circulation around the extended flaps but provides insight into how the wing stalls. Based on the tuft patterns displayed in Figures 48 and 51 it can be concluded that the wing stalls first at the tip and then progresses inward towards the fuselage.

Because flow visualizations were not taken IGE and OGE for the same angles of attack, except at 0^{o}, it was not possible to generalize many of the trends associated with the flow patterns that resulted for the full range of pitch angles studied. Based on Figures 47 and 50, limited insight is revealed into the effects of ground proximity at an angle of attack of 0^{o}. By comparing the outboard tufts along the outboard trailing edge, it can be

concluded that the strength of the wingtip vortices is reduced when the model is placed closest to the ground plane.

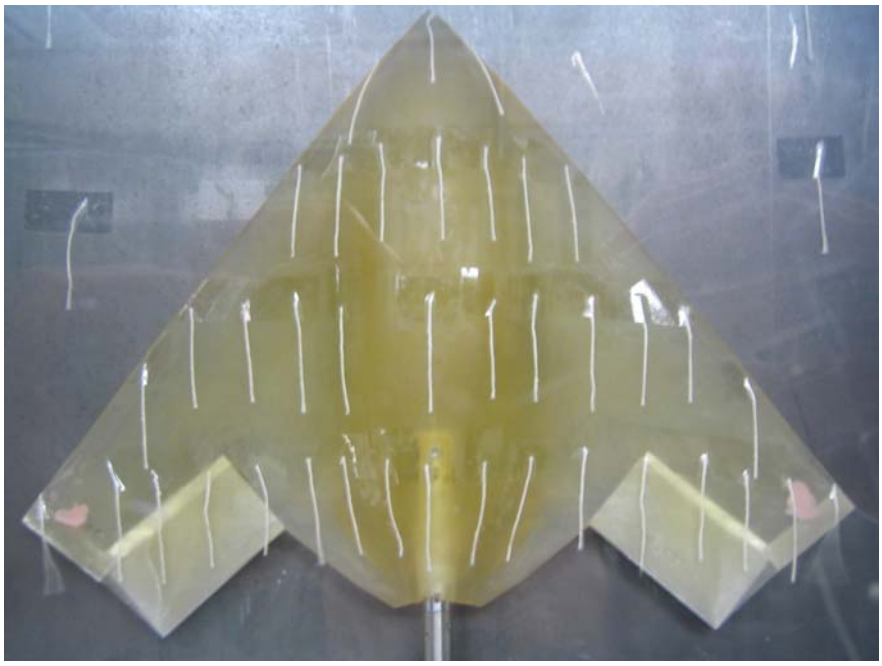

Figure 49: IGE (h/b = 0.05), Vel. = 100 mph, alpha = -4^{o}

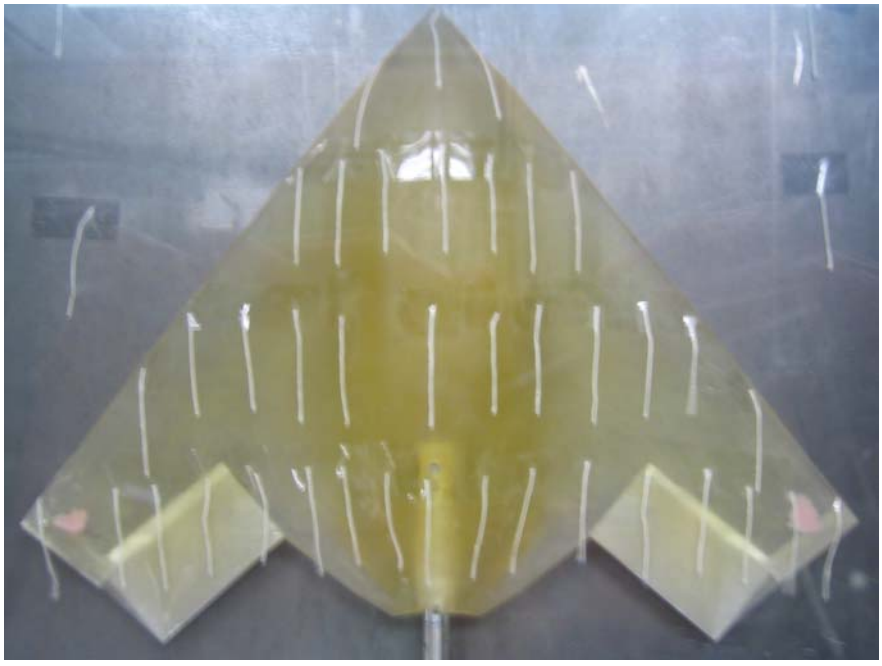

Figure 50: IGE (h/b = 0.05), Vel. = 100 mph, alpha = 0^{o}

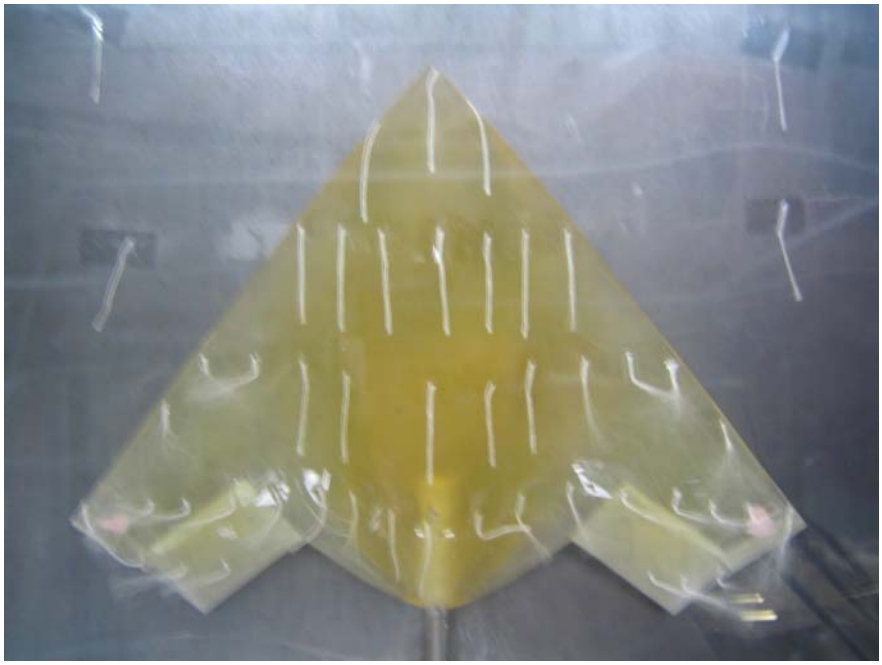

Figure 51: IGE (h/b = 0.05), Vel. = 100 mph, alpha = +13^{o}

Section 4 – Height-to-Span Ratio and Angle of Attack

As was mentioned earlier, the datum chosen as the reference point for vertical measurements above the ground planes was the interface between the 100 lb balance and the wind tunnel balance support; this location was chosen because it was the reference point studied in the previous ground effect research with the lambda model by In. It was hypothesized that for this location, the actual height above the ground planes would vary as the model was swept through the various angles of attack. This concept is illustrated in the Figure 52 below. Based on this diagram, it can be seen that for a given ground plane setting, the height measured with respect to the reference point would increase or decrease depending on the pitch angle. Because of this, the height-to-span ratios should be adjusted to account for this variance which would in turn, alter the ground effect plots that display the UCAV longitudinal characteristics as a function of h/b. In particular, as the angle of attack is increased, the curves for a given alpha should shift to the right.

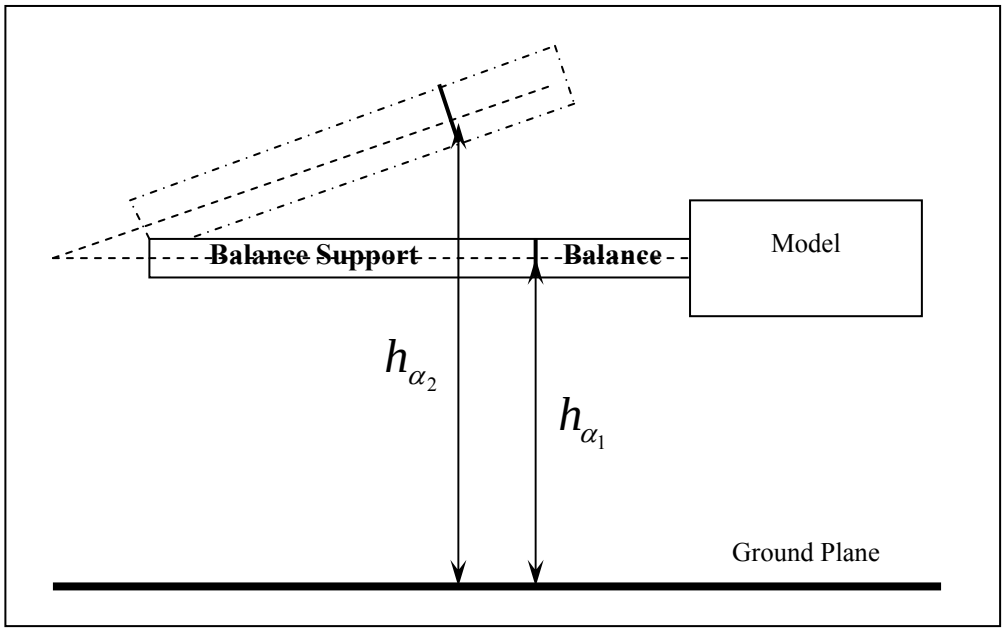

Figure 52: Variance of Height-Span-Ratio with AOA

In order to investigate the validity of this effect, additional measurements were obtained in the wind tunnel. Table 18 lists the vertical heights measured from the balance/support interface to the floor of the tunnel test section for the following pitch angles: $-4^o \leq \alpha \leq 8^o$. Based on these results, it is obvious that for this location, the vertical heights remained relatively constant as the sting mechanism pitched the model through the various angles of attack; therefore, adjustment of the IGE data was not required in this study. If another datum is chosen, such as the nose of the model, this effect will most likely have an impact of the final results. It should be noted that the choice of the reference point from which to measure the distance to the ground is arbitrary and can be varied (16).

Table 18: Variance of (h/b) Datum for Various AOA

AOA (deg)	h (in.)
-4	15.3
-2	15.3
0	15.25
2	15.28
4	15.25
6	15.25
8	15.25

VI. Conclusions and Recommendations

Section 1 – Conclusions

The ground effect region for the lambda UCAV with midboard and outboard flap deflections has been identified. The results indicate that the lift, drag, and the L/D are slightly affected between a height-to-span of 1.05 and 0.3, but vary significantly when $h/b < 0.3$. The variations in lift, drag, and L/D are further amplified for the same conditions when the flaps are deflected.

In terms of the variations in C_L, the results showed that for the no-flap configuration, the lift curve slope increased and the lift axis intercept decreased; for the split flap deflection configurations, the lift curve slope and the lift axis intercept both increased IGE. The lift axis intercept decrease associated with a no-flap, wing configuration has been well documented in previous work and is attributed to the Venturi effect that is generated when the area between the wing and the ground decrease as the airfoil moves closer to the surface. On the other hand, it was concluded that for the flap deflections, the lift axis increase was due to the additional lift generated by the flaps that dominated the lift decrease produced by the Venturi effect. The lift axis increase IGE was noted in other ground effect studies for split flap, wing configurations.

In order to validate the trends associated with the flap effects on the lift, a 2-D VORLAX panel code was used to theoretically predict the C_L variation IGE for a lambda-shaped UCAV. It was noted that the C_L values were not in good agreement to those predicted by the code. In particular, the C_L values were seen to be in better agreement for the no-flap case than when the flaps were deflected; the reason for this

discrepancy is that the panel code models wings as flat plates without camber. Based on this observation, it can be concluded that the VORLAX panel code will better predict the lift changes IGE for a wing without flaps and that a modeling tool that accounts for camber should be used for wings with flap deflections, IGE. However, the lift trends were similar to the VORLAX prediction and illustrated that flap deflections are to enhance the lift benefits associated with flying IGE.

With respect to the drag, it was determined that the drag coefficient increased as the lambda UCAV moved closer to the ground plane. This adverse effect was a result of the parasite drag increase that dominated the induced drag reduction at each angle of attack for a given flap configuration. The IGE drag rise was further amplified as the parasite drag increased from the larger momentum loss experienced when the flaps were set at a greater deflection angle. Because of this, it was determined that flap deflections decrease the L/D as compared to the no-flap case. Even though the L/D was less when the flaps were deflected, the L/D generally increased IGE. In addition, it was also concluded that the reduction of the induced drag IGE, for wings with split flap deflections, was in good agreement with McCormick's induced drag reduction theory.

In terms of the OGE data based on the deflection of the midboard and outboard flaps, it was determined that the longitudinal characteristics of the UCAV followed the trends that are to be expected for an aircraft with high-lift trailing edge devices: the lift curves were incrementally shifted upward without changing the slope; the drag was increased; and a nose-down pitching moment was approached as the flaps were deflected. Additionally, it was shown via a stability analysis that the lambda UCAV is longitudinally unstable whether the flaps are retracted or extended.

In order to determine the flow characteristics of the lambda UCAV IGE and OGE, a flow visualization was performed. The OGE visualization indicated that the flow pattern over the upper surface was similar to that of a delta wing, in that a spanwise outflow, which is characteristic of regions of high vorticity, developed over the suction side, along the entire length of the model at the higher angles of attack. The IGE visualization revealed that the wing of the UCAV will stall first at the tip and then progress inward towards the fuselage. It was also determined that the presence of the ground planes decreased the strength of the wingtip vortices which is to be expected for an aircraft flying in close proximity to the ground.

Section 2 – Recommendations

The results of this study allow for continued research and further investigation into the many facets associated with the flight characteristics of the lambda UCAV; in particular, the inherent aerodynamic behavior that is produced by employing trailing edge flap deflections while flying in-ground-effect. Based on the observations and findings of this study, the following are recommendations for future experiments:

1. Comprehensively analyze the boundary layer growth over the ground planes set for the following height-to-span ratios: 0.3, 0.15, 0.1 and 0.05.
2. Validate the boundary layer data collected in this experiment for a ground plane setting of 0.05.
3. Determine how to properly account for viscous effects in the MATLAB data reduction code.
4. Analyze the flow characteristics of the trailing edge flaps by means of a computational fluid dynamics program.

5. Analyze the effects of positive asymmetric flap deflections on the lateral stability of the lambda UCAV IGE and OGE.
6. Study the effects of deflecting either the midboard or outboard flaps separately.
7. Analyze the effects of using different flap configurations such as a plain flap or slotted flap.
8. Use another flow visualization technique in order to verify the results of the separation pattern over the upper surface of the lambda UCAV.
9. Investigate the affects of measuring h/b from a reference location on the model that varies with angle of attack for a given ground plane setting.

Appendix A: Additional UCAV Pictures

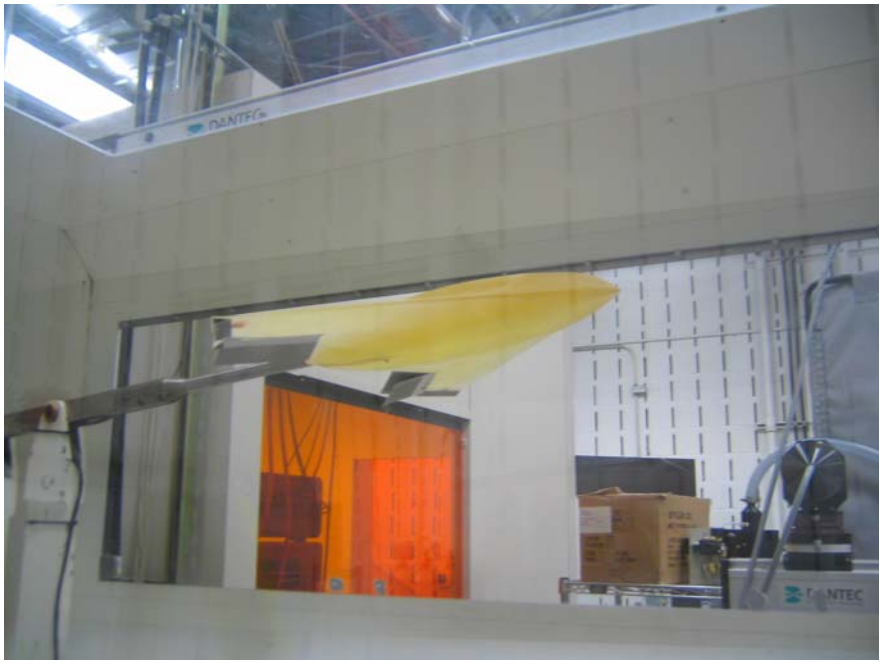

Figure 53: Lambda Model OGE with +20^{o} Symmetric Flap Deflections, AOA = +4^{o}

Figure 54: Lambda Model with +20^{o} Symmetric Flap Deflections, AOA = 0^{o}

Figure 55: Original Lambda UCAV Model

Figure 56: ½-Scaled Lambda UCAV with Mid/Outboard Trailing Edge Split Flaps

Appendix B: Ground Plane Schematics

Listed below in Figures 57-59 are the ground plane dimensions for the circular and front plates, and the mounting legs.

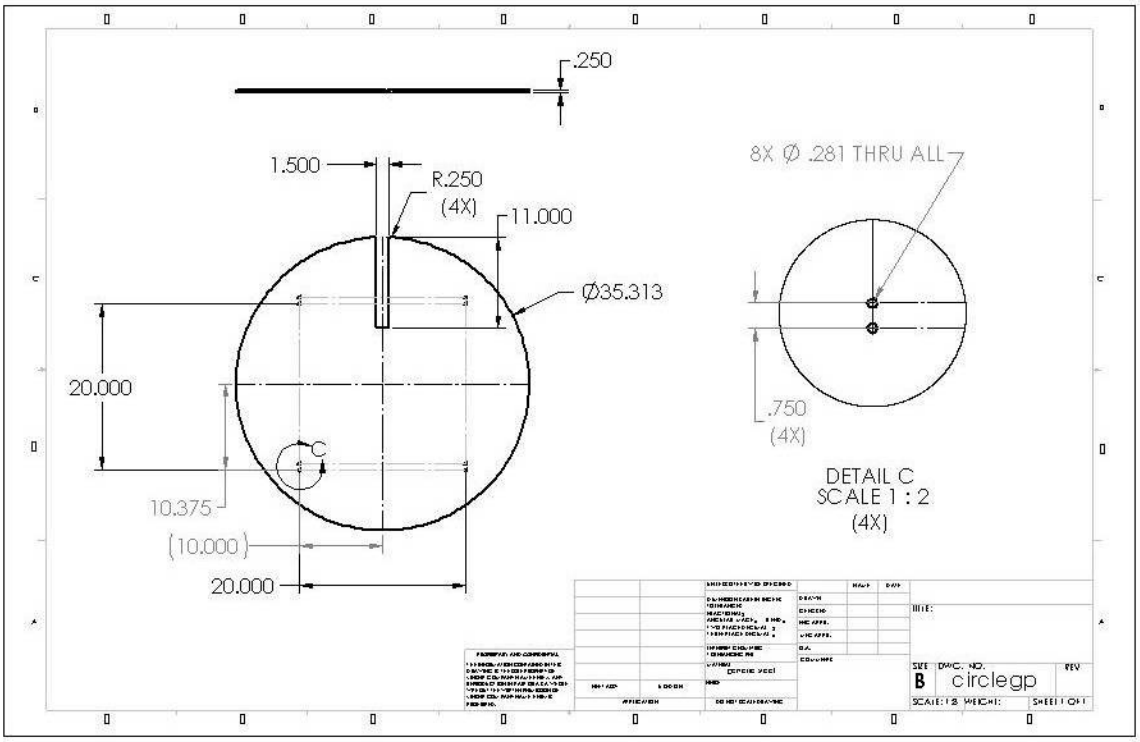

Figure 57: Dimensions of the ground plane circular plate (3)

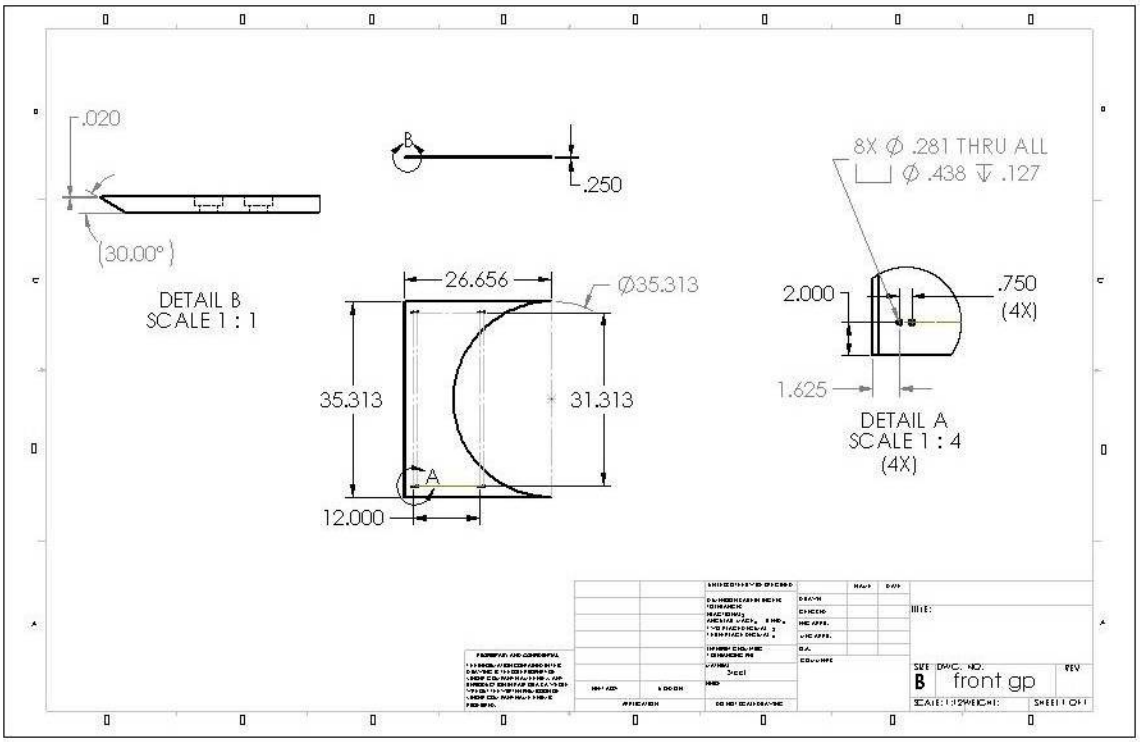

Figure 58: Dimensions of the ground plane front plate (3)

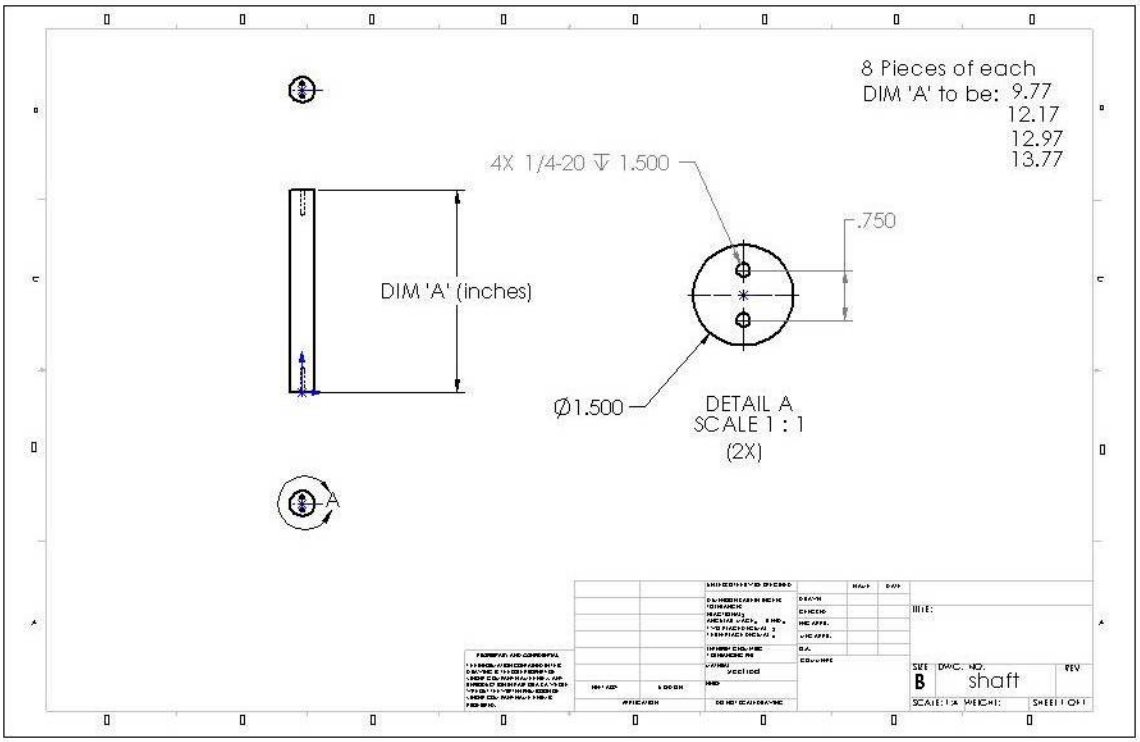

Figure 59: Dimensions of the ground plane mounting legs (3)

Appendix C: MATLAB Data Reduction Sample Calculation

The following section validates the accuracy of the MATLAB reduction code, found in Appendix G**,** used in this experiment to analyze the corresponding data collected by the six-component, strain gage balance. Table 19 lists the experimental test conditions and model specifications that are used in the sample calculation. It should be noted that this calculation corresponds to the wind tunnel tests conducted on the model with a symmetric midboard and outboard flap deflection configuration of $+20^{o}$. Equations 22-24 are used to calculate the density, the dynamic pressure and the speed of sound for the given test room conditions.

$$\rho = \frac{P}{RT} \qquad [22]$$

$$q_{\infty} = \frac{1}{2}\rho U_{\infty}^{2} \qquad [23]$$

$$a = \sqrt{\gamma RT} \qquad [24]$$

Table 19: Model specifications and test room conditions

Model Specifications
$c_r = 0.879$ ft
$S = 0.544$ ft^2
$b = 1.218$ ft
Wing Volume = 0.0317 ft^3
Test Room Conditions
$U_\infty = 60$ mph
$h/b = 0.15$
$\alpha = 2^o$
$T = 534.3^oR$
$P = 14.0187$ psia
$\gamma = 1.4$
$\mu = 0.372x10^{-6} \frac{slug}{ft - \sec}$
$R = 1716 \frac{ft - lb_f}{slug - {}^oR}$
$\rho = 0.0022 \frac{slug}{ft^3}$
$q_\infty = 8.5184 \frac{lb_f}{ft^2}$
$a = 1132.96 \frac{ft}{\sec}$

With an enclosed test section, the tunnel cross-sectional area, as compared to real world conditions, is decreased by the presence of the ground plane and model. As a

result, the air velocity increases in the vicinity of the model and reduces the precision of the balance measurements. This phenomenon is known as solid blockage and is corrected with the following equations (28):

$$\varepsilon_{total} = \varepsilon_{sb,wing} + (\varepsilon_{GP}\varepsilon_{tc} - 1) \quad [25]$$

$$\varepsilon_{sb,wing} = \frac{K_1 \tau_1 * WingVolume}{C^{3/2}} \quad [26]$$

$$\varepsilon_{tc} = \frac{U_{OT}}{U_{Tr}} \quad [27]$$

$$\varepsilon_{GP} = \frac{U_{GP}}{U_{OT}} \quad [28]$$

Where: $\varepsilon_{sb,\ wing}$ = solid blockage correction factor for the model = 9.7122 x 10^{-4}

ε_{GP} = solid blockage correction factor for the ground plane = 1.01

ε_{tc} = transducer correction factor due to differences in velocity measurements between the transducer and hot-wire = 0.911

K_1 = body shape factor, f(t/c) = 1.04

τ_1 = f(B/H, $\frac{2b}{B}$) = 0.83

C = Wind tunnel test section area = 9.4722 ft^2

Based on the above solid blockage correction factors, equations 29-32 are used to correct the following flight parameters, listed in Table 20, for blockage interference.

$$U_{\infty,corr} = U_{\infty} * (1 + \varepsilon_{total}) \quad [29]$$

$$q_{\infty,corr} = q_{\infty} * (1 + \varepsilon_{total})^2 \quad [30]$$

$$M = \frac{U_{\infty,corr}}{a} \quad [31]$$

$$\mathrm{Re} = \frac{\rho * U_{\infty,corr} * c_r}{\mu} \quad [32]$$

Table 20: Corrected Tunnel Flight Parameters for Solid Blockage Effects

Flight Parameter	
$U_{\infty,\,corr},\ \frac{ft}{sec}$	54.8171
$q_{\infty,\,corr},\ \frac{lb_f}{ft^2}$	7.1160
M	0.071
Re	4.1828×10^5

Before converting the forces and moments to the wind axis frame of reference, the following raw data (N_1, N_2, S_1, S_2, A_1, l), collected by the wind tunnel control computer, is adjusted for static tare effects and balance interactions. In order to account for the tare effects, the forces and moments measured by each sensor of the balance are empirically fit to a fourth order polynomial and then subtracted from the forces and moments that are collected during a corresponding dynamic test. Once the tare effects are removed, the forces and moments are corrected for the interactions that exist between the balance sensors. This step is necessary because every balance, to some degree, has inherent errors associated with the proximity between rosettes and the fact that each sensor is not perfectly perpendicular to another sensor; therefore, if a load is applied to one sensor, the

others will ultimately sense a component of that force (9). The computations associated with the tare and balance effects are beyond the scope of this sample calculation; a comprehensive discussion of this process can be found in Rivera (9). Table 21 lists the corrected forces and moments for the tare and balance effects that are obtained from Section VI, line 472 (Corrected_Data = (inv(Interactions_Kij) * Forces_minus_tare), of the MATLAB reduction code; it should be noted that the pitch angle, θ, and the yaw angle, ψ, are not computed in the above line of code but are obtained from the actual wind tunnel balance test files.

The values presented in Table 21 are required to convert the corrected data, measured initially in the UCAV's body axis, to the wind axis. Equations 33 and 34 convert the drag, side, and lift forces [D S* L] and the roll, pitch, and yaw moments [l m n] into the wind axis frame (28).

Table 21: Corrected Balance Measured Forces and Moments

$A = A_1$ corrected	0.164767 lb_f
$Y = S_1$ corrected	0.001518 lb_f
$N = N_1$ corrected	3.951459 lb_f
l = l corrected	0.037174 lb_f-in
$m = N_2$ corrected	-1.650225 lb_f-in
$n = S_2$ corrected	0.010705 lb_f-in
θ	0.1047 rad = 6^o
ψ	0^o

$$\begin{bmatrix} D \\ S^* \\ L \end{bmatrix}_{wind} = \begin{bmatrix} A\cos\theta\cos\psi + Y\sin\psi + N\sin\theta\cos\psi \\ -A\sin\psi\cos\theta + Y\cos\psi - N\sin\theta\sin\psi \\ -A\sin\theta + N\cos\theta \end{bmatrix} \quad [33]$$

$$\begin{bmatrix} l \\ m \\ n \end{bmatrix}_{wind,bc} = \begin{bmatrix} l\cos\theta\cos\psi - m\sin\psi + n\sin\theta\cos\psi \\ l\sin\psi\cos\theta + m\cos\psi + n\sin\theta\sin\psi \\ -l\sin\theta + n\cos\theta \end{bmatrix}_{body,bc} \quad [34]$$

Based on the above force equations, the following values for drag, side force and lift force, in the wind axis, are computed:

$$D = 0.245 \text{ lb}_f$$

$$S^* = 0.0122 \text{ lb}_f$$

$$L = 2.2941 \text{ lb}_f$$

Because a proper stability analysis reports the moments about the center of mass of an aircraft, it is necessary to transfer the moments measured at the balance center to the center of mass of the UCAV model by applying the following equations (28):

$$\begin{bmatrix} l_{w_{cm}} \\ m_{w_{cm}} \\ n_{w_{cm}} \end{bmatrix} = \begin{bmatrix} l_{w_{bc}} + S^* * z_{cm} + L * y_{cm} \\ m_{w_{bc}} - L * x_{cm} + D * z_{cm} \\ n_{w_{bc}} - D * y_{cm} - S^* * x_{cm} \end{bmatrix} \quad [35]$$

where $[x_{cm}\ y_{cm}\ z_{cm}]$ are the model center of mass coordinates in the wind axis. Since the model CG and balance centerline are located along the longitudinal axis: $x_{cmb} = 2.125$ in., $y_{cmb} = z_{cmb} = 0$. Equations 36-38 are used to calculate $[x_{cm}\ y_{cm}\ z_{cm}]$ (9); the results are listed in Table 22.

$$x_{cg,dist} = \sqrt{x_{cmb}^{\ 2} + z_{cmb}^{\ 2}} \quad [36]$$

$$w = \tan^{-1}\left(\frac{-z_{cmb}}{x_{cmb}}\right) \quad [37]$$

$$\begin{bmatrix} x_{cm} \\ y_{cm} \\ z_{cm} \end{bmatrix} = \begin{bmatrix} x_{cg,dist}\cos(\theta + w)\cos\psi \\ y_{cmb} + x_{cm}\tan\psi \\ -x_{cg,dist}\sin(\theta + w) \end{bmatrix} \quad [38]$$

Table 22: Model Center of Mass and Corresponding Moments

x_{cm}, in.	2.2137
y_{cm}, in.	0
z_{cm}, in.	-0.0472
$l_{w_{cm}}$, lb_f-in	0.036
$m_{w_{cm}}$, lb_f-in	0.9916
$n_{w_{cm}}$, lb_f-in	-0.0351

Non-dimensionalizing the lift, side force, and moments yields:

$$C_{L_w} = \frac{L}{q_{\infty,corr} * S} = 0.59282$$

$$C_{Y_w} = \frac{S^*}{q_{\infty,corr} * S} = 0.0031587$$

$$C_{l_{cg}} = \frac{l_{cg}}{q_{\infty,corr} * S * \bar{c}} = 6.359\text{x}10^{-4}$$

$$C_{m_{cg}} = \frac{m_{cg}}{q_{\infty,corr} * S * \bar{c}} = 0.04927$$

$$C_{n_{cg}} = \frac{n_{cg}}{q_{\infty,corr} * S * \bar{c}} = \text{-6.1977x10}^{-4}$$

Note: center of mass and center of gravity are used interchangeably as subscripts but mean the same thing.

Finally, equations 39-44 are applied to the drag force in order to correct for test section geometry and flow field interference and to the angle of attack to correct for upwash effects (9). The results are listed in Table 23.

$$C_{D,corr} = C_{D_u} + \Delta C_{D_w} \quad [39]$$

$$\alpha_{corr} = \alpha + \Delta\alpha_w \quad [40]$$

where:

$$\delta = \frac{b}{B} \quad [41]$$

$$\Delta C_{D_w} = \frac{\delta * S}{C}(C_{L_w})^2 \quad [42]$$

$$C_{D_u} = \frac{D}{q_{\infty,corr} * S} \quad [43]$$

$$\Delta\alpha_w = \frac{57.3 * \delta * S * C_{L_w}}{C} \quad [44]$$

Table 23: Drag Coefficient Correction Factors

δ	0.3322
ΔC_{D_w}	0.0067
C_{D_u}	0.0633
$C_{D,corr}$	0.0700
$\Delta\alpha_w$	0.6479^o
α_{corr}	2.6478^o

Table 24 summarizes the results obtained from this sample calculation and compares them to the results calculated by the MATLAB data reduction code. It is obvious from the table that a majority of the flight parameters are in good agreement with an exception for the roll moment coefficient that is shown to have a 29.8% discrepancy.

Table 24: MATLAB Reduction Code Flight Parameter Comparison

Flight Parameter	**Sample Calculation**	**MATLAB Code**	**Percent Error**
C_L	0.59282	0.59283	0
C_D	0.07000	0.07001	0
C_Y	0.00315869	0.00316	0.04
C_l	0.0006359	0.00049	29.77
C_m	0.04927	0.05642	12.67
C_n	-0.00061977	-0.0006	3.295

Appendix D: Ground Plane Boundary Layer Analysis

Based on the preliminary, theoretical boundary layer analysis presented in Chapter II, Section 2.1, it was determined that at the highest ground plane setting (h/b = 0.05) and a nominal test speed of 100 mph, the lambda UCAV would not interfere with the boundary layer. In order to obtain a more comprehensive look at the actual boundary layer development over the ground planes in the tunnel, several hot-wire experiments were conducted as outlined in Chapter IV, Section 1.2. Unfortunately, due to the limitations of the traversing mechanism in the +z-direction, the hot-wire could not be placed close enough to the lower ground plane settings (h/b = 0.3, 0.15, 0.1) and therefore within the boundary layer. As a result, it was only possible to acquire the velocity profiles over the highest ground plane setting (h/b = 0.05).

The velocity profiles obtained from the hot-wire tests are shown in Figures 60 and 61. In reference to these figures, several things should be noted: only the nominal test speeds of 40 and 100 mph were studied because it would provide the minimum and maximum boundary layer thicknesses that could develop over a given ground plane; the boundary layers related to the other two test speeds of 60 and 80 mph should fall within these two extremes and would only be redundant to present; the corrected velocities ($U_{\infty,corr}$) accounting for blockage effects are validated when comparing the profile velocities in Figures 60 and 62 to those seen in Table 11; for the ground plane set at h/b = 0.05, the corrected velocities for the nominal tunnel speeds of 40 and 100 mph are: 36.52 and 90.88 mph, respectively. In addition, the x-locations specified in each figure correspond to the distances measured from the leading edge of the ground plane where

the hot-wire probe was positioned for data acquisition. For h/b = 0.05, the closest the hot-wire could have been placed to the ground plane without touching the surface was ½ in.

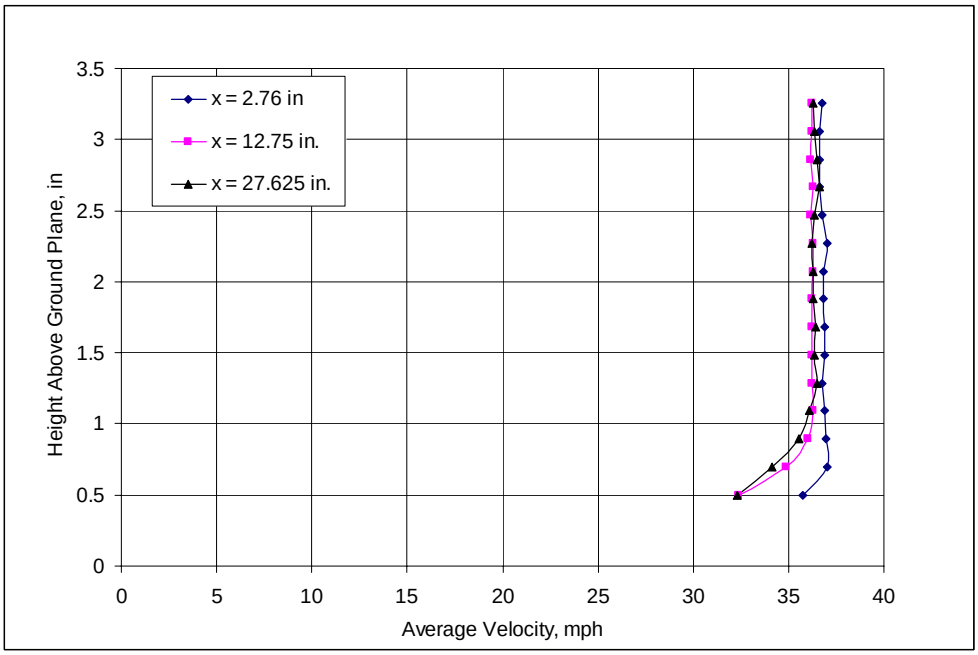

Figure 60: Boundary Layer Velocity Profiles, h/b = 0.05, $U_{\infty,corr}$ = 36.52 mph

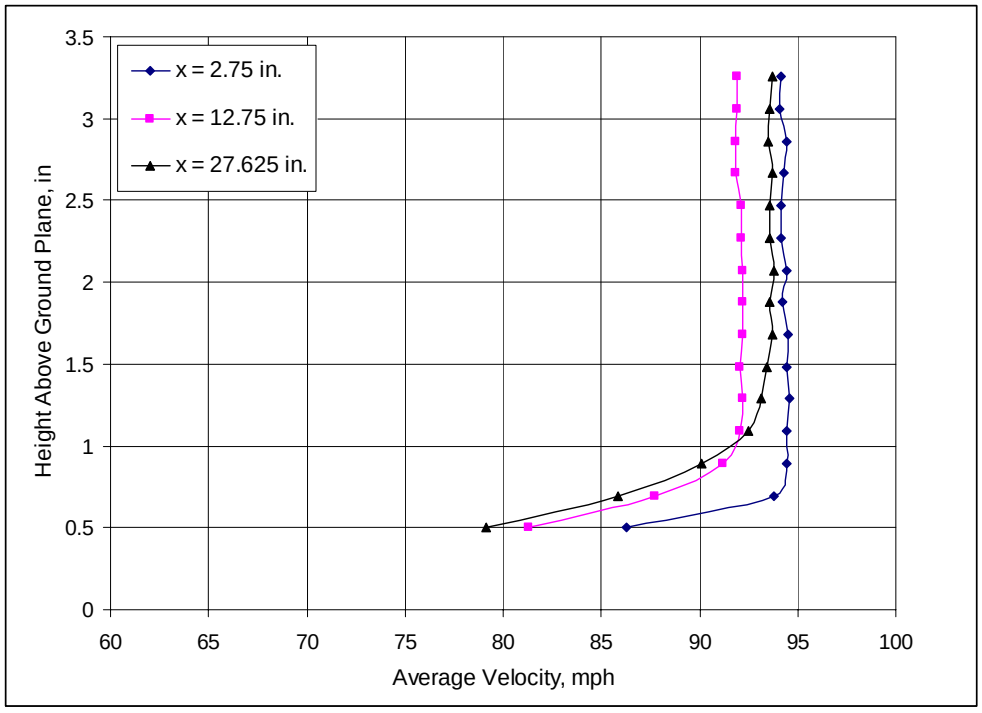

Figure 61: Boundary Layer Velocity Profiles, h/b = 0.05, $U_{\infty,corr}$ = 90.88 mph

Based on the velocity profiles at these two test speeds, the general boundary layer shapes, in terms of the boundary layer thickness, were estimated by noting the vertical heights where the velocities became nearly constant. Figure 62 displays the approximate boundary layer shapes that developed over the highest ground plane for 40 and 100 mph. Because velocity measurements were not acquired at the leading edge of the flat plate, the boundary layer was assumed to be zero at that location; in reality this might not have been the case but because the plate leading edge is well upstream of the UCAV, it is not of much interest to accurately model.

Figure 62 also compares the boundary layer thicknesses obtained from the hot-wire data to the theoretical boundary layer thicknesses determined from the conventional flat-plate laminar and turbulent boundary layer equations (see Equations 11 and 13), for the corrected tunnel velocities of 36.52 and 90.88 mph. It is clear from Figure 62 that the theoretical boundary layer equations have substantially under-predicted the boundary layer thickness and indicate that the boundary layer under the UCAV is in transition, whereas the hot-wire data collected in this study provides limited insight into the state of the boundary layers for the same x-locations. The reason for these discrepancies are unclear and further analysis will be required to substantiate the boundary layer data collected in this study. A possible explanation for these discrepancies might be how the flow curls around the leading edge of the ground plane. Even though the boundary layer thicknesses are not validated with theory, the remainder of this section will present a boundary layer analysis associated with the hot-wire data measured in this experiment.

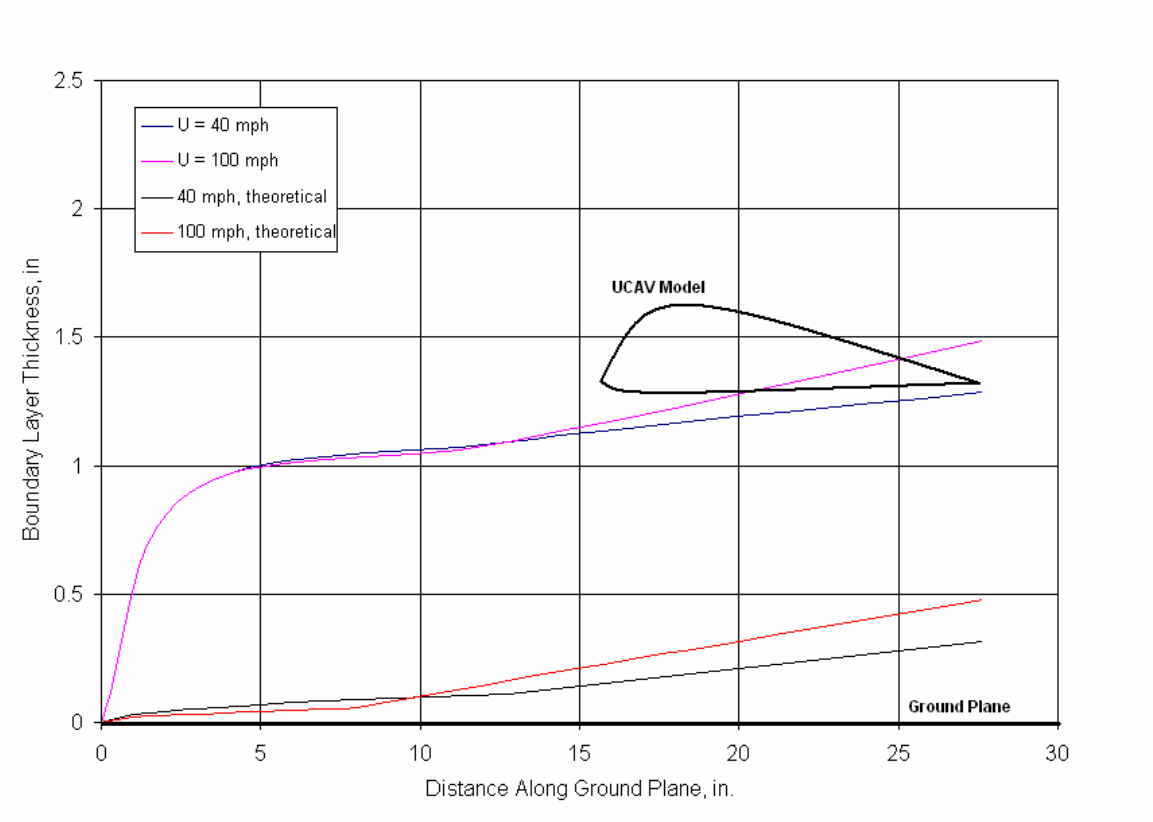

Figure 62: Ground Plane Boundary Layer Comparison, h/b = 0.05

From the results shown in Figure 62, it is possible to determine if the lambda UCAV was within the boundary layer during the tests conducted for a ground plane setting of h/b = 0.05 and an alpha sweep of -4° to +13°. Two key model positions were studied: the nose, which varied the most in the vertical direction with respect to the changing angles of attack; and the trailing edge which remained constant in the vertical axis for each angle tested. Table 25 compares the vertical positions of these two model locations, measured for the limiting angles of attack, to the corresponding boundary layer thicknesses as approximated from Figure 62.

Table 25: Boundary Layer Comparison, h/b = 0.05

	$\alpha = -4^o$	$\alpha = 0^o$	$\alpha = +13^o$
x_{nose}	16.63”	16.63”	16.63”
z_{nose}	0.56”	1.31”	3.75”
$x_{t.e}$	27.38”	27.38”	27.38”
$z_{t.e}$	1.0”	1.0”	1.0”
40 mph			
δ_{nose}	1.20”	1.20”	1.20”
$\delta_{t.e.}$	1.25”	1.25”	1.25”
100 mph			
δ_{nose}	1.25”	1.25”	1.25”
$\delta_{t.e.}$	1.49”	1.49”	1.49”

This first thing to note from Table 25 is that throughout the entire range of angles and speeds tested, some part of the lambda UCAV was within the boundary layer at h/b = 0.05. Because the nose of the model varied the most with angle of attack, it was only exposed to the boundary layer between -4^o and 0^o. On the other hand, the trailing edge was located near the point about which the model was pitched and therefore remained constant at about 1in. above the plate surface. For this vertical height, the boundary layer is seen to have extended well above 1.0 in. for each angle tested. It should be mentioned that the trailing edge height was measured for the no-flap configuration. For the two flap deflections studied in this experiment, $+10^o$ and $+20^o$, the trailing edge of the model would extend further into the boundary layer. Table 26 lists the vertical distances that the model extended into the boundary layer at the trailing edge for the two flap deflection angles; because the trailing edge of the flaps were located near the point of rotation, the vertical heights did not change with pitch, therefore, they are not presented for the various angles tested.

Table 26: Vertical Extensions of Trailing Edge Flaps into the Boundary Layer, h/b=0.05

δ_f	$+10^o$	$+20^o$
40 mph	0.51”	0.76”
100 mph	0.75”	1.0”

It is evident from the boundary layer analysis conducted in this experiment that a significant discrepancy exits between the theoretical predictions and the measured data, but based on the hot-wire results, it was concluded that the UCAV is within the boundary layer at the closest ground plane setting, and that a boundary layer removal technique, such as a moving belt ground plane, might need to be employed in future ground effect studies for h/b = 0.05. Because the hot-wire could not be placed close enough to the surface of the other ground planes, further investigation is necessary in order to accurately identify the boundary layer growth for h/b = 0.3, 0.15, and 0.1.

Appendix E: Additional Plots

The following are additional plots associated with the longitudinal flight characteristics OGE and IGE for various flap deflection configurations. It should be noted that the additional ground effect plots presented in this Appendix are based on symmetric deflections of the midboard and outboard trailing edge flaps.

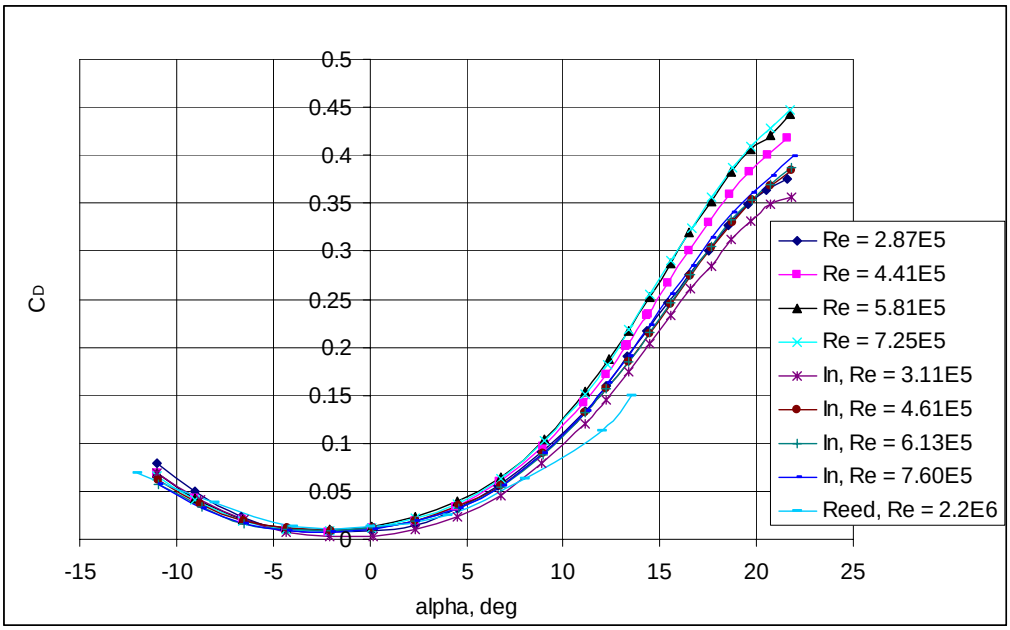

Figure 63: C_D vs. AOA, OGE, No Flaps

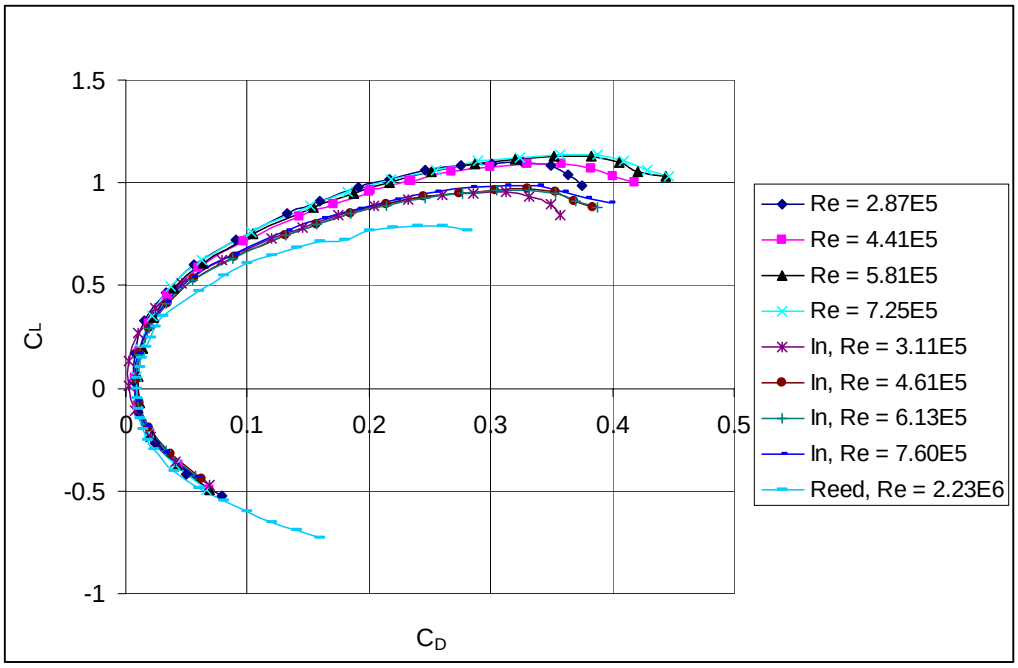

Figure 64: C_L vs. C_D, OGE, No Flaps

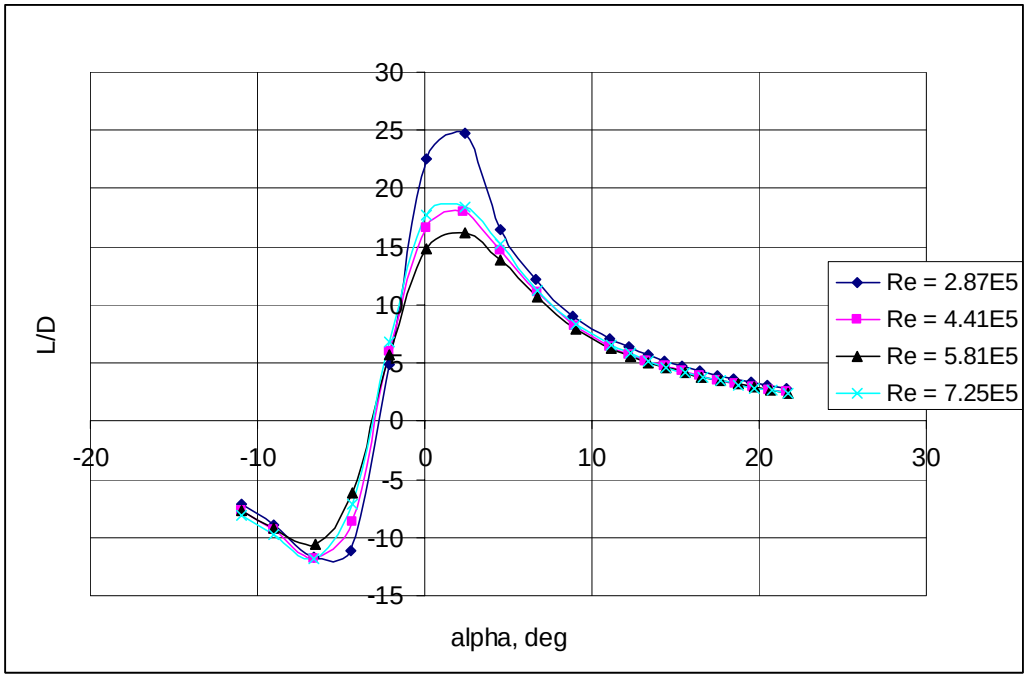

Figure 65: L/D vs. AOA, OGE, No Flaps

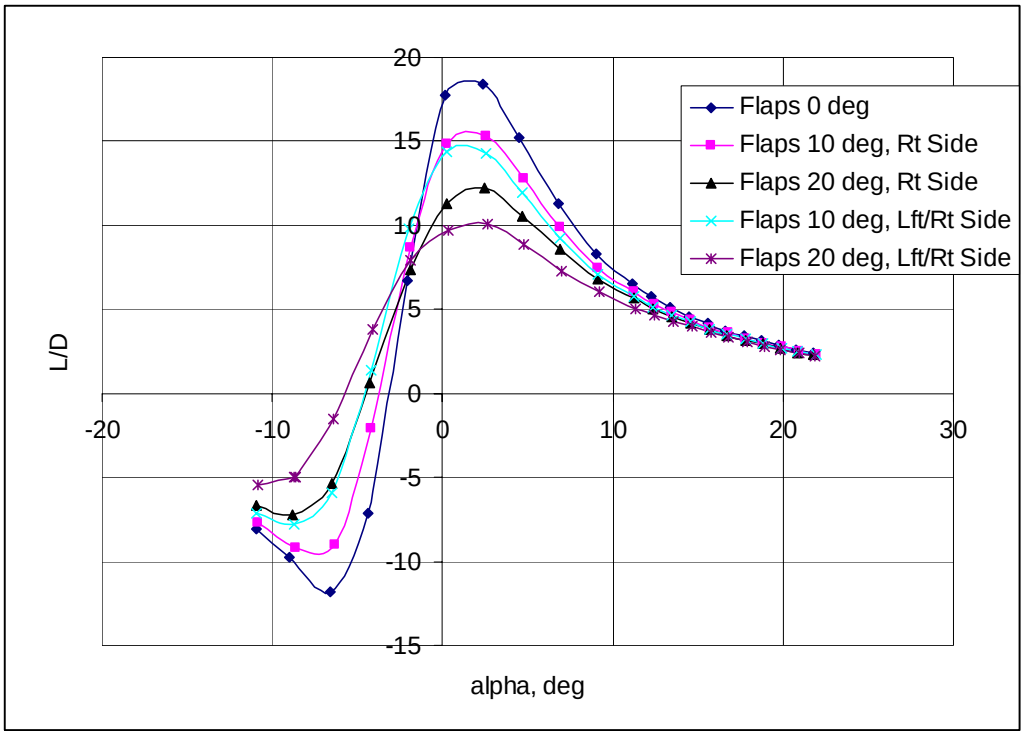

Figure 66: L/D vs. AOA, OGE, Flap Deflection Comparison, Vel. = 100 mph

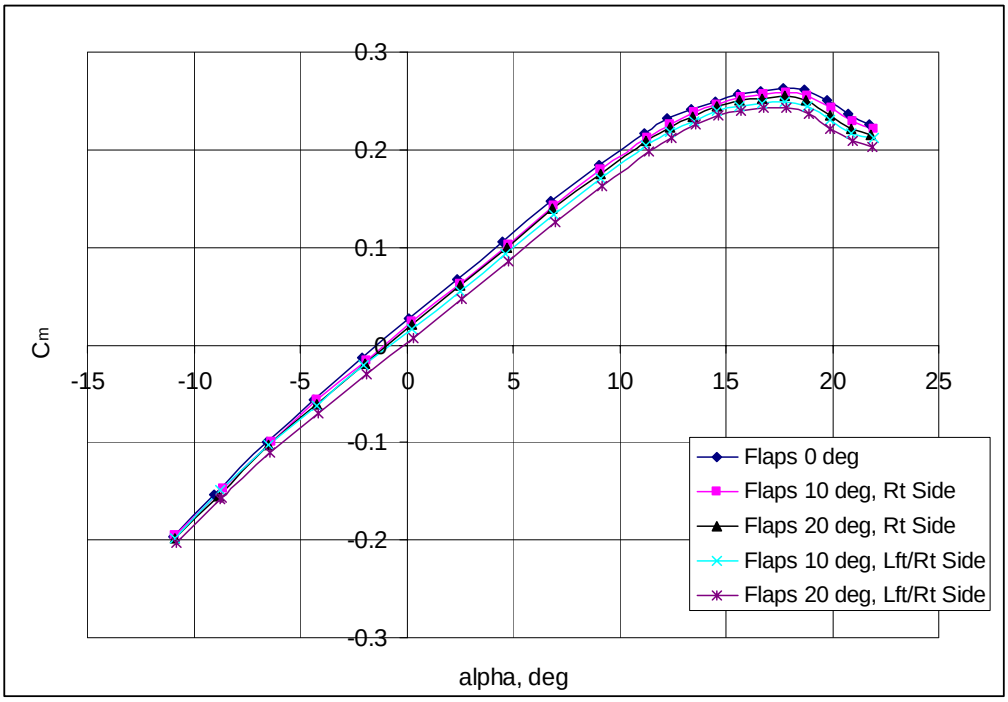

Figure 67: C_m vs. AOA, OGE, Flap Deflection Comparison, Vel. = 100 mph

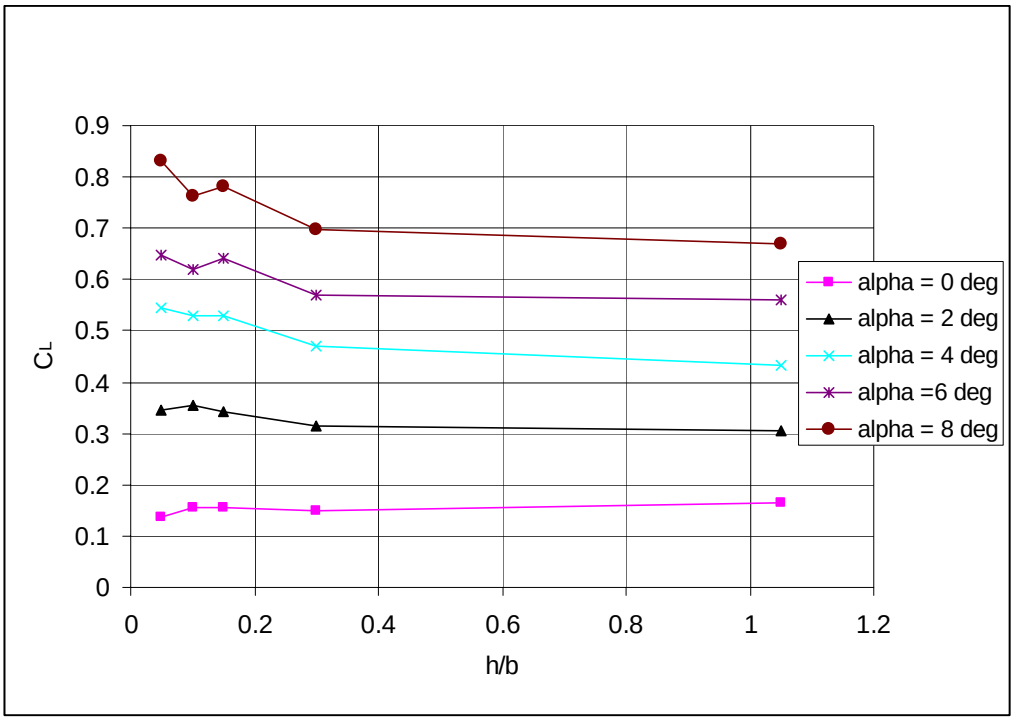

Figure 68: Ground Effect, C_L vs. (h/b), No Flaps, 40 mph

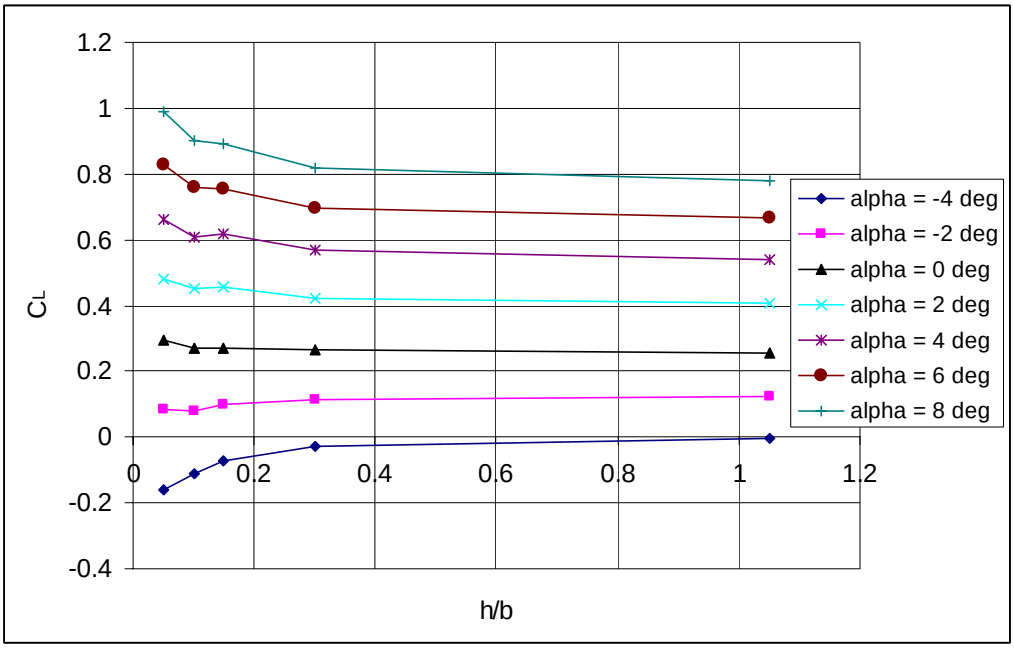

Figure 69: Ground Effect, C_L vs. (h/b), Flaps +10^o, 40 mph

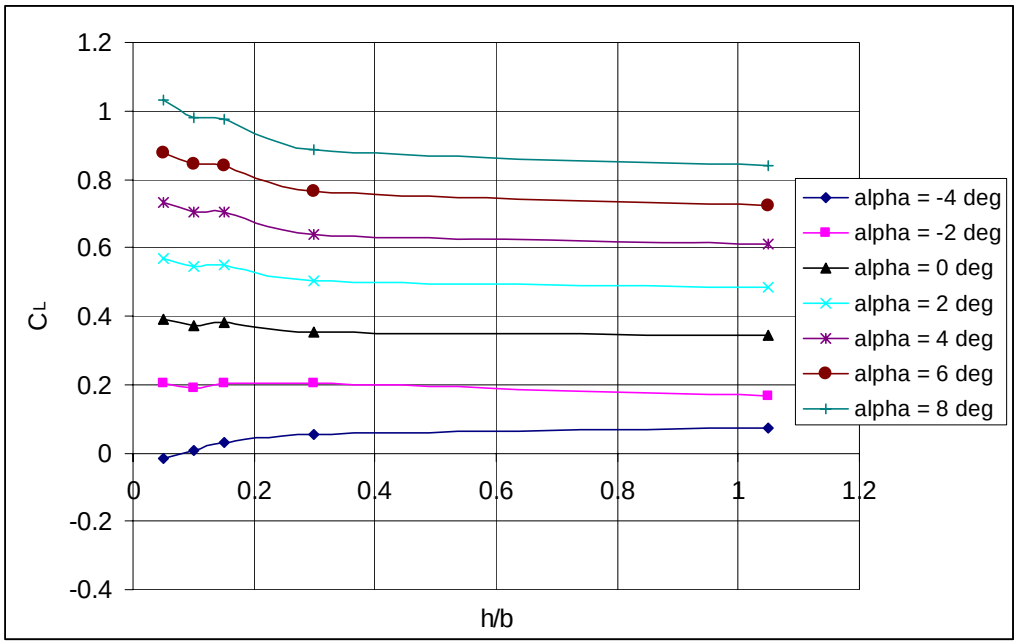

Figure 70: Ground Effect, C_L vs. (h/b), Flaps +20°, 40 mph

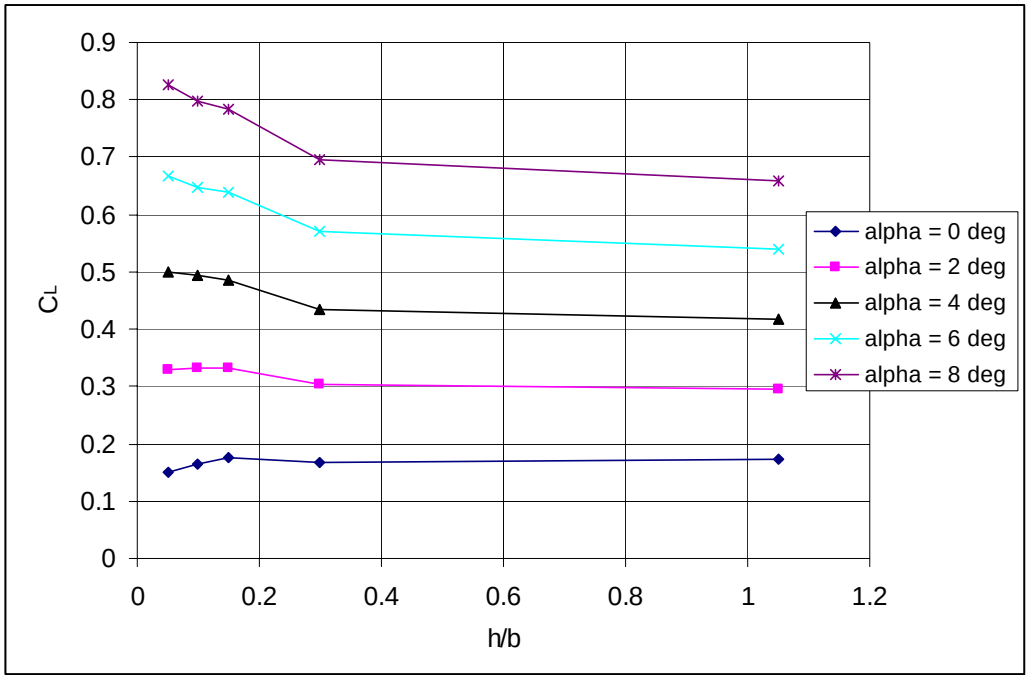

Figure 71: Ground Effect, C_L vs. (h/b), No Flaps, 60 mph

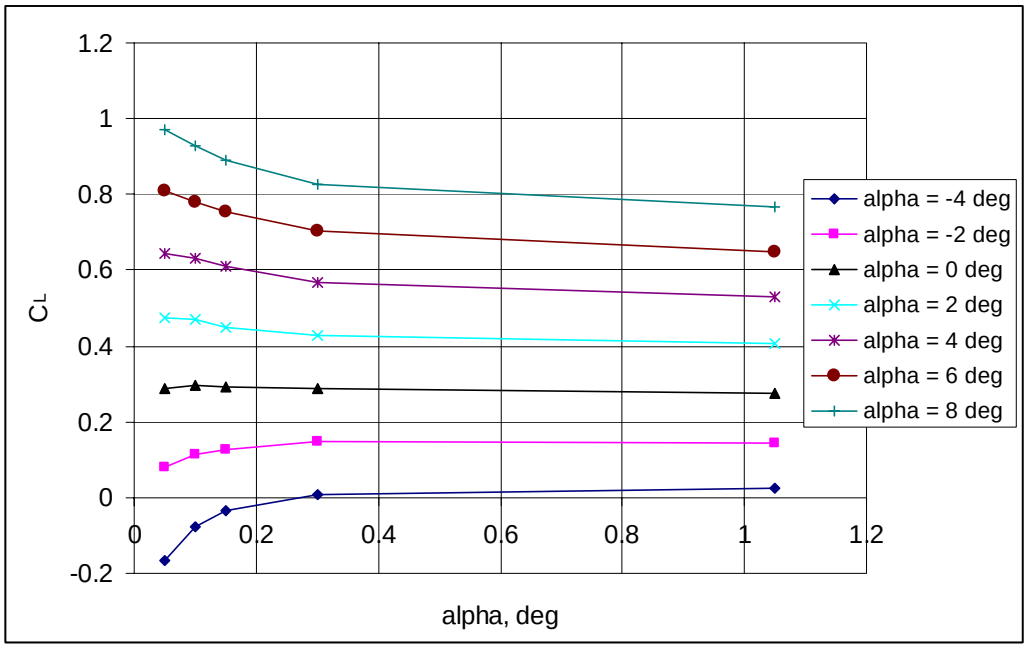

Figure 72: Ground Effect, C_L vs. (h/b), Flaps +10°, 60 mph

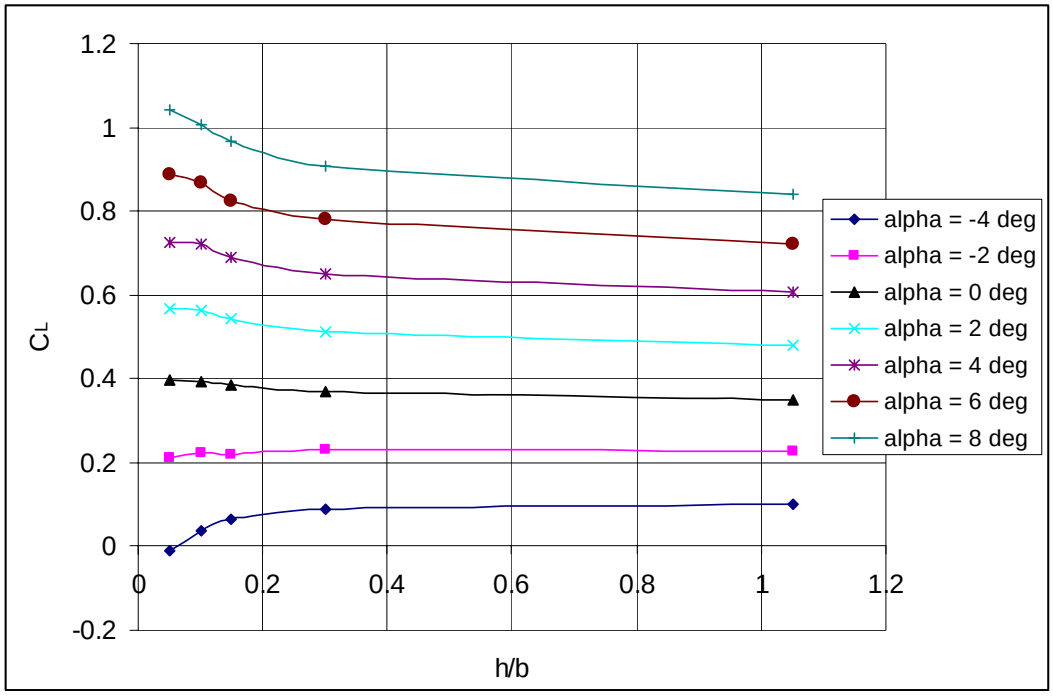

Figure 73: Ground Effect, C_L vs. (h/b), Flaps +20°, 60 mph

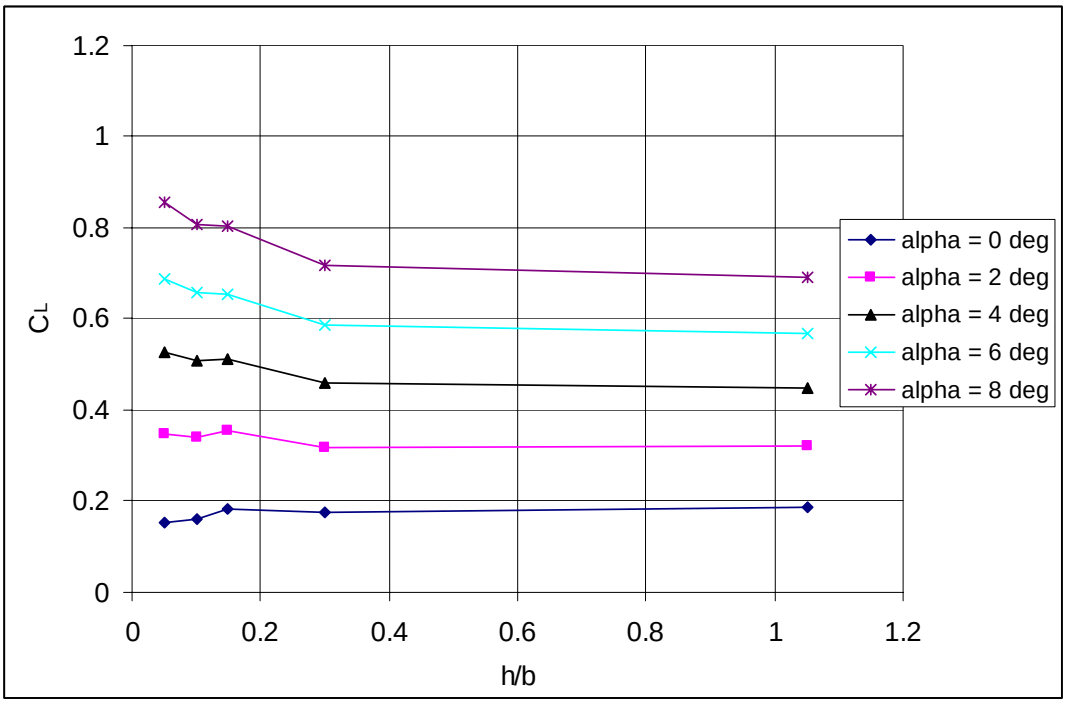

Figure 74: Ground Effect, C_L vs. (h/b), No Flaps, 80 mph

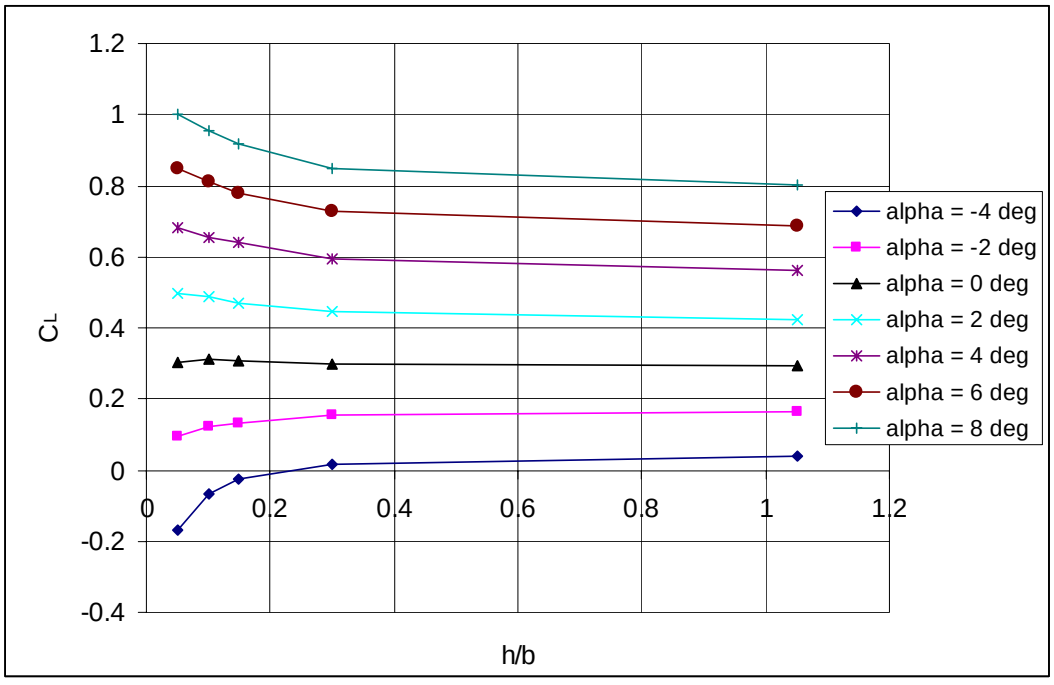

Figure 75: Ground Effect, C_L vs. (h/b), Flaps +10°, 80 mph

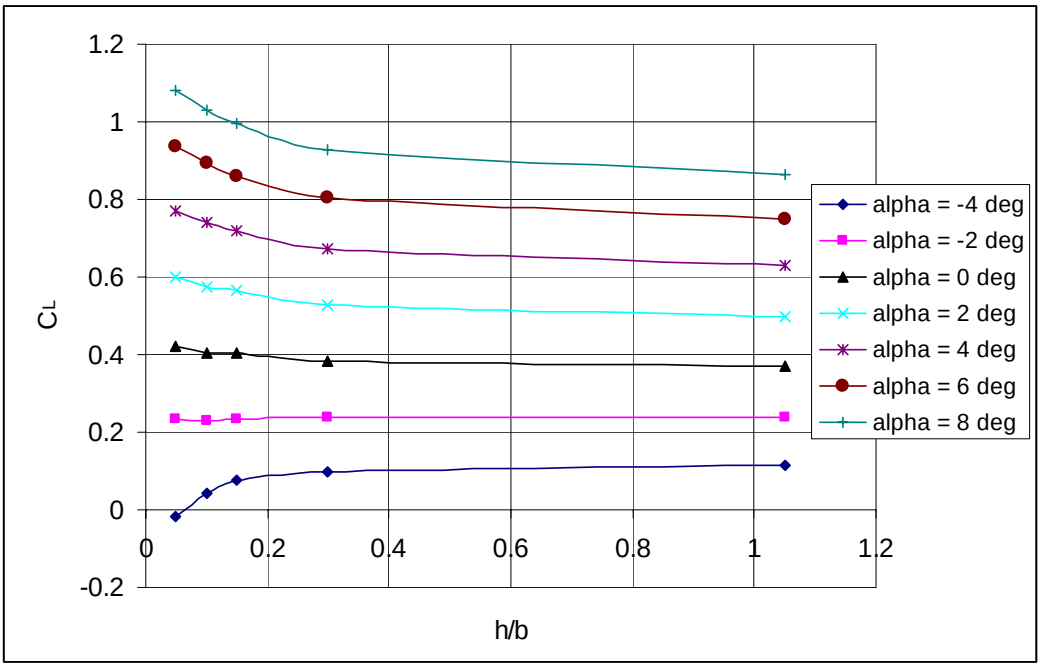

Figure 76: Ground Effect, C_L vs. (h/b), Flaps +20°, 80 mph

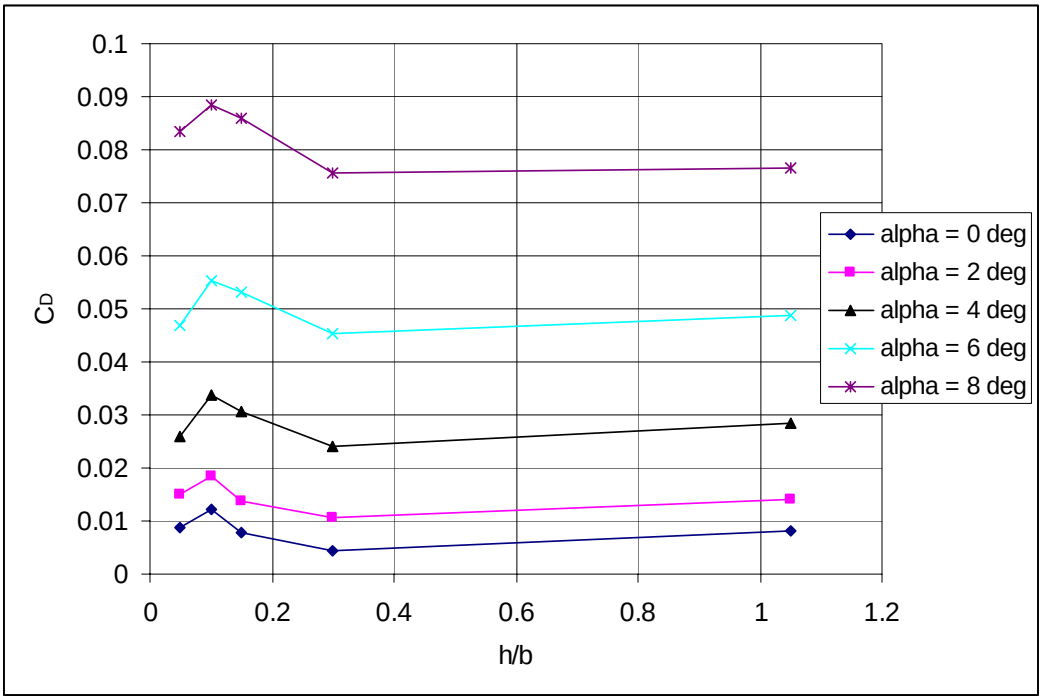

Figure 77: Ground Effect, C_D vs. (h/b), No Flaps, 40 mph

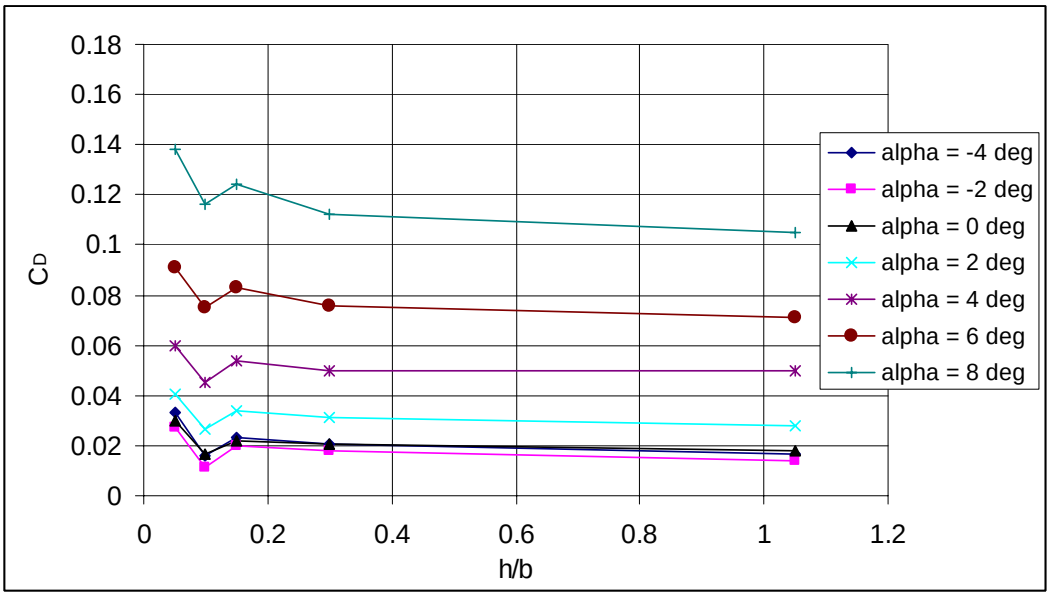

Figure 78: Ground Effect, C_D vs. (h/b), Flaps +10°, 40 mph

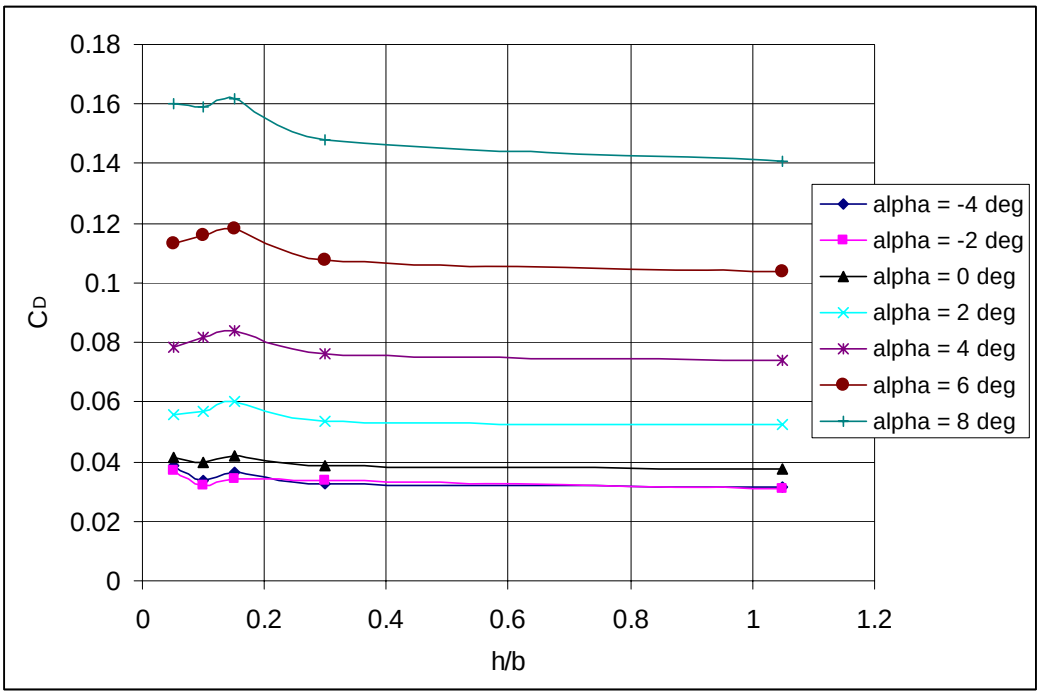

Figure 79: Ground Effect, C_D vs. (h/b), Flaps +20°, 40 mph

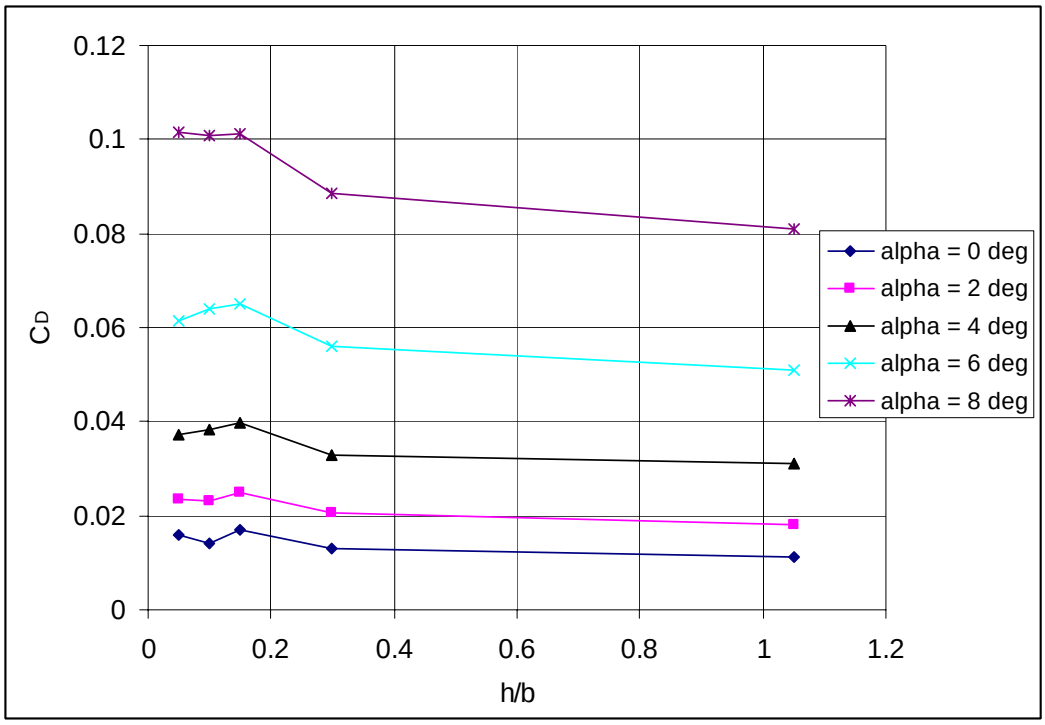

Figure 80: Ground Effect, C_D vs. (h/b), No Flaps, 60 mph

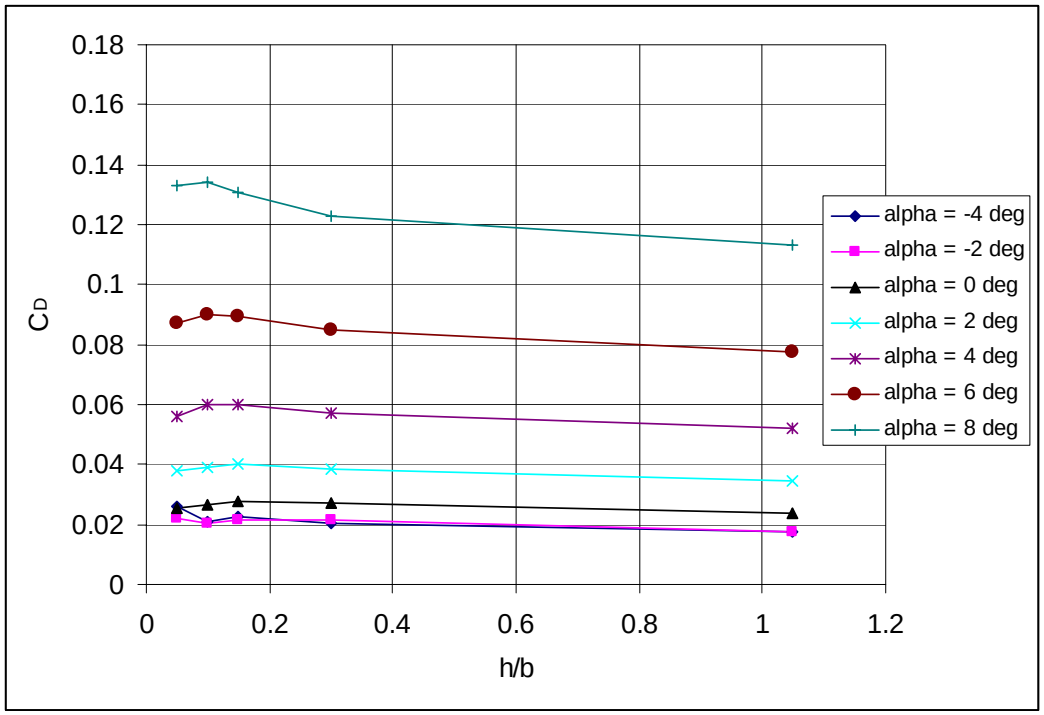

Figure 81: Ground Effect, C_D vs. (h/b), Flaps +10^o, 60 mph

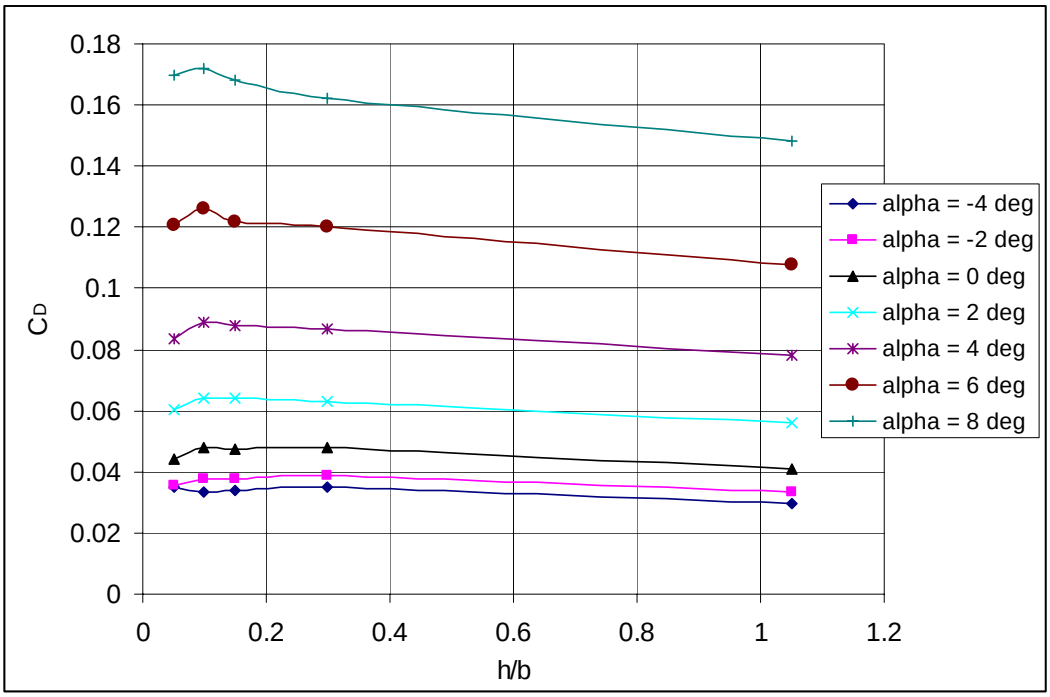

Figure 82: Ground Effect, C_D vs. (h/b), Flaps +20°, 60 mph

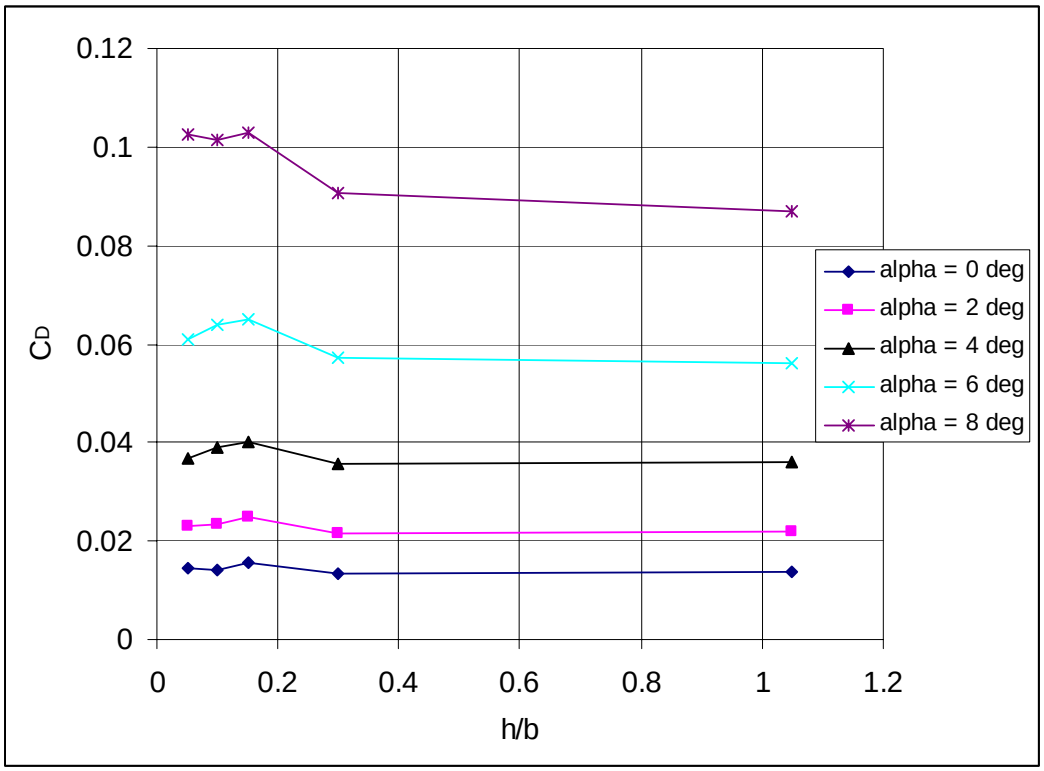

Figure 83: Ground Effect, C_D vs. (h/b), No Flaps, 80 mph

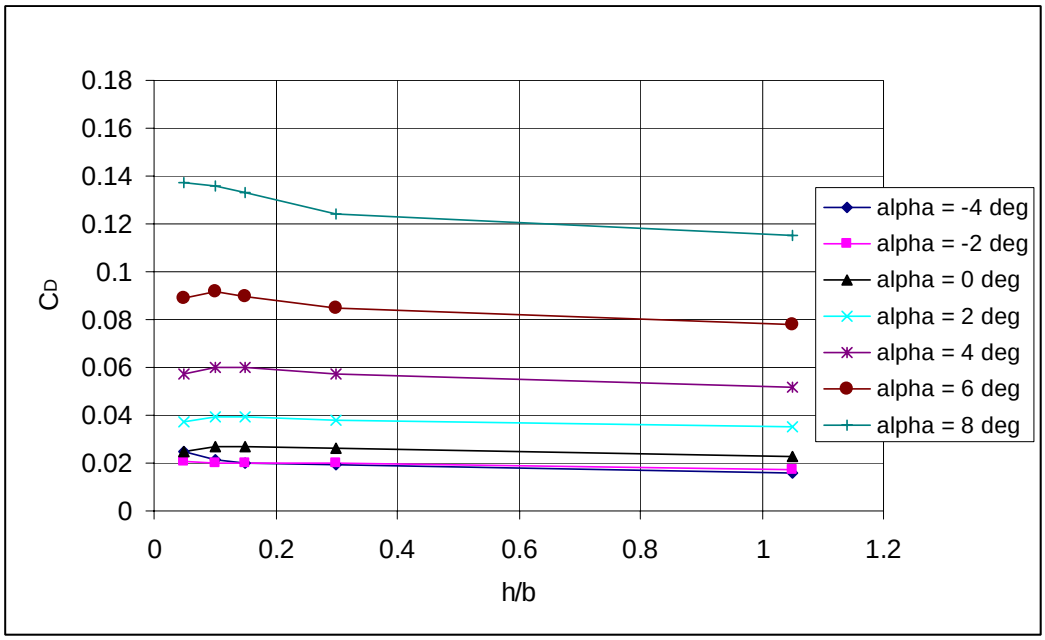

Figure 84: Ground Effect, C_D vs. (h/b), Flaps +10°, 80 mph

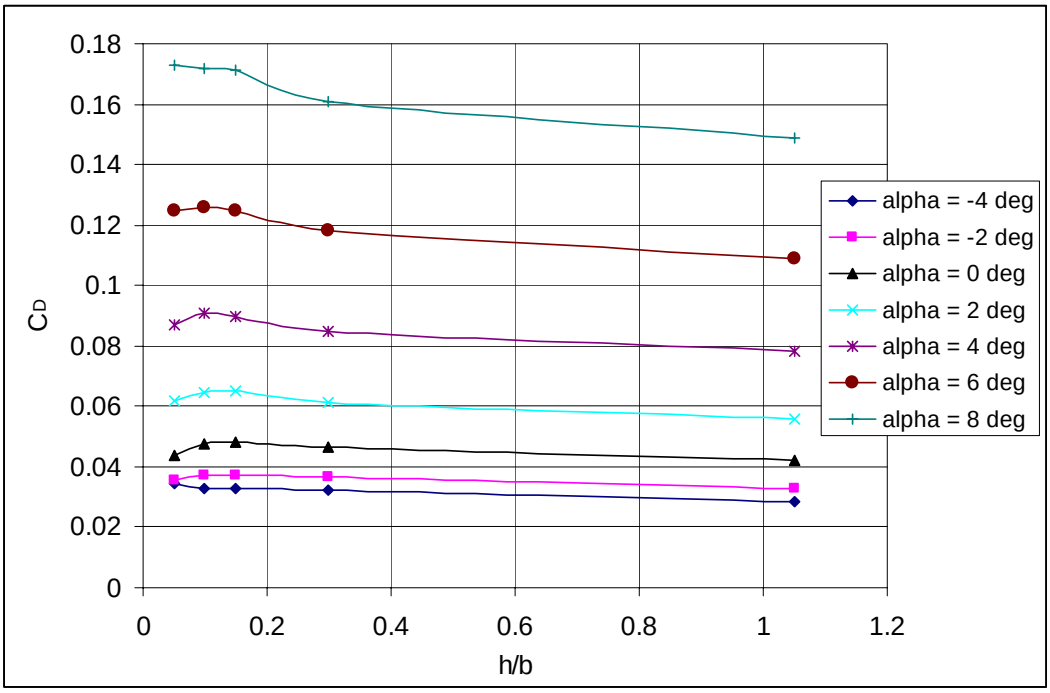

Figure 85: Ground Effect, C_D vs. (h/b), Flaps +20°, 80 mph

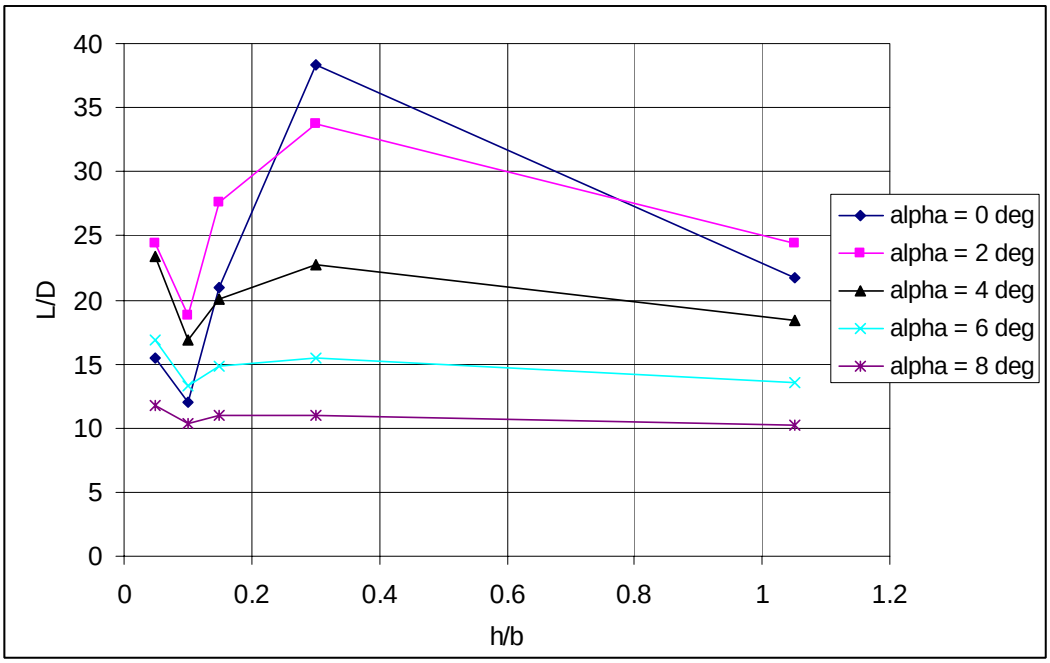

Figure 86: Ground Effect, L/D vs. (h/b), No Flaps, 40 mph

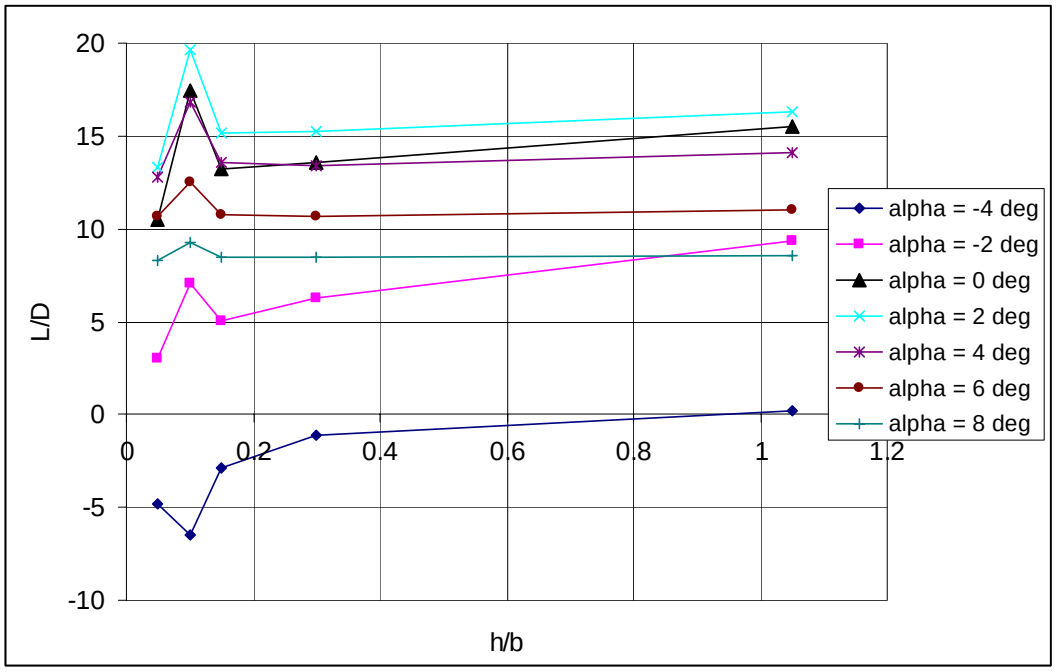

Figure 87: Ground Effect, L/D vs. (h/b), Flaps +10^{o}, 40 mph

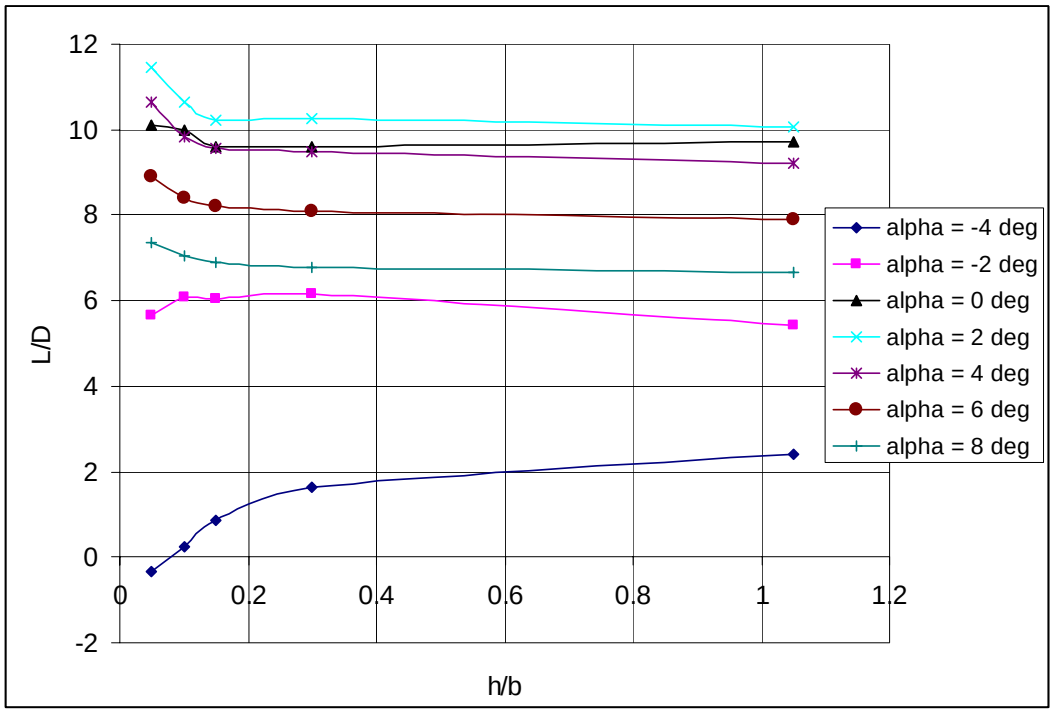

Figure 88: Ground Effect, L/D vs. (h/b), Flaps +20°, 40 mph

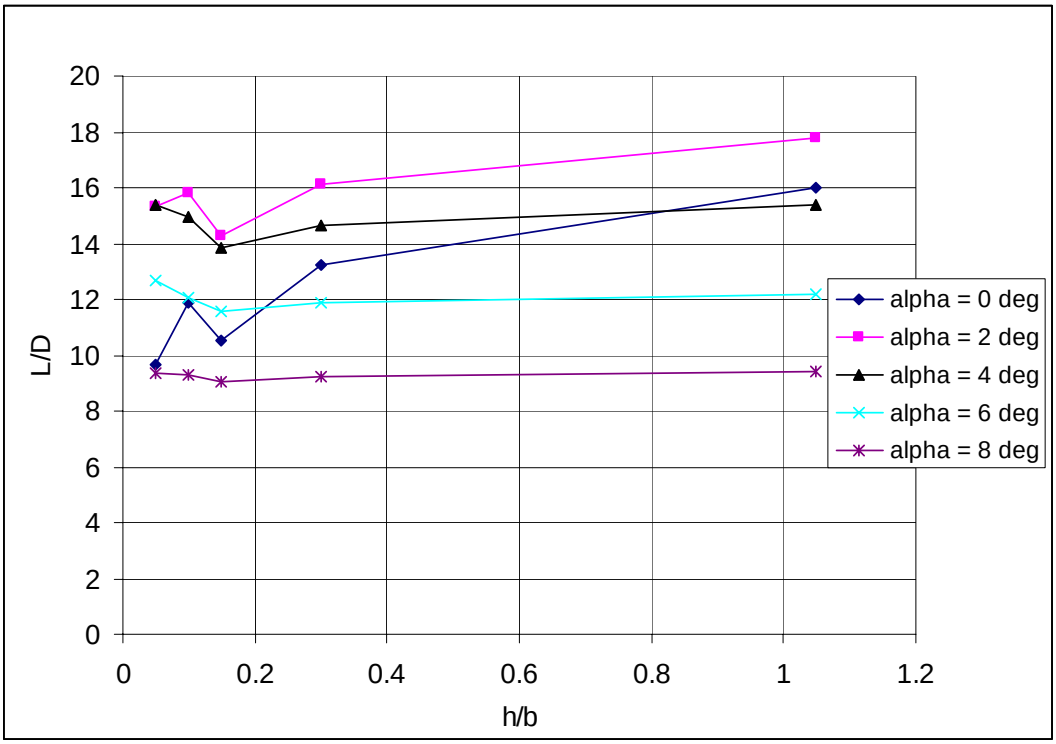

Figure 89: Ground Effect, L/D vs. (h/b), No Flaps, 60 mph

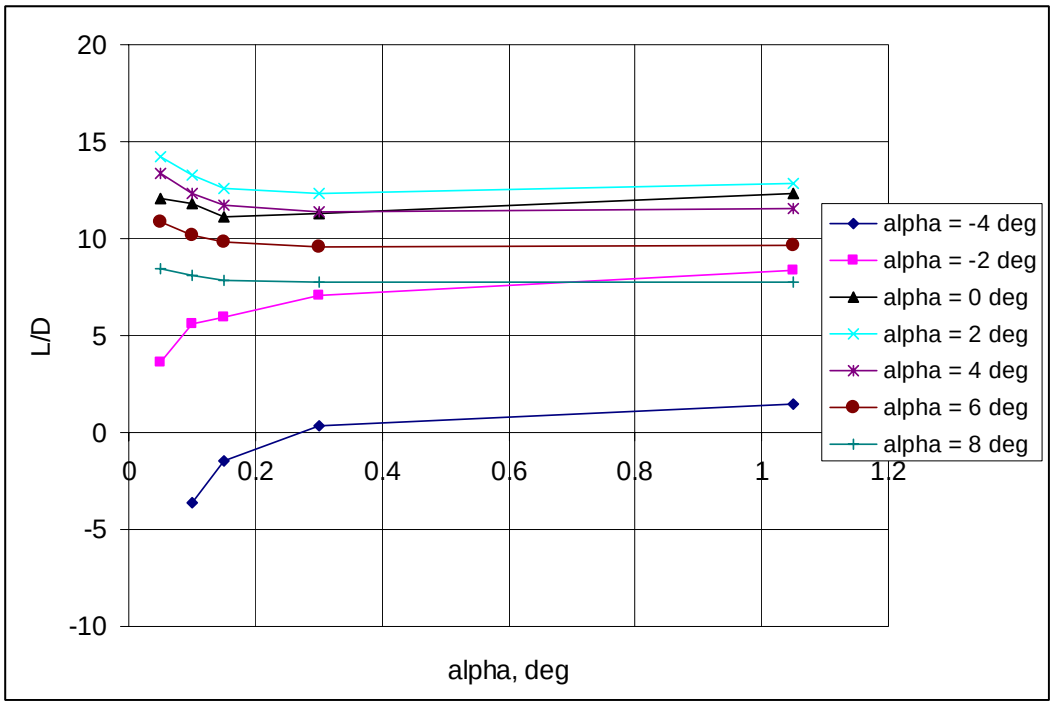

Figure 90: Ground Effect, L/D vs. (h/b), Flaps +10^{o}, 60 mph

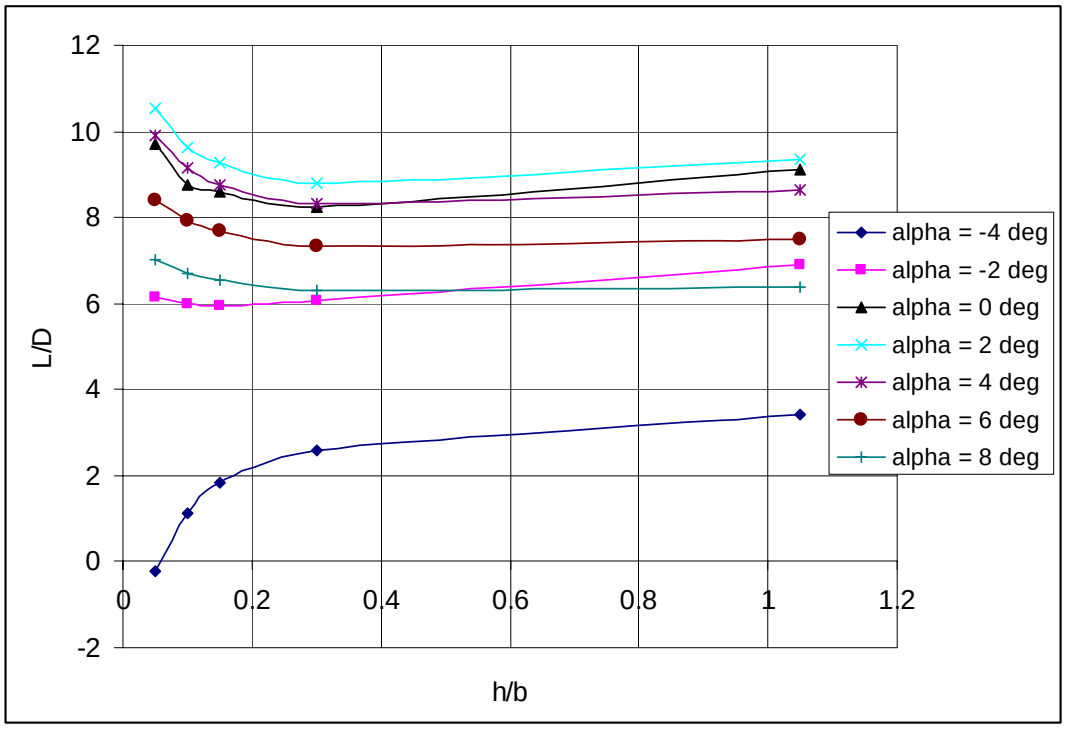

Figure 91: Ground Effect, L/D vs. (h/b), Flaps +20^{o}, 60 mph

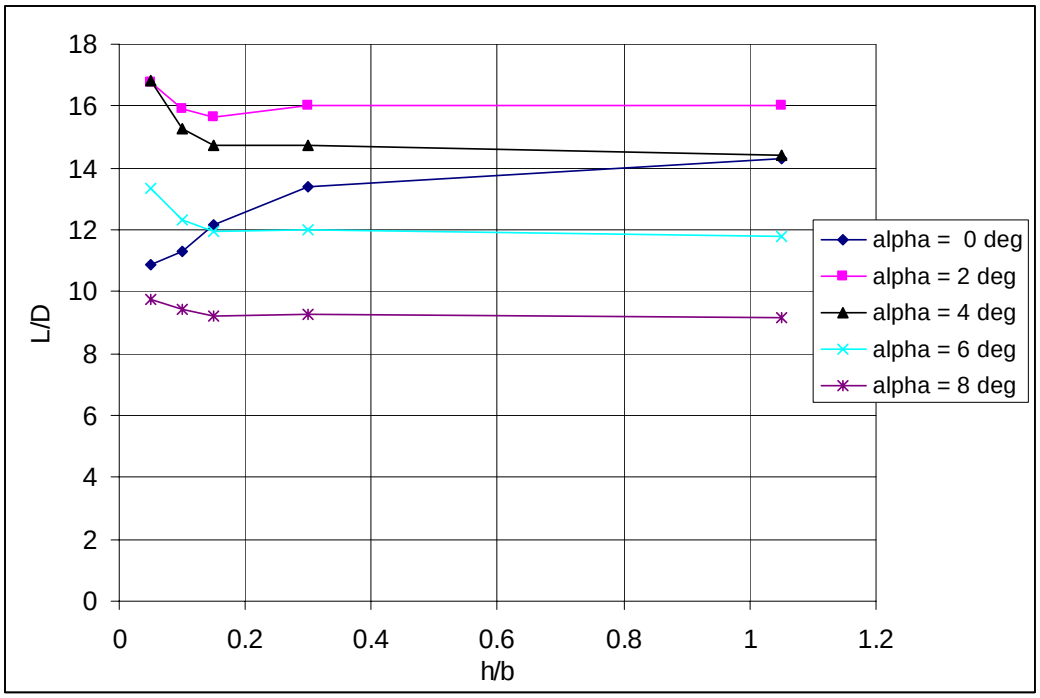

Figure 92: Ground Effect, L/D vs. (h/b), No Flaps, 80 mph

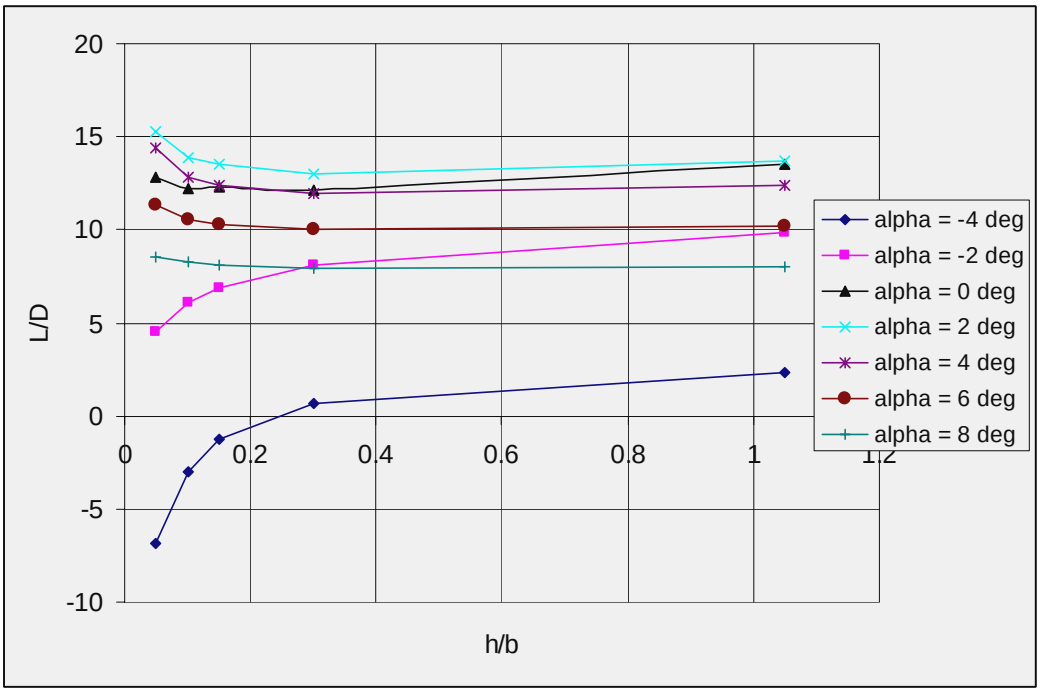

Figure 93: Ground Effect, L/D vs. (h/b), Flaps +10^{o}, 80 mph

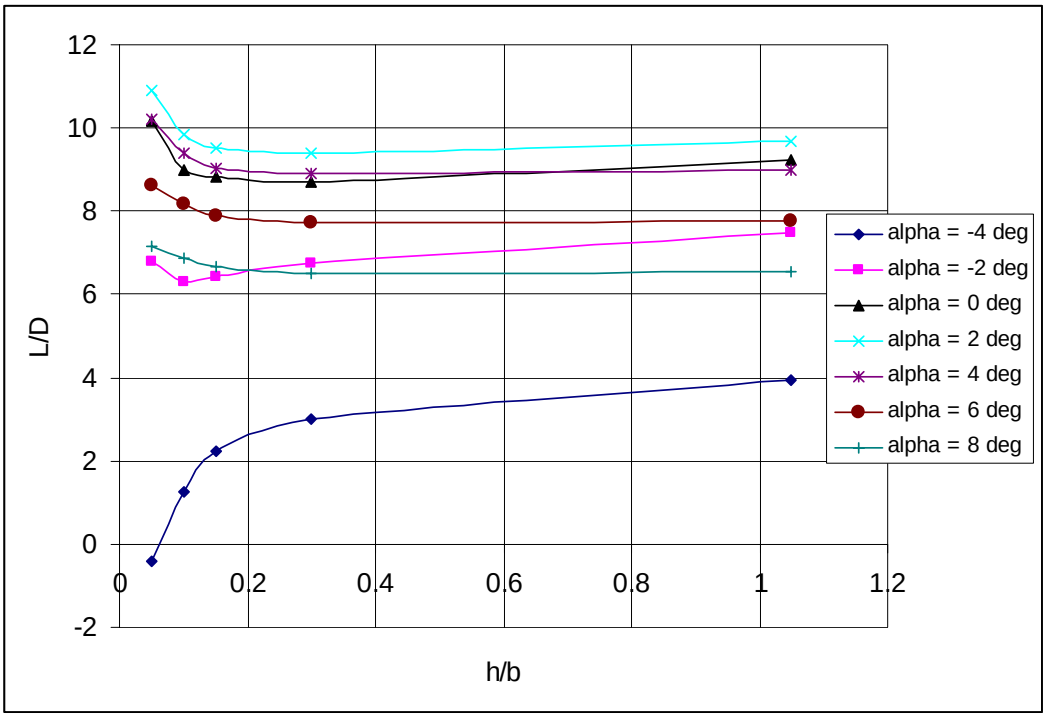

Figure 94: Ground Effect, L/D vs. (h/b), Flaps +20°, 80 mph

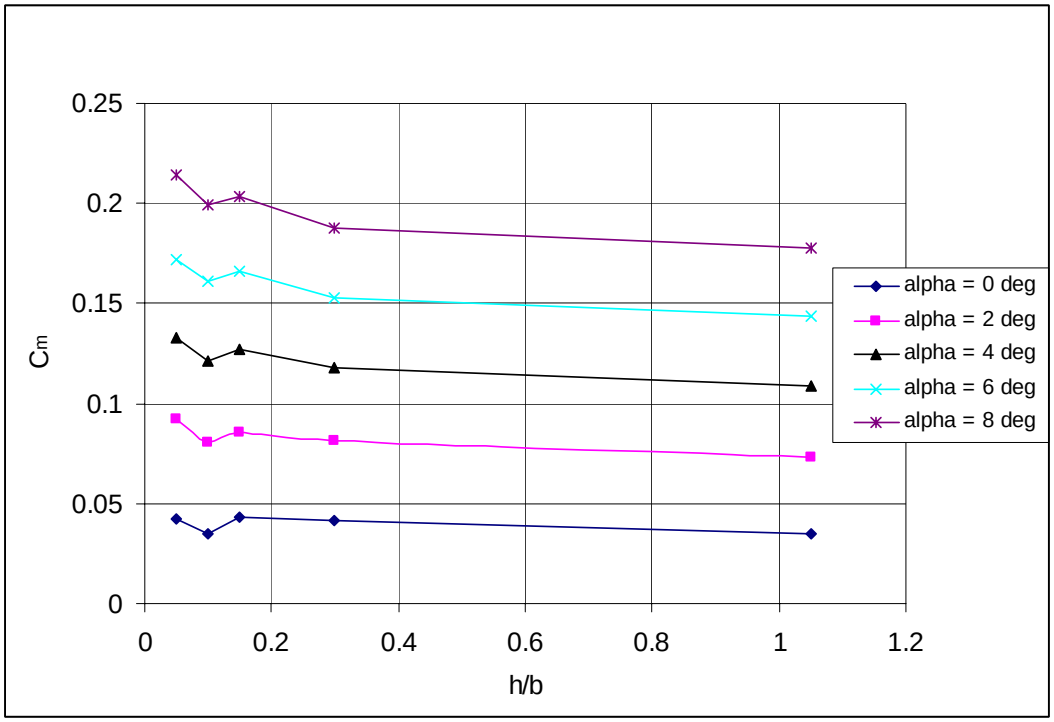

Figure 95: Ground Effect, C_m vs. (h/b), No Flaps, 40 mph

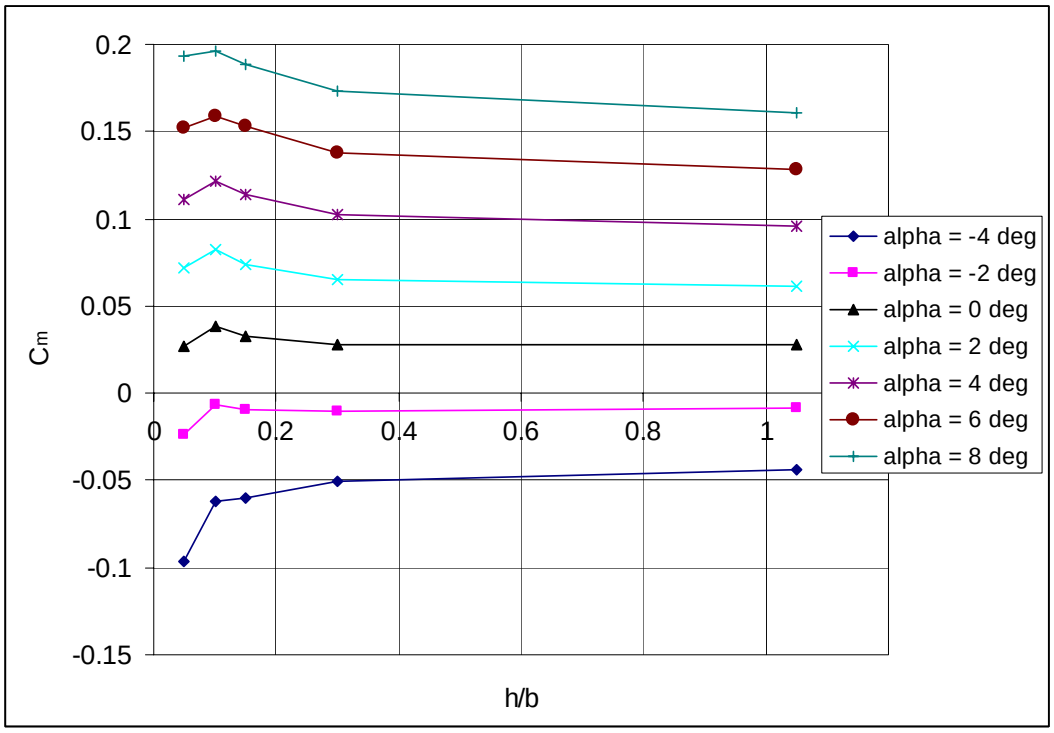

Figure 96: Ground Effect, C_m vs. (h/b), Flaps +10°, 40 mph

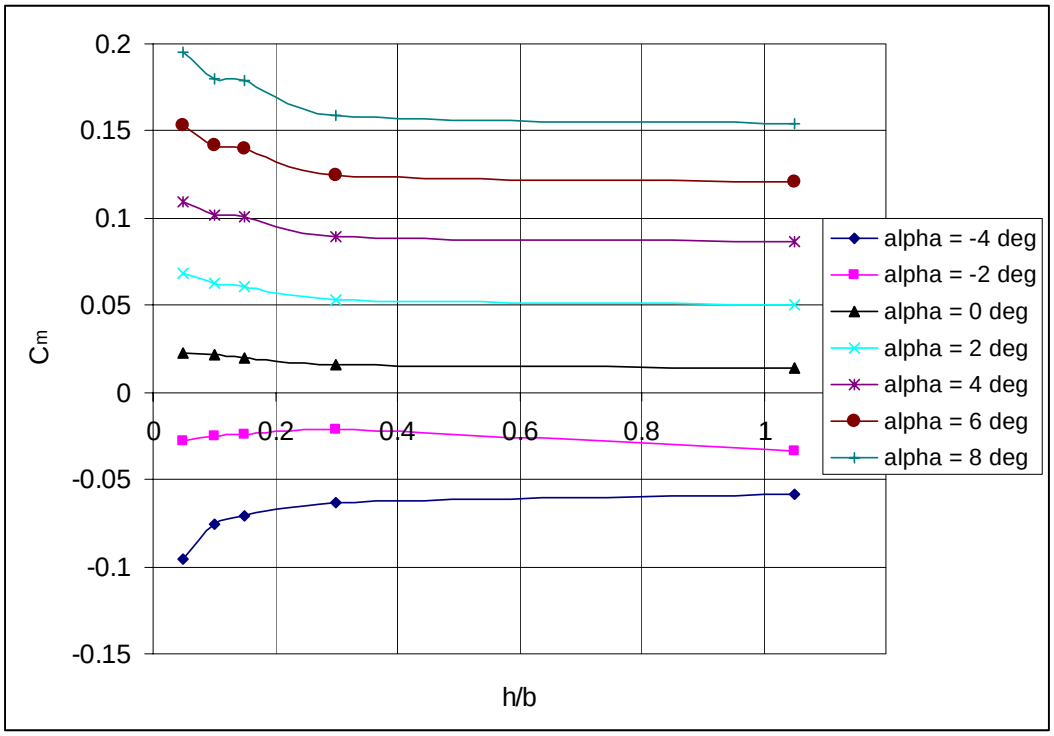

Figure 97: Ground Effect, C_m vs. (h/b), Flaps +20°, 40 mph

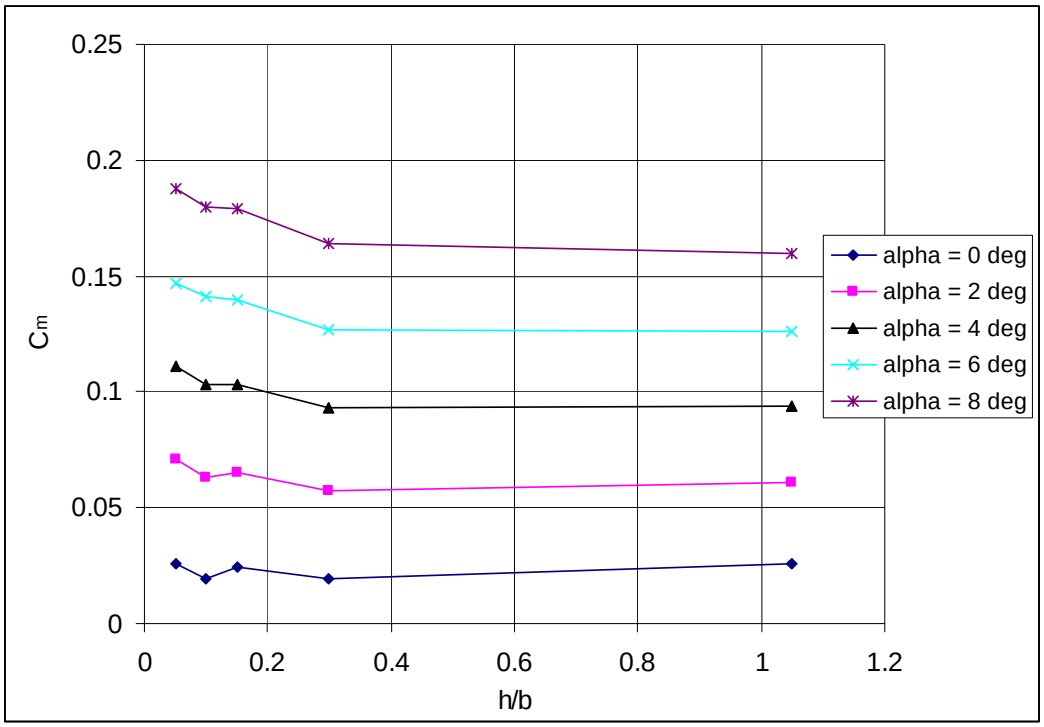

Figure 98: Ground Effect, C_m vs. (h/b), No Flaps, 60 mph

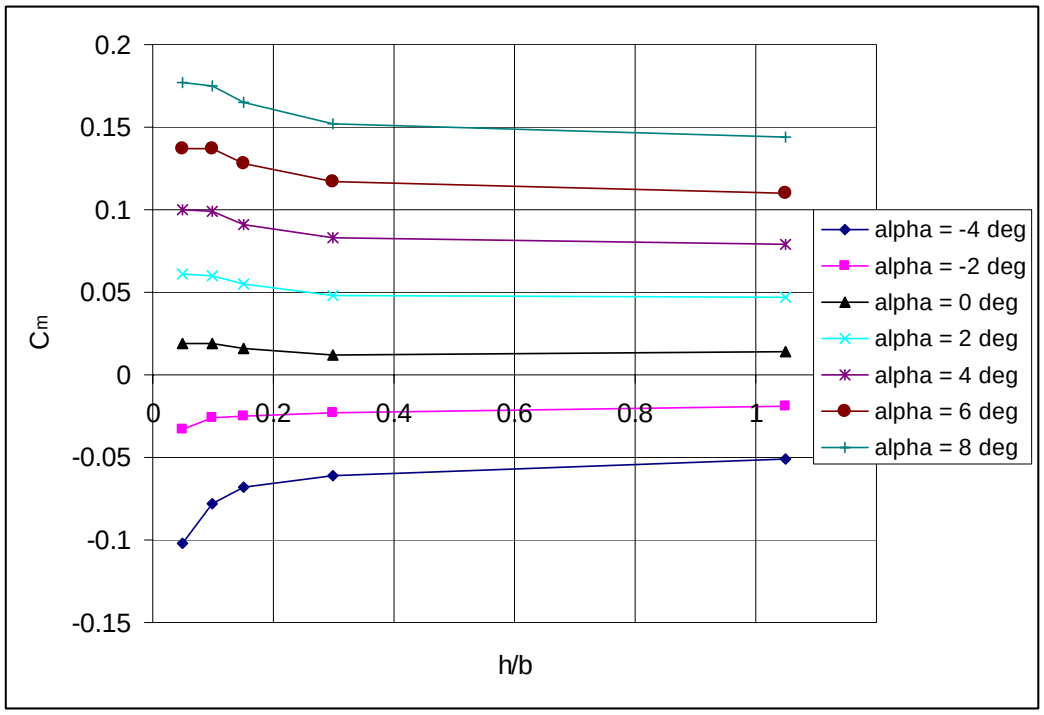

Figure 99: Ground Effect, C_m vs. (h/b), Flaps +10^o, 60 mph

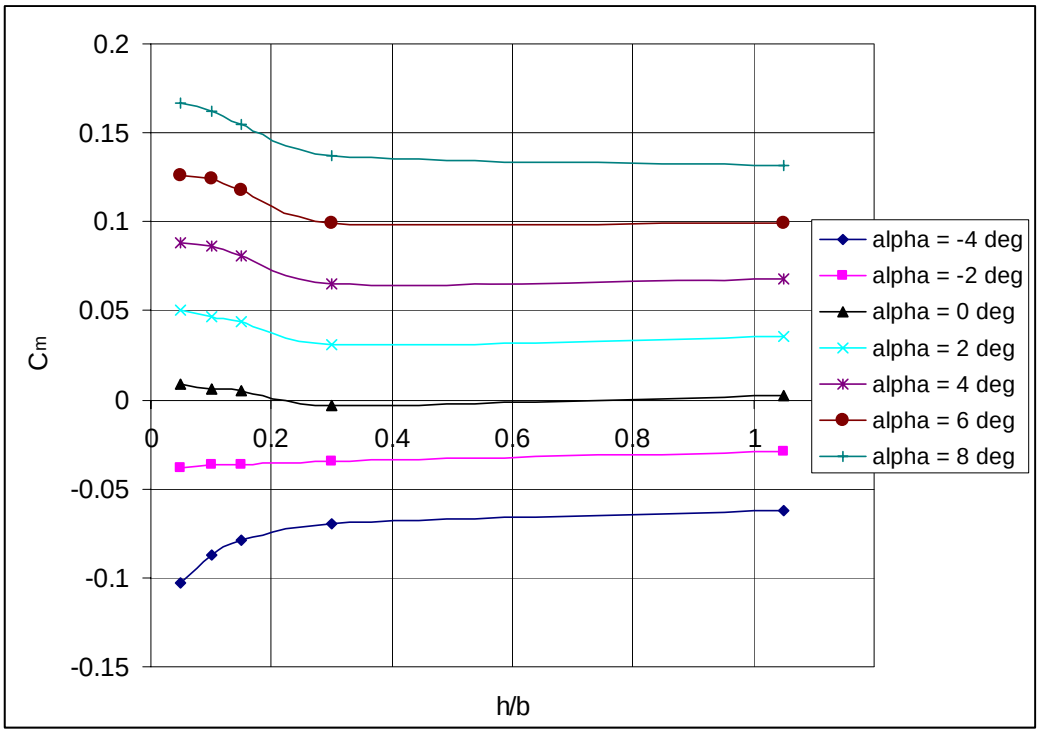

Figure 100: Ground Effect, C_m vs. (h/b), Flaps +20°, 60 mph

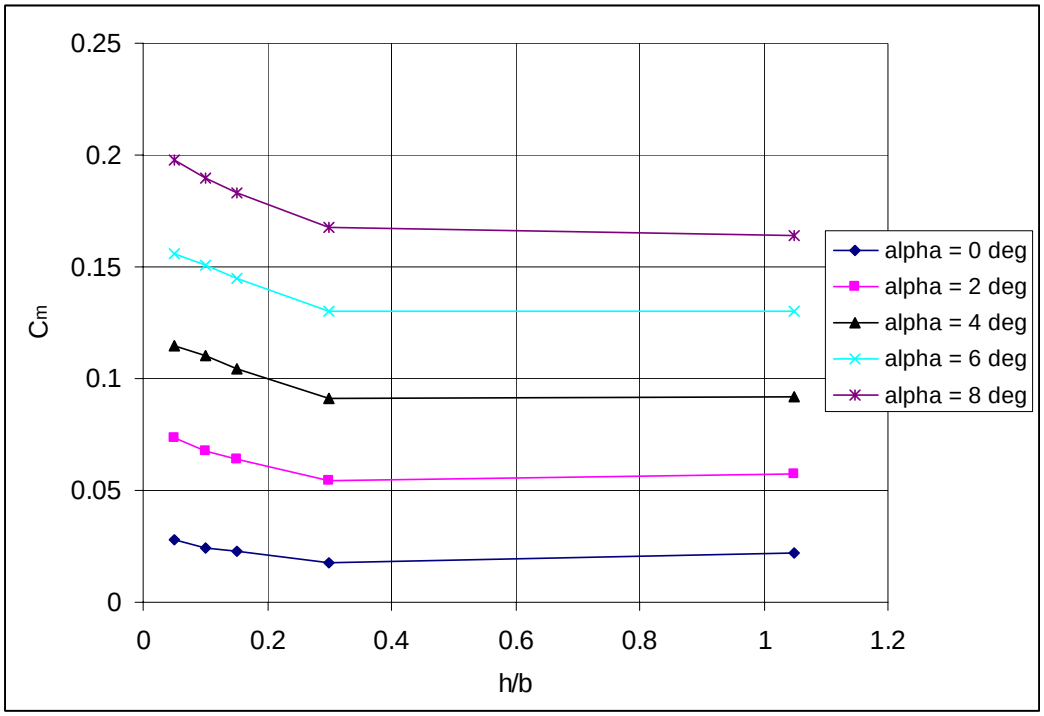

Figure 101: Ground Effect, C_m vs. (h/b), No Flaps, 80 mph

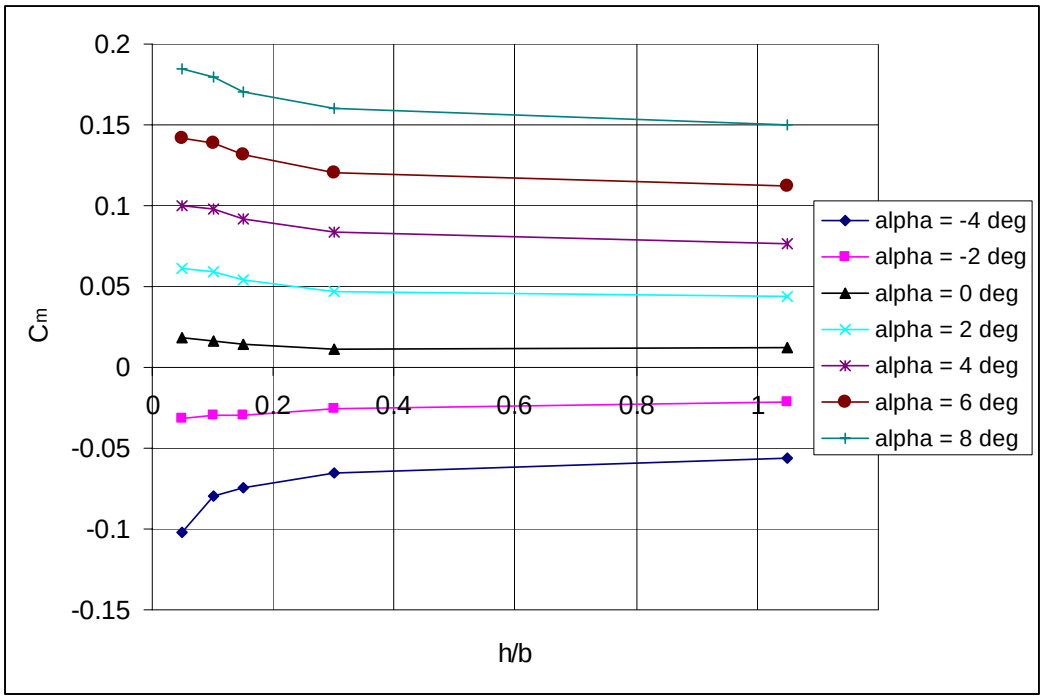

Figure 102: Ground Effect, C_m vs. (h/b), Flaps +10°, 80 mph

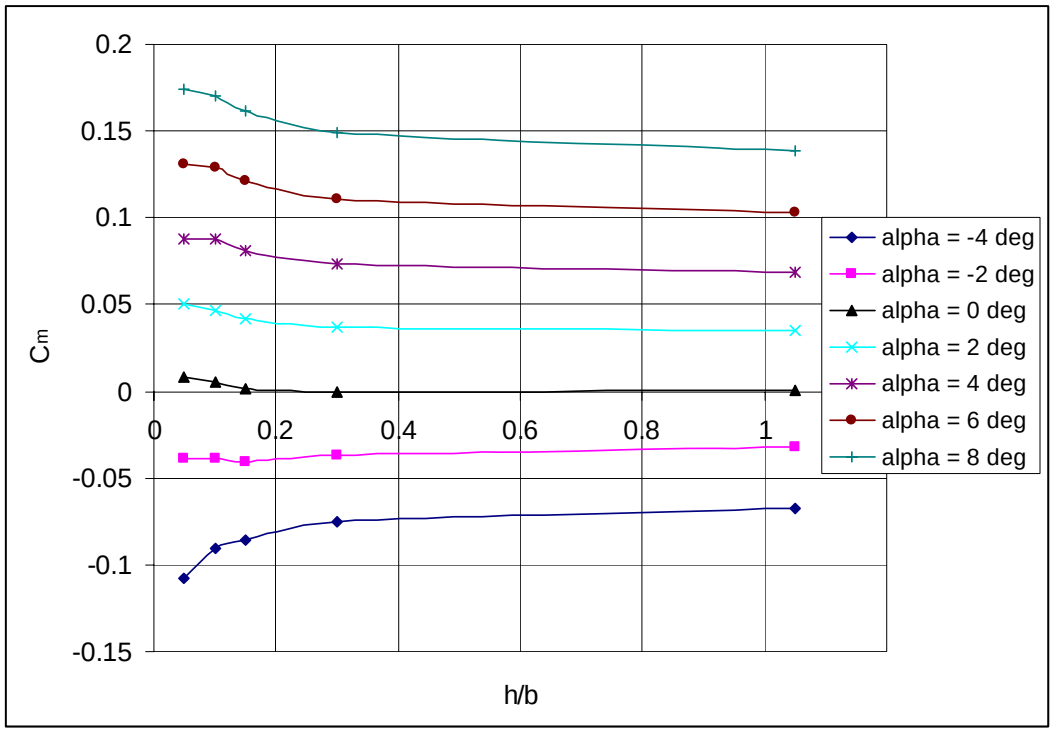

Figure 103: Ground Effect, C_m vs. (h/b), Flaps +20°, 80 mph

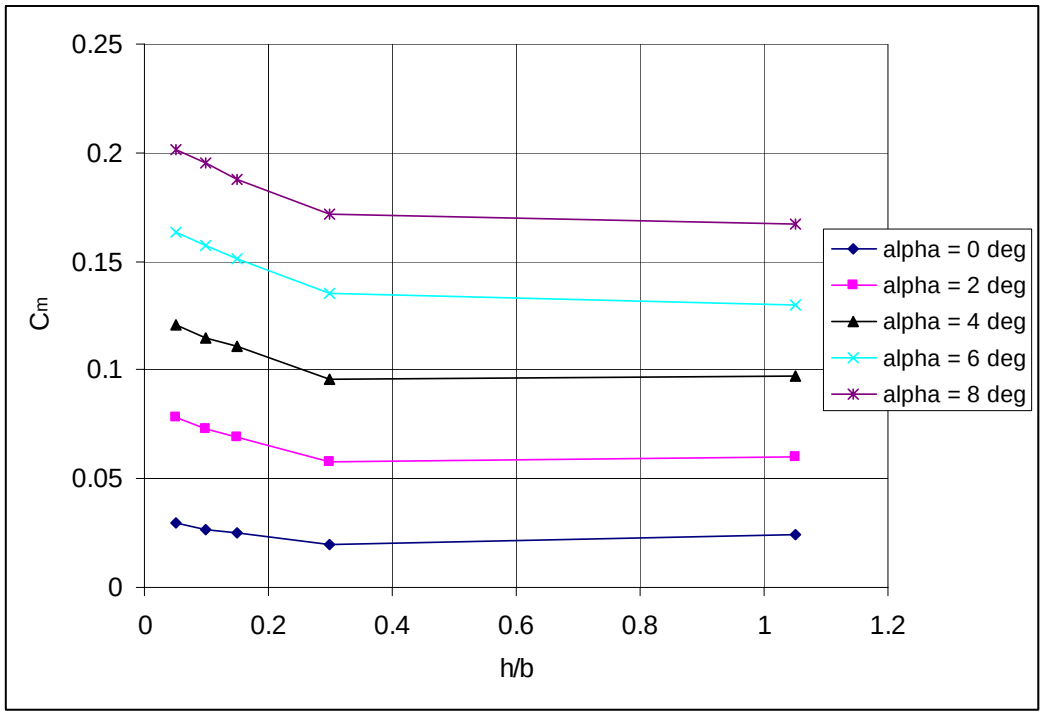

Figure 104: Ground Effect, C_m vs. (h/b), No Flaps, 100 mph

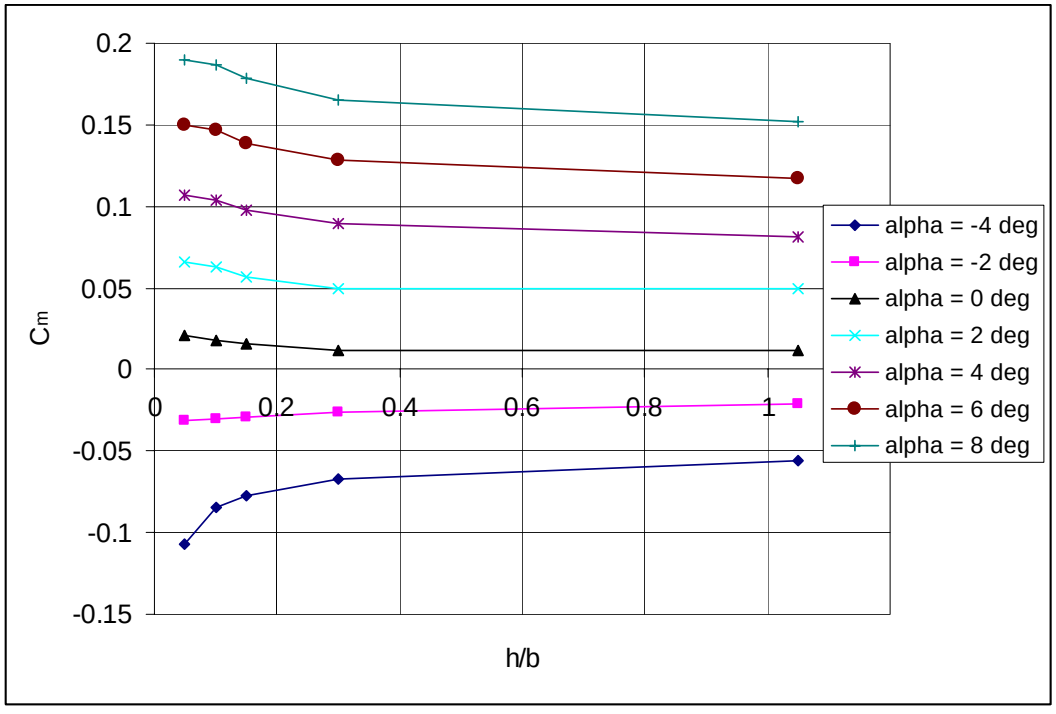

Figure 105: Ground Effect, C_m vs. (h/b), Flaps +10^o, 100 mph

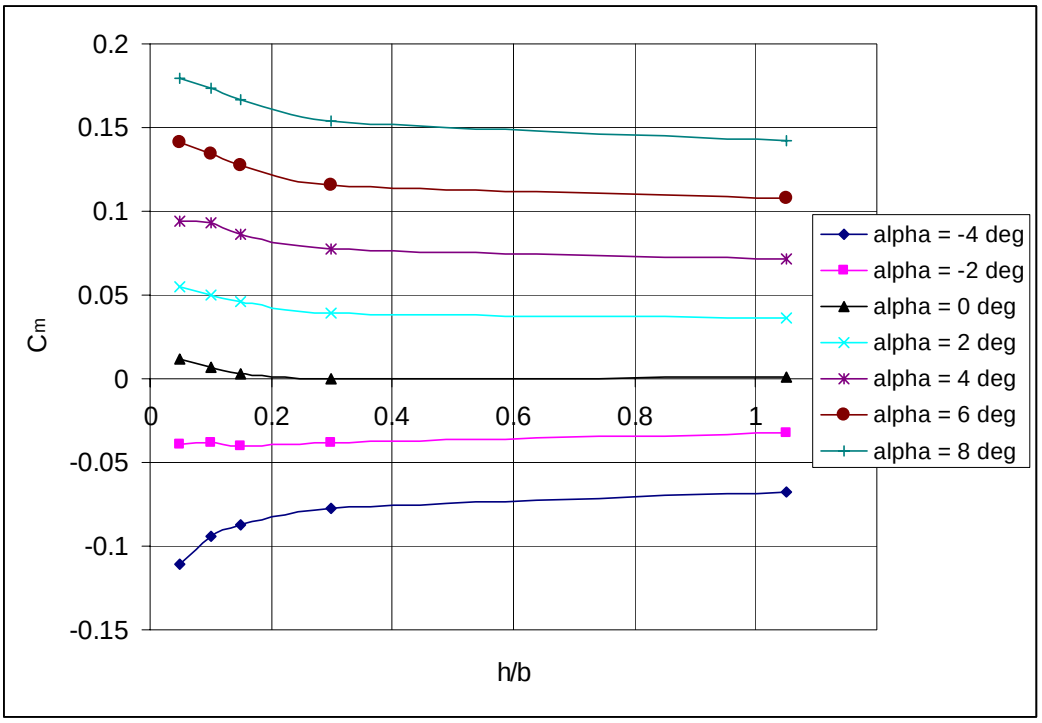

Figure 106: Ground Effect, C_m vs. (h/b), Flaps +20^o, 100 mph

Appendix F: Data Tables

The following tables were outputted by the MATLAB reduction code in an Excel file. These tables were used to produce the standard aerodynamic plots presented in this report.

Table 27: U_∞ = 40 mph, h/b = 1.05(OGE), $\delta_{mid/out} = +10^o$, Symmetric Deflections

M	Re#	q_c	Uinf	alpha_c	CL	CD_c	Cl_cg_w	Cm_cg_c_w	Cn_cg_w	C_Y	L/D
0.021513478	127422	0.65632	16.5969	1.03988	0.95155	0.12074	0.00189	0.06616	0.00131	-0.0083	9.196666
0.047808762	283165	3.24124	36.8827	-10.934	-0.4565	0.07513	-0.0002	-0.1879	0.00023	0.00093	-6.41544
0.047736383	282736	3.23143	36.8269	-8.7083	-0.3297	0.04703	0.00011	-0.1394	0.00038	-0.0008	-7.33232
0.047732868	282716	3.23095	36.8242	-6.4485	-0.1716	0.02537	0.00022	-0.0913	0.00048	-0.0023	-6.91628
0.04775314	282836	3.2337	36.8398	-4.2818	-0.019	0.01721	0.00044	-0.0489	0.0007	-0.0031	-1.10517
0.047784308	283020	3.23792	36.8639	-1.9479	0.12725	0.01358	0.00066	-0.0076	0.00069	-0.0046	9.589623
0.047811728	283183	3.24164	36.885	0.20977	0.27156	0.0182	0.00069	0.03162	0.00069	-0.0058	16.17138
0.047845006	283380	3.24615	36.9107	2.48424	0.44311	0.0309	0.00099	0.06998	0.00124	-0.01	16.31864
0.047913989	283788	3.25552	36.9639	4.73009	0.58846	0.05175	0.0011	0.1076	0.00117	-0.01	13.03586
0.047958315	284051	3.26155	36.9981	6.87171	0.71805	0.08403	0.0011	0.14244	0.00151	-0.0127	9.677906
0.047974485	284147	3.26375	37.0106	9.08578	0.83433	0.12603	0.00137	0.17927	0.0013	-0.0122	7.399871
0.04794566	283976	3.25983	36.9883	11.2179	0.95527	0.18025	0.00205	0.21194	0.00149	-0.0139	5.865995
0.04793945	283939	3.25898	36.9835	12.3248	1.01372	0.21135	0.00142	0.22391	0.00171	-0.0141	5.28675
0.047923162	283843	3.25677	36.971	13.438	1.07699	0.24624	0.00166	0.23734	0.00171	-0.0152	4.805543
0.04787887	283580	3.25075	36.9368	14.5378	1.12898	0.28271	0.00201	0.24815	0.0017	-0.0153	4.369113
0.047838092	283339	3.24522	36.9053	15.6167	1.16094	0.31869	0.00175	0.25873	0.00186	-0.0149	3.962492
0.047837272	283334	3.2451	36.9047	16.691	1.18956	0.3538	0.00274	0.26582	0.00153	-0.0165	3.63994
0.047845357	283382	3.2462	36.911	17.7369	1.19135	0.38468	0.00197	0.26852	0.00188	-0.0152	3.331437
0.047845357	283382	3.2462	36.911	18.7662	1.1788	0.41478	0.00413	0.26523	0.00079	-0.0185	3.035924
0.047784894	283024	3.238	36.8643	19.8496	1.13524	0.43623	0.00232	0.25138	0.00187	-0.0165	2.757754
0.047727478	282684	3.23022	36.82	20.8475	1.09392	0.45695	0.0031	0.23923	0.00125	-0.018	2.519802
0.047717635	282625	3.22889	36.8124	21.8557	1.06118	0.4749	0.00627	0.22835	-0.0019	-0.0252	2.34035

Table 28: U_∞ = 40 mph, h/b = 0.3, $\delta_{mid/out}$ = +10°, Symmetric Deflections

M	Re#	q_c	Uinf	alpha_c	CL	CD_c	Cl_cg_w	Cm_cg_c_w	Cn_cg_w	C_Y	L/D
0.023501127	139194	0.7832	18.1303	0.83564	0.84427	0.1197	0.00156	0.0642	0.0012	-0.0031	7.956976
0.047308752	280204	3.17379	36.497	-11.048	-0.5612	0.0911	0.00026	-0.2212	0.00083	-0.0081	-6.59458
0.04727437	280000	3.16918	36.4705	-8.8826	-0.4096	0.05935	0.00047	-0.161	0.00104	-0.0094	-7.29491
0.047266315	279952	3.1681	36.4642	-6.5968	-0.2277	0.03347	0.00048	-0.1059	0.00126	-0.0084	-7.01047
0.047271965	279986	3.16886	36.4686	-4.314	-0.0485	0.02068	0.00069	-0.0573	0.00144	-0.0087	-2.35115
0.047284842	280062	3.17059	36.4785	-2.0494	0.11401	0.01838	0.00082	-0.0107	0.00134	-0.0085	6.286036
0.047329991	280329	3.17664	36.5134	0.21849	0.27954	0.02092	0.00086	0.03232	0.0016	-0.009	14.38428
0.047370425	280569	3.18207	36.5446	2.50328	0.46053	0.03374	0.00108	0.07433	0.00179	-0.011	15.51034
0.047343349	280409	3.17844	36.5237	4.6722	0.6151	0.05674	0.0012	0.11479	0.00192	-0.0108	12.41973
0.047288449	280083	3.17107	36.4813	6.90828	0.75152	0.08957	0.00128	0.15384	0.00224	-0.0126	9.53744
0.047218321	279668	3.16167	36.4272	9.14029	0.88422	0.13608	0.00147	0.1925	0.00244	-0.0129	7.29737
0.047118806	279079	3.14836	36.3504	11.2849	1.01654	0.19421	0.00126	0.22429	0.00265	-0.0134	5.825387
0.04701193	278446	3.13409	36.268	12.4018	1.08412	0.22981	0.00136	0.23813	0.00292	-0.015	5.227204
0.046936072	277996	3.12399	36.2095	13.5283	1.15965	0.2684	0.00149	0.2521	0.00312	-0.0159	4.777157
0.046895438	277756	3.11858	36.1781	14.6255	1.20927	0.30642	0.00205	0.26355	0.003	-0.0153	4.341616
0.046897383	277767	3.11884	36.1796	15.7145	1.25041	0.34733	0.00248	0.27178	0.00273	-0.0153	3.9382
0.046872222	277618	3.11549	36.1602	16.784	1.27463	0.38391	0.00413	0.27889	0.00206	-0.0168	3.611673
0.046878246	277654	3.11629	36.1649	17.8309	1.27737	0.42008	0.00267	0.27761	0.00225	-0.0146	3.284108
0.046874279	277630	3.11577	36.1618	18.8584	1.26317	0.45114	0.00189	0.27288	0.00265	-0.0121	3.002445
0.046889307	277719	3.11777	36.1734	19.8599	1.22423	0.47951	0.00342	0.25525	0.00144	-0.0144	2.714929
0.04689487	277752	3.11851	36.1777	20.9478	1.18576	0.50119	0.00265	0.24641	0.00194	-0.0134	2.499608
0.046844705	277455	3.11184	36.139	21.9569	1.15377	0.52018	0.00381	0.23889	0.00057	-0.016	2.33184

Table 29: U_∞ = 40 mph, h/b = 0.15, $\delta_{mid/out}$ = +10°, Symmetric Deflections

M	Re#	q_c	Uinf	alpha_c	CL	CD_c	Cl_cg_w	Cm_cg_c_w	Cn_cg_w	C_Y	L/D
0.019992499	118413	0.5668	15.4235	1.01939	1.01241	0.14896	0.00143	0.07997	0.0019	-8E-05	7.823202
0.046216105	273732	3.02888	35.654	-11.313	-0.8038	0.12475	0.00067	-0.2949	0.00117	-0.0102	-7.14947
0.046159558	273397	3.02148	35.6104	-8.9841	-0.582	0.07359	0.00097	-0.2099	0.00146	-0.0106	-8.67083
0.046158208	273389	3.0213	35.6094	-6.6295	-0.3372	0.03821	0.00075	-0.1316	0.00145	-0.009	-9.3561
0.046151028	273347	3.02036	35.6038	-4.374	-0.1034	0.02394	0.00076	-0.0694	0.00147	-0.0082	-4.35491
0.046217171	273738	3.02902	35.6549	-2.0702	0.09498	0.02008	0.00082	-0.0107	0.00148	-0.0078	4.770447
0.046240465	273876	3.03208	35.6728	0.23281	0.29265	0.02232	0.00085	0.03775	0.00195	-0.0102	14.14971
0.046214021	273720	3.02861	35.6524	2.55382	0.50677	0.03774	0.00105	0.08511	0.00202	-0.0109	15.42909
0.046180556	273521	3.02423	35.6266	4.73589	0.67338	0.0622	0.00124	0.12897	0.00207	-0.0115	12.57525
0.046162446	273414	3.02185	35.6126	6.98637	0.82298	0.09986	0.00119	0.17135	0.00247	-0.013	9.465839
0.046093022	273003	3.01277	35.5591	9.2433	0.97847	0.15275	0.00149	0.21168	0.00271	-0.0139	7.275242
0.046083179	272945	3.01148	35.5515	11.4114	1.13227	0.2187	0.00112	0.24499	0.00297	-0.015	5.828984
0.046049477	272745	3.00708	35.5255	12.5412	1.21169	0.25836	0.00118	0.25773	0.00293	-0.0149	5.260074
0.046018296	272560	3.00301	35.5014	13.6705	1.28976	0.30146	0.0021	0.27246	0.00287	-0.0145	4.781637
0.045959003	272209	2.99528	35.4557	14.7722	1.3435	0.34485	0.0025	0.28402	0.00278	-0.0152	4.327941
0.04586156	271632	2.98259	35.3805	15.8728	1.39524	0.39327	0.00239	0.29181	0.00275	-0.0146	3.91768
0.04576022	271032	2.96942	35.3023	16.9227	1.40162	0.43036	0.00281	0.2974	0.00219	-0.0128	3.567445
0.045700691	270679	2.9617	35.2564	17.9659	1.40088	0.46939	0.00122	0.29741	0.00277	-0.0116	3.243102
0.04566573	270472	2.95717	35.2294	18.9695	1.36478	0.50236	0.00186	0.28369	0.00258	-0.0126	2.923474
0.045671229	270505	2.95788	35.2337	20.0584	1.32631	0.5309	0.00199	0.27046	0.0024	-0.0126	2.66676
0.045651567	270388	2.95534	35.2185	21.0698	1.29735	0.55952	0.00324	0.26111	0.0013	-0.0149	2.459802
0.045623542	270222	2.95171	35.1969	22.0973	1.2823	0.58512	0.00409	0.25922	0.00038	-0.0186	2.315622

Table 30: U_∞ = 40 mph, h/b = 0.1, $\delta_{mid/out}$ = +10°, Symmetric Deflections

M	Re#	q_c	Uinf	alpha_c	CL	CD_c	Cl_cg_w	Cm_cg_c_w	Cn_cg_w	C_Y	L/D
0.019312177	114384	0.52888	14.8986	1.14437	1.04716	0.13207	0.00122	0.10908	0.00162	-0.0034	9.421013
0.04712848	279136	3.14965	36.3579	-11.539	-1.0105	0.14101	0.0003	-0.4016	0.00085	-0.0108	-8.31473
0.047071842	278800	3.14209	36.3142	-9.1086	-0.696	0.07515	0.00196	-0.2577	0.00135	-0.0089	-10.5587
0.047069913	278789	3.14183	36.3127	-6.7104	-0.4112	0.03679	0.00125	-0.1503	0.00141	-0.0077	-12.2515
0.047123674	279107	3.14901	36.3542	-4.3317	-0.1443	0.01695	0.00076	-0.071	0.00126	-0.0056	-8.71437
0.047122602	279101	3.14887	36.3534	-2.0014	0.07829	0.01113	0.0007	-0.0066	0.00122	-0.005	7.110911
0.047118717	279078	3.14835	36.3504	0.22966	0.28976	0.01714	0.00062	0.04319	0.00146	-0.007	18.64817
0.047101703	278977	3.14607	36.3373	2.54461	0.49835	0.02967	0.001	0.09354	0.00173	-0.0084	19.99065
0.047113258	279046	3.14762	36.3462	4.82371	0.67414	0.05366	0.00096	0.13745	0.00176	-0.009	14.98167
0.04714176	279215	3.15143	36.3682	6.9942	0.83014	0.09232	0.00015	0.17772	0.00214	-0.0105	10.48495
0.047119467	279083	3.14845	36.351	9.25266	0.98703	0.14489	0.00094	0.21827	0.00217	-0.0105	7.814733
0.047059906	278730	3.14049	36.305	11.4078	1.12896	0.20688	0.00078	0.25199	0.00259	-0.0121	6.18363
0.047028919	278546	3.13636	36.2811	12.5386	1.20938	0.24646	0.00102	0.26606	0.00265	-0.0134	5.53321
0.046951151	278086	3.126	36.2211	13.6728	1.29185	0.29072	0.00141	0.28091	0.00275	-0.0131	4.989954
0.046908469	277833	3.12031	36.1882	14.7922	1.36178	0.33742	0.00176	0.29057	0.00288	-0.015	4.508487
0.046894362	277749	3.11844	36.1773	15.8856	1.40696	0.38357	0.00235	0.29973	0.00275	-0.0154	4.068499
0.046805743	277224	3.10666	36.1089	16.9186	1.39785	0.42211	0.00218	0.30098	0.00241	-0.0135	3.632211
0.046731712	276786	3.09684	36.0518	17.9582	1.39379	0.46102	0.00249	0.29619	0.00191	-0.0128	3.287482
0.046641164	276250	3.08485	35.982	18.9591	1.3553	0.49443	0.00085	0.27963	0.00293	-0.0118	2.950168
0.046559658	275767	3.07408	35.9191	20.062	1.32958	0.52736	0.0007	0.26582	0.00297	-0.0104	2.69338
0.046502508	275428	3.06654	35.875	21.091	1.31677	0.56019	0.00223	0.26274	0.00156	-0.0149	2.498048
0.046499654	275411	3.06616	35.8728	22.0589	1.32676	0.59514	0.00305	0.26328	0.00094	-0.0168	2.362581
0.046484784	275323	3.0642	35.8613	22.1289	1.31123	0.58864	0.00163	0.26366	0.00225	-0.0154	2.358975

Table 31: U_∞ = 40 mph, h/b = 0.05, $\delta_{mid/out}$ = +10°, Symmetric Deflections

M	Re#	q_c	Uinf	alpha_c	CL	CD_c	Cl_cg_w	Cm_cg_c_w	Cn_cg_w	C_Y	L/D
0.022158902	131244	0.69629	17.0948	0.94905	0.94805	0.12674	0.00183	0.08967	0.00011	0.0006	8.649929
0.046158906	273393	3.02139	35.6099	-4.4017	-0.2083	0.03554	0.00151	-0.1111	-6E-06	0.00089	-6.00071
0.046193767	273600	3.02596	35.6368	-3.2048	-0.0684	0.02766	0.00123	-0.0651	-4E-05	-0.0014	-2.48137
0.046214596	273723	3.02869	35.6529	-2.0963	0.07114	0.02749	0.00075	-0.0267	-0.0003	0.00293	2.59737
0.046161577	273409	3.02174	35.612	-0.909	0.20224	0.02743	0.00065	0.00458	-0.0002	0.00038	7.589054
0.046134831	273251	3.01824	35.5913	0.26534	0.32242	0.03041	0.00067	0.03351	0.00027	-0.0002	11.34348
0.0461585	273391	3.02134	35.6096	1.42813	0.43111	0.03669	0.00072	0.06033	0.00024	-0.0025	13.00841
0.046174714	273487	3.02346	35.6221	2.58496	0.53527	0.0446	0.00075	0.08447	0.00046	-0.0014	13.67671
0.046154713	273368	3.02084	35.6067	3.73912	0.63699	0.05639	0.00083	0.10572	0.00037	-0.0036	13.09305
0.04616205	273412	3.0218	35.6123	4.80178	0.73367	0.07161	0.00084	0.1274	0.00062	-0.0034	11.95938
0.046157198	273383	3.02117	35.6086	5.9404	0.82117	0.08942	0.00056	0.15081	0.00063	-0.0053	10.72535
0.046136251	273259	3.01843	35.5924	7.08409	0.9124	0.11437	0.00019	0.17383	0.001	-0.0045	9.263982
0.046123351	273183	3.01674	35.5825	8.23194	1.00834	0.14391	-0.0004	0.19771	0.00101	-0.0055	8.097842
0.046112227	273117	3.01528	35.5739	9.37031	1.09469	0.1738	-0.0004	0.21734	0.00131	-0.0048	7.252361
0.046120603	273166	3.01638	35.5804	10.5071	1.18052	0.20508	-0.0003	0.2361	0.00124	-0.0067	6.613557
0.04608477	272954	3.01169	35.5527	11.5628	1.27082	0.24425	-0.0004	0.25395	0.00165	-0.0069	5.953896
0.046067018	272849	3.00937	35.539	12.6981	1.35526	0.28618	-0.0003	0.2694	0.00172	-0.008	5.3963
0.046037431	272674	3.00551	35.5162	13.8374	1.44253	0.33314	0.00102	0.28486	0.00195	-0.0087	4.915667
0.045975837	272309	2.99747	35.4687	14.9831	1.53652	0.38612	0.00144	0.30154	0.00207	-0.012	4.50462

Table 32: U_∞ = 60 mph, h/b = 1.05 (OGE), $\delta_{mid/out}$ = +10°, Symmetric Deflections

M	Re#	q_c	Uinf	alpha_c	CL	CD_c	Cl_cg_w	Cm_cg_c_w	Cn_cg_w	C_Y	L/D
0.034952193	207017	1.73239	26.9643	0.89381	0.81788	0.08707	0.00228	0.049	-0.0001	0.00258	11.00552
0.073371064	434567	7.63388	56.6031	-10.887	-0.4137	0.06589	-0.0002	-0.1871	-0.0005	0.00197	-6.60562
0.073270146	433970	7.6129	56.5253	-8.6505	-0.2768	0.03944	4.6E-05	-0.1401	-0.0003	0.00168	-7.28874
0.073277948	434016	7.61452	56.5313	-6.3985	-0.1258	0.02225	5.3E-05	-0.0955	-0.0003	0.00135	-5.73324
0.073294735	434115	7.61801	56.5442	-4.2491	0.01092	0.01774	0.00039	-0.0556	-0.0002	0.00148	0.615582
0.073311876	434217	7.62157	56.5574	-1.9241	0.14905	0.01765	0.00048	-0.0173	-0.0002	0.00131	8.653189
0.073341665	434393	7.62777	56.5804	0.23252	0.29238	0.02453	0.00075	0.0177	8.7E-05	-0.0011	12.76603
0.073413762	434820	7.64277	56.636	2.4761	0.43566	0.0375	0.0006	0.05501	0.00025	-0.0019	12.85849
0.073523569	435471	7.66565	56.7208	4.70675	0.57595	0.0587	0.00084	0.08947	0.00035	-0.0031	10.99698
0.07359673	435904	7.68091	56.7772	6.85996	0.70731	0.09054	0.00067	0.124	0.00045	-0.003	8.732554
0.073633888	436124	7.68867	56.8059	9.07525	0.8247	0.13411	0.00044	0.16274	2.8E-06	0.00341	6.807878
0.073623787	436064	7.68656	56.7981	11.2067	0.94494	0.18623	0.00059	0.19354	0.0001	0.00404	5.584745
0.073624076	436066	7.68662	56.7983	12.3114	1.00144	0.21713	0.00082	0.20632	0.00034	0.0026	5.057648
0.073559403	435683	7.67312	56.7484	13.4184	1.05911	0.25095	0.00116	0.21909	0.00058	0.00065	4.61364
0.073518578	435441	7.66461	56.7169	14.5222	1.1147	0.28766	0.00157	0.23094	0.00076	-0.0013	4.222881
0.073485058	435243	7.65762	56.691	15.6053	1.1505	0.32488	0.00137	0.23772	0.00086	-0.0019	3.839603
0.07341945	434854	7.64395	56.6404	16.6729	1.17299	0.36116	0.00211	0.24163	0.00065	-0.0031	3.502316
0.073354787	434471	7.6305	56.5906	17.7346	1.18918	0.39605	0.0021	0.24436	0.00065	-0.0031	3.222024
0.073347157	434426	7.62891	56.5847	18.7724	1.18443	0.42722	0.00382	0.24093	-0.0005	-0.0044	2.957629
0.073346394	434421	7.62875	56.5841	19.8608	1.14551	0.45083	0.00239	0.22789	-3E-05	-0.0021	2.69023
0.073326179	434301	7.62454	56.5685	20.8592	1.1047	0.47118	0.00169	0.21545	0.0003	-2E-05	2.466374
0.073299334	434142	7.61896	56.5478	21.8603	1.06538	0.48715	0.00296	0.20669	-0.001	-0.0038	2.28867

Table 33: U_∞ = 60 mph, h/b = 0.3, $\delta_{mid/out}$ = +10°, Symmetric Deflections

M	Re#	q_c	Uinf	alpha_c	CL	CD_c	Cl_cg_w	Cm_cg_c_w	Cn_cg_w	C_Y	L/D
0.034225911	202716	1.66114	26.404	0.86124	0.8677	0.09931	0.00165	0.04712	-0.0004	0.00512	10.21372
0.07192955	426029	7.33686	55.491	-11.002	-0.519	0.08135	-9E-05	-0.2239	-0.0005	0.00017	-6.81028
0.071834437	425466	7.31747	55.4177	-8.8224	-0.3545	0.0496	-5E-05	-0.1675	-0.0004	0.00067	-7.50979
0.071844057	425523	7.31943	55.4251	-6.542	-0.1775	0.028	5.2E-05	-0.1128	-0.0004	0.00114	-6.47775
0.071922715	425989	7.33547	55.4858	-4.274	-0.0119	0.02031	0.00032	-0.0662	-0.0003	0.00181	-0.58639
0.071965593	426243	7.34422	55.5188	-2.0132	0.1471	0.02125	0.00047	-0.0234	-0.0003	0.00148	7.060984
0.072003855	426470	7.35203	55.5484	0.24935	0.30778	0.02792	0.00067	0.01646	1.2E-05	-0.0004	11.78804
0.072027718	426611	7.3569	55.5668	2.50965	0.46636	0.04161	0.00058	0.05722	0.0002	-0.0013	12.44806
0.072013987	426530	7.3541	55.5562	4.67599	0.61857	0.06439	0.0008	0.09486	0.00038	-0.0017	10.8344
0.071930664	426036	7.33709	55.4919	6.92068	0.76286	0.09956	0.00067	0.13158	0.00043	-0.0001	8.623764
0.071760396	425028	7.3024	55.3605	9.14927	0.89243	0.14728	0.00043	0.17351	3.7E-05	0.00484	6.756129
0.07155618	423818	7.26089	55.203	11.3032	1.03333	0.20648	0.00066	0.20709	0.00026	0.00364	5.552139
0.071437168	423113	7.23676	55.1112	12.4167	1.09783	0.2409	0.0008	0.2213	0.0005	0.00173	5.037898
0.071374177	422740	7.224	55.0626	13.5315	1.16255	0.2789	0.00123	0.23566	0.00075	0.00015	4.592756
0.071364578	422683	7.22206	55.0552	14.6336	1.21669	0.31859	0.00127	0.24701	0.00101	-0.0015	4.190302
0.071333982	422502	7.21587	55.0316	15.7266	1.26148	0.36057	0.00139	0.2544	0.00114	-0.0032	3.82012
0.071310585	422363	7.21114	55.0135	16.7963	1.28592	0.40024	0.00198	0.25903	0.00099	-0.0045	3.487687
0.071315504	422393	7.21213	55.0173	17.8465	1.29156	0.43592	0.00336	0.25955	0.00019	-0.0053	3.196122
0.071361938	422668	7.22153	55.0531	18.8762	1.27948	0.46916	0.00445	0.25227	-0.0005	-0.0064	2.921566
0.071383655	422796	7.22592	55.0699	19.8701	1.23363	0.4925	0.00308	0.23707	-0.0001	-0.0047	2.661715
0.071329662	422476	7.215	55.0282	20.9617	1.19847	0.51741	0.0024	0.2264	0.00014	-0.0038	2.445794
0.071294747	422270	7.20794	55.0013	21.9756	1.17091	0.54016	0.00242	0.22097	-9E-05	-0.0044	2.277987

Table 34: U_∞ = 60 mph, h/b = 0.15, $\delta_{mid/out}$ = +10°, Symmetric Deflections

M	Re#	q_c	Uinf	alpha_c	CL	CD_c	Cl_cg_w	Cm_cg_c_w	Cn_cg_w	C_Y	L/D
0.031449702	186273	1.40258	24.2623	1.04808	0.95906	0.11022	0.00194	0.06784	-0.0006	0.0062	10.34868
0.071133576	421315	7.17538	54.877	-11.248	-0.7439	0.11086	0.00059	-0.2937	-0.0005	0.0006	-7.4165
0.071033694	420723	7.15525	54.7999	-8.9042	-0.509	0.0638	0.00046	-0.2105	-0.0004	0.00051	-8.64691
0.071047066	420803	7.15794	54.8102	-6.5587	-0.2725	0.03297	0.00049	-0.1351	-0.0004	0.00147	-8.63571
0.071135603	421327	7.17579	54.8785	-4.3278	-0.0611	0.02288	0.0004	-0.075	-0.0004	0.0025	-2.67916
0.071190259	421651	7.18682	54.9207	-1.9442	0.13067	0.02143	0.00064	-0.0243	-0.0001	0.00058	6.192068
0.071204321	421734	7.18966	54.9315	0.25811	0.31579	0.02876	0.00078	0.02121	0.00013	-0.0008	11.75803
0.071152319	421426	7.17916	54.8914	2.54368	0.4975	0.04357	0.00061	0.06516	0.00035	-0.002	12.80453
0.071140398	421355	7.17676	54.8822	4.81867	0.66952	0.06888	0.00071	0.10618	0.00056	-0.003	11.09766
0.07116187	421483	7.18109	54.8988	6.98566	0.82233	0.10691	0.0009	0.14691	0.00035	0.00085	8.746556
0.071084795	421026	7.16554	54.8393	9.23673	0.97246	0.16079	0.00024	0.18796	6E-05	0.00382	6.812226
0.070994851	420493	7.14742	54.7699	11.3972	1.11933	0.22369	0.00064	0.2214	0.00054	0.00169	5.602458
0.07090451	419958	7.12924	54.7003	12.5143	1.18711	0.2613	0.00077	0.23638	0.00091	-0.0009	5.063972
0.070815398	419430	7.11134	54.6315	13.6374	1.25945	0.30293	0.00159	0.25148	0.00113	-0.0036	4.61886
0.070737597	418970	7.09572	54.5715	14.743	1.31672	0.34742	0.00137	0.26079	0.00139	-0.0046	4.188635
0.070690662	418692	7.08631	54.5353	15.8339	1.35972	0.39254	0.00147	0.26765	0.00152	-0.0062	3.805761
0.070642201	418405	7.07659	54.4979	16.894	1.37535	0.43355	0.00291	0.27146	0.00114	-0.0078	3.460219
0.070574657	418005	7.06307	54.4458	17.9353	1.37286	0.4714	0.00327	0.26873	0.00062	-0.0082	3.152709
0.070544471	417826	7.05703	54.4225	18.9451	1.34247	0.50322	0.00179	0.25559	0.00102	-0.0052	2.863349
0.070507905	417609	7.04971	54.3943	20.0312	1.30143	0.53256	0.00156	0.24072	0.00098	-0.0037	2.601502
0.070436963	417189	7.03553	54.3396	21.0541	1.28305	0.56085	0.00137	0.23603	0.00111	-0.0047	2.423365
0.070406854	417011	7.02952	54.3163	22.0749	1.26175	0.58592	0.00077	0.23189	0.00145	-0.0043	2.271138

Table 35: U_∞ = 60 mph, h/b = 0.1, $\delta_{mid/out}$ = +10°, Symmetric Deflections

M	Re#	q_c	Uinf	alpha_c	CL	CD_c	Cl_cg_w	Cm_cg_c_w	Cn_cg_w	C_Y	L/D
0.033876651	200647	1.62741	26.1346	0.99583	0.91124	0.10016	0.00112	0.06927	-0.0013	0.01111	10.80595
0.071177585	421576	7.18426	54.9109	-10.333	-0.8615	0.10749	0.00154	-0.3485	-0.0006	0.00208	-9.23012
0.071094947	421086	7.16759	54.8472	-9.1033	-0.6912	0.07748	0.00152	-0.28	-0.0006	0.00211	-10.1096
0.071142553	421368	7.17719	54.8839	-6.666	-0.3706	0.03735	0.00076	-0.165	-0.0007	0.00391	-10.6702
0.071247126	421988	7.19831	54.9646	-4.287	-0.1034	0.02131	0.00041	-0.0857	-0.0008	0.00557	-4.89968
0.071258944	422058	7.2007	54.9737	-1.961	0.11533	0.02021	0.00041	-0.0251	-0.0007	0.0046	5.778779
0.071245001	421975	7.19788	54.9629	0.26536	0.32243	0.02744	0.00041	0.02494	-0.0004	0.00318	12.66382
0.071250353	422007	7.19896	54.9671	2.56283	0.51502	0.04314	0.00044	0.07168	-0.0003	0.00199	13.52535
0.071261467	422072	7.20121	54.9756	4.84768	0.69607	0.06923	0.00036	0.1144	-6E-05	0.00066	11.60243
0.071256795	422045	7.20026	54.972	7.02244	0.85598	0.10927	-1E-05	0.15644	-0.0001	0.00364	8.98216
0.071204234	421733	7.18964	54.9315	9.28587	1.01743	0.16623	0.00014	0.19978	-0.0003	0.00602	6.945695
0.071115662	421209	7.17177	54.8631	11.4521	1.16956	0.23169	0.00013	0.23379	0.00042	0.00213	5.688496
0.071038219	420750	7.15616	54.8034	12.5774	1.2448	0.27128	0.00067	0.24915	0.00077	-0.0002	5.149644
0.07097165	420356	7.14275	54.752	13.7034	1.31985	0.3145	0.00154	0.26294	0.00102	-0.0038	4.692263
0.070914285	420016	7.13121	54.7078	14.8178	1.38522	0.36269	0.00147	0.273	0.00122	-0.0049	4.247855
0.070823575	419479	7.11298	54.6378	15.9144	1.43333	0.41028	0.00065	0.28016	0.00162	-0.0059	3.862418
0.070710397	418809	7.09026	54.5505	16.9579	1.43382	0.4535	0.00287	0.27959	0.00082	-0.0071	3.460868
0.070586463	418075	7.06543	54.4549	17.9855	1.4188	0.49178	0.00216	0.27151	0.00084	-0.0062	3.129336
0.070505875	417597	7.04931	54.3927	18.996	1.38903	0.52706	0.00099	0.25516	0.00108	-0.0042	2.833233
0.070473136	417403	7.04276	54.3675	20.0914	1.35651	0.55857	0.00181	0.24377	0.00041	-0.0051	2.591354
0.070433116	417166	7.03477	54.3366	21.1162	1.33985	0.58878	0.00092	0.23854	0.00109	-0.0036	2.416146
0.070387943	416899	7.02574	54.3017	22.1626	1.34203	0.62273	0.00251	0.2385	3E-05	-0.0088	2.280884

Table 36: U_∞ = 60 mph, h/b = 0.05, $\delta_{mid/out} = +10^o$, Symmetric Deflections

M	Re#	q_c	Uinf	alpha_c	CL	CD_c	Cl_cg_w	Cm_cg_c_w	Cn_cg_w	C_Y	L/D
0.034211355	202629	1.65973	26.3928	0.94105	0.86111	0.08991	0.00156	0.07161	-8E-05	-9E-05	11.36485
0.0714145	422979	7.23217	55.0937	-4.3997	-0.2066	0.02776	0.00168	-0.1138	-0.0002	-0.0003	-7.66433
0.071360831	422661	7.2213	55.0523	-3.1951	-0.0596	0.02242	0.00124	-0.0704	-0.0002	-0.0002	-2.6655
0.071352544	422612	7.21963	55.0459	-2.0867	0.07985	0.02206	0.00093	-0.0328	-0.0001	-0.0001	3.639219
0.071428088	423059	7.23492	55.1042	-0.9064	0.20458	0.02319	0.00069	-0.0016	-7E-05	-0.0003	9.136728
0.071493544	423447	7.24819	55.1547	0.26022	0.31773	0.02648	0.00061	0.02504	0.00012	-0.0016	12.93729
0.071491382	423434	7.24775	55.153	1.42149	0.42504	0.03349	0.00058	0.0499	0.00022	-0.0019	14.14508
0.071438297	423120	7.23699	55.112	2.57564	0.52674	0.04224	0.00069	0.07312	0.00041	-0.0025	14.2554
0.071454457	423216	7.24026	55.1245	3.71984	0.61935	0.0525	0.00072	0.09484	0.00052	-0.0034	13.70701
0.071457612	423234	7.2409	55.1269	4.77811	0.71201	0.06645	0.00074	0.11452	0.00041	-0.0028	12.53981
0.07143025	423072	7.23536	55.1058	5.92273	0.80501	0.08574	0.00033	0.13555	0.00013	0.00069	10.97003
0.071413075	422970	7.23188	55.0926	7.07091	0.90033	0.11113	-0.0003	0.1574	-1E-05	0.00365	9.411137
0.07144142	423138	7.23762	55.1145	8.20698	0.98549	0.13848	-0.0007	0.18145	-0.0002	0.00548	8.215713
0.071442621	423145	7.23787	55.1154	9.34067	1.06757	0.16763	-0.0005	0.2016	0.00016	0.00404	7.31765
0.071437109	423113	7.23675	55.1111	10.4749	1.15103	0.20059	-0.0002	0.21836	0.00056	0.00166	6.565169
0.07145307	423207	7.23998	55.1234	11.5233	1.23471	0.2364	-0.0004	0.23447	0.00106	-0.0009	5.955447
0.071412955	422970	7.23186	55.0925	12.6581	1.31867	0.27786	-8E-05	0.25098	0.00154	-0.0031	5.389116
0.071360831	422661	7.2213	55.0523	13.7904	1.39948	0.32202	0.00104	0.26567	0.00185	-0.0066	4.916161
0.071305409	422333	7.21009	55.0095	14.9214	1.47998	0.37146	0.00101	0.28043	0.00225	-0.0096	4.489036

Table 37: U_∞ = 80 mph, h/b = 1.05 (OGE), $\delta_{mid/out}$ = +10°, Symmetric Deflections

M	Re#	q_c	Uinf	alpha_c	CL	CD_c	Cl_cg_w	Cm_cg_c_w	Cn_cg_w	C_Y	L/D
0.046493315	275374	3.06533	35.8679	0.87432	0.80005	0.07683	0.00246	0.04411	0.00063	-0.0025	12.38004
0.096917793	574032	13.32	74.7686	-10.895	-0.4212	0.06434	-0.0002	-0.1939	-0.0004	0.00039	-6.90931
0.09671937	572856	13.2655	74.6155	-8.6523	-0.2784	0.03741	-4E-05	-0.1457	-0.0004	0.00116	-7.74862
0.096649298	572441	13.2463	74.5614	-6.3943	-0.122	0.02092	0.00025	-0.1001	-0.0002	0.00019	-5.91004
0.096652227	572459	13.2471	74.5637	-4.2368	0.02213	0.01575	0.00046	-0.0604	-7E-05	-0.0007	1.405622
0.096729825	572918	13.2683	74.6235	-1.994	0.16471	0.01721	0.00052	-0.0214	0.0002	-0.0013	9.868813
0.09682624	573489	13.2948	74.6979	0.25097	0.30926	0.02402	0.00097	0.01596	0.00038	-0.0022	13.93274
0.096974884	574370	13.3357	74.8126	2.50058	0.45806	0.03761	0.00081	0.05219	0.00037	-0.0019	13.63027
0.097104453	575137	13.3713	74.9126	4.66732	0.61063	0.05895	0.00054	0.08807	-2E-05	0.00299	11.7787
0.097186269	575622	13.3939	74.9757	6.89467	0.73907	0.09151	0.00053	0.12766	0.00074	-0.0011	9.113837
0.097210911	575768	13.4006	74.9947	9.11697	0.86288	0.13821	0.00215	0.16806	0.00174	-0.0079	6.958348
0.097147145	575390	13.3831	74.9455	11.2476	0.98241	0.19194	0.00185	0.19991	0.00226	-0.0111	5.661311
0.0970717	574943	13.3623	74.8873	12.356	1.04228	0.22402	0.00152	0.21273	0.00254	-0.0126	5.126797
0.097018445	574628	13.3476	74.8462	13.4634	1.10026	0.25903	0.00174	0.22527	0.00276	-0.0143	4.663282
0.096973716	574363	13.3353	74.8117	14.5598	1.1491	0.29595	0.00253	0.23578	0.00284	-0.0168	4.243932
0.096949191	574218	13.3286	74.7928	15.6437	1.18566	0.33442	0.00269	0.24171	0.00297	-0.0182	3.854392
0.096906563	573965	13.3169	74.7599	16.7137	1.21039	0.37181	0.00275	0.24571	0.00296	-0.0185	3.51988
0.096849727	573628	13.3013	74.716	17.7716	1.22307	0.40675	0.00352	0.24786	0.00264	-0.0186	3.23377
0.096771621	573166	13.2798	74.6558	18.8094	1.2183	0.43783	0.00434	0.24597	0.00216	-0.0195	2.974944
0.096731901	572931	13.2689	74.6251	19.898	1.17952	0.46214	0.00563	0.23307	0.00082	-0.0217	2.70776
0.0966675	572549	13.2512	74.5755	20.897	1.13927	0.48369	0.00448	0.21887	0.00133	-0.0191	2.482433
0.096598351	572140	13.2323	74.5221	21.9152	1.1156	0.50556	0.00431	0.21221	0.00132	-0.019	2.315369

Table 38: U_∞ = 80 mph, h/b = 0.3, $\delta_{mid/out}$ = +10°, Symmetric Deflections

M	Re#	q_c	Uinf	alpha_c	CL	CD_c	Cl_cg_w	Cm_cg_c_w	Cn_cg_w	C_Y	L/D
0.04890893	289681	3.39213	37.7315	0.74471	0.76107	0.0776	0.00185	0.04167	-0.0003	0.0044	11.43488
0.095175963	563715	12.8455	73.4248	-11.015	-0.5308	0.07997	3.6E-07	-0.2308	-0.0005	0.00058	-7.11554
0.095057283	563012	12.8135	73.3332	-8.8301	-0.3615	0.04808	-0.0001	-0.1735	-0.0005	0.00095	-7.9317
0.095052761	562985	12.8122	73.3297	-6.5393	-0.1751	0.0262	1E-04	-0.1173	-0.0004	0.00164	-6.83393
0.095114105	563349	12.8288	73.3771	-4.2667	-0.0052	0.01885	0.00032	-0.0703	-0.0004	0.00204	-0.27827
0.09516829	563669	12.8434	73.4189	-2.0023	0.15711	0.01994	0.00048	-0.0252	-1E-04	0.00062	8.067912
0.095203491	563878	12.8529	73.446	0.26161	0.31899	0.02717	0.00089	0.01626	0.00017	-0.0007	12.64623
0.095167235	563663	12.8431	73.4181	2.53031	0.48527	0.04155	0.00072	0.05699	0.00014	-2E-05	13.09372
0.095113749	563346	12.8287	73.3768	4.71013	0.64981	0.06474	0.00048	0.09632	-0.0002	0.00423	11.46324
0.094972379	562509	12.7906	73.2677	6.94746	0.78737	0.09991	0.00077	0.14003	0.00069	-0.0005	8.938868
0.094813555	561568	12.7478	73.1452	9.18437	0.92454	0.15188	0.00129	0.18215	0.00156	-0.006	6.81904
0.094691578	560846	12.7151	73.0511	11.3328	1.06037	0.2103	0.00141	0.21591	0.00221	-0.0098	5.614846
0.094551804	560018	12.6776	72.9433	12.4481	1.12649	0.24541	0.00117	0.23036	0.00259	-0.0118	5.092397
0.094453084	559433	12.6511	72.8671	13.5617	1.19019	0.28399	0.00193	0.24325	0.00284	-0.0144	4.631504
0.09438296	559018	12.6323	72.813	14.6619	1.24256	0.32463	0.00205	0.25374	0.00305	-0.0164	4.209435
0.094287206	558451	12.6067	72.7392	15.7522	1.28497	0.36776	0.00236	0.25987	0.00318	-0.0182	3.821189
0.094275459	558381	12.6036	72.7301	16.8273	1.31428	0.40887	0.00264	0.26538	0.00321	-0.0192	3.496078
0.094283528	558429	12.6057	72.7363	17.874	1.31676	0.44479	0.00289	0.26531	0.0031	-0.0194	3.19818
0.094326006	558681	12.6171	72.7691	18.8982	1.29958	0.47604	0.00277	0.25891	0.00305	-0.018	2.928085
0.094320311	558647	12.6156	72.7647	19.8911	1.25278	0.4996	0.00284	0.24322	0.0027	-0.0174	2.667356
0.094275103	558379	12.6035	72.7298	20.9943	1.22827	0.52867	0.00334	0.2333	0.00237	-0.0186	2.457071
0.094253756	558253	12.5978	72.7133	22.0127	1.20488	0.55278	0.00303	0.22722	0.0025	-0.0182	2.294601

Table 39: U_∞ = 80 mph, h/b = 0.15, $\delta_{mid/out}$ = +10°, Symmetric Deflections

M	Re#	q_c	Uinf	alpha_c	CL	CD_c	Cl_cg_w	Cm_cg_c_w	Cn_cg_w	C_Y	L/D
0.04550909	269544	2.93692	35.1086	0.92875	0.84986	0.08677	0.00236	0.05465	0.00037	0.00022	11.64201
0.093998047	556738	12.5295	72.5161	-11.278	-0.7718	0.11072	0.00057	-0.3093	-0.0002	-0.001	-7.76759
0.093926985	556317	12.5106	72.4613	-8.9192	-0.5227	0.06203	0.00054	-0.2234	-0.0002	-0.0007	-9.19932
0.093928165	556324	12.5109	72.4622	-6.558	-0.2718	0.03065	0.00055	-0.1424	-0.0002	0.00087	-9.2956
0.094017452	556853	12.5347	72.531	-4.317	-0.0513	0.02042	0.00062	-0.0812	-0.0001	0.00043	-2.51733
0.094062122	557118	12.5466	72.5655	-1.9313	0.14251	0.02018	0.00071	-0.0281	0.00022	-0.0015	7.200599
0.09405259	557061	12.544	72.5582	0.27699	0.33307	0.02777	0.00111	0.01999	0.00048	-0.0028	12.98296
0.094054425	557072	12.5445	72.5596	2.56964	0.52125	0.04339	0.00065	0.06466	0.00034	-0.0006	13.64076
0.09403035	556930	12.5381	72.541	4.85737	0.70493	0.06974	0.00057	0.10774	0.00021	0.00175	11.69667
0.093963945	556536	12.5204	72.4898	7.01461	0.84882	0.10798	0.00101	0.15393	0.00131	-0.0045	9.006833
0.093851989	555873	12.4906	72.4034	9.27291	1.00556	0.16452	0.00164	0.19635	0.00209	-0.0098	6.923711
0.09370812	555021	12.4523	72.2924	11.4328	1.15183	0.22862	0.00105	0.23092	0.00289	-0.0136	5.665295
0.093567667	554189	12.415	72.1841	12.5566	1.22582	0.26803	0.00181	0.24546	0.00319	-0.0166	5.121064
0.093522269	553920	12.403	72.149	13.6765	1.29524	0.31008	0.00277	0.25868	0.00336	-0.0196	4.657734
0.093462797	553568	12.3872	72.1031	14.7774	1.34825	0.355	0.00214	0.26699	0.00368	-0.0207	4.208917
0.093335957	552817	12.3536	72.0053	15.8766	1.39875	0.40333	0.00251	0.27438	0.0038	-0.0227	3.821521
0.093219375	552126	12.3228	71.9154	16.9213	1.40028	0.44172	0.00353	0.27554	0.00338	-0.023	3.463251
0.093127439	551582	12.2985	71.8444	17.9647	1.39977	0.48021	0.00412	0.27374	0.00301	-0.0231	3.160891
0.093045311	551095	12.2768	71.7811	18.9787	1.37325	0.51302	0.00349	0.26212	0.00294	-0.0218	2.878622
0.093064073	551206	12.2817	71.7955	20.0757	1.3421	0.54605	0.00284	0.2479	0.00331	-0.0207	2.622844
0.093049677	551121	12.2779	71.7844	21.0901	1.31595	0.57316	0.00314	0.23893	0.00301	-0.022	2.436325
0.092967804	550636	12.2563	71.7213	22.1249	1.30751	0.60406	0.00309	0.23622	0.00316	-0.0222	2.288018

Table 40: U_∞ = 80 mph, h/b = 0.1, $\delta_{mid/out}$ = +10°, Symmetric Deflections

M	Re#	q_c	Uinf	alpha_c	CL	CD_c	Cl_cg_w	Cm_cg_c_w	Cn_cg_w	C_Y	L/D
0.047654932	282254	3.22041	36.764	0.8974	0.82117	0.0813	0.00184	0.06134	-0.0001	0.00298	11.9989
0.094468126	559523	12.6551	72.8787	-9.1221	-0.7084	0.07767	0.00151	-0.2911	-0.0003	0.00135	-10.4015
0.094406417	559157	12.6386	72.8311	-6.6737	-0.3776	0.03624	0.00095	-0.1736	-0.0003	0.0018	-11.2645
0.094410833	559183	12.6398	72.8345	-4.3711	-0.1007	0.02182	0.00066	-0.0918	-0.0005	0.00325	-4.65774
0.094423872	559260	12.6433	72.8446	-1.9501	0.12527	0.02007	0.00069	-0.0287	-5E-05	0.00035	6.335563
0.094443312	559376	12.6485	72.8596	0.28119	0.33691	0.02792	0.00092	0.0233	0.00016	-0.0009	13.08094
0.094466887	559515	12.6548	72.8778	2.58711	0.53724	0.04341	0.00056	0.0706	-3E-05	0.00151	14.17303
0.094491467	559661	12.6614	72.8967	4.88602	0.73115	0.07097	0.00027	0.11535	0.0001	0.00167	12.03125
0.094473657	559555	12.6566	72.883	7.05345	0.88436	0.11163	0.00078	0.16252	0.00146	-0.0054	9.144156
0.094387599	559046	12.6336	72.8166	9.31889	1.04764	0.1696	0.00158	0.20556	0.00209	-0.0104	7.046684
0.094254574	558258	12.598	72.714	11.4854	1.19997	0.23637	0.00068	0.23958	0.00301	-0.0146	5.744138
0.094114015	557425	12.5604	72.6055	12.6136	1.27796	0.27726	0.00198	0.25414	0.00335	-0.0185	5.192636
0.094012806	556826	12.5334	72.5275	13.7379	1.35145	0.3216	0.00218	0.26751	0.00359	-0.0208	4.712784
0.093935617	556369	12.5129	72.4679	14.8476	1.41246	0.36952	0.00175	0.27624	0.00397	-0.0224	4.261191
0.093871607	555989	12.4958	72.4185	15.9461	1.46239	0.41992	0.00104	0.28194	0.0044	-0.0232	3.857164
0.093777607	555433	12.4708	72.346	16.984	1.4577	0.46115	0.00399	0.28101	0.00344	-0.0257	3.465524
0.09365122	554684	12.4372	72.2485	18.0125	1.44347	0.49929	0.00412	0.27454	0.003	-0.0243	3.141028
0.093512579	553863	12.4004	72.1416	19.0152	1.40658	0.53262	0.00285	0.25669	0.00314	-0.0228	2.842249
0.093409786	553254	12.3732	72.0623	20.1245	1.38674	0.56916	0.00212	0.24553	0.00368	-0.0204	2.604297
0.093352901	552917	12.3581	72.0184	21.1588	1.3788	0.60278	0.00153	0.24123	0.00437	-0.0195	2.43377
0.093281549	552495	12.3392	71.9633	22.2025	1.3785	0.63772	0.00269	0.23912	0.00345	-0.0237	2.291839

Table 41: U_∞ = 80 mph, h/b = 0.05, $\delta_{mid/out}$ = +10°, Symmetric Deflections

M	Re#	q_c	Uinf	alpha_c	CL	CD_c	Cl_cg_w	Cm_cg_c_w	Cn_cg_w	C_Y	L/D
0.05146277	304807	3.75562	39.7017	0.70018	0.72031	0.06844	0.00137	0.05846	7.5E-05	0.00088	12.30274
0.094405741	559153	12.6384	72.8306	-4.4244	-0.2292	0.02691	0.00157	-0.1182	-0.0004	0.00219	-8.84464
0.094370013	558941	12.6289	72.803	-3.2029	-0.0667	0.02105	0.00121	-0.0722	-0.0004	0.00209	-3.18074
0.094377976	558989	12.631	72.8092	-2.0817	0.0845	0.02069	0.00091	-0.034	-0.0002	0.00124	4.111544
0.09435033	558825	12.6236	72.7878	-0.8941	0.21582	0.02244	0.00073	-0.002	1.6E-05	0.00016	10.01567
0.094394944	559089	12.6355	72.8223	0.27698	0.33306	0.02642	0.00068	0.02528	0.00016	-0.0006	13.70133
0.094427574	559282	12.6443	72.8474	1.44566	0.44715	0.03326	0.00065	0.05024	0.00012	0.00031	15.18753
0.094434811	559325	12.6462	72.853	2.60833	0.55666	0.04211	0.00065	0.07318	-4E-05	0.00279	15.37728
0.094381061	559007	12.6318	72.8116	3.76804	0.66345	0.05338	0.00072	0.09555	-0.0002	0.00369	14.74875
0.094332057	558717	12.6187	72.7738	4.82856	0.75818	0.06815	0.00077	0.11738	0.00013	0.0019	13.25754
0.094300258	558528	12.6102	72.7492	5.96903	0.84737	0.08793	0.00059	0.14123	0.00096	-0.0022	11.41395
0.094328735	558697	12.6178	72.7712	7.10455	0.93112	0.11331	-0.0001	0.1674	0.00189	-0.0059	9.621157
0.094376196	558978	12.6305	72.8078	8.24419	1.01955	0.14288	0.0003	0.18996	0.00203	-0.0084	8.285201
0.094357686	558868	12.6256	72.7935	9.37831	1.10201	0.17297	0.00035	0.20929	0.00243	-0.0104	7.355914
0.094297634	558513	12.6095	72.7472	10.5138	1.18669	0.20676	0.00057	0.2272	0.00288	-0.0135	6.596333
0.09427273	558365	12.6028	72.728	11.5641	1.272	0.24338	7.5E-05	0.24355	0.00339	-0.0158	5.985396
0.094243897	558194	12.5951	72.7057	12.7046	1.3612	0.2861	0.00034	0.25966	0.00397	-0.0185	5.428342
0.094180299	557818	12.5781	72.6567	13.8416	1.44637	0.33313	0.00138	0.27456	0.00421	-0.0222	4.932429
0.094075884	557199	12.5503	72.5761	14.9761	1.53008	0.38466	0.00124	0.28828	0.00471	-0.0251	4.500183

Table 42: U_∞ = 100 mph, h/b = 1.05, $\delta_{mid/out}$ = +10°, Symmetric Deflections

M	Re#	q_c	Uinf	alpha_c	CL	CD_c	Cl_cg_w	Cm_cg_c_w	Cn_cg_w	C_Y	L/D
0.057996396	343505	4.76977	44.7421	0.75605	0.77144	0.07044	0.00165	0.04396	0.00043	4.1E-05	13.05537
0.120657034	714636	20.6443	93.0825	-10.903	-0.4287	0.06389	-0.0001	-0.1975	-0.0005	0.00034	-7.09907
0.120525531	713857	20.5994	92.9811	-8.7427	-0.2815	0.03768	1.9E-05	-0.1492	-0.0004	0.0006	-7.78549
0.120532445	713898	20.6017	92.9864	-6.4814	-0.1221	0.02097	0.00014	-0.1019	-0.0002	9.9E-05	-5.90131
0.120498095	713695	20.59	92.9599	-4.2368	0.02214	0.01593	0.0004	-0.0618	-7E-05	-0.0004	1.390947
0.120515452	713797	20.5959	92.9733	-1.9911	0.16741	0.01759	0.00051	-0.0212	0.00018	-0.0014	9.815369
0.120644965	714565	20.6402	93.0732	0.25836	0.31603	0.02394	0.00072	0.01658	0.00034	-0.0016	14.34124
0.120812265	715555	20.6975	93.2023	2.52026	0.47607	0.03773	0.00053	0.05532	7.6E-05	0.00187	14.2495
0.121009946	716726	20.7653	93.3548	4.67527	0.61791	0.05893	0.00081	0.0931	0.00078	-0.0023	11.9642
0.121096431	717239	20.795	93.4215	6.90094	0.7448	0.09119	0.00107	0.13381	0.00167	-0.008	9.239395
0.121059772	717021	20.7824	93.3932	9.12616	0.87128	0.13684	0.00282	0.17063	0.00319	-0.0169	7.120691
0.120957267	716414	20.7472	93.3141	11.2619	0.99554	0.19005	0.00347	0.20461	0.00369	-0.0215	5.816678
0.120868551	715889	20.7168	93.2457	12.3701	1.05518	0.22652	0.00169	0.21769	0.00348	-0.0183	5.140118
0.120823356	715621	20.7013	93.2108	13.4766	1.11234	0.26189	0.00243	0.22965	0.00367	-0.0213	4.667904
0.12075284	715203	20.6771	93.1564	14.5745	1.16262	0.30016	0.00256	0.23921	0.00389	-0.023	4.237238
0.120701938	714902	20.6597	93.1172	15.6527	1.19385	0.33798	0.00326	0.24396	0.00389	-0.0252	3.84127
0.120607839	714345	20.6275	93.0446	16.7215	1.21752	0.37505	0.00469	0.24754	0.0034	-0.0262	3.51094
0.120556469	714040	20.6099	93.0049	17.7757	1.22677	0.40917	0.00391	0.24925	0.00373	-0.0256	3.224351
0.120486654	713627	20.5861	92.9511	18.8106	1.21939	0.44006	0.00489	0.24441	0.00306	-0.0257	2.961792
0.120388715	713047	20.5526	92.8755	19.8954	1.17715	0.46375	0.00474	0.23095	0.00264	-0.0253	2.691732
0.120342937	712776	20.537	92.8402	20.8934	1.13593	0.48376	0.00435	0.21721	0.00266	-0.0256	2.473977
0.120289455	712459	20.5188	92.7989	21.9188	1.11892	0.50765	0.00466	0.21195	0.00221	-0.025	2.312893

Table 43: U_∞ = 100 mph, h/b = 0.3, $\delta_{mid/out}$ = +10°, Symmetric Deflections

M	Re#	q_c	Uinf	alpha_c	CL	CD_c	Cl_cg_w	Cm_cg_c_w	Cn_cg_w	C_Y	L/D
0.055339448	327768	4.34276	42.6924	0.8185	0.82858	0.08012	0.00178	0.04715	7.2E-05	0.00282	12.36123
0.118049144	699190	19.7616	91.0706	-11.034	-0.5481	0.0804	4.2E-05	-0.2378	-0.0004	-0.0002	-7.33994
0.117829739	697890	19.6882	90.9014	-8.7529	-0.3705	0.04658	-7E-05	-0.1785	-0.0003	1.2E-06	-8.42741
0.117825254	697864	19.6867	90.8979	-6.5435	-0.1789	0.02529	0.00024	-0.1203	-0.0003	0.00068	-7.25068
0.117895876	698282	19.7103	90.9524	-4.2662	-0.0048	0.01831	0.00043	-0.0721	-1E-04	-8E-05	-0.26196
0.117988963	698833	19.7414	91.0242	-1.9955	0.16337	0.01951	0.00056	-0.0257	0.00014	-0.001	8.59831
0.117979153	698775	19.7381	91.0166	0.2756	0.3318	0.02627	0.00078	0.01736	0.00023	-0.0007	13.72952
0.117941383	698552	19.7255	90.9875	2.55669	0.5094	0.04113	0.00065	0.06094	0.00012	0.0015	14.07931
0.117877515	698173	19.7042	90.9382	4.72886	0.66695	0.0643	0.001	0.10264	0.00087	-0.0032	11.94966
0.117709387	697177	19.648	90.8085	6.96676	0.80503	0.10008	0.00142	0.14718	0.00198	-0.0096	9.177795
0.117474819	695788	19.5698	90.6276	9.20835	0.94649	0.15003	0.00309	0.18621	0.00353	-0.0191	7.119312
0.117228606	694330	19.4878	90.4376	11.3644	1.08929	0.21254	0.00264	0.22307	0.00377	-0.0213	5.735693
0.117087677	693495	19.441	90.3289	12.4815	1.15711	0.25119	0.00192	0.23717	0.00382	-0.0206	5.12782
0.117007888	693023	19.4145	90.2673	13.592	1.21795	0.28999	0.00253	0.24962	0.00398	-0.0234	4.65396
0.116977082	692840	19.4043	90.2436	14.6908	1.26897	0.33163	0.00226	0.25838	0.00433	-0.0248	4.217002
0.116960203	692740	19.3987	90.2305	15.7778	1.30835	0.37516	0.00314	0.26369	0.00427	-0.0271	3.819832
0.116904273	692409	19.3801	90.1874	16.8432	1.32887	0.41488	0.00438	0.26711	0.00396	-0.0273	3.485991
0.116908151	692432	19.3814	90.1904	17.8931	1.33425	0.45077	0.00369	0.26796	0.00428	-0.0275	3.200998
0.116929515	692558	19.3885	90.2069	18.9112	1.31145	0.48154	0.00409	0.25862	0.00364	-0.0285	2.922545
0.116970708	692802	19.4022	90.2386	20.0045	1.27696	0.5101	0.0039	0.24462	0.00357	-0.0284	2.66588
0.11693943	692617	19.3918	90.2145	21.0123	1.24478	0.53539	0.00232	0.23415	0.00475	-0.0238	2.46082
0.116794251	691757	19.3437	90.1025	22.0336	1.22394	0.56073	0.00299	0.22844	0.00399	-0.0244	2.29995

Table 44: U_∞ = 100 mph, h/b = 0.15, $\delta_{mid/out}$ = +10°, Symmetric Deflections

M	Re#	q_c	Uinf	alpha_c	CL	CD_c	Cl_cg_w	Cm_cg_c_w	Cn_cg_w	C_Y	L/D
0.054632263	323580	4.23247	42.1468	0.94534	0.86505	0.08362	0.00188	0.0595	0.00012	0.00262	12.47473
0.116427562	689585	19.2224	89.8196	-11.321	-0.8108	0.11367	0.00064	-0.3231	-0.0002	-0.0014	-8.01697
0.116315979	688925	19.1856	89.7335	-8.9454	-0.5466	0.06264	0.00056	-0.2328	-9E-05	-0.001	-9.59984
0.116338989	689061	19.1932	89.7513	-6.571	-0.2837	0.0303	0.00088	-0.1478	-0.0002	-5E-05	-9.86408
0.116457168	689761	19.2322	89.8425	-4.2352	-0.056	0.01975	0.00062	-0.0833	-6E-05	-0.0002	-2.84363
0.116524112	690157	19.2543	89.8941	-1.9242	0.14901	0.02022	0.00076	-0.0274	0.00029	-0.0022	7.528039
0.116558399	690360	19.2656	89.9206	0.29129	0.34616	0.02716	0.00082	0.02181	0.00031	-0.0009	13.91441
0.116524895	690162	19.2545	89.8947	2.59912	0.54823	0.04314	0.00067	0.06991	0.0003	0.00021	14.65446
0.116485523	689929	19.2415	89.8643	4.87498	0.72105	0.06925	0.00102	0.11504	0.00115	-0.005	12.15184
0.116375349	689276	19.2052	89.7793	7.03803	0.87025	0.10869	0.00184	0.1616	0.00257	-0.013	9.234226
0.116260117	688594	19.1671	89.6905	9.29726	1.02785	0.16415	0.00255	0.20239	0.0038	-0.0209	7.137685
0.11605948	687405	19.101	89.5357	11.4689	1.18487	0.23442	0.00156	0.23874	0.00399	-0.0214	5.706253
0.115945564	686731	19.0636	89.4478	12.5931	1.2592	0.2741	0.00262	0.25338	0.00428	-0.0242	5.163678
0.115857917	686211	19.0348	89.3802	13.7064	1.32262	0.31692	0.00263	0.26453	0.00451	-0.0266	4.664429
0.115704682	685304	18.9844	89.262	14.8132	1.38102	0.36441	0.0026	0.27323	0.00476	-0.0281	4.210031
0.115520589	684214	18.9241	89.1199	15.9048	1.42453	0.41232	0.00282	0.27925	0.00492	-0.0293	3.812776
0.115389413	683437	18.8811	89.0187	16.9473	1.42406	0.45075	0.00365	0.27975	0.00474	-0.0297	3.455845
0.115319835	683024	18.8584	88.9651	17.9908	1.42363	0.49002	0.00428	0.27582	0.00422	-0.0316	3.154034
0.11533544	683117	18.8635	88.9771	19.0017	1.39424	0.52207	0.00288	0.26379	0.00476	-0.0291	2.874763
0.115314907	682995	18.8567	88.9613	20.0879	1.35332	0.55222	0.00352	0.24709	0.00412	-0.0287	2.616196
0.115288316	682838	18.848	88.9407	21.1135	1.33734	0.58243	0.00288	0.24128	0.00452	-0.0274	2.438982
0.115224992	682463	18.8273	88.8919	22.1531	1.33331	0.61535	0.00296	0.23962	0.00439	-0.0283	2.293119

Table 45: U_∞ = 100 mph, h/b = 0.1, $\delta_{mid/out}$ = +10°, Symmetric Deflections

M	Re#	q_c	Uinf	alpha_c	CL	CD_c	Cl_cg_w	Cm_cg_c_w	Cn_cg_w	C_Y	L/D
0.056360307	333815	4.50446	43.4799	0.94111	0.86117	0.07995	0.0016	0.06513	-5E-05	0.00426	13.08655
0.116815253	691882	19.3506	90.1187	-9.1891	-0.7696	0.08036	0.00183	-0.3144	-0.0002	-0.0003	-11.144
0.11669962	691197	19.3123	90.0295	-6.7055	-0.4068	0.0362	0.00117	-0.1848	-0.0002	0.00053	-12.3077
0.116717348	691302	19.3182	90.0432	-4.3794	-0.1083	0.02089	0.00075	-0.0956	-0.0002	0.00112	-5.24161
0.116768946	691607	19.3353	90.083	-1.9414	0.1332	0.01981	0.0008	-0.0295	0.00015	-0.0009	6.840973
0.116696448	691178	19.3113	90.0271	0.30016	0.35427	0.02665	0.00076	0.0255	0.00021	4.4E-05	14.60361
0.116690987	691146	19.3095	90.0229	2.62534	0.57222	0.04322	0.00075	0.07633	0.00036	-3E-05	15.47788
0.116719634	691315	19.319	90.045	4.91392	0.75668	0.07105	0.00083	0.12317	0.00126	-0.0056	12.58471
0.11675118	691502	19.3294	90.0693	7.08377	0.91211	0.11281	0.00151	0.16983	0.00298	-0.015	9.408926
0.116661714	690972	19.2998	90.0003	9.34911	1.07529	0.16989	0.0021	0.21124	0.00408	-0.0221	7.273518
0.116491245	689963	19.2434	89.8688	11.5277	1.23873	0.2434	0.00124	0.24675	0.00424	-0.0223	5.784817
0.116351069	689132	19.1971	89.7606	12.6594	1.31985	0.28553	0.00237	0.26141	0.00452	-0.0259	5.231034
0.116222727	688372	19.1548	89.6616	13.7816	1.39145	0.33154	0.00246	0.27335	0.00484	-0.0284	4.723017
0.116121621	687773	19.1215	89.5836	14.8929	1.45389	0.38189	0.00201	0.28099	0.0052	-0.0297	4.256415
0.116053081	687367	19.0989	89.5307	15.9864	1.49923	0.4327	0.003	0.28618	0.00515	-0.0317	3.845826
0.115885669	686376	19.0439	89.4016	17.009	1.48052	0.47097	0.00529	0.28293	0.00407	-0.0328	3.449791
0.115652538	684995	18.9673	89.2217	18.0348	1.46392	0.50982	0.00301	0.27287	0.0048	-0.0288	3.121736
0.115499971	684091	18.9173	89.104	19.0517	1.44001	0.54547	0.00299	0.2585	0.00467	-0.028	2.846303
0.115393543	683461	18.8825	89.0219	20.1594	1.41874	0.58132	0.00229	0.24788	0.00517	-0.0265	2.613092
0.11527057	682733	18.8422	88.9271	21.1973	1.41405	0.6174	0.00167	0.24315	0.00578	-0.025	2.441109
0.115184337	682222	18.8141	88.8605	22.2391	1.41198	0.6521	0.00229	0.24114	0.00512	-0.0277	2.299369

Table 46: U_∞ = 100 mph, h/b = 0.05, $\delta_{mid/out}$ = +10°, Symmetric Deflections

M	Re#	q_c	Uinf	alpha_c	CL	CD_c	Cl_cg_w	Cm_cg_c_w	Cn_cg_w	C_Y	L/D
0.057226878	338947	4.64404	44.1485	0.8308	0.83984	0.07688	0.00153	0.0694	-1E-04	0.00442	13.24089
0.117101473	693577	19.4456	90.3395	-4.4492	-0.2518	0.02696	0.00169	-0.1256	-0.0003	0.00163	-9.77932
0.117030585	693157	19.422	90.2848	-3.2125	-0.0755	0.02107	0.00118	-0.074	-0.0003	0.00176	-3.60189
0.117028517	693145	19.4213	90.2832	-2.0794	0.08654	0.02064	0.00096	-0.0335	-7E-05	0.00077	4.221135
0.117038765	693205	19.4247	90.2912	-0.8848	0.22435	0.02227	0.0008	-0.0003	8.5E-05	-0.0001	10.52608
0.117087298	693493	19.4409	90.3286	0.29515	0.34969	0.0263	0.00069	0.02802	6.2E-05	0.00094	14.59178
0.117093541	693530	19.4429	90.3334	1.47924	0.47788	0.03323	0.00068	0.05485	-9E-05	0.00302	16.54923
0.117066317	693369	19.4339	90.3124	2.64204	0.5875	0.04235	0.00091	0.07963	0.00037	0.00024	16.42485
0.117034428	693180	19.4233	90.2878	3.79295	0.68625	0.05398	0.00105	0.10252	0.00084	-0.0026	15.24994
0.117069864	693390	19.4351	90.3151	4.8554	0.78274	0.06869	0.00116	0.1256	0.00132	-0.0058	13.73053
0.117082586	693465	19.4393	90.325	5.99124	0.86769	0.08894	0.00098	0.15064	0.00236	-0.0109	11.63412
0.117087887	693496	19.4411	90.329	7.1334	0.95751	0.11465	1.9E-06	0.17416	0.00344	-0.0159	9.854924
0.117037941	693201	19.4245	90.2905	8.27275	1.04569	0.14328	-4E-05	0.19576	0.00395	-0.0188	8.541351
0.11705832	693321	19.4312	90.3062	9.41216	1.13299	0.17458	0.00028	0.2167	0.00441	-0.0214	7.548396
0.117117625	693673	19.4509	90.352	10.553	1.22254	0.2128	0.00068	0.23461	0.00408	-0.0208	6.633759
0.117064563	693358	19.4333	90.3111	11.6055	1.30988	0.25041	0.00017	0.2507	0.00463	-0.023	6.017373
0.116935103	692592	19.3903	90.2112	12.7499	1.40271	0.29511	0.00086	0.26675	0.00504	-0.0267	5.445552
0.116835917	692004	19.3575	90.1347	13.8898	1.49043	0.34401	0.00159	0.28148	0.00537	-0.03	4.940934
0.116755952	691530	19.331	90.073	15.0262	1.57587	0.3976	0.00169	0.29361	0.00577	-0.0324	4.499434

Table 47: U_∞ = 40 mph, h/b = 1.05 (OGE), $\delta_{mid/out}$ = +20°, Symmetric Deflections

M	Re#	q_c	Uinf	alpha_c	CL	CD_c	Cl_cg_w	Cm_cg_c_w	Cn_cg_w	C_Y	L/D
0.02195	129383	0.68085	16.9562	1.36414	1.24827	0.19193	0.00302	0.0363	-0.0021	0.01305	7.695242
0.047603	280590	3.20215	36.7724	-10.859	-0.3876	0.08269	0.00051	-0.197	9.5E-05	0.00091	-4.856
0.047531	280165	3.19246	36.7167	-8.7123	-0.2537	0.05628	0.00056	-0.1478	-0.0005	0.00407	-4.60857
0.047501	279987	3.1884	36.6934	-6.441	-0.0851	0.03669	0.00072	-0.1031	-0.0003	0.00283	-2.32876
0.047521	280105	3.1911	36.7089	-4.1888	0.06609	0.03147	0.00072	-0.0612	-0.0005	0.00275	2.105994
0.04758	280453	3.19903	36.7545	-1.8516	0.21542	0.03088	0.00085	-0.0196	-0.0004	0.00096	7.180797
0.047651	280868	3.20851	36.8089	0.31512	0.36796	0.03879	0.00113	0.01995	9.6E-05	-0.0015	10.1624
0.047698	281151	3.21498	36.846	2.5684	0.52012	0.05692	0.00115	0.06045	-4E-05	-0.0013	10.04876
0.047726	281312	3.21867	36.8671	4.71542	0.65465	0.0824	0.00105	0.09973	0.00035	-0.0041	8.819276
0.04773	281335	3.21917	36.87	6.93382	0.77489	0.11895	0.00081	0.13661	0.00066	-0.0062	7.208114
0.047756	281488	3.22269	36.8902	9.16468	0.90653	0.16563	0.00098	0.17239	0.00094	-0.008	6.045185
0.047749	281448	3.22176	36.8848	11.3034	1.03347	0.22244	0.00068	0.20707	0.00108	-0.0063	5.114385
0.047719	281270	3.21769	36.8615	12.4037	1.08589	0.2539	0.00088	0.22182	0.00103	-0.0068	4.69246
0.047716	281257	3.21739	36.8598	13.5218	1.1537	0.29022	0.00219	0.23604	0.00068	-0.0079	4.356381
0.047724	281301	3.21842	36.8657	14.6214	1.2055	0.32788	0.00154	0.24729	0.00093	-0.0073	4.01615
0.047673	281001	3.21155	36.8263	15.7043	1.2411	0.36515	0.00151	0.25709	0.00091	-0.0071	3.696211
0.047629	280743	3.20566	36.7925	16.769	1.26091	0.39993	0.00238	0.26639	0.00051	-0.0092	3.41151
0.047653	280885	3.2089	36.8112	17.8156	1.26335	0.43451	0.00029	0.26818	0.00117	-0.0045	3.126536
0.047648	280853	3.20816	36.8069	18.8462	1.25199	0.46451	0.00143	0.26306	0.00085	-0.0075	2.880683
0.047627	280728	3.2053	36.7905	19.9164	1.19639	0.48433	0.00231	0.24482	0.00028	-0.0087	2.617717
0.047602	280584	3.20202	36.7716	20.9048	1.14636	0.50176	0.00429	0.23089	-0.0013	-0.0139	2.404806
0.047596	280547	3.20118	36.7668	21.8357	1.12247	0.51983	0.00471	0.22705	-0.0016	-0.0154	2.263973

Table 48: U_∞ = 40 mph, h/b = 0.3, $\delta_{mid/out}$ = +20°, Symmetric Deflections

M	Re#	q_c	Uinf	alpha_c	CL	CD_c	Cl_cg_w	Cm_cg_c_w	Cn_cg_w	C_Y	L/D
0.020678	121886	0.60423	15.9736	1.317	1.28474	0.20945	0.00372	0.04848	0.00111	-0.0032	7.218897
0.047184	278121	3.14605	36.4489	-10.974	-0.4933	0.097	0.00091	-0.2284	0.00091	-0.0077	-5.34092
0.047121	277745	3.13755	36.3996	-8.8939	-0.3404	0.06525	0.0013	-0.173	0.0012	-0.008	-5.39926
0.047159	277972	3.14269	36.4294	-6.5015	-0.1405	0.04044	0.00141	-0.115	0.0009	-0.0064	-3.50663
0.047223	278350	3.15124	36.4789	-4.22	0.03751	0.03258	0.0012	-0.0676	0.00103	-0.0058	1.152116
0.047273	278641	3.15782	36.517	-1.9493	0.20564	0.03359	0.00111	-0.0205	0.00069	-0.0051	6.272927
0.047291	278748	3.16025	36.531	0.32292	0.3751	0.03958	0.00156	0.0217	0.00156	-0.0093	10.16596
0.047298	278791	3.16123	36.5367	2.59678	0.54609	0.05882	0.00144	0.06423	0.00155	-0.0098	10.27747
0.047284	278709	3.15937	36.5259	4.75464	0.69054	0.08531	0.00124	0.10349	0.00164	-0.0101	9.059926
0.047202	278224	3.14837	36.4623	6.98554	0.82222	0.12517	0.00089	0.14189	0.00178	-0.0106	7.322848
0.047095	277593	3.13413	36.3797	9.2322	0.96831	0.17681	0.00119	0.18064	0.00196	-0.0109	6.092842
0.04698	276919	3.11891	36.2913	11.379	1.10268	0.23745	0.00036	0.21732	0.00243	-0.0114	5.146416
0.046899	276437	3.10806	36.2281	12.5926	1.17919	0.27665	0.00077	0.23267	0.00245	-0.01	4.714337
0.046874	276294	3.10484	36.2094	13.6203	1.24386	0.31247	0.00158	0.24711	0.00214	-0.0117	4.395838
0.046842	276102	3.10054	36.1842	14.7292	1.30416	0.35383	0.00184	0.26147	0.00222	-0.0115	4.057919
0.046872	276278	3.1045	36.2074	15.8152	1.34258	0.39552	0.00185	0.27176	0.002	-0.0105	3.717609
0.046893	276404	3.10733	36.2238	16.8759	1.3588	0.43359	0.00211	0.27708	0.00136	-0.008	3.410801
0.046863	276227	3.10335	36.2007	17.9278	1.36602	0.4721	0.00165	0.27552	0.00134	-0.0066	3.129379
0.046853	276170	3.10206	36.1931	18.9472	1.34438	0.50335	0.00269	0.26707	0.00092	-0.0073	2.867217
0.046875	276298	3.10494	36.2099	19.926	1.28473	0.52611	0.00162	0.2459	0.00147	-0.0061	2.597365
0.046828	276022	3.09875	36.1738	20.9154	1.23573	0.54407	0.00231	0.23381	0.00098	-0.0093	2.399695
0.046784	275759	3.09285	36.1393	21.9371	1.21531	0.56644	0.00363	0.23057	-0.0003	-0.0126	2.257785

Table 49: U_∞ = 40 mph, h/b = 0.15, $\delta_{mid/out}$ = +20°, Symmetric Deflections

M	Re#	q_c	Uinf	alpha_c	CL	CD_c	Cl_cg_w	Cm_cg_c_w	Cn_cg_w	C_Y	L/D
0.022107	130308	0.69062	17.0774	1.41559	1.29535	0.19876	0.00302	0.05751	-0.0008	0.00996	7.767819
0.045978	271012	2.98727	35.5172	-11.227	-0.7244	0.12641	0.00164	-0.3001	0.00145	-0.0098	-6.22266
0.045924	270691	2.98021	35.4752	-9.0602	-0.4925	0.08217	0.00207	-0.2232	0.00104	-0.0095	-6.35158
0.045877	270413	2.97409	35.4388	-6.5895	-0.221	0.04753	0.00172	-0.1411	0.00087	-0.0065	-4.74201
0.045926	270705	2.98051	35.477	-4.2534	0.00691	0.03696	0.00117	-0.0774	0.00053	-0.0031	0.187058
0.045956	270881	2.98438	35.5	-1.8528	0.21433	0.03412	0.00111	-0.021	0.00035	-0.0028	6.446454
0.046011	271203	2.99148	35.5422	0.36342	0.41216	0.04361	0.00128	0.02744	0.00112	-0.0064	10.20866
0.04604	271374	2.99525	35.5646	2.66319	0.60686	0.06637	0.00117	0.07374	0.00134	-0.0071	10.22614
0.046003	271159	2.99053	35.5365	4.83533	0.76437	0.09483	0.00109	0.11753	0.00166	-0.0085	9.13328
0.045965	270935	2.98559	35.5072	7.08488	0.91312	0.13978	0.00051	0.16137	0.00179	-0.0092	7.371336
0.045867	270356	2.97284	35.4313	9.3415	1.06833	0.19392	0.00017	0.20401	0.00197	-0.0088	6.20575
0.0458	269960	2.96414	35.3794	11.5074	1.2201	0.26186	-0.0002	0.2417	0.0023	-0.0098	5.226057
0.045755	269697	2.95836	35.3449	12.628	1.29114	0.30076	-0.0001	0.26131	0.00185	-0.007	4.800472
0.045733	269567	2.95551	35.3279	13.7674	1.37841	0.34526	0.00098	0.27759	0.0018	-0.008	4.460602
0.045651	269082	2.94488	35.2642	14.8956	1.45638	0.39471	0.00078	0.29092	0.002	-0.0087	4.111064
0.045596	268759	2.93782	35.2219	15.9999	1.51157	0.44481	0.00208	0.30171	0.00172	-0.0096	3.767353
0.045547	268467	2.93144	35.1837	17.052	1.5199	0.49025	0.00395	0.30536	0.00084	-0.0102	3.406363
0.045501	268198	2.92557	35.1484	18.066	1.49247	0.52621	0.00043	0.2986	0.00197	-0.0065	3.085379
0.045498	268183	2.92523	35.1464	19.0703	1.45705	0.56005	0.00278	0.28384	0.0004	-0.0089	2.804396
0.045466	267994	2.92111	35.1217	20.1329	1.39447	0.58468	-0.0005	0.26291	0.00278	-0.0032	2.546554
0.045413	267677	2.9142	35.0801	21.0691	1.37635	0.61457	0.00188	0.25774	0.001	-0.0103	2.379392
0.045361	267374	2.90762	35.0405	22.1001	1.36441	0.64186	0.00142	0.25851	0.0016	-0.0103	2.250189

Table 50: U_∞ = 40 mph, h/b = 0.1, $\delta_{mid/out}$ = +20°, Symmetric Deflections

M	Re#	q_c	Uinf	alpha_c	CL	CD_c	Cl_cg_w	Cm_cg_c_w	Cn_cg_w	C_Y	L/D
0.023402	137938	0.77387	18.0773	1.32581	1.21319	0.18117	0.00254	0.05371	1.6E-05	0.00415	7.924198
0.04669	275207	3.08048	36.067	-11.47	-0.947	0.13884	0.00067	-0.4043	0.00062	-0.0084	-7.7788
0.046634	274877	3.07309	36.0237	-9.1817	-0.6036	0.0798	0.00243	-0.2685	0.00078	-0.0065	-8.28597
0.046636	274886	3.07328	36.0248	-6.6523	-0.2784	0.04525	0.00183	-0.159	0.00086	-0.0053	-6.36195
0.046671	275093	3.07792	36.052	-4.2819	-0.0192	0.03378	0.00141	-0.0827	0.00069	-0.0039	-0.56715
0.046696	275242	3.08125	36.0715	-1.8674	0.20093	0.03175	0.0013	-0.0217	0.00078	-0.0047	6.485374
0.046712	275334	3.08332	36.0836	0.35368	0.40325	0.04098	0.00129	0.02987	0.00116	-0.0068	10.64613
0.046727	275422	3.0853	36.0952	2.66019	0.60411	0.06364	0.00122	0.07591	0.00153	-0.0082	10.6588
0.046745	275533	3.08777	36.1097	4.83789	0.76672	0.09338	0.00086	0.1186	0.00163	-0.0096	9.331011
0.046729	275437	3.08561	36.0971	7.09021	0.918	0.13791	-2E-05	0.16347	0.0018	-0.0091	7.534823
0.046676	275121	3.07855	36.0557	9.34495	1.07149	0.19052	-0.0002	0.20497	0.0021	-0.0102	6.354148
0.04662	274796	3.07127	36.013	11.5101	1.22257	0.25778	-0.0005	0.24209	0.00249	-0.0101	5.33225
0.046535	274294	3.06007	35.9474	12.6447	1.30644	0.29978	-0.0006	0.26055	0.00231	-0.0081	4.888857
0.046488	274015	3.05385	35.9108	13.7876	1.39688	0.34488	0.00112	0.27492	0.0021	-0.0079	4.54022
0.046473	273927	3.05188	35.8992	14.9212	1.47984	0.39315	0.00083	0.29155	0.00229	-0.0091	4.211425
0.046464	273874	3.05071	35.8923	16.0466	1.5543	0.44511	0.00074	0.30569	0.00239	-0.0092	3.895159
0.046441	273736	3.04764	35.8742	17.1501	1.60966	0.49874	9.8E-05	0.31379	0.00244	-0.0092	3.582414
0.046393	273455	3.04138	35.8374	18.0577	1.48489	0.52754	0.00228	0.28664	0.00095	-0.0091	3.058515
0.046266	272709	3.0248	35.7396	19.0482	1.43685	0.56107	0.00085	0.2644	0.00172	-0.0076	2.754183
0.046132	271919	3.0073	35.6361	20.1467	1.40706	0.59449	0.00106	0.25117	0.00155	-0.0086	2.527356
0.046048	271424	2.99637	35.5712	21.0947	1.39972	0.62755	0.00112	0.24861	0.0015	-0.0098	2.371649
0.046012	271209	2.99161	35.543	22.1457	1.40618	0.66259	0.00159	0.25185	0.0012	-0.0108	2.250333

Table 51: U_∞ = 40 mph, h/b = 0.05, $\delta_{mid/out}$ = +20°, Symmetric Deflections

M	Re#	q_c	Uinf	alpha_c	CL	CD_c	Cl_cg_w	Cm_cg_c_w	Cn_cg_w	C_Y	L/D
0.020754	122331	0.60865	16.032	1.44267	1.39973	0.21546	0.00226	0.07636	-0.0022	0.01485	7.859544
0.045799	269954	2.964	35.3786	-4.2173	-0.0396	0.03942	0.00147	-0.1041	0.00015	0.00117	-1.00569
0.045791	269907	2.96297	35.3724	-3.1248	0.08436	0.03613	0.00121	-0.0619	8.1E-05	-0.0005	2.343783
0.045811	270024	2.96552	35.3877	-1.9448	0.20973	0.03682	0.00108	-0.026	8.7E-05	-0.0004	5.828603
0.045806	269994	2.96487	35.3837	-0.7791	0.32106	0.03867	0.00101	0.00502	2.7E-06	-0.0003	8.74844
0.045833	270153	2.96837	35.4046	0.37924	0.42663	0.04303	0.00101	0.03191	0.00067	-0.0044	10.78558
0.045838	270185	2.96908	35.4088	1.53215	0.52629	0.0511	0.00103	0.05855	0.00058	-0.0045	11.48572
0.04584	270196	2.9693	35.4102	2.68444	0.62631	0.0624	0.00089	0.08174	0.00036	-0.0044	11.40375
0.04588	270434	2.97454	35.4414	3.82096	0.71187	0.07562	0.00065	0.10515	0.00042	-0.0045	10.79257
0.045859	270311	2.97183	35.4253	4.87301	0.79885	0.09266	0.00059	0.1273	0.00077	-0.0063	9.924841
0.045841	270200	2.96941	35.4108	5.99943	0.87518	0.11291	-0.0001	0.1534	0.00077	-0.0058	8.903146
0.045869	270366	2.97306	35.4326	7.14014	0.96368	0.13993	-0.0004	0.17706	0.00104	-0.0065	7.884762
0.045882	270443	2.97474	35.4426	8.27655	1.04916	0.16673	-0.0008	0.20029	0.00094	-0.0067	7.198958
0.045857	270299	2.97157	35.4237	9.42266	1.14259	0.19706	-0.0008	0.22109	0.0012	-0.0071	6.636649
0.045838	270184	2.96904	35.4087	10.4747	1.23047	0.23148	-0.0007	0.24058	0.00122	-0.0068	6.073303
0.045848	270245	2.97039	35.4167	11.6072	1.31145	0.26724	-0.0004	0.2608	0.0016	-0.0085	5.594115
0.0458	269959	2.96412	35.3793	12.7449	1.39812	0.30942	-0.0006	0.27908	0.00175	-0.0087	5.137558
0.045765	269753	2.95959	35.3522	13.8927	1.49307	0.35898	0.0003	0.29856	0.00173	-0.0098	4.718013
0.04576	269723	2.95892	35.3483	15.0239	1.57381	0.40735	-2E-05	0.3152	0.00186	-0.0091	4.370344

Table 52: U_∞ = 60 mph, h/b = 1.05 (OGE), $\delta_{mid/out}$ = +20°, Symmetric Deflections

M	Re#	q_c	Uinf	alpha_c	CL	CD_c	Cl_cg_w	Cm_cg_c_w	Cn_cg_w	C_Y	L/D
0.0335	197461	1.58585	25.8781	1.23978	1.13447	0.15697	0.00313	0.02692	-0.0024	0.01178	8.566698
0.073159	431226	7.56324	56.5139	-10.807	-0.3401	0.06995	0.00037	-0.1936	-0.0008	0.0043	-5.0209
0.073057	430621	7.54204	56.4346	-8.6524	-0.199	0.04526	0.00073	-0.1483	-0.0006	0.00381	-4.47089
0.073026	430442	7.53576	56.4111	-6.3959	-0.0438	0.03101	0.00078	-0.1046	-0.0006	0.00369	-1.41552
0.073068	430690	7.54445	56.4436	-4.16	0.09241	0.0295	0.00078	-0.065	-0.0007	0.00387	3.149707
0.073089	430809	7.54862	56.4592	-1.9218	0.23077	0.03375	0.00077	-0.0278	-0.0005	0.00277	7.050685
0.07314	431114	7.55932	56.4992	0.15254	0.35997	0.04121	0.00115	0.00447	-0.0006	0.00173	9.291871
0.073249	431753	7.58174	56.583	2.56333	0.51547	0.06003	0.00068	0.04509	-0.0005	0.00137	9.37904
0.073327	432213	7.59791	56.6432	4.71075	0.65038	0.08681	0.00044	0.08	-0.0004	0.00086	8.259905
0.073369	432461	7.60664	56.6758	6.93492	0.7759	0.12326	0.00015	0.11422	-0.0004	0.0029	6.94138
0.073381	432530	7.60906	56.6848	9.16858	0.9101	0.17415	0.00019	0.15163	-0.0004	0.00489	5.747145
0.073359	432402	7.60455	56.668	11.2939	1.02477	0.22785	6.4E-05	0.18686	0.00029	0.00187	4.931099
0.073306	432089	7.59356	56.627	12.4052	1.0873	0.26077	0.0004	0.20094	0.00054	-0.0005	4.564236
0.073275	431905	7.58708	56.6029	13.512	1.14472	0.29597	0.00115	0.21435	0.00071	-0.0029	4.224425
0.07323	431643	7.57787	56.5685	14.6109	1.19588	0.33322	0.00196	0.22631	0.00083	-0.0051	3.90874
0.073189	431399	7.5693	56.5365	15.6911	1.22898	0.37084	0.00189	0.23368	0.00102	-0.0073	3.593206
0.073171	431295	7.56565	56.5229	16.7589	1.25167	0.40808	0.00241	0.2379	0.00079	-0.0078	3.309563
0.073127	431036	7.55659	56.489	17.8139	1.2618	0.44389	0.00241	0.23906	0.00078	-0.0076	3.051349
0.073093	430838	7.54962	56.463	18.8515	1.25681	0.47679	0.00304	0.23385	0.0004	-0.0082	2.813773
0.073081	430766	7.54712	56.4536	19.9396	1.2176	0.50182	0.00287	0.21908	-1E-05	-0.0069	2.571276
0.073076	430732	7.54594	56.4492	20.9217	1.16183	0.5179	0.00222	0.20425	0.00019	-0.0056	2.360691
0.073032	430477	7.537	56.4158	21.8414	1.12772	0.53316	0.00278	0.19748	-0.0005	-0.0072	2.215948

Table 53: U_∞ = 60 mph, h/b = 0.3, $\delta_{mid/out}$ = +20°, Symmetric Deflections

M	Re#	q_c	Uinf	alpha_c	CL	CD_c	Cl_cg_w	Cm_cg_c_w	Cn_cg_w	C_Y	L/D
0.033547	197739	1.59032	25.9145	1.18837	1.16703	0.17078	0.00387	0.01751	-0.0018	0.00759	8.059417
0.071922	423933	7.30959	55.5581	-10.918	-0.442	0.08655	0.00047	-0.2049	-0.0005	0.00145	-5.33613
0.07181	423270	7.28675	55.4713	-8.8253	-0.2775	0.05658	0.00091	-0.1609	-0.0006	0.00197	-5.03499
0.071706	422661	7.2658	55.3915	-6.4398	-0.084	0.03667	0.00103	-0.1145	-0.0005	0.00223	-2.29937
0.071727	422780	7.26989	55.407	-4.1758	0.07793	0.03443	0.00101	-0.0733	-0.0006	0.0032	2.271043
0.071821	423338	7.28907	55.4801	-1.9174	0.23484	0.0388	0.00079	-0.0336	-0.0005	0.00255	6.220752
0.071892	423758	7.30354	55.5351	0.34682	0.39697	0.04908	0.00126	0.0028	-0.0006	0.00124	8.615927
0.07186	423565	7.2969	55.5099	2.60397	0.55266	0.06811	0.00067	0.04079	-0.0004	0.00089	8.872606
0.071766	423015	7.27795	55.4377	4.77078	0.70531	0.09766	0.00044	0.07855	-0.0004	0.00131	7.999301
0.07167	422450	7.25852	55.3637	7.00693	0.84179	0.1374	0.00037	0.11719	-0.0004	0.00394	6.795025
0.071545	421711	7.23318	55.267	9.25169	0.98615	0.19241	0.00032	0.1619	-0.0005	0.0055	5.67214
0.071368	420667	7.19739	55.1301	11.3947	1.11699	0.25239	-0.0002	0.20224	0.00039	0.00183	4.886244
0.071263	420047	7.17618	55.0488	12.5161	1.1888	0.29006	-0.0002	0.22118	0.00086	-0.0007	4.518255
0.071198	419664	7.16311	54.9986	13.6328	1.25525	0.32931	0.00061	0.23965	0.00107	-0.0035	4.194542
0.071174	419526	7.15839	54.9805	14.7385	1.31264	0.3712	0.00164	0.2566	0.00111	-0.0059	3.879637
0.071196	419653	7.16275	54.9972	15.8169	1.34414	0.41239	0.0011	0.26767	0.00144	-0.0077	3.556599
0.071205	419707	7.16458	55.0043	16.8813	1.36371	0.4534	0.00154	0.2764	0.00125	-0.0082	3.263016
0.071147	419363	7.15285	54.9592	17.9356	1.37314	0.49225	0.00239	0.28167	0.00053	-0.0079	3.009372
0.071109	419139	7.1452	54.9298	18.9676	1.36311	0.52791	0.00263	0.28017	0.00033	-0.0084	2.7679
0.071107	419130	7.14488	54.9286	19.9397	1.29724	0.54811	0.00209	0.26248	8.4E-05	-0.0065	2.513974
0.071057	418832	7.13474	54.8896	20.9315	1.25044	0.56786	0.00217	0.254	-0.0002	-0.0075	2.324053
0.071074	418932	7.13815	54.9027	21.0242	1.25567	0.57063	0.00196	0.25675	0.00033	-0.0053	2.322897
0.071047	418773	7.13274	54.8819	21.9574	1.23389	0.59252	0.00144	0.25669	0.00057	-0.0068	2.189746

Table 54: U_∞ = 60 mph, h/b = 0.15, $\delta_{mid/out}$ = +20°, Symmetric Deflections

M	Re#	q_c	Uinf	alpha_c	CL	CD_c	Cl_cg_w	Cm_cg_c_w	Cn_cg_w	C_Y	L/D
0.038065	224369	2.04751	29.4045	1.09442	1.00146	0.13861	0.00256	0.03309	-0.0023	0.01382	8.381962
0.070924	418049	7.1081	54.787	-11.162	-0.6652	0.11052	0.00133	-0.2957	4.4E-05	-0.0001	-6.5164
0.070817	417417	7.08659	54.7041	-8.9802	-0.4193	0.06771	0.00137	-0.2189	-0.0004	0.0016	-6.51467
0.070797	417300	7.08263	54.6888	-6.5215	-0.1588	0.03877	0.00132	-0.1409	-0.0007	0.00349	-4.14741
0.070862	417685	7.09572	54.7393	-4.2086	0.04798	0.03368	0.00111	-0.0833	-0.0009	0.00512	1.426534
0.070913	417985	7.10592	54.7786	-1.8341	0.23146	0.0378	0.00079	-0.0323	-0.0006	0.00432	6.293148
0.070933	418103	7.10991	54.794	0.36844	0.41675	0.04943	0.00127	0.01229	-0.0008	0.00367	9.037438
0.070963	418279	7.11591	54.8171	2.64786	0.59283	0.07001	0.00049	0.05642	-0.0006	0.00316	9.364385
0.070951	418212	7.11363	54.8083	4.894	0.7473	0.09982	0.00032	0.09777	-0.0005	0.00317	8.380689
0.070899	417904	7.10315	54.7679	7.07002	0.89952	0.1441	7.4E-05	0.13676	-0.0003	0.00356	6.991087
0.070828	417483	7.08885	54.7128	9.33064	1.05839	0.20186	-0.0003	0.18102	-0.0001	0.00377	5.863884
0.070717	416833	7.06679	54.6276	11.4877	1.20211	0.26744	-0.0004	0.21735	0.00084	-0.0002	5.011268
0.070625	416288	7.04833	54.5562	12.6126	1.27701	0.30808	-0.0004	0.23419	0.00122	-0.0025	4.610537
0.07057	415964	7.03735	54.5137	13.7439	1.35695	0.35167	0.00123	0.25058	0.00139	-0.0066	4.286646
0.070496	415529	7.02266	54.4568	14.8625	1.42614	0.39849	0.00152	0.26382	0.0017	-0.0092	3.964795
0.070467	415356	7.0168	54.4341	15.958	1.47323	0.44611	0.00134	0.27276	0.00196	-0.0106	3.640177
0.070383	414863	7.00014	54.3694	16.9952	1.46791	0.48921	0.00173	0.27203	0.00172	-0.0107	3.275742
0.070272	414206	6.97801	54.2834	18.0263	1.45614	0.52782	0.00237	0.2647	0.00107	-0.0095	2.987666
0.070204	413805	6.96449	54.2308	19.0388	1.42818	0.5628	0.00252	0.25089	0.00039	-0.0096	2.72606
0.070167	413591	6.95728	54.2027	20.1109	1.3743	0.58898	0.00197	0.23188	0.00055	-0.0078	2.485359
0.070183	413685	6.96045	54.215	21.1299	1.35234	0.61767	0.00105	0.22717	0.0014	-0.0071	2.320449
0.070116	413290	6.94716	54.1633	22.0697	1.33664	0.64209	0.00053	0.2252	0.00202	-0.0065	2.198369

Table 55: U_∞ = 60 mph, h/b = 0.1, $\delta_{mid/out}$ = +20°, Symmetric Deflections

M	Re#	q_c	Uinf	alpha_c	CL	CD_c	Cl_cg_w	Cm_cg_c_w	Cn_cg_w	C_Y	L/D
0.0343	202176	1.66249	26.496	1.3123	1.20083	0.1683	0.00272	0.04323	-0.0027	0.01712	8.528767
0.070658	416481	7.05488	54.5815	-10.234	-0.7715	0.10334	0.00205	-0.3427	-0.0005	0.00233	-8.38681
0.070618	416244	7.04683	54.5504	-9.1852	-0.6069	0.07834	0.00232	-0.2847	-0.0007	0.00293	-8.50923
0.070666	416529	7.05648	54.5877	-6.6093	-0.2391	0.04117	0.0017	-0.1674	-0.0009	0.00468	-5.96707
0.070711	416793	7.06545	54.6224	-4.2419	0.01745	0.03307	0.00131	-0.0933	-0.0009	0.00464	0.527549
0.070738	416952	7.07082	54.6432	-1.9242	0.22859	0.03797	0.00096	-0.0348	-0.0004	0.00254	6.182976
0.070752	417035	7.07363	54.654	0.38116	0.42839	0.04973	0.00124	0.01437	-0.0006	0.0021	9.266145
0.070779	417193	7.079	54.6748	2.67459	0.61729	0.07049	0.00054	0.06035	-0.0005	0.00219	9.763239
0.070783	417216	7.07979	54.6778	4.85781	0.78495	0.10157	0.00014	0.10278	-0.0005	0.00349	8.739534
0.070774	417165	7.07807	54.6712	7.12029	0.94552	0.14924	-0.0004	0.14409	-0.0003	0.00416	7.152689
0.070719	416843	7.06714	54.629	9.38038	1.10391	0.20702	-0.0007	0.18956	0.00012	0.00365	6.006795
0.070661	416499	7.05546	54.5838	11.5456	1.2551	0.27517	-0.0006	0.22578	0.00091	-0.0006	5.120253
0.070605	416171	7.04438	54.5409	12.6765	1.33549	0.31724	-0.001	0.24246	0.00159	-0.0028	4.715262
0.070518	415654	7.02688	54.4731	13.8144	1.42145	0.36274	0.00135	0.25903	0.00169	-0.0075	4.384413
0.070444	415218	7.01214	54.416	14.9431	1.4999	0.41103	0.00125	0.27399	0.00202	-0.0094	4.074408
0.070424	415102	7.00821	54.4007	16.066	1.57206	0.46288	0.00132	0.28629	0.00243	-0.0126	3.781294
0.070346	414645	6.9928	54.3409	17.149	1.60868	0.51638	0.00068	0.29072	0.00262	-0.0123	3.444545
0.0702	413783	6.96375	54.2279	18.0893	1.51381	0.55117	0.00201	0.26642	0.00116	-0.0093	2.983087
0.070024	412742	6.92878	54.0915	19.0918	1.47671	0.58866	0.00165	0.24492	0.00068	-0.0076	2.699327
0.069853	411735	6.89499	53.9595	20.1805	1.43803	0.62079	-0.0004	0.22994	0.00223	-0.0034	2.473608
0.069802	411439	6.88507	53.9207	21.226	1.44033	0.6583	0.00147	0.22968	0.00105	-0.0093	2.327855
0.069824	411566	6.88933	53.9373	22.1775	1.43529	0.68817	0.00192	0.22992	0.00083	-0.0119	2.211939

Table 56: U_∞ = 60 mph, h/b = 0.05, $\delta_{mid/out}$ = +20°, Symmetric Deflections

M	Re#	q_c	Uinf	alpha_c	CL	CD_c	Cl_cg_w	Cm_cg_c_w	Cn_cg_w	C_Y	L/D
0.032661	192515	1.5074	25.2299	1.23938	1.21372	0.15868	0.00177	0.05012	-0.0025	0.0147	9.294174
0.070919	418020	7.10711	54.7832	-4.211	-0.0339	0.03534	0.00143	-0.1106	-0.0007	0.00445	-0.95864
0.070894	417872	7.10206	54.7638	-3.1115	0.09658	0.0344	0.00105	-0.071	-0.0008	0.00453	2.822216
0.070879	417787	7.09918	54.7526	-1.9338	0.21982	0.03563	0.00088	-0.0359	-0.0008	0.00412	6.33399
0.070901	417913	7.10346	54.7691	-0.7673	0.33192	0.03994	0.00092	-0.0077	-0.0006	0.00293	8.771947
0.070933	418102	7.1099	54.794	0.38623	0.43304	0.04623	0.00082	0.0179	-0.0005	0.00276	10.15223
0.070966	418296	7.11649	54.8194	1.53665	0.53041	0.0555	0.00081	0.04159	-0.0006	0.00189	10.58084
0.070974	418342	7.11805	54.8254	2.68349	0.62544	0.06742	0.00053	0.06374	-0.0005	0.00166	10.43025
0.070953	418220	7.11389	54.8093	3.82178	0.71263	0.0808	0.00031	0.08419	-0.0005	0.00177	10.02039
0.070965	418291	7.11632	54.8187	4.87367	0.79946	0.09801	0.00026	0.10521	-0.0005	0.00194	9.315012
0.070928	418074	7.10894	54.7903	6.01338	0.88795	0.12074	-0.0003	0.1263	-0.0001	0.00077	8.400634
0.070936	418123	7.1106	54.7967	7.16357	0.98512	0.14963	-0.001	0.14852	-0.0002	0.00241	7.513255
0.070977	418365	7.11885	54.8284	8.29007	1.06153	0.17663	-0.0013	0.17348	1.7E-05	0.00186	6.842548
0.070983	418396	7.11988	54.8324	9.42162	1.14164	0.20685	-0.0011	0.1946	0.00058	-0.001	6.272876
0.070954	418229	7.1142	54.8105	10.4718	1.2278	0.23952	-0.0007	0.21239	0.00102	-0.0031	5.82535
0.070934	418110	7.11016	54.795	11.6054	1.30986	0.27718	-0.0005	0.2295	0.00144	-0.0057	5.358216
0.070916	418001	7.10645	54.7807	12.7418	1.39525	0.32016	-0.0007	0.24691	0.00199	-0.0078	4.929726
0.070884	417813	7.10005	54.756	13.8802	1.48167	0.36643	0.00049	0.26446	0.00242	-0.0119	4.565112
0.070825	417467	7.0883	54.7107	15.0114	1.56239	0.41658	0.00055	0.27964	0.00281	-0.0148	4.222442

Table 57: U_∞ = 80 mph, h/b = 1.05, $\delta_{mid/out}$ = +20°, Symmetric Deflections

M	Re#	q_c	Uinf	alpha_c	CL	CD_c	Cl_cg_w	Cm_cg_c_w	Cn_cg_w	C_Y	L/D
0.044041	259591	2.74081	34.0205	1.20346	1.10124	0.14789	0.00336	0.02101	-0.0014	0.00497	8.826747
0.096675	569834	13.2067	74.6789	-10.818	-0.3505	0.06844	0.00037	-0.2003	-0.0005	0.00285	-5.30206
0.096524	568946	13.1656	74.5626	-8.7476	-0.2064	0.04407	0.00081	-0.1549	-0.0004	0.00263	-4.77143
0.096491	568750	13.1565	74.5369	-8.6581	-0.2041	0.04351	0.00093	-0.1539	-0.0004	0.00225	-4.77865
0.096505	568835	13.1605	74.5481	-6.3936	-0.0417	0.02939	0.001	-0.1089	-0.0003	0.00148	-1.42077
0.096533	568996	13.1679	74.5692	-4.147	0.10432	0.02838	0.0009	-0.0698	-0.0002	0.0009	3.703239
0.096665	569777	13.2041	74.6715	-1.9079	0.24346	0.03302	0.00086	-0.0303	-0.0002	0.00021	7.633455
0.096817	570673	13.2456	74.7889	0.34074	0.39141	0.04398	0.00124	0.00658	-0.0003	1.5E-06	9.534081
0.096894	571125	13.2666	74.8482	2.58227	0.53281	0.06007	0.00093	0.04494	-0.0005	0.00155	9.74909
0.096946	571435	13.281	74.8888	4.74567	0.68233	0.08828	0.00051	0.08097	-0.0002	0.00181	8.593317
0.097005	571782	13.2972	74.9343	6.9658	0.80415	0.12513	0.00072	0.12022	0.00076	-0.0036	7.129033
0.096992	571706	13.2936	74.9243	9.19742	0.93648	0.17681	0.00175	0.16	0.00154	-0.0094	5.850114
0.096954	571478	13.283	74.8944	11.3284	1.05639	0.23215	0.00108	0.19422	0.00242	-0.0132	5.009848
0.096842	570817	13.2523	74.8078	12.4382	1.1175	0.26571	0.0011	0.20871	0.00267	-0.0149	4.619804
0.096773	570411	13.2335	74.7547	13.5478	1.17745	0.30201	0.00202	0.22187	0.00282	-0.0175	4.272873
0.096733	570175	13.2225	74.7237	14.6441	1.22623	0.3395	0.00294	0.23352	0.00281	-0.0205	3.945157
0.096668	569796	13.2049	74.674	15.7263	1.26124	0.3788	0.00249	0.2399	0.00313	-0.0211	3.619411
0.096608	569441	13.1885	74.6275	16.7905	1.28064	0.41727	0.00346	0.24254	0.00272	-0.023	3.317773
0.096567	569197	13.1772	74.5955	17.8448	1.29009	0.45266	0.0037	0.24361	0.00252	-0.023	3.064985
0.09651	568864	13.1618	74.5519	18.8844	1.28691	0.48622	0.00434	0.24043	0.00214	-0.0229	2.830651
0.096444	568473	13.1437	74.5007	19.8824	1.24485	0.50996	0.0036	0.22578	0.00209	-0.0199	2.591274
0.09642	568334	13.1373	74.4824	20.9514	1.18902	0.52745	0.00439	0.20907	0.00125	-0.0213	2.375716
0.096343	567881	13.1163	74.423	21.8821	1.16496	0.54803	0.00401	0.20265	0.00128	-0.0217	2.231106

Table 58: U_∞ = 80 mph, h/b = 0.3, $\delta_{mid/out}$ = +20°, Symmetric Deflections

M	Re#	q_c	Uinf	alpha_c	CL	CD_c	Cl_cg_w	Cm_cg_c_w	Cn_cg_w	C_Y	L/D
0.039152	230773	2.16605	30.2438	1.33409	1.30038	0.18437	0.00382	0.02608	-0.001	0.00361	8.548217
0.094948	559655	12.7391	73.345	-10.931	-0.4542	0.08445	0.00045	-0.2362	-0.0001	0.0003	-5.64108
0.094888	559304	12.7231	73.299	-8.8337	-0.2852	0.05419	0.0008	-0.1809	-0.0002	0.00055	-5.41855
0.094862	559151	12.7162	73.2789	-6.4392	-0.0834	0.03418	0.00103	-0.1243	-0.0002	0.00087	-2.45041
0.094924	559513	12.7326	73.3264	-4.1674	0.08562	0.0318	0.00105	-0.0789	-8E-05	0.00031	2.704271
0.094981	559852	12.7481	73.3708	-1.9061	0.24513	0.03663	0.00084	-0.0348	-1E-04	-0.0004	6.907538
0.095015	560053	12.7572	73.3972	0.36229	0.41112	0.04859	0.00132	0.00642	-0.0002	-0.0005	9.062901
0.095011	560028	12.7561	73.3939	2.62218	0.56933	0.06596	0.0009	0.04809	-0.0003	0.00156	9.523781
0.094892	559326	12.7241	73.3018	4.79989	0.73194	0.09616	0.00049	0.08776	-0.0002	0.00184	8.516241
0.094714	558279	12.6766	73.1647	7.0327	0.86537	0.1369	0.00069	0.13078	0.00097	-0.0043	7.057571
0.094562	557380	12.6357	73.0468	9.27677	1.0091	0.19289	0.00116	0.17231	0.00179	-0.0093	5.817159
0.094434	556624	12.6015	72.9478	11.4235	1.14333	0.25356	0.00062	0.20826	0.00267	-0.0131	5.000827
0.094337	556053	12.5757	72.873	12.5417	1.21217	0.2906	0.0008	0.22413	0.00301	-0.0156	4.616395
0.09429	555779	12.5633	72.8371	13.6594	1.27964	0.33026	0.00234	0.23854	0.00308	-0.0187	4.279365
0.094249	555533	12.5522	72.8049	14.7606	1.33285	0.37189	0.00269	0.25069	0.00328	-0.0214	3.943215
0.094168	555056	12.5306	72.7423	15.843	1.368	0.41488	0.00301	0.25694	0.00332	-0.0234	3.607683
0.094071	554487	12.5049	72.6677	16.9111	1.39096	0.45796	0.0026	0.26097	0.00346	-0.0235	3.303487
0.093999	554062	12.4858	72.612	17.9627	1.39794	0.49691	0.00308	0.26012	0.0032	-0.0232	3.041356
0.094009	554118	12.4883	72.6193	18.9901	1.38369	0.53061	0.00434	0.25346	0.00228	-0.0241	2.800461
0.094054	554384	12.5003	72.6542	19.9748	1.32937	0.55371	0.0042	0.23399	0.00184	-0.0234	2.556433
0.0941	554657	12.5126	72.69	21.0624	1.29056	0.57845	0.00357	0.22228	0.0022	-0.0222	2.360714
0.094126	554813	12.5196	72.7104	21.9912	1.2648	0.59997	0.00273	0.2164	0.00288	-0.0201	2.221062

Table 59: U_∞ = 80 mph, h/b = 0.15, $\delta_{mid/out}$ = +20°, Symmetric Deflections

M	Re#	q_c	Uinf	alpha_c	CL	CD_c	Cl_cg_w	Cm_cg_c_w	Cn_cg_w	C_Y	L/D
0.044694	263439	2.82266	34.5248	1.26386	1.1565	0.15846	0.00288	0.03019	-0.0015	0.00968	8.698809
0.093702	552312	12.407	72.3827	-11.192	-0.6928	0.11042	0.00099	-0.311	0.00044	-0.0019	-6.84192
0.093638	551937	12.3902	72.3335	-8.9945	-0.4324	0.06674	0.00127	-0.2305	-6E-05	1.6E-05	-6.84404
0.093633	551906	12.3888	72.3295	-6.519	-0.1565	0.03735	0.00142	-0.1487	-0.0003	0.00159	-4.2426
0.093717	552402	12.4111	72.3945	-4.1959	0.05954	0.03281	0.00132	-0.09	-0.0002	0.0016	1.818404
0.093736	552513	12.4161	72.4091	-1.8156	0.24836	0.03758	0.00098	-0.0368	-0.0002	0.00058	6.822526
0.093707	552341	12.4083	72.3864	0.38977	0.43627	0.05089	0.00124	0.0093	-0.0002	0.00081	9.231654
0.093705	552332	12.4079	72.3853	2.67427	0.617	0.07119	0.0009	0.05513	-0.0003	0.00125	9.651302
0.093698	552286	12.4058	72.3793	4.95217	0.79168	0.10399	0.00076	0.09885	0.0001	0.00036	8.602249
0.093625	551857	12.3866	72.3231	7.10851	0.93474	0.14795	0.00038	0.14399	0.0015	-0.0061	7.120144
0.093471	550947	12.3458	72.2038	9.36745	1.09207	0.20664	0.00127	0.18871	0.002	-0.0109	5.938502
0.093325	550087	12.3072	72.0911	11.5293	1.24017	0.27412	0.00025	0.22441	0.00304	-0.0149	5.06629
0.093207	549392	12.2762	72	12.6566	1.3173	0.31497	0.00066	0.24049	0.00343	-0.0175	4.673301
0.093111	548825	12.2509	71.9257	13.7892	1.39838	0.36009	0.00246	0.2563	0.00355	-0.0217	4.3321
0.093059	548519	12.2372	71.8855	14.9023	1.46254	0.40735	0.00241	0.26881	0.00385	-0.0237	3.990002
0.093015	548265	12.2258	71.8522	15.9854	1.49834	0.45587	0.00166	0.2744	0.00425	-0.0243	3.627504
0.092921	547710	12.2011	71.7795	17.0256	1.49573	0.49916	0.00156	0.27469	0.00419	-0.0245	3.276568
0.092823	547130	12.1753	71.7036	18.0583	1.48543	0.53662	0.00259	0.26927	0.00361	-0.0242	3.003701
0.092706	546439	12.1446	71.613	19.0746	1.46095	0.57326	0.00313	0.25505	0.00302	-0.0242	2.743316
0.092627	545972	12.1238	71.5519	20.1565	1.41605	0.60362	0.0013	0.23731	0.00433	-0.0194	2.504617
0.092612	545887	12.12	71.5407	21.1806	1.39872	0.63465	0.00159	0.23088	0.0041	-0.0208	2.341584
0.092562	545594	12.107	71.5022	22.1225	1.38493	0.66236	0.00118	0.2279	0.00454	-0.0205	2.213132

Table 60: U_∞ = 80 mph, h/b = 0.1, $\delta_{mid/out}$ = +20°, Symmetric Deflections

M	Re#	q_c	Uinf	alpha_c	CL	CD_c	Cl_cg_w	Cm_cg_c_w	Cn_cg_w	C_Y	L/D
0.04169	245735	2.45602	32.2045	1.37067	1.25424	0.16993	0.00317	0.04514	-0.0013	0.0087	8.963629
0.093732	552488	12.4149	72.4057	-8.993	-0.5902	0.07458	0.00216	-0.2834	-0.0002	0.00065	-8.68645
0.093676	552158	12.4001	72.3625	-6.6139	-0.2433	0.04041	0.0019	-0.1737	-0.0004	0.00162	-6.19504
0.093734	552501	12.4155	72.4074	-4.2377	0.02128	0.03276	0.00148	-0.0974	-0.0003	0.00137	0.649542
0.093815	552976	12.4369	72.4697	-1.916	0.23611	0.03719	0.00099	-0.0365	-8E-05	0.00039	6.534769
0.093806	552925	12.4346	72.4631	0.39242	0.4387	0.05001	0.00134	0.01374	-0.0001	0.00039	9.46662
0.093777	552754	12.4269	72.4407	2.69482	0.6358	0.07111	0.0009	0.06138	-0.0002	0.00155	10.02805
0.093784	552796	12.4288	72.4461	4.89511	0.81908	0.10387	0.00058	0.10581	0.0003	-2E-06	8.993222
0.093804	552911	12.4339	72.4611	7.14458	0.96775	0.14967	0.0006	0.15241	0.00188	-0.0076	7.341984
0.093727	552458	12.4136	72.4018	9.40646	1.12778	0.20902	0.00063	0.1976	0.00241	-0.0113	6.103826
0.093601	551715	12.3802	72.3045	11.5726	1.27983	0.27856	0.00026	0.2329	0.00318	-0.0156	5.174793
0.09351	551182	12.3563	72.2346	12.7094	1.36562	0.32183	0.0003	0.24906	0.00372	-0.0182	4.770469
0.093458	550874	12.3425	72.1943	13.8459	1.45027	0.36791	0.00251	0.26483	0.00386	-0.0225	4.424284
0.093363	550313	12.3174	72.1207	14.974	1.52819	0.4174	0.00191	0.2789	0.00435	-0.0249	4.098533
0.093246	549621	12.2864	72.0301	16.0909	1.59484	0.4701	0.00147	0.28963	0.00474	-0.0266	3.782886
0.093106	548796	12.2495	71.9219	17.1417	1.60195	0.52228	-0.0041	0.29001	0.00618	-0.0226	3.384367
0.092939	547811	12.2056	71.7928	18.1038	1.52709	0.55677	0.00234	0.26835	0.00375	-0.0254	2.980881
0.092785	546905	12.1653	71.6741	19.1078	1.49138	0.59261	0.00256	0.24807	0.00308	-0.0235	2.710684
0.092662	546180	12.133	71.5791	20.2014	1.45716	0.62648	0.00244	0.23318	0.003	-0.0234	2.486679
0.092585	545725	12.1128	71.5194	21.246	1.45864	0.66389	0.00071	0.23056	0.00483	-0.0203	2.340145
0.092493	545184	12.0888	71.4486	22.1974	1.45351	0.69561	0.00061	0.22965	0.00493	-0.0226	2.218016

Table 61: U_∞ = 80 mph, h/b = 0.05, $\delta_{mid/out}$ = +20°, Symmetric Deflections

M	Re#	q_c	Uinf	alpha_c	CL	CD_c	Cl_cg_w	Cm_cg_c_w	Cn_cg_w	C_Y	L/D
0.03718	219152	1.95339	28.7207	1.47934	1.43329	0.18223	0.00226	0.05819	-0.0018	0.01072	10.01963
0.09361	551770	12.3827	72.3116	-4.2223	-0.0442	0.03485	0.00161	-0.1166	-0.0006	0.00338	-1.27061
0.093571	551539	12.3723	72.2814	-3.1083	0.09948	0.03363	0.00126	-0.0743	-0.0005	0.00219	2.974271
0.093559	551468	12.3691	72.2721	-1.919	0.2333	0.03546	0.00099	-0.0389	-0.0003	0.00105	6.778104
0.093597	551694	12.3793	72.3017	-0.7501	0.34765	0.04001	0.00099	-0.0087	-0.0002	0.00074	9.220205
0.093626	551862	12.3868	72.3238	0.40753	0.45252	0.04636	0.00088	0.01768	-0.0002	0.00068	10.66021
0.093646	551980	12.3921	72.3391	1.56708	0.55826	0.0569	0.00086	0.04104	-0.0003	0.00104	10.95621
0.093683	552200	12.402	72.368	2.7289	0.66699	0.06999	0.00048	0.06423	-0.0003	0.00083	10.84411
0.093673	552140	12.3993	72.3602	3.87386	0.76029	0.08487	0.00043	0.08549	-2E-05	0.00026	10.29543
0.093645	551977	12.392	72.3388	4.93267	0.85344	0.10297	0.00051	0.10738	0.00049	-0.0028	9.580678
0.093681	552188	12.4014	72.3664	6.06657	0.93663	0.12549	-0.0003	0.1317	0.00151	-0.0069	8.612272
0.093725	552444	12.413	72.4	7.1993	1.01781	0.15228	-0.0008	0.15798	0.00214	-0.0101	7.680327
0.093726	552455	12.4134	72.4014	8.33688	1.10436	0.18224	-0.0005	0.18117	0.00225	-0.0121	6.946749
0.093677	552166	12.4004	72.3635	9.47167	1.18744	0.21364	-0.0005	0.20104	0.00272	-0.0144	6.3586
0.093626	551862	12.3868	72.3237	10.5225	1.27421	0.24769	3.9E-05	0.21936	0.00316	-0.0177	5.879445
0.093599	551707	12.3798	72.3033	11.6615	1.36117	0.28738	-0.0002	0.23673	0.00367	-0.0197	5.40059
0.093624	551851	12.3863	72.3222	12.7996	1.4482	0.3312	3.4E-05	0.25342	0.00421	-0.023	4.973284
0.093584	551614	12.3757	72.2913	13.9407	1.53702	0.37947	0.00115	0.26999	0.00453	-0.0268	4.596201
0.093477	550982	12.3473	72.2084	15.073	1.61878	0.43101	0.00067	0.28481	0.00497	-0.0292	4.248393

Table 62: U_∞ = 100 mph, h/b = 1.05, $\delta_{mid/out}$ = +20°, Symmetric Deflections

M	Re#	q_c	Uinf	alpha_c	CL	CD_c	Cl_cg_w	Cm_cg_c_w	Cn_cg_w	C_Y	L/D
0.008254	48651.1	0.09627	6.37591	8.35648	7.64666	2.09381	0.02326	0.1453	-0.0055	0.04623	7.813563
0.091934	541891	11.9432	71.017	0.60039	0.629	0.07501	0.00186	0.01236	-0.0005	0.00259	9.323201
0.120639	711089	20.5658	93.1911	-10.825	-0.3569	0.06754	0.00037	-0.2035	-0.0002	0.00034	-5.48188
0.120527	710428	20.5276	93.1044	-8.7545	-0.2128	0.04363	0.00086	-0.158	-0.0003	0.00094	-4.975
0.120431	709860	20.4948	93.03	-8.6623	-0.208	0.04272	0.00084	-0.1568	-0.0003	0.00116	-4.96568
0.120417	709778	20.4901	93.0193	-6.3944	-0.0425	0.02861	0.00101	-0.1106	-0.0002	0.00023	-1.48575
0.120424	709820	20.4925	93.0247	-4.1469	0.10445	0.02765	0.0008	-0.0706	-0.0001	7.3E-05	3.806954
0.120443	709934	20.499	93.0396	-1.8994	0.25127	0.03304	0.00115	-0.0304	-0.0003	1.1E-05	7.891864
0.120564	710643	20.54	93.1326	0.34978	0.39968	0.04416	0.00125	0.00671	-0.0002	0.00058	9.721633
0.120716	711544	20.5921	93.2506	2.60825	0.55658	0.06122	0.00131	0.04704	-0.0001	-0.0001	10.06221
0.12083	712212	20.6308	93.3382	4.75706	0.69275	0.08733	0.00108	0.08513	0.00075	-0.0043	8.861739
0.12087	712448	20.6445	93.3692	6.97852	0.81579	0.12465	0.00101	0.1255	0.00179	-0.0105	7.28678
0.120826	712186	20.6294	93.3349	9.20995	0.94796	0.17479	0.00151	0.16216	0.00327	-0.0188	6.013169
0.120749	711738	20.6034	93.276	11.3499	1.07606	0.23439	0.00192	0.19806	0.0034	-0.0202	5.068321
0.120638	711078	20.5652	93.1896	12.4587	1.13622	0.26876	0.00153	0.21167	0.00363	-0.0213	4.654034
0.120494	710233	20.5164	93.0789	13.5723	1.19987	0.30607	0.00305	0.22557	0.00366	-0.0254	4.306557
0.12043	709855	20.4945	93.0293	14.6631	1.24368	0.34393	0.00329	0.23565	0.00388	-0.0273	3.95537
0.120437	709898	20.497	93.0349	15.7385	1.27238	0.38262	0.00285	0.24059	0.00412	-0.0279	3.617368
0.120405	709706	20.4859	93.0098	16.8017	1.29091	0.42063	0.00414	0.24302	0.00359	-0.0292	3.319888
0.120285	708998	20.4451	92.917	17.855	1.29938	0.45645	0.00413	0.24324	0.00351	-0.0296	3.062771
0.120217	708597	20.4219	92.8644	18.8881	1.2903	0.4883	0.00324	0.23735	0.00384	-0.0267	2.82619
0.120233	708694	20.4276	92.8772	19.8796	1.24232	0.50959	0.00431	0.22147	0.00278	-0.0254	2.587357
0.120191	708445	20.4132	92.8445	20.9672	1.20346	0.53246	0.00458	0.20952	0.0023	-0.0276	2.383881
0.120095	707882	20.3808	92.7708	21.8955	1.17725	0.55188	0.00494	0.2028	0.00181	-0.0277	2.240471

Table 63: U_∞ = 100 mph, h/b = 0.3, $\delta_{mid/out}$ = +20°, Symmetric Deflections

M	Re#	q_c	Uinf	alpha_c	CL	CD_c	Cl_cg_w	Cm_cg_c_w	Cn_cg_w	C_Y	L/D
0.059303	349554	4.96965	45.8104	1.0748	0.98351	0.12831	0.00265	0.02208	-0.0009	0.00586	8.951975
0.117806	694391	19.6113	91.0027	-10.947	-0.4682	0.08439	0.00041	-0.2425	-0.0001	-0.0006	-5.83692
0.117728	693927	19.5851	90.9419	-8.8407	-0.2916	0.0534	0.00089	-0.1863	-0.0001	0.00013	-5.63194
0.117626	693330	19.5514	90.8637	-6.441	-0.0851	0.03367	0.00117	-0.1279	-0.0003	0.00098	-2.53781
0.117721	693885	19.5827	90.9364	-4.1631	0.08955	0.03161	0.00093	-0.0806	-0.0001	8.8E-05	2.846937
0.117834	694555	19.6206	91.0242	-1.8075	0.25572	0.03687	0.00099	-0.0344	-0.0002	-0.0002	7.178767
0.11786	694706	19.6291	91.0439	0.37785	0.42537	0.0489	0.00125	0.00753	-0.0002	0.00087	9.358581
0.117787	694278	19.6049	90.9879	2.6558	0.60009	0.06778	0.00117	0.05183	-4E-05	0.00028	9.851743
0.117596	693149	19.5412	90.8399	4.81879	0.74924	0.096	0.00104	0.09336	0.00078	-0.0042	8.784376
0.117476	692445	19.5015	90.7476	7.05111	0.88222	0.13689	0.00114	0.13687	0.00204	-0.011	7.228332
0.117243	691073	19.4243	90.5678	9.30225	1.03242	0.19237	0.00151	0.17759	0.00345	-0.0194	6.000932
0.117041	689882	19.3574	90.4117	11.4612	1.17786	0.25951	0.00126	0.21566	0.00367	-0.0203	5.054195
0.116916	689144	19.3161	90.3151	12.5767	1.24421	0.2971	0.00115	0.23039	0.00399	-0.0219	4.649944
0.116844	688720	19.2923	90.2595	13.6971	1.31408	0.33794	0.00313	0.24523	0.00404	-0.0264	4.30839
0.116793	688416	19.2752	90.2196	14.7916	1.36125	0.38015	0.00296	0.25494	0.0043	-0.0281	3.947829
0.116762	688233	19.265	90.1957	15.8688	1.39158	0.42382	0.00285	0.25979	0.00449	-0.0289	3.596831
0.116728	688034	19.2539	90.1696	16.9284	1.40683	0.46525	0.00233	0.26258	0.0046	-0.0293	3.290819
0.116732	688058	19.2552	90.1727	17.9812	1.41483	0.50373	0.00413	0.26141	0.00373	-0.0301	3.039044
0.116747	688146	19.2601	90.1842	18.9969	1.38988	0.53483	0.00511	0.25019	0.00297	-0.029	2.791002
0.116672	687701	19.2353	90.126	20.0728	1.33947	0.56134	0.0032	0.23238	0.00387	-0.026	2.541115
0.116621	687406	19.2187	90.0872	21.0889	1.31482	0.5889	0.00324	0.22373	0.00382	-0.0258	2.365083
0.116547	686969	19.1943	90.03	22.0271	1.29768	0.6141	0.00406	0.22008	0.00296	-0.0278	2.229764
0.116547	686966	19.1942	90.0297	22.1139	1.2975	0.61648	0.00348	0.21938	0.00338	-0.027	2.220328

Table 64: U_∞ = 100 mph, h/b = 0.15, $\delta_{mid/out}$ = +20°, Symmetric Deflections

M	Re#	q_c	Uinf	alpha_c	CL	CD_c	Cl_cg_w	Cm_cg_c_w	Cn_cg_w	C_Y	L/D
0.059761	352254	5.04674	46.1643	1.10986	1.01559	0.1305	0.00267	0.03202	-0.0005	0.00437	9.163477
0.116335	685720	19.1246	89.8663	-11.236	-0.7325	0.11251	0.00093	-0.3225	0.00062	-0.004	-7.1624
0.116206	684958	19.0821	89.7664	-9.0208	-0.4565	0.06662	0.00138	-0.2398	0.00026	-0.0023	-7.28631
0.116345	685779	19.1278	89.874	-6.5279	-0.1646	0.03661	0.00167	-0.1525	-8E-05	-0.0002	-4.56215
0.116373	685944	19.137	89.8956	-4.1977	0.05789	0.03234	0.00137	-0.0912	4.2E-05	-0.0005	1.793355
0.11636	685865	19.1327	89.8853	-1.8078	0.25552	0.03658	0.00108	-0.0353	8.2E-05	-0.0011	7.232177
0.116404	686127	19.1473	89.9197	0.40793	0.45289	0.05082	0.00128	0.01204	-6E-06	0.0004	9.654494
0.116403	686121	19.147	89.9189	2.70661	0.64658	0.07144	0.00133	0.06046	0.00029	-0.0013	10.18844
0.116331	685693	19.1231	89.8628	4.97097	0.80888	0.10289	0.00121	0.10566	0.00122	-0.006	8.94693
0.116265	685307	19.1016	89.8122	7.13588	0.95978	0.14835	0.00116	0.15117	0.00292	-0.0149	7.338587
0.116109	684384	19.0501	89.6912	9.38773	1.11064	0.20489	0.00133	0.19318	0.00384	-0.0214	6.12369
0.115904	683177	18.983	89.5331	11.5602	1.26849	0.27821	0.0006	0.22994	0.00411	-0.0216	5.124853
0.115708	682025	18.919	89.3821	12.6942	1.35175	0.3214	0.00156	0.24694	0.00451	-0.025	4.717291
0.115647	681664	18.899	89.3347	13.8244	1.43058	0.36687	0.00337	0.26159	0.00453	-0.029	4.363697
0.11562	681501	18.8899	89.3133	14.9231	1.48154	0.41385	0.0021	0.27071	0.00501	-0.0297	3.982778
0.115409	680262	18.8213	89.151	16.0031	1.51455	0.46191	0.00211	0.27594	0.00524	-0.0302	3.621972
0.115222	679155	18.7601	89.006	17.0379	1.507	0.5049	0.00235	0.27468	0.00496	-0.0302	3.26483
0.115151	678740	18.7372	88.9515	18.068	1.49425	0.54188	0.00322	0.26572	0.00459	-0.031	2.992704
0.115122	678569	18.7278	88.9291	19.0847	1.47021	0.57769	0.00399	0.25203	0.00374	-0.0294	2.740577
0.115032	678038	18.6985	88.8596	20.1681	1.42668	0.60809	0.00289	0.23538	0.00421	-0.0261	2.506172
0.114929	677428	18.6648	88.7796	21.1986	1.41524	0.64122	0.00283	0.23044	0.00438	-0.0262	2.346898
0.114904	677285	18.657	88.7609	22.2353	1.40858	0.67416	0.00299	0.22833	0.00414	-0.0281	2.213626

Table 65: U_∞ = 100 mph, h/b = 0.1, $\delta_{mid/out}$ = +20°, Symmetric Deflections

M	Re#	q_c	Uinf	alpha_c	CL	CD_c	Cl_cg_w	Cm_cg_c_w	Cn_cg_w	C_Y	L/D
0.056504	333052	4.51151	43.6478	1.14022	1.12297	0.14255	0.00296	0.04221	-0.0006	0.00561	9.476658
0.116264	685300	19.1012	89.8113	-9.0494	-0.6418	0.07651	0.00243	-0.3028	0.00011	-0.0023	-9.34804
0.11621	684984	19.0835	89.7699	-6.6314	-0.2593	0.03975	0.00225	-0.1817	5.3E-05	-0.0011	-6.74222
0.116241	685164	19.0936	89.7935	-4.2401	0.01911	0.0325	0.00153	-0.1006	-0.0002	0.00071	0.588145
0.116285	685422	19.108	89.8273	-1.9055	0.24573	0.03623	0.00102	-0.036	0.00012	-0.0006	7.005012
0.116314	685592	19.1174	89.8495	0.41947	0.46345	0.05064	0.00136	0.01581	-1E-05	0.00084	9.95723
0.116333	685709	19.124	89.8649	2.72955	0.66758	0.0717	0.00124	0.06613	0.0004	-0.0014	10.56231
0.116352	685821	19.1302	89.8796	4.91884	0.84079	0.1036	0.00104	0.11234	0.00141	-0.0069	9.330282
0.116304	685534	19.1142	89.842	9.43639	1.15516	0.20986	0.00125	0.20208	0.00417	-0.0224	6.264103
0.116142	684578	19.0609	89.7167	11.6162	1.31967	0.28606	0.00046	0.23856	0.00435	-0.0223	5.219389
0.115938	683379	18.9942	89.5595	12.7557	1.40799	0.33005	0.00131	0.2551	0.00467	-0.0258	4.817966
0.115785	682474	18.944	89.441	13.8983	1.49823	0.37874	0.00272	0.27144	0.00499	-0.03	4.460025
0.115677	681841	18.9088	89.358	15.0185	1.56885	0.42905	0.00239	0.28311	0.0054	-0.032	4.105743
0.115558	681140	18.8699	89.266	16.1229	1.6241	0.4836	0.00192	0.29053	0.00578	-0.0327	3.748289
0.115388	680138	18.8145	89.1348	17.0974	1.56146	0.526	0.00215	0.27848	0.00523	-0.0317	3.256467
0.115184	678933	18.7479	88.9768	18.1303	1.5513	0.56681	0.00317	0.26692	0.00468	-0.0306	2.978067
0.115014	677932	18.6926	88.8457	19.1261	1.50812	0.60131	0.00086	0.24526	0.00585	-0.0249	2.70308
0.114875	677112	18.6475	88.7383	20.1556	1.4948	0.63858	0.00131	0.23471	0.00555	-0.0257	2.508185
0.114744	676338	18.6048	88.6368	21.269	1.47968	0.67337	0.00097	0.22929	0.00594	-0.0248	2.342709
0.114695	676053	18.5891	88.5994	22.2341	1.48708	0.70915	0.00204	0.22983	0.00504	-0.0281	2.2296

Table 66: U_∞ = 100 mph, h/b = 0.05, $\delta_{mid/out}$ = +20°, Symmetric Deflections

M	Re#	q_c	Uinf	alpha_c	CL	CD_c	Cl_cg_w	Cm_cg_c_w	Cn_cg_w	C_Y	L/D
0.050871	299852	3.6569	39.2968	1.31429	1.28226	0.15084	0.00216	0.05777	-0.0012	0.00524	10.73196
0.115818	682669	18.9548	89.4665	-4.2363	-0.057	0.03441	0.00173	-0.1207	-0.0005	0.00239	-1.65937
0.11578	682445	18.9424	89.4372	-3.1101	0.09786	0.03252	0.00135	-0.075	-0.0003	0.00133	3.025868
0.115774	682409	18.9404	89.4325	-1.9125	0.23929	0.03472	0.00109	-0.0368	-0.0002	0.00069	7.115566
0.115863	682936	18.9696	89.5015	-0.7354	0.36111	0.03941	0.00098	-0.0055	-0.0002	0.00079	9.779644
0.115881	683043	18.9756	89.5155	0.43816	0.48055	0.04701	0.00095	0.02131	-0.0002	-0.0004	11.27796
0.115868	682963	18.9711	89.505	1.60964	0.5972	0.05779	0.00085	0.04672	2.6E-05	-0.0003	11.71317
0.115843	682816	18.963	89.4858	2.76222	0.69747	0.07013	0.00061	0.06984	0.00046	-0.0029	11.46175
0.11581	682624	18.9523	89.4606	3.90611	0.7898	0.08512	0.00062	0.09228	0.00094	-0.0057	10.78611
0.115788	682493	18.945	89.4435	4.96384	0.88197	0.10305	0.00073	0.11557	0.0015	-0.009	9.997952
0.115795	682532	18.9472	89.4485	6.09783	0.96523	0.12653	-0.0002	0.14139	0.00282	-0.0147	8.874625
0.115805	682595	18.9507	89.4567	7.23576	1.05119	0.15339	-0.0013	0.16471	0.00368	-0.019	7.944413
0.115823	682698	18.9564	89.4703	8.3697	1.13439	0.1824	-0.0014	0.18628	0.00408	-0.0219	7.186367
0.115828	682727	18.958	89.4741	9.51856	1.23035	0.21925	8.6E-06	0.20922	0.00386	-0.0219	6.462779
0.115799	682559	18.9487	89.4521	10.5708	1.31846	0.2546	0.00025	0.22754	0.00419	-0.0244	5.953788
0.115738	682200	18.9287	89.405	11.7127	1.40796	0.29581	-0.0005	0.24461	0.00475	-0.0262	5.457254
0.115677	681840	18.9088	89.3579	12.8608	1.50422	0.34227	0.00054	0.26205	0.0052	-0.0306	5.028937
0.115657	681722	18.9022	89.3423	14.0039	1.59482	0.39221	0.00124	0.27863	0.00562	-0.0343	4.640185
0.115614	681470	18.8883	89.3094	15.1381	1.67832	0.44621	0.00126	0.29264	0.00607	-0.0365	4.276088

Appendix G: MATLAB Data Reduction Code

```
%*********************************************************************
%*********************************************************************
%***************     Lt. Gebbie & Capt Anthony DeLuca    ***************
%********   Adapted for the Balance AFIT 1 by Lt. Rivera Parga    *********
%**************    Re-adapted by Troy Leveron, ENS, USNR    **************
%**** Re-adapted by Brett Jones, ENS, USNR for UCAV Ground Effects Test****
%****** Re-adapted by Won In, Capt, USAF for UCAV Ground Efects Test *****
%**Re-adapted by Jason Mostaccio, Ens, USN for UCAV Ground Efects Test*****
%******************* Calculation of Lift, Drag, Moments ******************
%*********************************************************************
%*********************************************************************

%This Code will transfer measured Forces and Moments on the AFIT-1 balance to Wind
%(earth) centered frame of reference by correcting for tare effects, balance
%interactions, and wind tunnel irregularities, then gives a file with all the
%corrected data

clear
clc
close all;
format long
%#########################################################################
####
%INPUT DECK
%FIRST FILL THE FOLLOWING INFORMATION
%#########################################################################
####

%Masskg=1.235;                          % Mass of the UCAV in KGS
Masskg=1.065;                          % Mass of the Lamda UCAV in KGS
%T_room = mean([73.4 74 74.7]) + 459.67       %deg R  ****Changed for each day of
testing****
T_room = mean([72.4 75.2 76.3]) + 459.67       %deg R  ****Changed for each day of
testing****
%P_barro = mean([28.6823 28.6130 28.6228]) * 0.4911541   %Psi   ****Changed for
each day of testing****
P_barro = mean([28.5495 28.5456 28.532]) * 0.4911541    %Psi   ****Changed for each
day of testing****

% INPUT DATA FILE AND INPUT DATA TARE FILE
% load tarefile.txt;                  %tarefile GP42005tearA-10to+20B0model
% TareFile = tarefile(:,1:9);
% load datafile.txt;                  %datafile (Raw Data file name here)
% DataFile = datafile(:,1:9);
```

```
load Lambda_LR20_NP_tarefile.txt;           %tarefile Lamda_tA-10to+20B0NP.txt
TareFile = Lambda_LR20_NP_tarefile(:,1:9);
load Lambda_LR20_P2_60mph_datafile.txt;       %datafile Lamda_40MA-
10to+20B0NP.txt
DataFile = Lambda_LR20_P2_60mph_datafile(:,1:9);

%Offset distances from the Mounting Block to the Model C.G. (inches)
Y_cmb =  0;
X_cmb = 2.125;                    %inches  (from origin @ balance center w/ + right)
Z_cmb = 0;


% Required for the Solid body blockage corrections due to wing
% and fuselage
Body_Volume = 54.70258 / 12^3 ;        %ft^3: From Solid Works "Mass Properties"
Wing_Area = 78.309 / 12^2             %ft^2 Estimated from Solid Works schematic

%#########################################################################
#
%I.-   Room Conditions and Model Specifics :
%      UNITS are in Ft, Sec, lbm, Psf, Rankine, fps
%#########################################################################
#

Mass = (Masskg * 1000) * 0.0022046;               %lbm (UCAV)
Gas_Const = 1716;                              %ft-lbf/Slug-R
Density = (P_barro * 144)/(1716 * T_room);         %lbm/ft^3 or lbf-s^2/ft^4
Root_Chord = 10.54818/12;                          %ft
Span = 14.61858 / 12;                             %ft
Aspect_Ratio = Span^2 / Wing_Area;
Kinematic_Viscosity = .372e-6;                     %slug/ft-s
Speed_of_Sound = sqrt(1.4 * T_room * Gas_Const);    %fps

%Distances between sensors (inches) to calculate moments

D1 = (2.10 / 2); D2 = D1; D3 = (1.7 / 2); D4 = D3;

%#########################################################################
#
%II.-     Solid body blockage corrections due to wing and fuselage (Pope
%pg 369
%#########################################################################
#

K_1 = 1.04;                        % t/c=.15, 4 digit airfoil
delta = 0.3322;                     %boundary correction factor (2b/B), B=44 in. (Ch. 10)
```

```
Tau_1 = 0.86;                       %factor from pg 369, fun. of tunnel shape and b/B
X_Section = (31/12)*(44/12);          %ft^2
Wing_Volume = Body_Volume;            %ft^3   Flying Wing UCAV
Epsilon_sb_w = (K_1*Tau_1*Wing_Volume) / X_Section^(3/2)
Epsilon_tunnel_correction = 0.911;   %from Hot-wire data... ratio between hotwire and
transducer vel
Epsilon_sb_gp = 1.01;               %Plane # Vel / Open Tunnel Vel as measured by the hot-
wire
Epsilon_tot = Epsilon_sb_w+ (Epsilon_sb_gp*Epsilon_tunnel_correction-1)

%#########################################################################
#
%VI.- CORRECT FORCES AND MOMENTS FOR BALANCE INTERACTIONS
(body axis)
%#########################################################################
####

%Balance Interactions with off axis elements for the 100 lb balance
%Using average of the 100 lb calibration runs for N1 & N2 and the
%50 lb calibration for S1, S2 & A and 40 lb calibration for L then normalizing by the
actual
%sensor (N1, N2,...) in question.  The sensor sequence in each row vector is:
%[N1 N2 S1 S2 A L]

N1_I = ([7.316 -0.735 0.195 0.018 -0.113 -0.073 ] + [7.207 -0.74 0.297 0.021 -0.062
0.021])/2;
   N11 = N1_I(1,1)/100;

N2_I = ([-0.109 7.64 0.015 0.118 0.043 -0.017] + [-0.173 7.481 0.041 0.151 0.064
0.02])/2;
   N22 = N2_I(1,2)/100;

S1_I = ([0.01 0.01  7.517 -0.439 0.058 -0.005] + [0.021 0.01 7.36 -0.443 0.053 0.048])/2;
   S11 = S1_I(1,3)/50;

S2_I = ([-0.005 -0.006 -0.108 7.286 -0.027 0.028] + [0 0 -0.132 7.015 -0.019 -0.031])/2;
   S22 = S2_I(1,4)/50;

A_I = ([0 0.004 -0.01 0.011 7.612 0.104] + [-0.05 0.042 -0.02 0.01 7.546 0.054])/2;
   A11 = A_I(1,5)/50;

L_I = ([-0.079 0.066 0.033 0.025 0.525 8.695] + [-0.09 0.04 0 -0.03 0.492 8.709])/2;
   L11 = L_I(1,6)/40;

N1_normalized = (N1_I/100)  .* [N11 N22 S11 S22 A11 L11].^(-1);
N2_normalized = (N2_I/100) .* [N11 N22 S11 S22 A11 L11].^(-1);
```

```
S1_normalized = (S1_I/50)  .* [N11 N22 S11 S22 A11 L11].^(-1);
S2_normalized = (S2_I/50)  .* [N11 N22 S11 S22 A11 L11].^(-1);
A_normalized = (A_I/50)    .* [N11 N22 S11 S22 A11 L11].^(-1);
L_normalized = (L_I/40)    .* [N11 N22 S11 S22 A11 L11].^(-1);

Interactions_Kij = [N1_normalized' N2_normalized' S1_normalized' S2_normalized'
A_normalized' L_normalized'];

%#########################################################################
#
% III.-  Load the static tare data for the alpha sweep w/o the wind ,
%       separate each force from the file, and fit a 4th order poly
%       as an x-y plot (AoA vs.Force) for each of the 6 force sensors.
%#########################################################################
#

%load tare1.txt;                    %Raw tare data file to be read in.
FILE=TareFile(:,1:9);                %GP42005tearA-10to+20B0model

j=1;
k=1;
L=length(FILE);

for i=1:L                           %Run for all data points # of rows
   if i~=L                          %if current row is not last row, go to next
      NEXT=i+1;                     %set next equal to the value of the next row
      VALUE2=FILE(NEXT,1);          %set value2 as next row column 1
   else if i==L                     %unless the it is the last value
      VALUE2=50;                    %value2 set to 50 to end the sequence
   end
   end
   A(j,:)=FILE(i,:);                %set row j of A equal to row i of FILE
   VALUE1=FILE(i,1);                %set value1 equal to row i column 1 of FILE
   if VALUE1==VALUE2                %if value1 equals value2, go to next row
      j=j+1;
   else if VALUE1~=VALUE2           %if value1 and value2 are different check
      if length(A(:,1))<5           %if less than 20 values, ignored due to angle change
         j=1;
         clear A;
      else if length(A(:,1))>5      %if more than 20 values
            C=length(A(:,1));       %find length of A
            for m=1:9               %Average all rows of the like values in A
               B(k,m)=mean(A(4:C,m));  %disregarding first 10 for vibrations
            end
            j=1;
            k=k+1;
```

```
            clear A
        end
        end

    end
    end
end

if B(k-1,1)<B((k-2),1)
    B=B(1:(k-2),:)
end

tare=[B];

%_____________________________________End of inserted code
[row,col] = size(tare);


for k = 1:row;

theta_tare(k,:,:)   = tare(k,1).* (pi/180);
% NF_tare(k,:,:)      = tare(k,4);
N1_tare(k,:,:)      = tare(k,4);
% PM_tare(k,:,:)      = tare(k,5);
N2_tare(k,:,:)      = tare(k,5);
% SF_tare(k,:,:)      = tare(k,7);
S1_tare(k,:,:)      = tare(k,7);
% YM_tare(k,:,:)      = tare(k,8);
S2_tare(k,:,:)      = tare(k,8);
% AF_tare(k,:,:)       = tare(k,6);
A_tare(k,:,:)       = tare(k,6);
% RM_tare(k,:,:)       = tare(k,9);
L_tare(k,:,:)       = tare(k,9);
end

% NF_poly = polyfit(theta_tare,NF_tare,4);
N1_poly = polyfit(theta_tare,N1_tare,4);
% PM_poly = polyfit(theta_tare,PM_tare,4);
N2_poly = polyfit(theta_tare,N2_tare,4);
% SF_poly = polyfit(theta_tare,SF_tare,4);
S1_poly = polyfit(theta_tare,S1_tare,4);
% YM_poly = polyfit(theta_tare,YM_tare,4);
S2_poly = polyfit(theta_tare,S2_tare,4);
% AF_poly  = polyfit(theta_tare,AF_tare,4);
A_poly  = polyfit(theta_tare,A_tare,4) ;
% RM_poly  = polyfit(theta_tare,RM_tare,4);
```

```
L_poly  = polyfit(theta_tare,L_tare,4) ;

clear ('B','C','D','L')
%#########################################################################
#
%IV.- Load the specific test run files,
%#########################################################################
#

%clear ('AA','B','C','L')

%load data1.txt;                    %Raw data file to be read in:
FILE=DataFile(:,:);                  %Same as above

j=1;
k=1;
L=length(FILE);

for i=1:L                           %Run for all data points # of rows
   if i~=L                          %if current row is not last row, go to next
      NEXT=i+1;                     %set next equal to the value of the next row
      VALUE2=FILE(NEXT,1);          %set value2 as next row column 1
   else if i==L                     %unless the it is the last value
      VALUE2=50;                    %value2 set to 50 to end the sequence
   end
   end
   A(j,:)=FILE(i,:);                %set row j of A equal to row i of FILE
   VALUE1=FILE(i,1);                %set value1 equal to row i column 1 of FILE
   if VALUE1==VALUE2                %if value1 equals value2, go to next row
      j=j+1;
   else if VALUE1~=VALUE2           %if value1 and value2 are different check
      if length(A(:,1))<5           %if less than 20 values, ignored due to angle change
         j=1;
         clear A;
      else if length(A(:,1))>5      %if more than 20 values
            C=length(A(:,1));       %find length of A
            for m=1:9               %Average all rows of the like values in A
               B(k,m)=mean(A(4:C,m));    %disregarding first 10 for vibrations
            end
            j=1;
            k=k+1;
            clear A
      end
      end
   end
   end
```

```
end

if B(k-1,1)<B((k-2),1)
   B=B(1:(k-2),:)
end

sample_data=[B];

%_____________________________________End of inserted code
[row2,col2] = size(sample_data);


for i = 1:row2;

%Angles of the model during test runs (Roll, Pitch {AoA}, Yaw {Beta}):

phi               = 0;
theta(i,:)        = sample_data(i,1) .* (pi/180);       %radians
si(i,:)           = sample_data(i,2) .* (pi/180);       %radians
Wind_Speed(i,:)   = sample_data(i,3) .* (5280/3600);    %fps

%Flight Parameters (Re#, Ma#, Dynamic Pressure):

q = (.5 * Density) .* Wind_Speed.^2;                    %lbf/ft^2
q_Corrected = q .* (1 + Epsilon_tot)^2;                 %lbf/ft^2
Wind_Speed_Corrected = Wind_Speed .* (1 + Epsilon_tot); %fps
Wind_Speed_Corrected_mph = Wind_Speed_Corrected.*(3600/5280);
Mach_Number = Wind_Speed_Corrected ./ Speed_of_Sound;   %NonDimensional
Reynolds_Number = ((Density * Root_Chord) .* Wind_Speed_Corrected) ./
Kinematic_Viscosity; %NonDimensional
Flight_Parameters = [Mach_Number Reynolds_Number q_Corrected];

%individual forces and moments for each sensor:

%NEW NOTATION
% NF_test(i,:,:)      = sample_data(i,4);
N1_test(i,:,:)      = sample_data(i,4);
% PM_test(i,:,:)      = sample_data(i,5);
N2_test(i,:,:)      = sample_data(i,5);
% SF_test(i,:,:)      = sample_data(i,7);
S1_test(i,:,:)      = sample_data(i,7);
% YM_test(i,:,:)      = sample_data(i,8);
S2_test(i,:,:)      = sample_data(i,8);
% AF_test(i,:,:)       = sample_data(i,6);
A_test(i,:,:)       = sample_data(i,6);
% RM_test(i,:,:)       = sample_data(i,9);
```

```
L_test(i,:,:)       = sample_data(i,9);
%#########################################################################
#
%V.-   Subtract the effect of the static
%      weight with the tare polynominals above
%#########################################################################
#

%Evaluating the actual test theta angle (AoA) in the tare polynominal to
%determine the tare values for the angles tested in each run.

% NF_eval = polyval(NF_poly,theta);
N1_eval = polyval(N1_poly,theta);
% PM_eval = polyval(PM_poly,theta);
N2_eval = polyval(N2_poly,theta);
% SF_eval = polyval(SF_poly,theta);
S1_eval = polyval(S1_poly,theta);
% YM_eval = polyval(YM_poly,theta);
S2_eval = polyval(S2_poly,theta);
% AF_eval  = polyval(AF_poly,theta);
A_eval  = polyval(A_poly,theta);
% RM_eval  = polyval(RM_poly,theta);
L_eval  = polyval(L_poly,theta);

%The Time-Averaged (raw) forces and momentums NF,AF,SF,PM,YM AND RM
measurd in the wind
%tunnel (body axis) with the tare effect of the weight subtracted off.

% NF_resolved = NF_test - (NF_eval);
N1_resolved = N1_test - (N1_eval);
% PM_resolved = PM_test - (PM_eval);
N2_resolved = N2_test - (N2_eval);
% SF_resolved = SF_test - (SF_eval);
S1_resolved = S1_test - (S1_eval);
% YM_resolved = YM_test - (YM_eval);
S2_resolved = S2_test - (S2_eval);
% AF_resolved  = AF_test -  (AF_eval);
A_resolved  = A_test -  (A_eval);
% RM_resolved  = RM_test -  (RM_eval);
L_resolved  = L_test -  (L_eval);

%Forces_minus_tare = [NF_resolved, AF_resolved, PM_resolved, RM_resolved,
YM_resolved, SF_resolved]';
Forces_minus_tare = [N1_resolved N2_resolved S1_resolved S2_resolved A_resolved
L_resolved]';
```

```
%Forces N1, N2, S1, S2, A, & L corrected for the balance interactions (body axis)

% Corrected_Data(:,i)= [NF(n);AF(n);PM(n);RM(n);YM(n);SF(n)];

%Forces N1, N2, S1, S2, A, & L corrected for the balance interactions (body axis)

Corrected_Data = (inv(Interactions_Kij) * Forces_minus_tare)

%#########################################################################
#
%VII.- Calculation of the Axial, Side, & Normal Forces from the corrected balance
%      forces in the Body Axis reference frame
%#########################################################################
#

%Forces_b(:,i) = [Corrected_Data(2,i); Corrected_Data(6,i); Corrected_Data(1,i)]
Forces_b(:,i) = [Corrected_Data(5,i); Corrected_Data(3,i) + Corrected_Data(4,i);
Corrected_Data(1,i) + Corrected_Data(2,i)];

%Calculation of the Drag, Side, & Lift Forces in the Wind Axis reference
%frame

% Forces_w =
[Forces_b(1,:).*cos(theta').*cos(si')+Forces_b(2,:).*sin(si')+Forces_b(3,:).*sin(theta').*co
s(si');
%           -Forces_b(1,:).*sin(si').*cos(theta')+Forces_b(2,:).*cos(si')-
Forces_b(3,:).*sin(theta').*sin(si');
%           -Forces_b(1,:).*sin(theta')+Forces_b(3,:).*cos(theta')];

Forces_w =
[Forces_b(1,:).*cos(theta').*cos(si')+Forces_b(2,:).*sin(si')+Forces_b(3,:).*sin(theta').*co
s(si');
          -Forces_b(1,:).*sin(si').*cos(theta')+Forces_b(2,:).*cos(si')-
Forces_b(3,:).*sin(theta').*sin(si');
          -Forces_b(1,:).*sin(theta')+Forces_b(3,:).*cos(theta')];

% Calculate lift-to-drag ratio
L_D = Forces_w(3,:)./Forces_w(1,:);

%First entry is the moments calculated by the balance or direct calculation
%in the Body Reference Frame.  Balance measures Roll (l), Yaw is about the
%z-axis (n), and Pitch is about the y-axis (m).  Distances from strain
%gages to C.G. are in INCHES.  Moments are in-lbf

% m = Corrected_Data(3,i);
m = Corrected_Data(1,i) * D1 - Corrected_Data(2,i) * D2;
```

```
% n = Corrected_Data(5,i);
n = Corrected_Data(3,i) * D3 - Corrected_Data(4,i) * D4;
% l = Corrected_Data(4,i);

%Moments_b(:,i) = [l; m; n]
Moments_b(:,i) = [Corrected_Data(6,i); m; n];

%Second entry is the conversion from the "Balance Centeric" moments to the
%Wind Reference monments with respect to the Balance Center (bc)

% Moments_w_bc = [Moments_b(1,:).*cos(theta').*cos(si')-
Moments_b(2,:).*sin(si')+Moments_b(3,:).*sin(theta').*cos(si');
%
Moments_b(1,:).*sin(si').*cos(theta')+Moments_b(2,:).*cos(si')+Moments_b(3,:).*sin(the
ta').*sin(si');
%               -Moments_b(1,:).*sin(theta')+Moments_b(3,:).*cos(theta')];

Moments_w_bc = [Moments_b(1,:).*cos(theta').*cos(si')-
Moments_b(2,:).*sin(si')+Moments_b(3,:).*sin(theta').*cos(si');

Moments_b(1,:).*sin(si').*cos(theta')+Moments_b(2,:).*cos(si')+Moments_b(3,:).*sin(the
ta').*sin(si');
          -Moments_b(1,:).*sin(theta')+Moments_b(3,:).*cos(theta')];


%Finally, the balance centered moments are converted to moments about the
%Model's Center of Mass (cm) or Center of Gravity (CG)

cgdist=sqrt((X_cmb)^2+(Z_cmb)^2);       %Obtaining the direct distance between the
center of the balance and %the center of mass
w=atan(-Z_cmb/X_cmb);                   %Obtaining the angle between cgdist and the x axes
at zero angle of %attack

X_cm(i,:)= cos(theta(i,:)+w)*cos(si(i,:))*(cgdist);
Y_cm(i,:) = Y_cmb + X_cm(i,:)*tan(si(i,:));
Z_cm(i,:)= -sin(theta(i,:)+w)*(cgdist);

% Moments_w_cg_u = [Moments_w_bc(1,:) + Z_cm(i,:)*Forces_w(2,:) +
Forces_w(3,:)* Y_cm(i,:);
%               Moments_w_bc(2,:) - Forces_w(3,:)* X_cm(i,:) + Forces_w(1,:)*
Z_cm(i,:);
%               Moments_w_bc(3,:) - Forces_w(1,:)* Y_cm(i,:) - Forces_w(2,:)*
X_cm(i,:)];

Moments_w_cg_u = [Moments_w_bc(1,:) + Z_cm(i,:)*Forces_w(2,:) + Forces_w(3,:)*
Y_cm(i,:);
```

```
            Moments_w_bc(2,:) - X_cm(i,:)*Forces_w(3,:) + Forces_w(1,:)* Z_cm(i,:);
            Moments_w_bc(3,:) - Y_cm(i,:)*Forces_w(1,:) - Forces_w(2,:)* X_cm(i,:)];

%#########################################################################
#

%VIII.- Calculation of the actual Lift and Drag nondimensional Coefficients, uncorrected
for tunnel effects, %(Cl and Cd)
%#########################################################################
#

C_D_u = Forces_w(1,:) ./ (q_Corrected' .* Wing_Area);
C_Y_u = Forces_w(2,:) ./ (q_Corrected' .* Wing_Area);
C_L_u = Forces_w(3,:) ./ (q_Corrected' .* Wing_Area);  %Keuthe & Chow pg 178
Coefficients = [C_L_u; C_D_u; C_Y_u]';
% Ave_Cl = mean(Coefficients(:,1));
% Ave_Cd = mean(Coefficients(:,2));

end

%#########################################################################
#
%IX         Drag Coefficient Correction
%#########################################################################
#

C_D_o = min(Coefficients(:,2));
C_L_u_sqrd = Coefficients(:,1).^2;
Delta_C_D_w = ((delta * Wing_Area) / X_Section) .* C_L_u_sqrd;
C_D_Corrected = C_D_u' + Delta_C_D_w;

%#########################################################################
#
%X.-  Angle of Attack due to upwash Correction
%#########################################################################
#

alpha = sample_data(:,1);
Delta_alpha_w = ((delta * Wing_Area) / X_Section) .* (57.3 * C_L_u);
alpha_Corrected = alpha + Delta_alpha_w';

%#########################################################################
#
%XI.-  Pitching Moment Correction
%#########################################################################
#
```

```
c_bar = (mean([7.42, 7.42, 7.42, 3.7442, 0])) / 12; %ft = Mean Chord of wing taken at
five equal stations

Cl_w_cg =   Moments_w_cg_u(1,:) ./ (q_Corrected' .* (Wing_Area * Span*12));
Cm_w_cg_u = Moments_w_cg_u(2,:) ./ (q_Corrected' .* (Wing_Area * c_bar*12));
Cn_w_cg =   Moments_w_cg_u(3,:) ./ (q_Corrected' .* (Wing_Area * Span*12));

Cm_w_cg_corrected = Cm_w_cg_u;         %No Tail
Corrected_Moment_Coefficients = [Cl_w_cg' Cm_w_cg_corrected' Cn_w_cg'];

%OBTAINING THE MOMENTS COEFFICIENTS CORRECTED ABOUT THE
CENTER OF THE
%BALANCE

Cl_w_bc =   Moments_w_bc(1,:) ./ (q_Corrected' .* (Wing_Area * Span*12));
Cm_w_bc_u = Moments_w_bc(2,:) ./ (q_Corrected' .* (Wing_Area * c_bar*12));
Cn_w_bc =   Moments_w_bc(3,:) ./ (q_Corrected' .* (Wing_Area * Span*12));

Cm_w_bc_corrected = Cm_w_bc_u;
Corrected_Moment_Coefficients_bc = [Cl_w_bc' Cm_w_bc_corrected' Cn_w_bc'];

%##########################################################################
#
%XII.- OUTPUT VARIABLES FORMATING
%##########################################################################
#

alpha = sample_data(:,1);

fprintf('   Mach Number Reynolds Number Dynamic Pressure(Psf)\r')
Flight_Parameters
fprintf(' \r');
fprintf(' Loads are in lbf and arranged [D S L] across the top and increments of alpha
down the side \r')
Forces_w'
fprintf(' \r')
fprintf(' Lift-to-Drag Ratio')
L_D'
fprintf(' \r')
fprintf(' Moments are in in-lbf and arranged [L M N] down the side and increments of
alpha along the top \r')
Moments_w_cg_u
fprintf(' \r')
fprintf('      Cl_u          Cd_u          CY_u \r');
Coefficients
```

```
fprintf(' \r')
fprintf('    Del_CD_w       CD_u     CD_Corrected \r');
Compare_CD = [Delta_C_D_w C_D_u' C_D_Corrected]
fprintf(' \r')
fprintf('    Del_alpha_w    alpha_g     alpha_Corrected \r');
Compare_alpha = [Delta_alpha_w' alpha alpha_Corrected ]
fprintf(' \r')
fprintf('    Cl_cg_wind    Cm_cg_corrected_w     Cn_cg_wind \r');
Corrected_Moment_Coefficients
fprintf(' \r')
fprintf('      M#          Re#          q_c          Uoo        alpha_c        C_L        C_D_c
Cl_cg_w       Cm_cg_c_w    Cn_cg_w       C_Y\r');
YY=[Flight_Parameters (Wind_Speed_Corrected .* (3600/5280)) alpha_Corrected
C_L_u' C_D_Corrected Corrected_Moment_Coefficients C_Y_u']%pressure]
%XX=['M#' 'Re#' 'q_c'  'Uoo' 'alpha_c' 'C_L' 'C_D_c' 'Cl_cg_w' 'Cm_cg_c_w' 'Cn_cg_w
\r'];

%ZZ=[XX; YY];
wk1write('output.xls',YY,2,1)
```

Appendix H: Lambda UCAV Flap Specifications

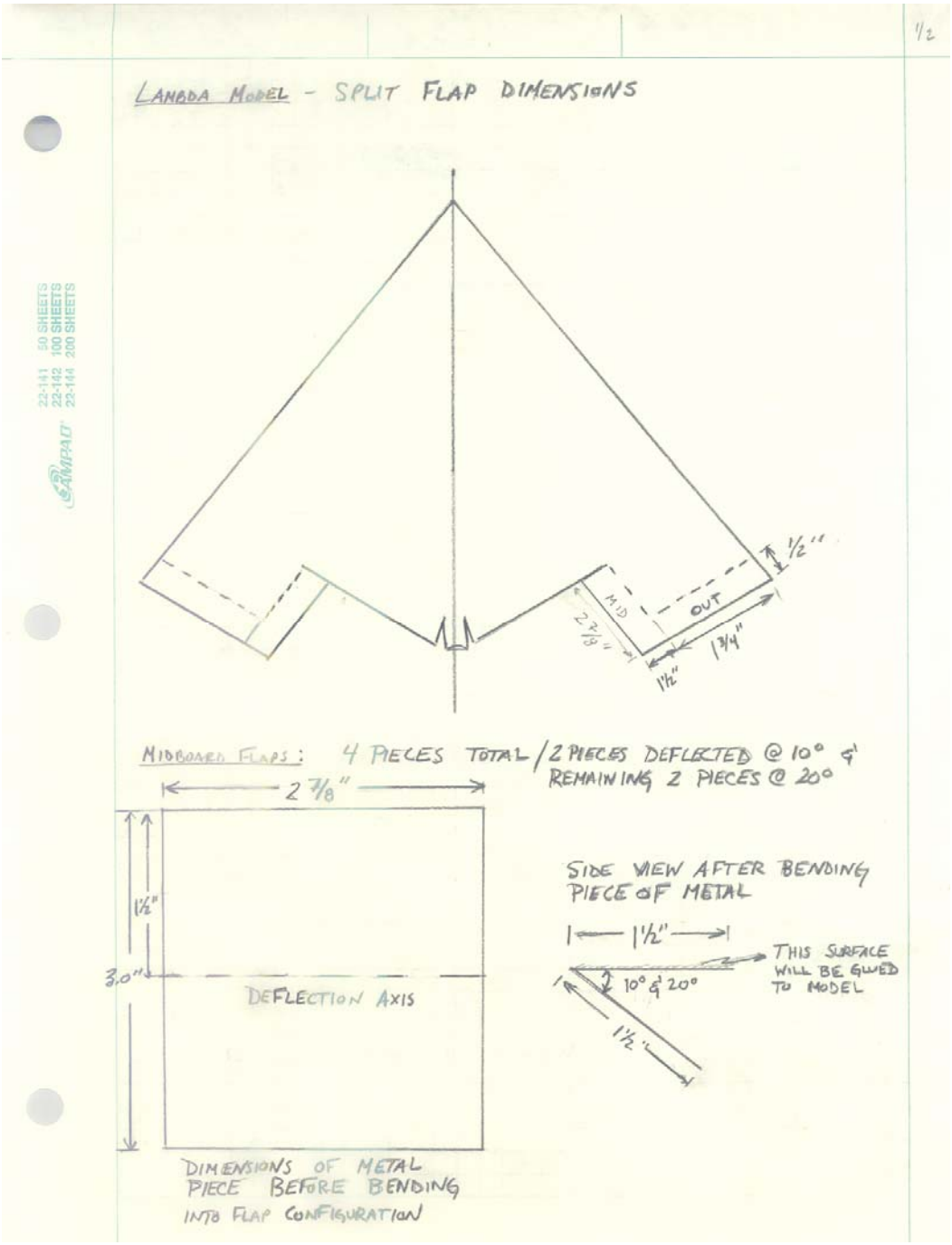

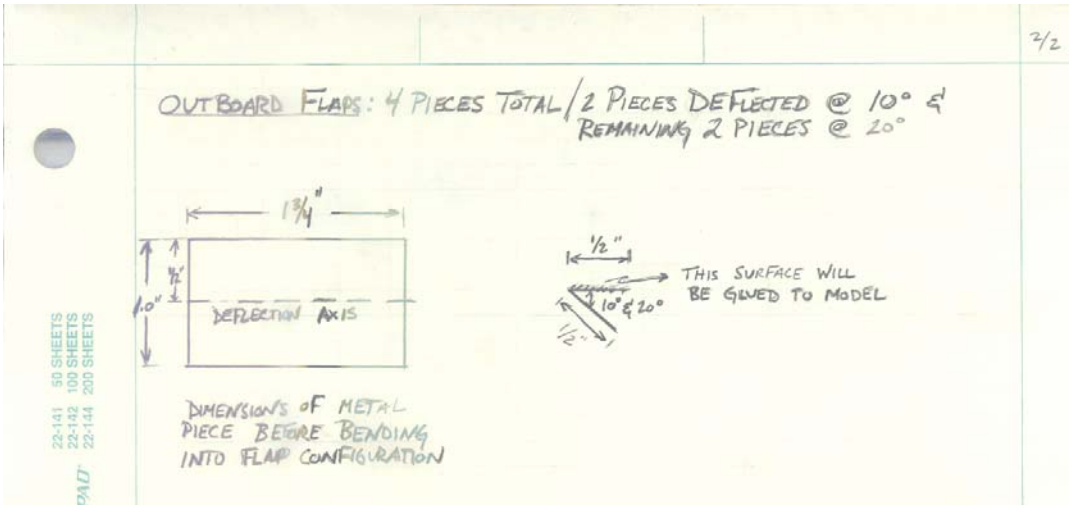
2/2
OUTBOARD FLAPS: 4 PIECES TOTAL / 2 PIECES DEFLECTED @ 10° &
REMAINING 2 PIECES @ 20°
1 3/4"
1/2"
1.0"
DEFLECTION AXIS
1/2"
THIS SURFACE WILL
BE GLUED TO MODEL
10° & 20°
1 1/2"
DIMENSIONS OF METAL
PIECE BEFORE BENDING
INTO FLAP CONFIGURATION
22-141 50 SHEETS
22-142 100 SHEETS
22-144 200 SHEETS

References

1. Edwards, L.C. "Experimental Study of Wing-in-Ground Effects in the AFIT 5-foot Wind Tunnel," MS thesis, AFIT/GAE/AA/87M-1, Department of Aeronautics and Astronautics, Air For Institute of Technology (AU),Wright-Patterson AFB, OH, March 1987.

2. van Opstal, Edwin and others. "Wing in Ground Effect Aerodynamics," *The WIG Page*. 5 Jan 2006 http://www.setechnology.com/wig/html/main.php?open=aero &code=0.

3. Jones, Brett L. "Experimental Investigation into the Aerodynamic Ground Effect of a Tailless Chevron-Shaped UCAV," MS thesis, AFIT/GAE/ENY/05-J04, Department of Aeronautics and Astronautics, Air For Institute of Technology (AU),Wright-Patterson AFB, OH, June 2005.

4. Phillips, Warren F. *Mechanics of Flight*. New Jersey: John Wiley and Sons, Inc., 2004.

5. Herring, Sharolyn. "History of the Hovercraft," Neoteric Hovercraft, Inc. 17 Jan 2006 http://www.neoterichovercraft.com/general_info/historyof.htm#2.

6. Cole, William. "The Pelican: A Big Bird for the Long Haul," *Boeing Frontiers Online*, 1 (5) (September 2002) n.pag. 8 Jan 2006 http://www.boeing.com/ news/frontiers/archive/2002/september/i_pw.html.

7. "Unmanned Aerial Vehicle," *Wikipedia Encyclopedia*. 9 Jan 2006 http://en.wikipedia.org/wiki/UAV.

8. Newcome, Laurence R. *Unmanned Aviation A Brief History of Unmanned Aerial Vehicles*. Virginia: American Institute of Aeronautics and Astronautics, Inc., 2004.

9. Rivera Parga, Jose R. "Wind Tunnel Investigation of the Static Stability and Control Effectiveness a Rotary Tail in a Portable UAV," MS thesis, AFIT/GAE/ ENY/04-D02, Department of Aeronautics and Astronautics, Air For Institute of Technology (AU),Wright-Patterson AFB, OH, 2004.

10. Reed, Shad A. "Experimental Aerodynamic Development of Advanced Unmanned Combat Aerial Vehicle Configurations," Final Report, Air Vehicles Directorate Air Force Laboratory, Wright-Patterson AFB, OH, October 1998.

11. In, Won. "Experimental Investigation into the Aerodynamic Ground Effect of a Chevron and Lambda UCAV," MS thesis, AFIT/ENY/GA-06M, Department of Aeronautics and Astronautics, Air Force Institute of Technology, Wright-Patterson AFB, OH, 2006.

12. Wieselsberger, C. *Wing Resistance Near the Ground.* NACA TM 77, 1922.

13. McCormick, Barnes W. *Aerodynamics, Aeronautics, and Flight Mechanics.* New York: John Wiley and Sons, Inc, 1995.

14. Fink, Marvin P. and James L. Lastinger. *Aerodynamic Characteristics of Low-Aspect-Ratio Wings in Close Proximity to the Ground.* NASA TN D-926, 1961.

15. Le Sueur, Maurice. *Ground Effect on the Take-off and Landing of Airplanes.* NACA TM 771, 1934.

16. Recant, Isidore G. *Wind-tunnel Investigation of Ground Effect on Wings with Flaps.* NACA TN 705, 1939.

17. Baker, Paul A., William G. Schweikhard, and William R. Young. *Flight Evaluation of Ground Effect on Several Low-Aspect-Ratio Airplanes.* NASA TN D-6053, 1970.

18. Bertin, John J. *Aerodynamics for Engineers* (4th Edition). New Jersey: Prentice-Hall, 1989.

19. Corda, Stephen and others. *Dynamic Ground Effects Flight Test of an F-15 Aircraft.* NASA TM 4604, 1994.

20. Kuethe, Arnold M. and Chuen-Yen Chow. *Foundations of Aerodynamics* (4th Edition). New York: John Wiley and Sons, 1986.

21. White, Frank M. *Viscous Fluid Flow* (3rd Edition). New York: McGraw Hill, 2006.

22. Kemmerly, Guy T. and John W. Paulson, Jr. *Investigation of a Moving-Model Technique for Measuring Ground Effects.* NASA TM 4080, 1989.

23. Turner, Thomas R. "Endless-belt Technique for Ground Simulation," *Proceedings of Conference on VTOL/STOL Aircraft,* NASA SP 116, Paper 25: 445, (1966).

24. Lee, Pai Hung, C. Edwards Lan, and Vincent U. Muirhead. *An Experimental Investigation of Dynamic Ground Effect.* NASA CR 4105, 1987.

25. Curry, Robert E. and Lewis R. Owens. *Ground-Effect Characteristics of the Tu-144 Supersonic Transport Airplane.* NASA TM 2003-212035, 2003.

26. DeLuca, Anthony M."Experimental Investigation into the Aerodynamic Performance of Both Rigid and Flexible Wing Structured Micro-Air-Vehicles," MS thesis, AFIT/GAE/ENY/04-M06, Department of Aeronautics and Astronautics, Air Force Institute of Technology (AU), Wright-Patterson AFB, OH, March 2004.

27. Gebbie, David A. "Experimental Study of the Subsonic Aerodynamics of a Blended Wing Body Air Vehicle with a Focus on Rapid Technology Assessment," MS thesis, AFIT/GAE/ENY/05-M09, Department of Aeronautics and Astronautics, Air Force Institute of Technology (AU), Wright-Patterson AFB, OH, March 2005.

28. Barlow**,** Rae, and Alan Pope. *Low-Speed Wind Tunnel Testing (Third Edition)*. New York: John Wiley & Sons, Inc., 1999.

29. Nickel, Karl and Michael Wohlfahrt. *Tailless Aircraft in Theory and Practice*. Washington, DC: American Institute of Aeronautics and Astronautics, Inc., 1994.

30. Plumley, Ryan, private communication, January 2006.

31. Franke, Jones, and Eric Stephen. *Aerodynamic Ground Effects of a Tailless Chevron-Shaped UCAV Model*. American Institute of Aeronautics and Astronautics, Inc., 2006.

Vita

Jason Thomas Mostaccio was born in Patterson, New Jersey. He graduated from Vernon Township High School in 2000 and five years later earned his bachelor of science degree in aerospace engineering and a minor in leadership from Virginia Tech. While at Virginia Tech, he was a midshipman in the Navy ROTC program and a member of the Corps of Cadets and regimental band. On 13 May 2005, he received a Commission into the United States Navy. Upon completion of his master's degree at the Air Force Institute of Technology, he will proceed to his next assignment in Pensacola, Florida, where he will have the opportunity to achieve his life long dream as a naval aviator.

REPORT DOCUMENTATION PAGE

Form Approved
OMB No. 074-0188

1. REPORT DATE *(DD-MM-YYYY)*	**2. REPORT TYPE**	**3. DATES COVERED** *(From – To)*
13 Jun 06	**Master's Thesis**	27 Jun 05 – 13 Jun 06

4. TITLE AND SUBTITLE

EXPERIMENTAL INVESTIGATION OF THE AERODYAMIC GROUND EFFECT OF A TAILLESS LAMBDA-SHAPED UCAV WITH WING FLAPS

5a. CONTRACT NUMBER

5b. GRANT NUMBER

5c. PROGRAM ELEMENT NUMBER

6. AUTHOR(S)

MOSTACCIO, JASON, Ensign, USN

5d. PROJECT NUMBER

5e. TASK NUMBER

5f. WORK UNIT NUMBER

7. PERFORMING ORGANIZATION NAMES(S) AND ADDRESS(S)
Air Force Institute of Technology
Graduate School of Engineering and Management (AFIT/EN)
2950 Hobson Way
WPAFB OH 45433-7765

8. PERFORMING ORGANIZATION REPORT NUMBER

AFIT/GAE/ENY/06-J11

9. SPONSORING/MONITORING AGENCY NAME(S) AND ADDRESS(ES)
AFRL/VAAA
Attn: Mr. Dieter Multhopp
3550 Aberdeen Rd. SE
WPAFB OH 454XX-5776 DSN: 246-2871

10. SPONSOR/MONITOR'S ACRONYM(S)

11. SPONSOR/MONITOR'S REPORT NUMBER(S)

12. DISTRIBUTION/AVAILABILITY STATEMENT
APPROVED FOR PUBLIC RELEASE; DISTRIBUTION UNLIMITED.

13. SUPPLEMENTARY NOTES

14. ABSTRACT

This experimental study adequately identified the ground effect region of a lambda-shaped unmanned combat air vehicle (UCAV). The lambda planform used in this study was originally tested in a previous experiment to determine the stability and control characteristics generated out-of-ground-effect. The following study extends the existing database by analyzing the inherent aerodynamic behavior that is produced by employing trailing edge flap deflections while flying in-ground-effect (IGE). To accomplish this objective, static ground effect tests were performed in the AFIT 3' x 3' subsonic wind tunnel where a ground plane was used to simulate the forces and moments on the UCAV IGE. Removable aluminum flap pieces were attached to the model, in a split flap configuration, along the midboard and outboard trailing edges of the UCAV, and the corresponding IGE data was collected for symmetric and asymmetric deflections of $+10^{o}$ and $+20^{o}$.

Based on the results of this study, the ground effect region for the lambda UCAV, with flaps deployed was characterized by an increase in the lift, a reduction in the induced drag but an increase in the overall drag, and an increase in the lift-to-drag ratio. These trends were noted in previous ground effect studies for aircraft with trailing edge flaps, and similar aspect ratios and wing sweep. Additionally, a flow visualization analysis revealed that a vortical flow pattern, that is characteristic of delta wing configurations, developed over the upper surface of the wing at high angles of attack.

15. SUBJECT TERMS
Ground Effect Analysis with Flap Deflections; Flow Visualization of the Lambda UCAV; Boundary Layer Analysis of the Ground Plane

16. SECURITY CLASSIFICATION OF:			**17. LIMITATION OF ABSTRACT**	**18. NUMBER OF PAGES**	**19a. NAME OF RESPONSIBLE PERSON**
REPORT	**ABSTRACT**	**c. THIS PAGE**			Milton E. Franke
U	**U**	**U**	**UU**	209	**19b. TELEPHONE NUMBER** *(Include area code)* (937) 785-3636, e-mail: milton.franke@afit.edu